



**Supramolecular Complexes of Some First Row d-Block and d<sup>10</sup>  
Elements: Synthesis, Characterization and Their Possible  
Applications**

**Sirinart Chooset**

**A Thesis Submitted in Fulfillment of the Requirements for the  
Degree of Doctor of Philosophy in Chemistry**

**Prince of Songkla University**

**2017**

**Copyright of Prince of Songkla University**



**Supramolecular Complexes of Some First Row d-Block and d<sup>10</sup>  
Elements: Synthesis, Characterization and Their Possible  
Applications**

**Sirinart Chooset**

**A Thesis Submitted in Fulfillment of the Requirements for the  
Degree of Doctor of Philosophy in Chemistry**

**Prince of Songkla University**

**2017**

**Copyright of Prince of Songkla University**

**Thesis Title**           Supramolecular Complexes of Some First Row d-Block and d<sup>10</sup>  
Elements: Synthesis, Characterization and Their Possible  
Applications

**Author**                   Miss Sirinart Chooset

**Major Program**        Chemistry

---

**Major Advisor**

.....  
(Assoc. Prof. Dr. Sumpun Wongnawa)

**Co-advisor**

.....  
(Dr. Anob Kantacha)

**Examining Committee :**

.....Chairperson  
(Asst. Prof. Dr. Chomchai Suksai)

.....Committee  
(Assoc. Prof. Dr. Sumpun Wongnawa)

.....Committee  
(Dr. Anob Kantacha)

.....Committee  
(Asst. Prof. Dr. Kanidtha Hansongnern)

.....Committee  
(Asst. Prof. Dr. Saowanit Saithong)

The Graduate School, Prince of Songkla University, has approved this thesis  
as fulfillment of the requirements for the Doctor of Philosophy Degree in Chemistry

.....  
(Assoc. Prof. Dr. Teerapol Srichana)  
Dean of Graduate School

This is to certify that the work here submitted is the result of the candidate's own investigations. Due acknowledgement has been made of any assistance received.

.....Signature  
(Assoc. Prof. Dr. Sumpun Wongnawa)  
Major Advisor

.....Signature  
(Dr. Anob Kantacha)  
Co-advisor

.....Signature  
(Miss Sirinart Chooset)  
Candidate



I hereby certify that this work has not been accepted in substance for any degree, and is not being currently submitted in candidature for any degree.

.....Signature

(Miss Sirinart Chooset)

Candidate

ชื่อวิทยานิพนธ์	สารประกอบเชิงซ้อนซูปราโมเลกุลของธาตุกลุ่ม d แถวแรกและ d <sup>10</sup> บางชนิด: การสังเคราะห์, การศึกษาคุณลักษณะและการใช้ประโยชน์
ผู้เขียน	นางสาว สิรินาถ ชุเศษ
สาขาวิชา	เคมี
ปีการศึกษา	2559

### บทคัดย่อ

ได้สังเคราะห์สารประกอบเชิงซ้อนซูปราโมเลกุลของโลหะแทรนซิชันซึ่งมีลิแกนด์ที่ประกอบด้วยออกซิเจนและไนโตรเจนเป็นอะตอมผู้ให้ได้แก่  $[\text{Cd}(\text{Cin})_2(\text{H}_2\text{O})_2]$  (1),  $[\text{Zn}(4,4'\text{-bpy})_{0.5}(\text{Cin})_2]_n$  (2),  $[\text{Cd}_3(4,4'\text{-bpy})_2(\text{cin})_6(\text{H}_2\text{O})_2]_n$  (3),  $[\text{Cd}(4,4'\text{-bpy})(3\text{-Npt})(\text{H}_2\text{O})]_n$  (4),  $[\text{Mn}_2(\text{bpp})(3\text{-Npt})_2(\text{H}_2\text{O})_2]_n$  (5),  $[\text{Ni}(\text{bpp})(3\text{-Npt})(\text{H}_2\text{O})]_n$  (6),  $\{[\text{Ag}_2(\text{bpp})_2] \cdot (4\text{H}_2\text{O}) \cdot (3\text{-Npt})\}_n$  (7),  $\{[\text{Ag}_2(\text{bpe})_2(3\text{-Npt})] \cdot 7\text{H}_2\text{O}\}_n$  (8),  $[\text{Zn}(\text{bpp})_2(\text{sal})_2]_n$  (9),  $[\text{Zn}_2(\text{bpe})_2(\text{sal})_4]$  (10),  $\{[\text{Co}(\text{bpp})_2(\text{H}_2\text{O})_2](4\text{-abs})_2 \cdot \text{H}_2\text{O}\}_n$  (11),  $[\text{Mn}_{0.5}(\text{bpp})(\text{H}_2\text{O})_2] \cdot (4\text{-abs})$  (12),  $\{[\text{Cd}_{0.5}(\text{bpp})(4\text{-abs})] \cdot (\text{H}_2\text{O})\}_n$  (13),  $[\text{Zn}_{0.5}(\text{bpp})(\text{H}_2\text{O})_2] \cdot (4\text{-abs})$  (14),  $\{[\text{Zn}(4,4'\text{-bpy})(\text{H}_2\text{O})_4] \cdot (4\text{-abs})_2 \cdot 2\text{H}_2\text{O}\}_n$  (15),  $\{[\text{Cd}(4,4'\text{-bpy})_{1.5}(\text{H}_2\text{O})_3] \cdot (4\text{-abs}) \cdot (4,4'\text{-bpy}) \cdot (\text{H}_2\text{O}) \cdot \text{NO}_3\}_n$  (16),  $\{[\text{Cd}_{0.5}(\text{bpe})(4\text{-abs})] \cdot \text{H}_2\text{O}\}_n$  (17),  $\{[\text{Cd}(\text{bpp})_2(\text{H}_2\text{O})_2] \cdot (3\text{-abs})_2 \cdot 2\text{H}_2\text{O}\}_n$  (18),  $[\text{Zn}(\text{bpp})_2(\text{Mbs})_2]_n$  (19),  $[\text{Cd}(\text{bpp})_2(\text{Mbs})_2]_n$  (20),  $\{[\text{Cd}(\text{bpp})(\text{sdz})_2] \cdot 2\text{H}_2\text{O}\}_n$  (21) และ  $\{[\text{Zn}(\text{bpe})(\text{sdz})(\text{ac})] \cdot \text{H}_2\text{O}\}_n$  (22) [เมื่อ bpy = 4,4'-bipyridine, bpp = 1,3-bis(4-pyridyl)propane, bpe = 1,2-bis(4-pyridyl)ethane, cin = Cinnamate, 3-Npt = 3-Nitroptalate, sal = Salicylate, 4-abs = Sulfanilate, sdz = Sulfadiazine, 3-abs = 3-aminobenzinesulfonate และ Mbs = *p*-Toluenesulfonate] ด้วยวิธีที่เหมาะสมและทำการศึกษาคุณลักษณะสารประกอบเชิงซ้อนทั้งหมดด้วยเทคนิคฟูรีเยร์ทรานสฟอร์มอินฟราเรดสเปกโทรสโกปี การวิเคราะห์ธาตุองค์ประกอบ เทคนิคการวิเคราะห์การสูญเสีย น้ำหนักทางความร้อน เทคนิคการเลี้ยวเบนของรังสีเอกซ์ทั้งแบบผงและแบบผลึกเดี่ยว เทคนิคนิวเคลียร์แมกเนติกเรโซแนนซ์ เทคนิคยูวี-วิสิเบิลสเปกโทรสโกปี และเทคนิคโฟโตลูมิเนสเซนซ์ และจากการศึกษาพบว่าสารประกอบเชิงซ้อน (2), (9), (10), (13), (14), (17), (18), (19), และ (20) แสดงสมบัติโฟโตลูมิเนสเซนซ์ ในสถานะของแข็งที่อุณหภูมิห้อง นอกจากนี้ได้ศึกษาการประยุกต์ใช้งานในด้านการดูดซับ การเป็นตัวเร่งเชิงแสง การเป็นตัวตรวจวัดโลหะ และการยับยั้งเชื้อแบคทีเรียซึ่งให้ผลดังนี้ จากการศึกษาสมบัติการเป็นตัวเร่งเชิงแสงของสารประกอบเชิงซ้อน (7) และ (8) พบว่าสารประกอบเชิงซ้อนทั้งสองชนิดสามารถสลายสีข้อมเมทิลีนบลู (MB) และ โรดามีน บี (RhB) ภายใต้แสงยูวี

และแสงวิชิเบิล ส่วนสารประกอบเชิงซ้อน (9) และ (10) มีความจำเพาะเจาะจงและความไวในการตรวจวัดไอออนของโลหะทองแดง เมื่อทำการทดลองเปรียบเทียบกับโลหะอื่นเช่น  $\text{Cd}^{2+}$ ,  $\text{Mn}^{2+}$ ,  $\text{Sr}^{2+}$ ,  $\text{K}^+$ ,  $\text{Na}^+$ ,  $\text{Ni}^{2+}$ ,  $\text{Co}^{2+}$  และ  $\text{Ca}^{2+}$  โดยกลไกจะเกิดผ่าน fluorescence quenching ค่าความเข้มข้นต่ำสุดในการตรวจวัดโลหะทองแดงของสารประกอบเชิงซ้อน(9) และ (10) อยู่ที่ประมาณ  $3.9 \times 10^{-7}$  และ  $8.9 \times 10^{-7}$  โมลต่อลิตร ตามลำดับ นอกจากนี้ผลการศึกษาฤทธิ์ การยับยั้งแบคทีเรียของสารประกอบเชิงซ้อน (9) และ (10) ในตัวทำละลายไดเมทิลซัลฟอกไซด์ (DMSO) ที่ศึกษาโดยการวัดโซนไฮของการยับยั้งแสดงให้เห็นว่าสารประกอบเชิงซ้อนทั้งสองชนิด มีฤทธิ์ ใการยับยั้งแบคทีเรียแกรมลบมากกว่าแบคทีเรียแกรมบวก สำหรับการศึกษาศสมบัติการดูดซับของสีย้อมออเรนจ์ จี(OG) บนตัวดูดซับสารประกอบเชิงซ้อน (7) ได้ทำการศึกษาถึงผลของเวลา ปริมาณตัวดูดซับ และความเข้มข้น โดยจากการศึกษากลไกการดูดซับพบว่ารูปแบบการดูดซับเป็นแบบแลงเมียร์

<b>Thesis Title</b>	Supramolecular Complexes of Some First Row d-Block and d <sup>10</sup> Elements: Synthesis, Characterization and Their Possible Applications
<b>Author</b>	Miss Sirinart Chooset
<b>Major Program</b>	Chemistry
<b>Academic Year</b>	2016

### ABSTRACT

Supramolecular complexes based on transition metals with O-donor and N-donor ligand, namely  $[\text{Cd}(\text{Cin})_2(\text{H}_2\text{O})_2]$  (**1**),  $[\text{Zn}(4,4'\text{-bpy})_{0.5}(\text{Cin})_2]_n$  (**2**),  $[\text{Cd}_3(4,4'\text{-bpy})_2(\text{cin})_6(\text{H}_2\text{O})_2]_n$  (**3**),  $[\text{Cd}(4,4'\text{-bpy})(3\text{-Npt})(\text{H}_2\text{O})]_n$  (**4**),  $[\text{Mn}_2(\text{bpp})(3\text{-Npt})_2(\text{H}_2\text{O})_2]_n$  (**5**),  $[\text{Ni}(\text{bpp})(3\text{-Npt})(\text{H}_2\text{O})]_n$  (**6**),  $\{[\text{Ag}_2(\text{bpp})_2] \cdot (4\text{H}_2\text{O}) \cdot (3\text{-Npt})\}_n$  (**7**),  $\{[\text{Ag}_2(\text{bpe})_2(3\text{-Npt})] \cdot 7\text{H}_2\text{O}\}_n$  (**8**),  $[\text{Zn}(\text{bpp})_2(\text{sal})_2]_n$  (**9**),  $[\text{Zn}_2(\text{bpe})_2(\text{sal})_4]$  (**10**),  $\{[\text{Co}(\text{bpp})_2(\text{H}_2\text{O})_2] \cdot (4\text{-abs})_2 \cdot \text{H}_2\text{O}\}_n$  (**11**),  $[\text{Mn}_{0.5}(\text{bpp})(\text{H}_2\text{O})_2] \cdot (4\text{-abs})$  (**12**),  $\{[\text{Cd}_{0.5}(\text{bpp})(4\text{-abs})] \cdot (\text{H}_2\text{O})\}_n$  (**13**),  $[\text{Zn}_{0.5}(\text{bpp})(\text{H}_2\text{O})_2] \cdot (4\text{-abs})$  (**14**),  $\{[\text{Zn}(4,4'\text{-bpy})(\text{H}_2\text{O})_4] \cdot (4\text{-abs})_2 \cdot 2\text{H}_2\text{O}\}_n$  (**15**),  $\{[\text{Cd}(4,4'\text{-bpy})_{1.5}(\text{H}_2\text{O})_3] \cdot (4\text{-abs}) \cdot (4,4'\text{-bpy}) \cdot (\text{H}_2\text{O}) \cdot \text{NO}_3\}_n$  (**16**),  $\{[\text{Cd}_{0.5}(\text{bpe})(4\text{-abs})] \cdot \text{H}_2\text{O}\}_n$  (**17**),  $\{[\text{Cd}(\text{bpp})_2(\text{H}_2\text{O})_2] \cdot (3\text{-abs})_2 \cdot 2\text{H}_2\text{O}\}_n$  (**18**),  $[\text{Zn}(\text{bpp})_2(\text{Mbs})_2]_n$  (**19**),  $[\text{Cd}(\text{bpp})_2(\text{Mbs})_2]_n$  (**20**),  $\{[\text{Cd}(\text{bpp})(\text{sdz})_2] \cdot 2\text{H}_2\text{O}\}_n$  (**21**), and  $\{[\text{Zn}(\text{bpe})(\text{sdz})(\text{ac})] \cdot \text{H}_2\text{O}\}_n$  (**22**) [where bpy = 4,4'-bipyridine, bpp = 1,3-bis(4-pyridyl)propane, bpe = 1,2-bis(4-pyridyl)ethane, cin = Cinnamate, 3-Npt = 3-Nitroptalate sal = Salicylate, 4-abs = Sulfanilate, sdz = Sulfadiazine, 3-abs = 3-aminobenzinesulfonate, and Mbs = *p*-Toluenesulfonate] have been synthesized under suitable conditions. All complexes were characterized by Fourier-transformed infrared spectroscopy, Elemental analysis, Thermogravimetric analysis, Powder X-ray diffraction, Single crystal X-ray diffraction, Nuclear magnetic resonance, UV-Visible spectrophotometer, and photoluminescence spectroscopy. The complexes (**2**), (**9**), (**10**), (**13**), (**14**), (**17**), (**18**), (**19**), and (**20**) showed strong photoluminescence in the solid state at room temperature. Other applications such as adsorption property,

photocatalytic property, fluorescence sensing for metal ions property, and antibacterial activity were also investigated. The photodegradation study of complex (7) and complex (8) showed that both complexes were active photocatalysts for degradation MB and RhB dyes under UV and visible light. Complexes (9) and (10) exhibited selectivity and sensitivity to  $\text{Cu}^{2+}$  compared with other metal ions such as  $\text{Cd}^{2+}$ ,  $\text{Mn}^{2+}$ ,  $\text{Sr}^{2+}$ ,  $\text{K}^+$ ,  $\text{Na}^+$ ,  $\text{Ni}^{2+}$ ,  $\text{Co}^{2+}$ , and  $\text{Ca}^{2+}$  via a fluorescence quenching mechanism. The detection limit for  $\text{Cu}^{2+}$  of complexes (9) and (10) were about  $3.9 \times 10^{-7}$  mol/L and  $8.9 \times 10^{-7}$  mol/L, respectively. Moreover, antibacterial studies of complexes (9) and (10) in dimethylsulfoxide (DMSO) solution were carried out in order to measure zone of inhibition values. The antibacterial activity of complexes for Gram negative bacteria was higher than Gram positive bacteria. The adsorption study for the adsorption of orange G (OG) dye onto complex (7) as a function of effect of contact time, adsorbent dose, and initial dye concentration were investigated. The data suggested that the Langmuir isotherm was the favored model over the Freundlich isotherm for OG dye.

## ACKNOWLEDGMENTS

First and foremost, I would like to thank my advisor, Assoc. Prof. Dr. Sumpun Wongnawa who suggested this research problem, for his suggestion comment on my research, guidance, and assistance in reading, correcting, and criticizing the manuscript.

Secondly, I would like to express my profound gratitude to my co-advisor, Dr. Anob Kantacha Faculty of Science, Thanksin University, for the valuable suggestion and guidance on my thesis.

I am grateful to my examining committee, Asst. Prof. Dr. Chomchai Suksai of the Department of Chemistry, Burapha University. Asst. Prof. Dr. Kanidtha Hansongnern and Asst. Prof. Dr. Saowanit Saithong of Faculty of Science, Prince of Songkla University, for the kindness, comments and helpful suggestion.

I would like to thank, Asst. Prof. Dr. Kittipong Chainok, Department of Physics, Faculty of Science and Technology, Thammasart University, for X-ray collecting data and teaching X-ray structure determination on olex2 program.

I would like to thank Dr. Matthias Zeller and Dr. Arunpatcha Nimthong, Department of Chemistry, Youngstown State University, for help in collecting the data of single crystal X-ray

I am grateful to the Songklanagarind Scholarship for Graduate Studies from Prince of Songkla University, for the financial supports and laboratory expenses throughout this research.

I would like to thank the Department of Chemistry, Faculty of Science, Prince of Songkla University, for all necessary laboratory facilities used throughout this research.

My deep gratitude is also due to all my friends and staffs who give me their help and shared a hard time with me during my study.

Finally, I would like to express my deepest appreciation to my parents for great understanding, encouragement, and support.

Sirinart Chooset

## CONTENTS

	<b>Page</b>
CONTENTS	xi
LIST OF TABLES	xiii
LIST OF FIGURES	xvi
LIST OF ABBREVIATIONS AND SYMBOLS	xxv
CHAPTER 1: INTRODUCTION	1
1.1. Introduction	1
1.2. Types of ligands used for synthesis in supramolecular and coordination Polymer	5
1.3. Application of supramolecular chemistry	9
1.4. Review of literatures	12
1.5. Objectives	40
CHAPTER 2: EXPERIMENTAL	41
2.1 Chemicals	41
2.2 Synthesis of supramolecular complex	42
2.3 Instrument	47
2.4 Photocatalytic experiments	49
2.5 Metal ions sensing experiments	50
2.6 Antibacterial activity	50
2.7 Adsorption experiment procedure	51
CHAPTER 3: RESULTS AND DISCUSSION	53
3.1 Characterization	
3.1.1 Single crystal X-ray diffraction	56
3.1.2 Elemental analysis	109
3.1.3 Infrared spectroscopy	110
3.1.4 Thermogravimetric analysis	115
3.1.5 Electronic absorption spectra	120
3.1.6 wder X-ray diffraction (PXRD)	Po 121
3.1.7 Nuclear magnetic resonance spectroscopy	122
3.1.8 Photoluminescent Property	123
3.2 Luminescent sensing for metal ions	128
3.3 Test for photocatalytic activity	134
3.4 Biological activity	142
3.5 Adsorption studies	143



**CONTENTS (continued)**

	<b>Page</b>
CHAPTER 4: CONCLUSIONS	153
REFERENCES	156
Appendix A	167
Appendix B	210
VITAE	234

## LIST OF TABLES

<b>Table</b>		<b>Page</b>
1	Classification of hydrogen bonds	2
2	The catalytic activity for complexes 1-5 in the cyanosilylation of benzaldehyde and acetophenone with 3 h of reaction time	28
3	The preparation of complexes	53
4	The solubilities of all complexes	54
5	Selected bond distances and angles of $[\text{Cd}(\text{Cin})_2(\text{H}_2\text{O})_2](\mathbf{1})$	57
6	Selected bond distances and angles of $[\text{Zn}(4,4'\text{-bpy})_{0.5}(\text{Cin})_2]_n(\mathbf{2})$	59
7	Selected bond distances and angles of $[\text{Cd}_3(4,4'\text{-bpy})_2(\text{cin})_6(\text{H}_2\text{O})_2]_n(\mathbf{3})$	61
8	Hydrogen-bond geometry ( $\text{\AA}$ , $^\circ$ ) of $[\text{Cd}_3(4,4'\text{-bpy})_2(\text{cin})_6(\text{H}_2\text{O})_2]_n(\mathbf{3})$	62
9	Selected bond distances and angles of $[\text{Cd}(4,4'\text{-bpy})(3\text{-Npt})(\text{H}_2\text{O})]_n(\mathbf{4})$	64
10	Hydrogen-bond geometry ( $\text{\AA}$ , $^\circ$ ) of $[\text{Cd}(4,4'\text{-bpy})(3\text{-Npt})(\text{H}_2\text{O})]_n(\mathbf{4})$	64
11	Selected bond distances and angles of $[\text{Mn}_2(\text{bpp})(3\text{-Npt})_2(\text{H}_2\text{O})_2]_n(\mathbf{5})$	66
12	Hydrogen-bond geometry ( $\text{\AA}$ , $^\circ$ ) of $[\text{Mn}_2(\text{bpp})(3\text{-Npt})_2(\text{H}_2\text{O})_2]_n(\mathbf{5})$	67
13	Selected bond distances and angles of $[\text{Ni}(\text{bpp})(3\text{-Npt})(\text{H}_2\text{O})]_n(\mathbf{6})$	69
14	Selected bond distances and angles of $\{[\text{Ag}_2(\text{bpp})_2]\cdot 3\text{-Npt}\}_n(\mathbf{7})$	71
15	Selected bond distances and angles of $\{[\text{Ag}_2(\text{bpe})_2(3\text{-Npt})]\cdot 7\text{H}_2\text{O}\}_n(\mathbf{8})$	73
16	Selected bond distances and angles of $[\text{Zn}(\text{bpp})_2(\text{Sal})_2]_n(\mathbf{9})$	76
17	Hydrogen-bond geometry ( $\text{\AA}$ , $^\circ$ ) of $[\text{Zn}(\text{bpp})_2(\text{Sal})_2]_n(\mathbf{9})$	77
18	Selected bond distances and angles of $[\text{Zn}_2(\text{bpe})_2(\text{Sal})_4](\mathbf{10})$	79
19	Hydrogen-bond geometry ( $\text{\AA}$ , $^\circ$ ) of $[\text{Zn}_2(\text{bpe})_2(\text{Sal})_4](\mathbf{10})$	80
20	Selected bond distances and angles of $\{[\text{Co}(\text{bpp})_2(\text{H}_2\text{O})_2]\cdot (4\text{-abs})_2\cdot \text{H}_2\text{O}\}_n(\mathbf{11})$	81
21	Hydrogen-bond geometry ( $\text{\AA}$ , $^\circ$ ) of $\{[\text{Co}(\text{bpp})_2(\text{H}_2\text{O})_2]\cdot (4\text{-abs})_2\cdot \text{H}_2\text{O}\}_n(\mathbf{11})$	82
22	Selected bond distances and angles of $[\text{Mn}_{0.5}(\text{bpp})(\text{H}_2\text{O})_2]\cdot (4\text{-abs})(\mathbf{12})$	84
23	Selected bond distances and angles of $[\text{Zn}_{0.5}(\text{bpp})(\text{H}_2\text{O})]\cdot (4\text{-abs})(\mathbf{14})$	84
24	Hydrogen-bond geometry ( $\text{\AA}$ , $^\circ$ ) of $[\text{Mn}_{0.5}(\text{bpp})(\text{H}_2\text{O})_2]\cdot (4\text{-abs})(\mathbf{12})$	85

### LIST OF TABLES (continued)

Table		Page
25	Hydrogen-bond geometry (Å, °) of [Zn <sub>0.5</sub> (bpp)(H <sub>2</sub> O)]·(4-abs)( <b>14</b> )	86
26	Selected bond distances and angles of {[Cd <sub>0.5</sub> (bpp)(4-abs)]·(H <sub>2</sub> O)} <sub>n</sub> ( <b>13</b> )	88
27	Hydrogen-bond geometry (Å, °) of {[Cd <sub>0.5</sub> (bpp)(4-abs)]·(H <sub>2</sub> O)} <sub>n</sub> ( <b>13</b> )	88
28	Selected bond distances and angles of {[Zn(4,4'-bpy)(H <sub>2</sub> O) <sub>4</sub> ]· (4-abs) <sub>2</sub> ·2H <sub>2</sub> O} <sub>n</sub> ( <b>15</b> )	90
29	Hydrogen-bond geometry (Å, °) of {[Zn(4,4'-bpy)(H <sub>2</sub> O) <sub>4</sub> ]· (4-abs) <sub>2</sub> ·2H <sub>2</sub> O} <sub>n</sub> ( <b>15</b> )	91
30	Selected bond distances and angles of {[Cd(4,4'-bpy) <sub>1.5</sub> (H <sub>2</sub> O) <sub>3</sub> ]· (4,4'bpy)·(4-abs)·(H <sub>2</sub> O)·NO <sub>3</sub> } <sub>n</sub> ( <b>16</b> )	93
31	Hydrogen-bond geometry (Å, °) of {[Cd(4,4'-bpy) <sub>1.5</sub> (H <sub>2</sub> O) <sub>3</sub> ]· (4,4'bpy)·(4-abs)·(H <sub>2</sub> O)·NO <sub>3</sub> } <sub>n</sub> ( <b>16</b> )	94
32	Selected bond distances and angles of {[Cd <sub>0.5</sub> (bpe)(4-abs)]·H <sub>2</sub> O} <sub>n</sub> ( <b>17</b> )	96
33	Hydrogen-bond geometry (Å, °) of {[Cd <sub>0.5</sub> (bpe)(4-abs)]·H <sub>2</sub> O} <sub>n</sub> ( <b>17</b> )	97
34	Selected bond distances and angles of {[Cd(bpp) <sub>2</sub> (H <sub>2</sub> O) <sub>2</sub> ]·(3-abs) <sub>2</sub> · 2H <sub>2</sub> O} <sub>n</sub> ( <b>18</b> )	99
35	Hydrogen-bond geometry (Å, °) of {[Cd(bpp) <sub>2</sub> (H <sub>2</sub> O) <sub>2</sub> ]· (3-abs) <sub>2</sub> ·2H <sub>2</sub> O} <sub>n</sub> ( <b>18</b> )	99
36	Selected bond distances and angles of [Zn(bpp) <sub>2</sub> (Mbs) <sub>2</sub> ] <sub>n</sub> ( <b>19</b> )	102
37	Selected bond distances and angles of [Cd(bpp) <sub>2</sub> (Mbs) <sub>2</sub> ] <sub>n</sub> ( <b>20</b> )	102
38	Hydrogen-bond geometry (Å, °) of [Zn(bpp) <sub>2</sub> (Mbs) <sub>2</sub> ] <sub>n</sub> ( <b>19</b> )	102
39	Hydrogen-bond geometry (Å, °) of [Cd(bpp) <sub>2</sub> (Mbs) <sub>2</sub> ] <sub>n</sub> ( <b>20</b> )	103
40	Selected bond distances and angles of {[Cd(bpp)(sdz) <sub>2</sub> ]·2H <sub>2</sub> O} <sub>n</sub> ( <b>21</b> )	104
41	Hydrogen-bond geometry (Å, °) of {[Cd(bpp)(sdz) <sub>2</sub> ]·2H <sub>2</sub> O} <sub>n</sub> ( <b>21</b> )	105
42	Selected bond distances and angles of {[Zn(bpe)(sdz)(ac)]·2H <sub>2</sub> O} <sub>n</sub> ( <b>22</b> )	107

**LIST OF TABLES (continued)**

<b>Table</b>		<b>Page</b>
43	Hydrogen-bond geometry( $\text{\AA}$ , $^\circ$ ) of $\{[\text{Zn}(\text{bpe})(\text{sdz})(\text{ac})]\cdot 2\text{H}_2\text{O}\}_n$ ( <b>22</b> )	107
44	Analytical data (%) calcd (found) of complexes.	109
45	Characteristic IR vibration frequencies ( $\text{cm}^{-1}$ ) of the prepared complexes	111
46	Characteristic IR vibration frequencies ( $\text{cm}^{-1}$ ) of the prepared complexes	114
47	Thermal behavior of complexes	115
48	Chemical shift of protons from aromatic ring (ppm)	122
49	Diameter of zones of inhibition (mm) of complex.	142
50	The constant values of Langmuir and Freundlich isotherms and linear correlation coefficient for adsorption of OG dye by the as-synthesized complex ( <b>7</b> )	150

## LIST OF FIGURES

<b>Figure</b>		<b>Page</b>
1	Partial positive and negative charges associated with the hydrogen atom (H), the donor atom (D) and the acceptor atom (A) in a hydrogen bond	2
2	Face-to-face stacking between two aromatic rings	3
3	Offset stacking between two aromatic rings	3
4	Edge-on interaction (C-H... $\pi$ ) between two aromatic rings	4
5	Cation- $\pi$ interaction between benzene and a sodium cation	4
6	The coordination modes of carboxylate group	6
7	The coordination modes of sulfonate ligand	7
8	Molecular structure of 4,4'-Bipyridine	7
9	TT, TG, GG, and GG' conformations (T = trans, G=gauche) of 1,3-Bi(4-pyridyl)propane (bpp)	8
10	gauche (left) or anti (right) conformation of 1,2-Bis(4-pyridyl)ethane	8
11	A simplified model of the photocatalytic reaction mechanism of dyes degradation	11
12	Molecular structure of $[\text{Zn}(4,4'\text{-bpy})(\text{H}_2\text{O})_4]\cdot(\text{ADC})\cdot 4\text{H}_2\text{O}$	12
13	(a) The UV-vis spectra and (b) the decolorization efficiency of the Bismarck brown dye in the presence of complex. Reaction conditions: dye solution(100ml, 10ppm) and catalyst(110mg).	12
14	Molecular structure of $[\text{Cu}(\text{bipy})(\text{SO}_4)]_n$	13
15	Adsorption isotherms of the Congo red, Orange G, and X-3B dyes on $[\text{Cu}(\text{bipy})(\text{SO}_4)]_n$	14
16	Molecular structure of $[\text{Co}(\text{C}_8\text{H}_{12}\text{O}_4)(\text{C}_{10}\text{H}_8\text{N}_2)]\cdot\text{H}_2\text{O}$	15
17	Molecular structure of $[\text{Cd}(\text{C}_8\text{H}_{12}\text{O}_4)(\text{C}_{10}\text{H}_8\text{N}_2)]\cdot\text{H}_2\text{O}$	15
18	Molecular structure of $[\text{Ag}_2\text{L}_1(\text{biim})_2]\cdot 2\text{H}_2\text{O}$	16
19	Molecular structure of $\text{AgL}_2(\text{biim})$	16
20	Molecular structure of $[\text{Ag}(\text{HL}_3)(\text{Pic})_2]\cdot\text{H}_2\text{O}$	17
21	Molecular structure of $[\text{Ag}_3(\text{L}_3)(\text{HL}_3)(4,4'\text{-bipy})_3(\text{H}_2\text{O})_2]\cdot 4\text{H}_2\text{O}$	17

## LIST OF FIGURES (continued)

<b>Figure</b>		<b>Page</b>
22	Solid-state photoluminescent spectra of <b>1</b> (a), <b>2</b> (b), and <b>3</b> (c) and free ligands [H <sub>2</sub> L1(a'), HL2(b'), H <sub>2</sub> L3(c'), biim(a''), and Pic ('')] at room temperature	18
23	Molecular structure of {(bmpp)[Ag <sub>2</sub> Br <sub>4</sub> ]} <sub>n</sub>	19
24	Molecular structure of {(bmpp)[Ag <sub>4</sub> I <sub>6</sub> ]} <sub>n</sub>	19
25	Photocatalytic decomposition of MB solution (a), RhB solution (b) under UV light irradiation with the use of complexes 1–2 and the control experiment without any catalyst under the same conditions	20
26	Molecular structure of [Ag <sub>4</sub> (dpe) <sub>4</sub> ](btec)	21
27	Molecular structure of [Ag <sub>4</sub> (bpy) <sub>4</sub> ](btec)·12H <sub>2</sub> O	22
28	MO concentration versus irradiation time in the dark and under irradiation by Hg lamp in the presence of complexes 1 and 2	22
29	Molecular structure of {Co(btbb) <sub>0.5</sub> (ndc)(H <sub>2</sub> O)} <sub>n</sub>	23
30	Molecular structure of {[Co(btbp) <sub>2</sub> (3-npa)]·2H <sub>2</sub> O} <sub>n</sub>	24
31	Molecular structure of {[Co(btbb)(bpdc)]·1.5H <sub>2</sub> O} <sub>n</sub>	24
32	Absorption spectra of the MO solution during decomposition reaction under simulated natural sunlight irradiation in the presence of complex 1	25
33	Decomposition of MO solution in a photocatalytic process	25
34	The fluorescence emission spectra of 1 in the DMSO in the presence of various contents of analytes (λ <sub>ex</sub> = 371 nm)	26
35	Molecular structure of [Co(H <sub>2</sub> TTTA) <sub>2</sub> (4,4'-bpy) <sub>2</sub> ]	27
36	Solid state photoluminescence properties of the free H <sub>3</sub> TTTA ligand and all complexes	27
37	Molecular structure of [Co(BPY) <sub>2</sub> (H <sub>2</sub> O) <sub>2</sub> ](BPY)(BS) <sub>2</sub> (H <sub>2</sub> O) <sub>4</sub>	29
38	Molecular structure of [Co(BPY) <sub>2</sub> (H <sub>2</sub> O) <sub>4</sub> ](ABS) <sub>2</sub> (H <sub>2</sub> O) <sub>2</sub>	29
39	Molecular structure of [Co(BPY)(H <sub>2</sub> O) <sub>4</sub> ](MBS) <sub>2</sub>	30

## LIST OF FIGURES (continued)

<b>Figure</b>		<b>Page</b>
40	Molecular structure of $\{[\text{Cu}_3(\text{btb})_3(\text{nbta})_2] \cdot (\text{H}_2\text{O})_2\}_n$	31
41	Solid-state fluorescence spectra of free btb and the complex.	31
42	Adsorption result of congo red over the complex	32
43	Molecular structure of $[\text{Co}(\text{L}_1)(\text{tp})]_n$ (1) and $[\text{Co}(\text{L}_2)(\text{Htp})(\text{tp})_{0.5}]_n$ (2)	32
44	Emission spectra of complexes 1, 2 and free ligands in the solid state at room temperature	33
45	Adsorption results of congo red over complexes 1 and 2	33
46	Molecular structure of $\text{Mn}_3(\text{btde})_3(\text{DMF})_4$ .	34
47	Molecular structure of $\text{Co}(\text{btde})(\text{DMF})_3$	35
48	Molecular structure of $\text{Zn}(\text{btde})(\text{DMF})_3$	35
49	Molecular structure of $\text{Zn}(\text{btde})(4,4'\text{-bpy})_{0.5}$	36
50	(a) Fluorescent emission spectra of the $\text{H}_2\text{btde}$ ligand and crystals 1-4 in the solid state at room temperature and fluorescent images of complexes 3 and 4.	36
51	Molecular structure of methylene blue	37
52	Molecular structure of Rhodamine B	38
53	Molecular structure of Orange G	38
54	Molecular structure of N- and O- donor ligands used for synthesis in this thesis	39
55	Molecular structure of $\text{Cd}(\text{Cin})_2(\text{H}_2\text{O})_2$ (ellipsoid probability at 50%).	56
56	Packing diagram of $\text{Cd}(\text{Cin})_2(\text{H}_2\text{O})_2$ plotted down b axis	57
57	View of the supramolecular network via O–H---O interactions	58
58	Molecular structure of $\text{Zn}(4,4'\text{-bpy})_{0.5}(\text{Cin})_2$ (ellipsoid probability at 50%)	58
59	Packing diagram of $[\text{Zn}(4,4'\text{-bpy})_{0.5}(\text{Cin})_2]$ plotted down c axis	59
60	The $\pi$ - $\pi$ interactions between aromatic rings of 4,4'-bpy and Cin ligand	60
61	Molecular structure of $[\text{Cd}_3(4,4'\text{-bpy})_2(\text{cin})_6(\text{H}_2\text{O})_2]_n$ (ellipsoid probability at 50%)	61
62	Packing diagram of $[\text{Cd}_3(4,4'\text{-bpy})_2(\text{cin})_6(\text{H}_2\text{O})_2]_n$ plotted down b axis	62

## LIST OF FIGURES (continued)

Figure	Page
63 O–H ... O hydrogen bond between hydrogen atom of water molecule and oxygen atom of cinnamate ligand	62
64 Molecular structure of $[\text{Cd}(4,4'\text{-bpy})(3\text{-Npt})_2(\text{H}_2\text{O})]_n$ (ellipsoid probability at 50%)	63
65 Packing diagram of $[\text{Cd}(4,4'\text{-bpy})(3\text{-Npt})_2(\text{H}_2\text{O})]_n$ plotted down a axis	64
66 Intramolecular hydrogen bond interaction of $[\text{Cd}(4,4'\text{-bpy})(3\text{-Npt})(\text{H}_2\text{O})]_n$	65
67 Molecular structure of $[\text{Mn}_2(\text{bpp})(3\text{-Npt})_2(\text{H}_2\text{O})_2]_n$ (ellipsoid probability at 50%)	65
68 View of the 3D supramolecular network via O–H---O interactions	67
69 Molecular structure of $[\text{Ni}(\text{bpp})(3\text{-Npt})_2(\text{H}_2\text{O})]_n$ (ellipsoid probability at 50%)	68
70 Packing diagram of $[\text{Ni}(\text{bpp})(3\text{-Npt})_2(\text{H}_2\text{O})]_n$ plotted down a axis	69
71 View of the hydrogen bonds interaction via strong O–H---O	70
72 ORTEP representation of the asymmetric unit of $\{[\text{Ag}_2(\text{bpp})_2]\cdot 3\text{-Npt}\}_n$ (Thermal ellipsoids are drawn at 40% probability)	70
73 Packing diagram of $\{[\text{Ag}_2(\text{bpp})_2]\cdot 3\text{-Npt}\}_n$ plotted down b axis	71
74 $\pi$ - $\pi$ Stacking interactions of $\{[\text{Ag}_2(\text{bpp})_2]\cdot 3\text{-Npt}\}_n$	72
75 ORTEP representation of the asymmetric unit of $\{[\text{Ag}_2(\text{bpe})_2(3\text{-Npt})]\cdot 7\text{H}_2\text{O}\}_n$ (Thermal ellipsoids are drawn at 50% probability)	73
76 Packing diagram of $\{[\text{Ag}_2(\text{bpe})_2(3\text{-Npt})]\cdot 7\text{H}_2\text{O}\}_n$ plotted down a axis	74
77 3-D supramolecular network by hydrogen bonding.	75
78 ORTEP representation of the asymmetric unit of $[\text{Zn}(\text{bpp})_2(\text{Sal})_2]_n$ (Thermal ellipsoids are drawn at 50% probability)	76
79 Packing diagram of $[\text{Zn}(\text{bpp})_2(\text{Sal})_2]_n$ plotted down a axis	77
80 Intramolecular interaction via strong O–H---O interactions	78



## LIST OF FIGURES (continued)

Figure	Page
81 ORTEP representation of the asymmetric unit of $[\text{Zn}_2(\text{bpe})_2(\text{Sal})_4]$ (Thermal ellipsoids are drawn at 50% probability)	78
82 Packing diagram of $[\text{Zn}_2(\text{bpe})_2(\text{Sal})_4]$ plotted down b axis	79
83 View of the hydrogen bond via strong O–H---O interactions	80
84 Molecular structure of $\{[\text{Co}(\text{bpp})_2(\text{H}_2\text{O})_2]\cdot(4\text{-abs})_2\cdot\text{H}_2\text{O}\}_n$ (ellipsoid probability at 50%)	81
85 Packing diagram of $\{[\text{Co}(\text{bpp})_2(\text{H}_2\text{O})_2]\cdot(4\text{-abs})_2\cdot\text{H}_2\text{O}\}_n$ plotted down b axis	82
86 View of the 3D supramolecular network via O–H---O and N–H---O interactions	83
87 ORTEP representation of the asymmetric unit of $[\text{Mn}_{0.5}(\text{bpp})(\text{H}_2\text{O})_2]\cdot$ (4-abs) (Thermal ellipsoids are drawn at 50% probability)	84
88 Packing diagram of $[\text{M}_{0.5}(\text{bpp})(\text{H}_2\text{O})_2]\cdot(4\text{-abs})$ plotted down a axis	85
89 View of the 3D supramolecular network via O–H---O and N–H---O interactions	86
90 View of the 3D supramolecular network via N–H---O interactions	87
91 ORTEP representation of the asymmetric unit of $\{[\text{Cd}(\text{bpp})_2(4\text{-abs})_2]\cdot$ ( $\text{H}_2\text{O}$ ) $\}_n$ (Thermal ellipsoids are drawn at 50% probability)	87
92 Intermolecular hydrogen bonding occurs between the oxygen of lattice water molecule and oxygen of monodentate 4-abs ligand	89
93 ORTEP representation of the asymmetric unit of $\{[\text{Zn}(4,4'\text{-bpy})(\text{H}_2\text{O})_4]\cdot$ (4-abs) $_2\cdot 2\text{H}_2\text{O}\}_n$ (Thermal ellipsoids are drawn at 50% probability)	90
94 Packing diagram of $\{[\text{Zn}(4,4'\text{-bpy})(\text{H}_2\text{O})_4]\cdot(4\text{-abs})_2\cdot 2\text{H}_2\text{O}\}_n$	91
95 Three-dimensional supramolecular structure of $\{[\text{Zn}(4,4'\text{-bpy})$ ( $\text{H}_2\text{O}$ ) $_4]\cdot(4\text{-abs})_2\cdot 2\text{H}_2\text{O}\}_n$	92
96 2-D honeycomb-like supramolecular network in complex generated from the basic building blocks through hydrogen-bonding interactions	92

## LIST OF FIGURES (continued)

Figure		Page
97	ORTEP representation of the asymmetric unit of $\{[\text{Cd}(4,4'\text{-bpy})_{1.5}(\text{H}_2\text{O})_3]\cdot(4,4'\text{bpy})\cdot(4\text{-abs})\cdot(\text{H}_2\text{O})\cdot\text{NO}_3\}_n$ (Thermal ellipsoids are drawn at 50% probability)	93
98	Packing diagram of $\{[\text{Cd}(4,4'\text{-bpy})_{1.5}(\text{H}_2\text{O})_3]\cdot(4,4'\text{bpy})\cdot(4\text{-abs})\cdot(\text{H}_2\text{O})\cdot\text{NO}_3\}_n$ plotted down b axis	94
99	3-D supramolecular network of $\{[\text{Cd}(4,4'\text{-bpy})_{1.5}(\text{H}_2\text{O})_3]\cdot(4,4'\text{bpy})\cdot(4\text{-abs})\cdot(\text{H}_2\text{O})\cdot\text{NO}_3\}_n$	95
100	ORTEP representation of the asymmetric unit of $\{[\text{Cd}_{0.5}(\text{bpe})(4\text{-abs})]\cdot\text{H}_2\text{O}\}_n$ (Thermal ellipsoids are drawn at 50% probability)	95
101	Packing diagram of $\{[\text{Cd}_{0.5}(\text{bpe})(4\text{-abs})]\cdot\text{H}_2\text{O}\}_n$ plotted down c axis	96
102	Hydrogen bonding of $\{[\text{Cd}_{0.5}(\text{bpe})(4\text{-abs})]\cdot\text{H}_2\text{O}\}_n$ between water molecule and sulfonate ligands	97
103	ORTEP representation of the asymmetric unit of $\{[\text{Cd}(\text{bpp})_2(\text{H}_2\text{O})_2]\cdot(3\text{-abs})_2\cdot 2\text{H}_2\text{O}\}_n$ (Thermal ellipsoids are drawn at 50% probability)	98
104	Packing diagram of $\{[\text{Cd}(\text{bpp})_2(\text{H}_2\text{O})_2]\cdot(3\text{-abs})_2\cdot 2\text{H}_2\text{O}\}_n$ plotted down c. axis	98
105	O–H···O hydrogen bonding of $\{[\text{Cd}(\text{bpp})_2(\text{H}_2\text{O})_2]\cdot(3\text{-abs})_2\cdot 2\text{H}_2\text{O}\}_n$	100
106	ORTEP representation of the asymmetric unit of $[\text{Zn}(\text{bpp})_2(\text{Mbs})_2]_n$ (Thermal ellipsoids are drawn at 50% probability)	101
107	Weak C–H···O hydrogen bond interactions of $[\text{M}(\text{bpp})_2(\text{Mbs})_2]_n$	103
108	ORTEP representation of the asymmetric unit of $\{[\text{Cd}(\text{bpp})(\text{sdz})_2]\cdot 2\text{H}_2\text{O}\}_n$ (Thermal ellipsoids are drawn at 50% probability)	104
109	Packing diagram of $\{[\text{Cd}(\text{bpp})(\text{sdz})_2]\cdot 2\text{H}_2\text{O}\}_n$ plotted down c axis	105
110	Coordination polymer chain are linked by O–H···O hydrogen bonding	106
111	ORTEP representation of the asymmetric unit of $\{[\text{Zn}(\text{bpe})(\text{sdz})(\text{ac})]\cdot 2\text{H}_2\text{O}\}_n$ (Thermal ellipsoids are drawn at 50% probability)	106
112	View of the O—H···O hydrogen bonds of $\{[\text{Zn}(\text{bpe})(\text{sdz})(\text{ac})]\cdot 2\text{H}_2\text{O}\}_n$	108
113	Ultraviolet absorption spectrum for $\{[\text{Co}(\text{bpp})_2(\text{H}_2\text{O})_2](4\text{-abs})_2\cdot\text{H}_2\text{O}\}_n$ ( <b>11</b> )	120

## LIST OF FIGURES (continued)

<b>Figure</b>	<b>Page</b>
114 Visible absorption spectrum for $\{[\text{Co}(\text{bpp})_2(\text{H}_2\text{O})_2] \cdot (4\text{-abs})_2 \cdot \text{H}_2\text{O}\}_n$ ( <b>11</b> )	121
115 Solid-state emission spectrum of complex ( <b>2</b> ) at room temperature	123
116 The emission spectra of complexes ( <b>9</b> )-(10) at room temperature	124
117 Fluorescent image of complex ( <b>9</b> ) in DMSO solution at room temperature	124
118 Luminescent spectra of complex ( <b>9</b> ) in the solid state (—) and dissolved state (- - -) in DMSO ( $\lambda_{\text{ex}}=320$ nm)	125
119 Solid-state emission spectra of complexes ( <b>11</b> )-(14) at room temperature	126
120 Solid-state emission spectra of complexes ( <b>17</b> )-(18) at room temperature	127
121 Solid-state emission spectra of complexes ( <b>19</b> )-(20) at room temperature	128
122 The quenching efficiency of complex ( <b>9</b> ) in the DMSO upon addition of metal ion aqueous solution	129
123 The quenching efficiency of complex ( <b>10</b> ) in the DMSO upon addition of metal ion aqueous solution	130
124 Fluorescent images of complex ( <b>10</b> ) in the DMSO upon addition of metal ion aqueous solution	130
125 The fluorescence emission spectrum of complex ( <b>9</b> ) in the DMSO upon incremental addition of $\text{Cu}^{2+}$ aqueous solution	131
126 The relationship between the quenching efficiency and the logarithmic concentration of $\text{Cu}^{2+}$ of complex ( <b>9</b> )	131
127 The fluorescence emission spectrum of complex ( <b>10</b> ) in the DMSO upon incremental addition of $\text{Cu}^{2+}$ aqueous solution	132
128 The relationship between the quenching efficiency and the logarithmic concentration of $\text{Cu}^{2+}$ of complex ( <b>10</b> )	132
129 The quenching efficiency of complex ( <b>9</b> ) in the DMSO solutions upon addition of different counter anions to $\text{Cu}^{2+}$ aqueous solutions	133
130 The quenching efficiency of complex ( <b>10</b> ) in the DMSO solutions upon addition of different counter anions to $\text{Cu}^{2+}$ aqueous solutions	133

## LIST OF FIGURES (continued)

<b>Figure</b>	<b>Page</b>
131 The efficiencies of photocatalytic degradation of MB dye on complex (7) and complex (8) under UV irradiation (n=3)	134
132 The efficiencies of photocatalytic degradation of RhB dye on complex (7) and complex (8) under UV irradiation (n=3)	134
133 The efficiencies of photocatalytic degradation of MB dye on complex (7) and complex (8) under visible light irradiation (n=3)	135
134 The efficiencies of photocatalytic degradation of RhB dye on complex (7) and complex (8) under visible light irradiation (n=3)	136
135 UV–visible diffuse reflectance spectra of absorbance versus energy (eV) for complex (7)	137
136 UV–visible diffuse reflectance spectra of absorbance versus energy (eV) for complex (8)	137
137 The propose mechanisms of photocatalytic reactions between of dyes and complex (8)	138
138 The photodegradation efficiencies of MB dye on complexes (7) and (8) from the recyclability test under UV-irradiation	139
139 The photodegradation efficiencies of RhB dye on complexes (7) and (8) from the recyclability test under UV-irradiation	140
140 The photodegradation efficiencies of MB dye on complexes (7) and (8) from the recyclability test under visible irradiation	140
141 The photodegradation efficiencies of Rh B dye on complexes (7) and (8) from the recyclability test under visible irradiation	141
142 PXRD patterns of complex (7) before (—) and after (.....) photocatalytic process	141
143 PXRD patterns of complex (8) before (—) and after (.....) photocatalytic process	142
144 The UV-visible spectrum of OG solution in the range of $1 \times 10^{-5}$ to $5 \times 10^{-5}$ M	144

**LIST OF FIGURES (continued)**

<b>Figure</b>		<b>Page</b>
145	The standard calibration graph of OG solution in the range of $1 \times 10^{-5}$ to $5 \times 10^{-5}$ M	144
146	Effect of the contact time on OG dye removal by complex (7)	145
147	Effect of the dosage of adsorbent on OG dye removal by the complex (7)	146
148	Effect of the initial concentration of OG dye on dye removal by the complex (7)	147
149	Non-linearized (a), linearized Langmuir (b) and Freudlich (c) adsorption isotherms of OG dye for the complex (7)	150
150	The photographs of complex (7) with OG dye: (a) used and (b) regenerated complex (7)	152

**LIST OF ABBREVIATION AND SYMBOLS**

K	=	kelvin
cm <sup>-1</sup>	=	wavenumber
bpp	=	1,3-bis(4-pyridyl)propane
bpy	=	4,4'-bipyridine
bpe	=	1,2-bis(4-pyridyl)ethane
4-abs	=	4-aminobenzene sulfonic acid
3-abs	=	3-aminobenzene sulfonic acid
3-npt	=	3-Nitrophthalic acid
Cin	=	cinnamic acid
nm	=	nanometer
sal	=	salicylate
OG	=	orange G
MB	=	methylene blue
RhB	=	rhodamine B
$\lambda_{em}$	=	lambda emission
$\lambda_{ex}$	=	lambda excitation
MLCT	=	metal-to-ligand charge-transfer
LMCT	=	ligand -to- metal charge-transfer
HOMO	=	highest occupied molecular orbital
LOMO	=	lowest unoccupied molecular orbital
$\delta$	=	chemical shift
Å	=	angstrom
h $\nu$	=	energy
M	=	molar; mass

mmol	=	millimole
Vis	=	visible
UV	=	ultraviolet
DMSO	=	dimethyl sulfoxide
1-D	=	one-dimensional
2-D	=	two-dimensional
3-D	=	three-dimensional
NMR	=	nuclear magnetic resonance
Calc	=	calculated
ppm	=	parts per million

## CHAPTER 1

### INTRODUCTION

#### **Supramolecular chemistry**

Supramolecular chemistry is one of the popular and speedy growing areas in the group of chemistry. It is highly interdisciplinary in nature and, as a result, attracts not just chemists but biochemists, biologists, environmental scientists, and others. Supramolecular chemistry extends beyond the realm of individual molecules to focus on intermolecular non-covalent interactions between two or more entities to create structure (Steed *et al.*, 2000).

Definition of supramolecular chemistry was given by Jean Marie Lehn, who received the Nobel prize in chemistry for his work area on supramolecular chemistry in 1987, as “Supramolecular chemistry is the chemistry of the intermolecular bond, covering the structures and functions of the entities formed by association of two or more chemical species.” (Lehn, 1995)

#### **Coordination polymer**

A coordination polymer is an inorganic polymer structure containing metal cation centers linked by organic ligands, when a ligand has the ability to form many coordination bonds and acts as a bridge between metal and another metal centers. More formally, a coordination polymer is a coordination compound with repeating coordination entities extending in one-dimensional structure (extends in a straight line (along the x axis)), two-dimensional structure (extends in a plane (two directions, x and y axes)), and three-dimensional structure (extends in all three directions (x, y, and z axes)) (Bao *et al.*, 2005, Stuart *et al.*, 2013 and [https://en.wikipedia.org/Coordination polymer](https://en.wikipedia.org/Coordination%20polymer)).

#### **Intermolecular forces**

Supramolecular chemistry, coordination polymers, and crystal engineering are related and their structures and architectures are controlled by intermolecular interactions. Therefore, study of intermolecular forces is important for understanding the molecular structures. The significantly non-covalent interactions involved in coordination chemistry may be several types of interaction as follows.



### Hydrogen bonding interactions

Hydrogen bonding interactions has become very important in supramolecular chemistry. Hydrogen bonding occurs between acidic hydrogen atoms and electronegative atom or electron withdrawing group such as nitrogen (N), sulfur (S), fluorine (F) and an another acceptor as show in **Figure 1**. Hydrogen bonds are widely exploited in molecular crystal engineering. Generally, types of hydrogen bonds are based on the distance between the acceptor and donor atom which is divided into three types as: strong, medium, and weak hydrogen bonds. The classification of hydrogen bonds are summarized in **Table 1**.

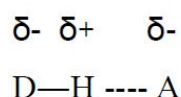


**Figure 1.** Partial positive and negative charges associated with the hydrogen atom (H), the donor atom (D) and the acceptor atom (A) in a hydrogen bond.

**Table 1.** Classification of hydrogen bonds. (Steed *et al.*, 2007)

	<b>strong</b>	<b>medium</b>	<b>weak</b>
<b>Interaction type</b>	mostly covalent	mostly electrostatic	electrostatic
<b>Bond lengths (Å)</b>	D---H = H...A	D---H < H...A	D---H << H...A
<b>D---A</b>	2.2 - 2.5	2.5 - 3.2	3.2 - 4.0
<b>H...A</b>	1.2 - 1.5	1.5 - 2.2	2.2 - 3.2
<b>Bond energy (kcal/mol)</b>	14-40	4-14	0-4
<b>Bond angle &lt;DHA (°)</b>	175-180	130-180	90-150
<b>Reduction in IR stretch frequency</b>	25%	10-25%	<10%
<b>Examples</b>	proton sponges, HF complexes, hydrated protons	carboxylic acids, alcohols, biomolecules	C-H...O/N O/N-H...π

IR spectroscopy is a useful tool to study and understand the hydrogen bonds interaction. The data of H-bonding from IR spectroscopy are shown as the shift in vibration of -OH groups. Another important technique is the X-ray crystallography which reveals the existence of hydrogen bonding in the obtained crystal structure.

### $\pi$ - $\pi$ interactions

$\pi$ - $\pi$  stacking interactions are non-covalent interactions between two aromatic rings. There are two general types: face-to-face and offset interactions. The evidence for  $\pi$ - $\pi$  stacking interactions comes from X-ray crystallography (Mutasem *et al.*, 2002).

#### Face-to-face interaction

The  $\pi$ - $\pi$  stacking that occurs between one aromatic ring over the other aromatic ring in a perfectly aligned style is called *face-to-face interaction*. The centroid-centroid distance of aromatic molecule is equal with the interplanar distance (Figure 2). The distance between the aromatic rings in  $\pi$ - $\pi$  interaction obtained by measuring centroid-to-centroid is about 3.3–3.8 Å

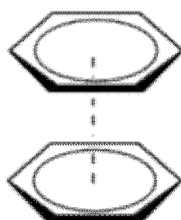


**Figure 2.** Face-to-face stacking between two aromatic rings. (Mutasem *et al.*, 2002)

#### Offset interaction

The stacking that occurs between one aromatic ring over the other aromatic ring in a slightly parallel displaced style is called *offset interaction*. The other names used to denote is *parallel displaced* or *slipped interaction* (Figure 3). The distance between the aromatic rings is equal with Face-to-face interaction

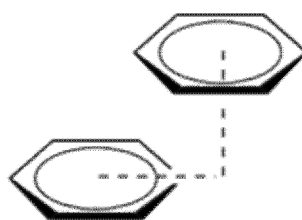


**Figure 3.** Offset stacking between two aromatic rings. (Mutasem *et al.*, 2002)

### C-H... $\pi$ interactions

The C-H ...  $\pi$  interaction occurs between the positively charged hydrogen of an aromatic ring with the  $\pi$ -cloud of another aromatic molecule is called *C-H...  $\pi$  interaction*. The other names are *edge-to-face*, *point-to-face*, *edge-on*, and *T-shaped interaction*. This type is generally included in the  $\pi$ -type of interactions (**Figure 4**).

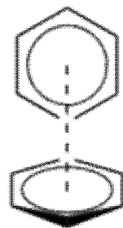


**Figure 4.** Edge-on interaction (C-H ...  $\pi$ ) between two aromatic rings. (Mutasem *et al.*, 2002)

### Cation- $\pi$ interactions

The cation- $\pi$  interaction is a weak non-covalent molecular interaction between partial negative charge of the electron-rich  $\pi$  orbitals from an aromatic ring such as benzene and the adjacent positive charge from cation such as alkali metal ions (**Figure 5**). The cation- $\pi$  interaction is the important force for molecular recognition in biological systems (Jennifer *et al.*, 1997).

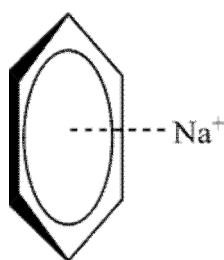


**Figure 5** Cation- $\pi$  interaction between benzene and a sodium cation. (Jennifer *et al.*, 1997)

### Dipole-dipole interaction

Dipole-dipole interactions are electrostatic interactions between polar molecules where the negative end of one molecule attracts the positive end of another molecule. The strength of the dipole-dipole interaction depends on the distance,

strength of the dipoles, and relative orientation of the dipoles. The energies of dipole-dipole interaction are in the range 5-50 kJ/mol. Only polar molecules can exhibit this type of forces and are considered to be quite strong.

### **Types of ligands used for synthesis in supramolecular and coordination polymer**

The general synthetic procedure for designing supramolecular involves using multidentate ligands containing O-, S-, P-, or N- as donor atoms, such as monocarboxylic acid, polycarboxylic acids, and bipyridines etc. Ligand will donate a lone pair of electrons to a metal cation to form a coordination complex by a Lewis acid and base relationship. Example of ligands for synthesis in supramolecular are as follows.

#### **Oxygen donor ligands**

##### **Carboxylate ligand**

Carboxylate ligands are a large group of O-donor ligands and are popular for synthesis of supramolecular complex. Carboxylate ligands exhibit various mode of coordination such as monodentate, bridging, chelating, and chelating-bridging as shown in **Figure 6**. When, the number of donor atoms in carboxylate ligands and the number of chelating rings increase will result in the complexes higher stability. In addition, the ability of the carboxylate groups to form chelating and bridging coordination modes indicates that they do not operate as linear linking groups and this makes the coordination networks ranging from zero-dimensional discrete molecules to three-dimensional architectures.

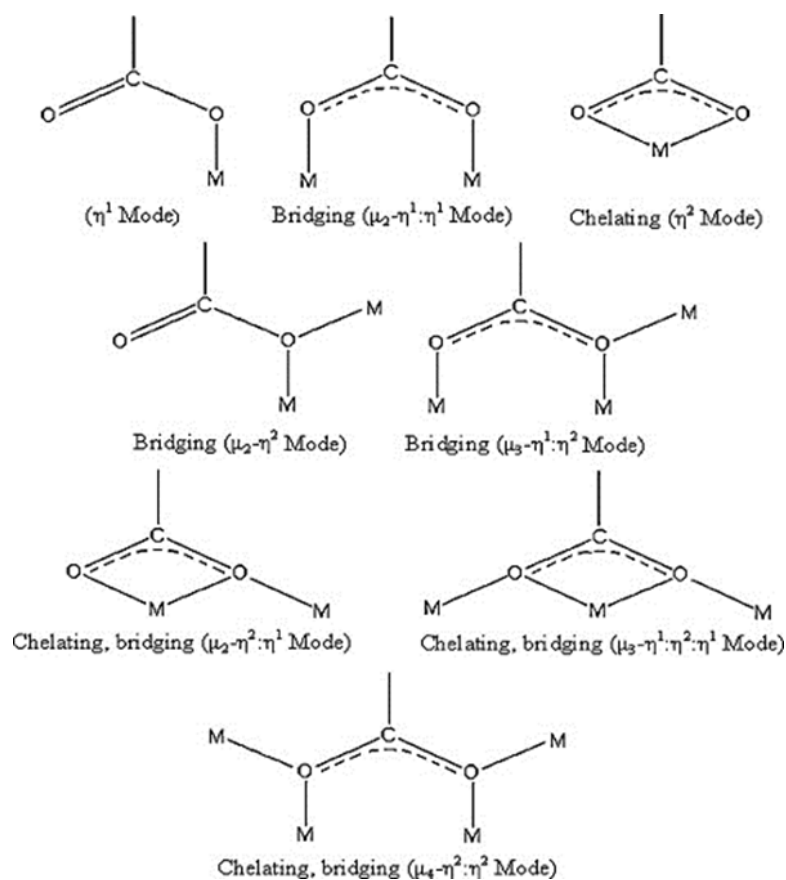


**Figure 6.** The coordination modes of carboxylate group. (Mao *et al.*, 2011)

### Sulfonate ligand

Sulfonate ligands are a large group of O-donor ligands with the general formula  $\text{RSO}_3^-$  (where R is an aromatic group or aliphatic). Sulfonate compounds have important functions in several fields such as chemical separation, medicine, and catalysis. Salts of sulfonic acid are applied as surfactants and dyes in industry. In addition, sulfonate ligands containing -OH and -NH<sub>2</sub> groups have a potential for hydrogen bonding acceptor and donor interactions to construct new metal-organic coordination networks and enhance crystal stability. Sulfonate ligand exhibit various modes of coordination, such as monodentate, bridging, chelating, and chelating-bridging (Deng *et al.*, 2010 and Swiderski *et al.*, 2013) are shown in **Figure 7**.

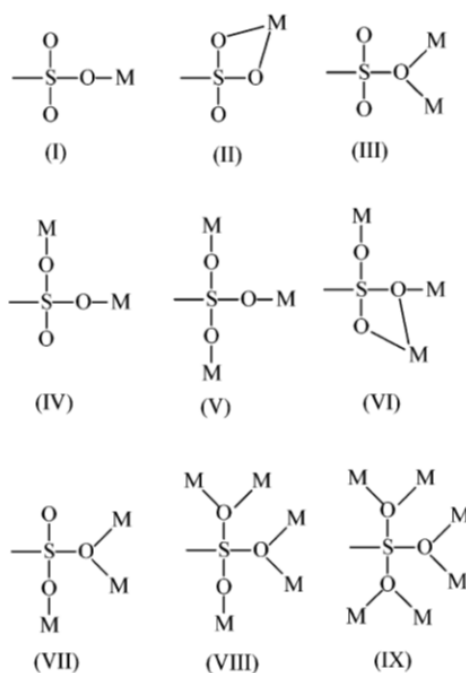


**Figure 7.** The coordination modes of sulfonate ligand. (Ma *et al.*, 2005)

### Nitrogen donor ligands

Nitrogen donor ligands have been widely employed as linkers in supramolecular synthesis. N-donor organic ligands is an important strategy of constructing coordination polymers, due to abilities of coordinating to metal ions, H-bonds or  $\pi$ - $\pi$  stacking interactions, and altering the coordination environment of central ions and the dimension of the frameworks. The pyridine ligands show better donor ability towards the transition metal atom in comparison to primary amines, producing more stable networks.

4,4'-Bipyridine (4,4'-bipy) is a rigid linear bidentate bridging ligand with coordination sites at two ends of the rigid molecule and has been widely used in crystal engineering of coordination polymers and supramolecular chemistry. (Seidel *et al.*, 2011)

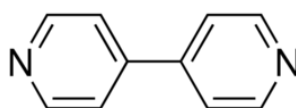


**Figure 8.** Molecular structure of 4,4'-Bipyridine.

The flexible 1,3-bis(4-pyridyl)propane shows good coordinating ability resulting in multi-dimensional systems. The free rotation of the pyridine rings and the propyl group ( $-\text{CH}_2-\text{CH}_2-\text{CH}_2-$ ) can assume TT, TG, GG, and GG' conformations (Lucia *et al.*, 2002).

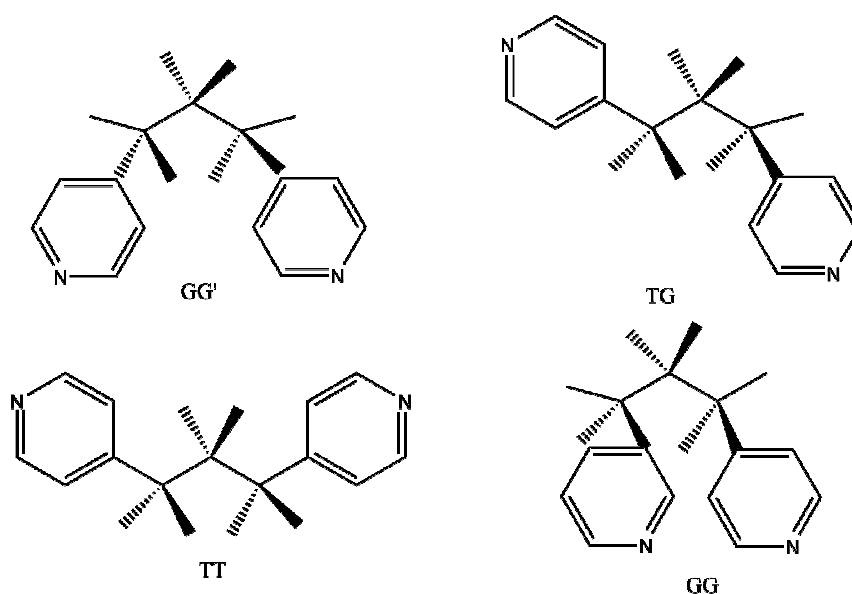


**Figure 9.** TT, TG, GG, and GG' conformations (T = trans, G=gauche) of 1,3-Bi(4-pyridyl)propane (bpp). (Lucia *et al.*, 2002)

Flexible 1,2-Bis(4-pyridyl)ethane ligand acts as bridging ligand, and can bend, rotate around bonds, and reorient themselves which can exist in either gauche or anti conformational isomers (Jacqueline *et al.*, 2002). Two conformations of 1,2-Bis(4-pyridyl)ethane are shown in **Figure 10**. These different conformations create more variety in the structure from 1-D to 3-D frameworks.

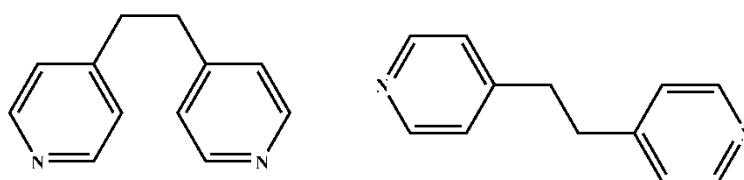


**Figure 10.** gauche (left) or anti (right) conformation of 1,2-Bis(4-pyridyl)ethane. (Jacqueline *et al.*, 2002)

## Application of supramolecular chemistry

### Organic pollutant degradation in coordination complexes

The past decades, organic dyes widely used in textile, plastics, printing, cosmetic and food industries represent a source of wastewaters. Most of dyes cause to be toxic mutagenic, and carcinogenic on humans. Several techniques such as coagulation, adsorption, oxidation, photo-catalysis, ozonation, electrochemical, and biosorption have been used for the removal of organic dye pollutants from wastewaters of the industries. In the field of environmental remediation, coordination complexes such as MOF have been developed for uses as photocatalysts or as efficient adsorbents for the degradation of organic pollutants from wastewater. There have been reports that many MOF's have good photocatalytic performances for the degradation of dye pollutants.

The hypothesis for organic pollutant degradation mechanism of MOF and coordination complexes come from highest occupied molecular orbital (HOMO) and lowest unoccupied molecular orbital (LUMO). In the ground state, there are two electrons in the HOMO, and no electrons in the LUMO. In the presence of energy light, one electron of the HOMO is transferred to the LUMO form which it can easily be lost, while the HOMO strongly demands one electron to return to its stable state. Generally, the excited  $M^{2+}$  center decays to its ground state quickly. (Wang *et al.*, 2014)

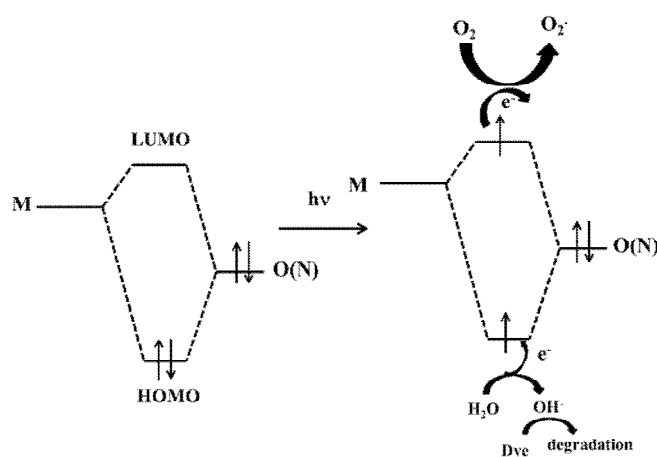


**Figure 11.** A simplified model of the photocatalytic reaction mechanism of dyes degradation. (Wang *et al.*, 2014)



### **Fluorescence sensing in coordination complexes**

Generally, luminescence through excitation of an organic/inorganic molecule upon UV light photons is a phenomenon termed as photoluminescence. It is formally divided into two parts: fluorescence and phosphorescence depending upon the electronic configuration of the excited state and the emission pathway which, if the electrons fall back to original state is short, the process is called fluorescence, but if the electrons fall back is long the process is called phosphorescence.

Photoluminescent of supramolecular and metal coordination polymer has been of significant interest due to their applications in many areas such as light-emitting diodes (LEDs), trace metal analysis, and molecular sensor. In recent years, some metal–organic coordination complexes from  $d^{10}$  metal centers and functional organic ligands (Flexible ligands) or conjugated organic ligands could exhibit strong luminescence, particularly in the blue green, and red region, which attracted great interest for panel display applications.

In addition, luminescence material of supramolecular and metal coordination polymer has been of significant interest to the development of selective and sensitive detection for detecting nitroaromatic explosives such as 2,4,6-trinitrophenol (TNP) 2,4,6-trinitrotoluene (TNT) and 2,6-dinitrotoluene (2,6-DNT) which it is used in the synthesis of explosives (Ye *et al.*, 2016 , Zhang *et al.*, 2016 and Buragohain *et al.*, 2016).

However, metal ion sensing has become very important for both biological and environmental applications. In response, a large class of cation sensors based on coordination chemistry has been developed. Several are selective for either alkali alkaline earth metals, and transition or heavy metal in which detection is necessary to monitor and regulate a number of cellular functions. Heavy metal cations such as lead and mercury have also been studied, due to their deleterious effects on biological systems while  $\text{Cu}^{2+}$  can contaminate surrounding environment and is harmful to human health, which may lead to some metabolism disorders such as Wilson's disease and neurodegenerative disorders like Alzheimer's disease (Faller, 2012).

### **Antibacterial activity in coordination complexes**

For decades, great effort has been devoted to the study of coordination complexes and coordination polymers (CPs). Pharmaceutical scientists, biologists, medicinal and inorganic chemists have also been engaged in the research of coordination complexes for biomedical applications. These studies encompass other types of weak supramolecular interactions such as  $\pi$ - $\pi$  interactions, H-bonding and van der Waals force as well. The combination of weaker supramolecular interactions may also be used as a supramolecular chemistry approach for drug delivery in some specific cases (Ma *et al.*, 2011).

The mechanism in antimicrobial activity of the metal complexes and coordination polymer can be explained based on the basis the overtone's concept and chelation theory. According to the overtone concept of cell permeability, the lipid membrane that surrounds the cell favours the passage of only lipid-soluble materials in which liposolubility is an important factor that controls the antimicrobial activity. On chelation, polarity of the metal ion is reduced to a greater extent due the overlapping of the orbital from ligand and partial sharing of the positive charge of the metal ion with donor groups. This increases the delocalization of  $\pi$ -electrons, over the whole chelate ring and enhances the lipophilicity of complexes. This lipophilicity enhances the penetration of the complexes into the lipid membranes and blocks the metal binding sites in the enzymes of microorganisms. Furthermore, these coordination complexes annoy the respiration process of the cell and thus block the synthesis of proteins of cell, which restricts further growth of the organism (Sivakami *et al.*, 2014). In general, metal complexes are more active than ligands as they may serve as principal cytotoxic species in pharmaceutical industry as an antimicrobial agent, after testing its toxicity.

These above mentioned aspects interest me to initiate this research to synthesize and characterize supramolecular complexes and coordination polymer with O and N donor ligand and study their possible applications such as adsorption property, photocatalytic property, fluorescence sensing for metal ions property, and antibacterial activity.

### Literature reviews

Abbasi *et al.* (2016) studied the synthesis of 1D-[Zn(4,4'-bpy)(H<sub>2</sub>O)<sub>4</sub>](ADC)·4H<sub>2</sub>O (4,4'-bpy = 4,4'-bipyridine and H<sub>2</sub>ADC = acetylenedicarboxylic acid) with Zn(CH<sub>3</sub>COO)<sub>2</sub>·2H<sub>2</sub>O, 4,4'-bipyridine and acetylenedicarboxylic acid as starting materials. The obtained complex was characterized by Fourier-transformed infrared spectroscopy (FT-IR), single crystal x-ray diffraction (SCXRD), powder X-ray diffraction (PXRD), and thermogravimetric analysis (TGA). Single crystal X-ray diffraction analysis showed that coordination complex was one dimension polymer. The octahedral geometry Zn atom was coordinated by four oxygen atoms from water molecules and two nitrogen atoms from 4,4'-bpy while ADC<sup>2-</sup> was not coordinated to zinc atom as shown in **Figure 12**.

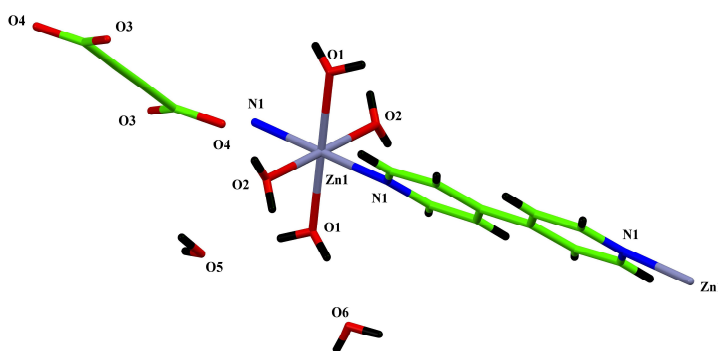


**Figure 12.** Molecular structure of [Zn(4,4'-bpy)(H<sub>2</sub>O)<sub>4</sub>](ADC)·4H<sub>2</sub>O. (Abbasi *et al.*, 2016)

In this study, [Zn(4,4'-bpy)(H<sub>2</sub>O)<sub>4</sub>](ADC)·4H<sub>2</sub>O was investigated in the color removal of Bismarck brown dye as dye pollutant in water (**Figure 13**).

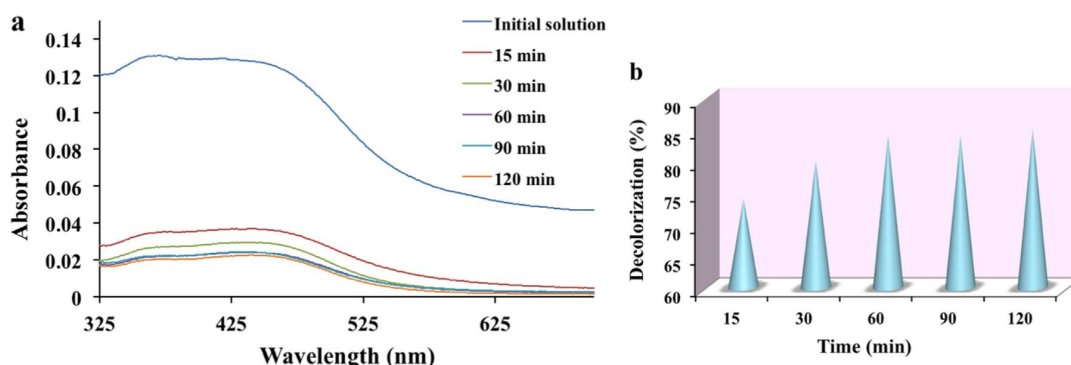


**Figure 13.** (a) The UV-vis spectra and (b) the decolorization efficiency of the Bismarck brown dye in the presence of complex. Reaction conditions: dye solution (100ml, 10ppm) and catalyst (110mg). (Abbasi *et al.*, 2016)

From the data, the obtained complex exhibited good catalytic activity and stability in the decolorization of Bismarck brown, color changed from brown to colorless after 120 min and could be easily recovered and reused for at least three cycles.

Xiao *et al.* (2015) reported the synthesis and characterization of  $[\text{Cu}(\text{bipy})(\text{SO}_4)]_n$  which the obtained complex was prepared by hydrothermal method at 110 °C for 24 h with  $\text{CuSO}_4$  and 4,4'-bipy as starting materials. The single crystal X-ray data indicated that the complex crystallized in hexagonal system space group  $P65(150)$ . The Cu atom was six-coordinated in an octahedral environment to the three oxygen atoms from three water molecules, one oxygen atom from sulfate ligand and two nitrogen atoms from 4,4'-bipy ligand. Bipy ligand acted as a bridging ligand which linked Cu atoms to form 1-D chain. Molecular structure of this complex is shown in **Figure 14**.

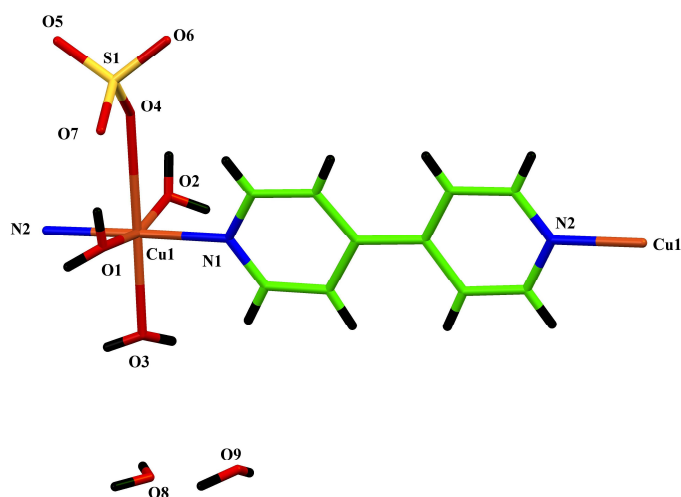


**Figure 14.** Molecular structure of  $[\text{Cu}(\text{bipy})(\text{SO}_4)]_n$ . (Xiao *et al.*,2015)

In addition,  $[\text{Cu}(\text{bipy})(\text{SO}_4)]_n$  was tested as an adsorbent for remove Congo red, Orange G, and X-3B (**Figure 15**).  $[\text{Cu}(\text{bipy})(\text{SO}_4)]_n$  showed great adsorption capacity for all dyes. The experimental value of maximal adsorption capacity for Congo red, Orange G, and X-3B were 2429 mg/g, 1333 mg/g, and 915 mg/g,

respectively, and color of complex changed from blue to the colors of the dyes. Basic isotherm models of Langmuir and Freundlich were used to fit the experimental data which the correlation coefficients of Langmuir isotherms for all dyes were much better than that of Freundlich isotherms for all dyes.

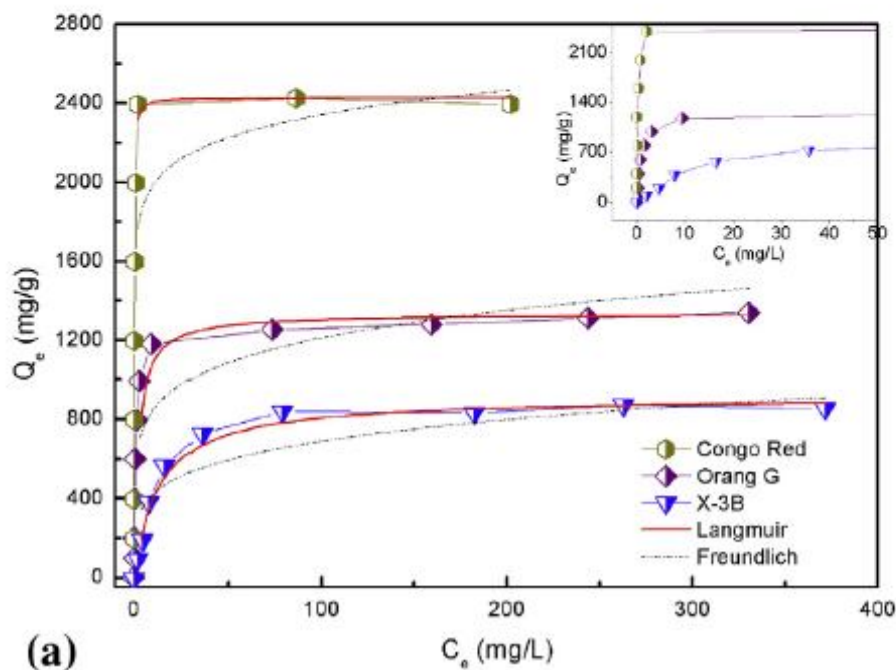


**Figure 15.** Adsorption isotherms of the Congo red, Orange G, and X-3B dyes on  $[\text{Cu}(\text{bipy})(\text{SO}_4)]_n$ . (Xiao *et al.*, 2015)

Xie *et al.* (2010) studied coordination polymers,  $[\text{M}(\text{C}_8\text{H}_{12}\text{O}_4)(\text{C}_{10}\text{H}_8\text{N}_2)] \cdot \text{H}_2\text{O}$  [ $\text{M}=\text{Co}$  (1),  $\text{Cd}$  (2);  $\text{C}_{10}\text{H}_8\text{N}_2 = 4,4\text{-bipyridine}$ ,  $\text{C}_8\text{H}_{14}\text{O}_4 = \text{subaric acid}$ ] obtained from the reaction between the metal salts [ $\text{Co}(\text{ac})_2 \cdot 4\text{H}_2\text{O}$  for complex (1) and  $\text{CdCO}_3 \cdot 4\text{H}_2\text{O}$  for complex (2)], bipy and subaric acid by hydrothermal method. The obtained complex was characterized by Fourier-transformed infrared spectroscopy (FT-IR), single crystal X-ray diffraction (SCXRD), powder X-ray diffraction (PXRD), and thermogravimetric analysis (TGA). Single crystal X-ray diffraction analysis showed that complex (1) Co atom was coordinated by four oxygen atoms from subarate ligand and two nitrogen atoms from 4,4'-bpy. Both subarate ligand and 4,4'-bpy acted as bridging ligand extending into a two-dimensional coordination polymer (**Figure 16**). In complex (2), Cd atom was coordinated by five oxygen atoms from subarate ligand and two nitrogen atoms from 4,4'-bpy forming a decahedral geometry. Subarate

ligand and 4,4'-bpy acted as bridging ligand extending into a two-dimensional coordination polymer (**Figure 17**).

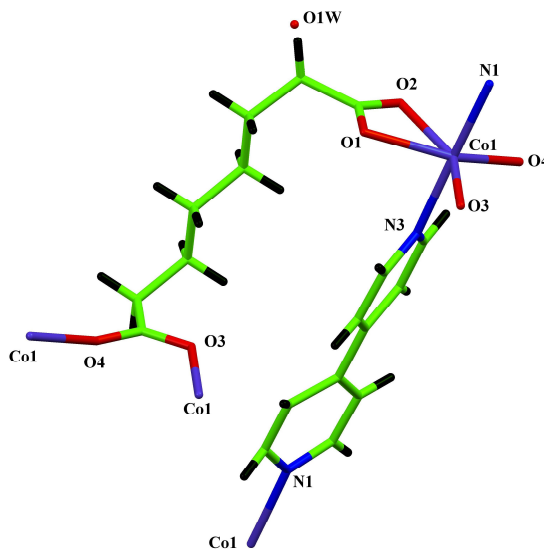


**Figure 16.** Molecular structure of  $[\text{Co}(\text{C}_8\text{H}_{12}\text{O}_4)(\text{C}_{10}\text{H}_8\text{N}_2)] \cdot \text{H}_2\text{O}$ .

(Xie *et al.*, 2010)

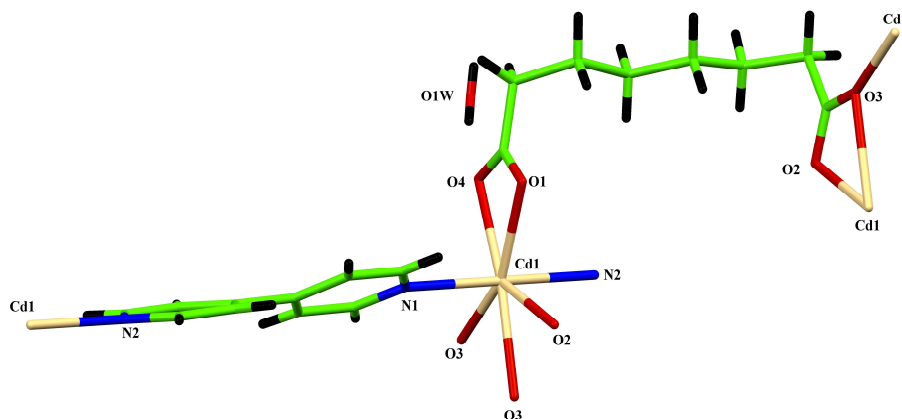


**Figure 17.** Molecular structure of  $[\text{Cd}(\text{C}_8\text{H}_{12}\text{O}_4)(\text{C}_{10}\text{H}_8\text{N}_2)] \cdot \text{H}_2\text{O}$ .

(Xie *et al.*, 2010)

Li *et al.* (2010) synthesized silver(I) sulfonate coordination polymers,  $[\text{Ag}_2\text{L}_1(\text{biim})_2] \cdot 2\text{H}_2\text{O}$  (1),  $\text{AgL}_2(\text{biim})$  (2),  $[\text{Ag}(\text{HL}_3)(\text{Pic})_2] \cdot \text{H}_2\text{O}$  (3), and  $[\text{Ag}_3(\text{L}_3)(\text{HL}_3)(4,4'\text{-bipy})_3(\text{H}_2\text{O})_2] \cdot 4\text{H}_2\text{O}$  (4) [ $\text{L}_1$  = 3-carboxy-4-hydroxybenzenesulfonate,  $\text{L}_2$  = *p*-aminobenzenesulfonate,  $\text{H}_2\text{L}_3$  = *p*-hydroxybenzenesulfonic acid,  $\text{biim}$  = 1,1'-(1,4-butanediyl)-bis(imidazole),  $\text{Pic}$  =  $\beta$ -

picoline, 4,4'-bipy = 4,4'-bipyridine]. For complexes (1) and (2), Ag atom coordinated with two nitrogen atoms from biim ligands to form a one-dimensional (1D) chain, and L<sub>1</sub> and L<sub>2</sub> sulfonate ligands acted as counter anion without coordinating to the silver atom. Complex (3) existed as a binuclear structure with the two silver cations connected by two HL<sub>3</sub> ligands. In complex (4), Ag(1) atom is four-coordinated by two nitrogen atoms from two 4,4'-bipy ligands, one oxygen atom from sulfonate of L<sub>3</sub> ligand and one oxygen atom from water molecule. Molecular structure of the complexes (1)-(4) are shown in **Figures 18-21**. In addition, complexes 1-3 displayed photoluminescent properties at room temperature (**Figure 22**).

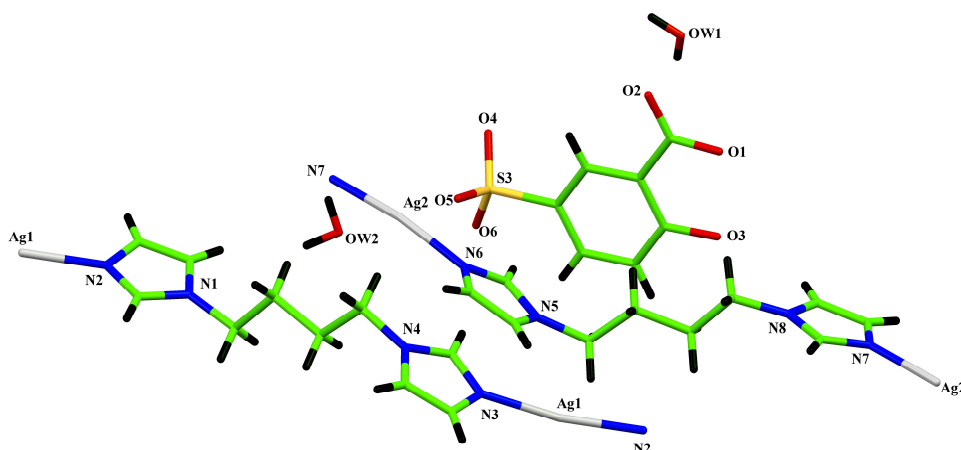


**Figure 18.** Molecular structure of  $[Ag_2L_1(biim)_2] \cdot 2H_2O$ . (Li *et al.*, 2010)

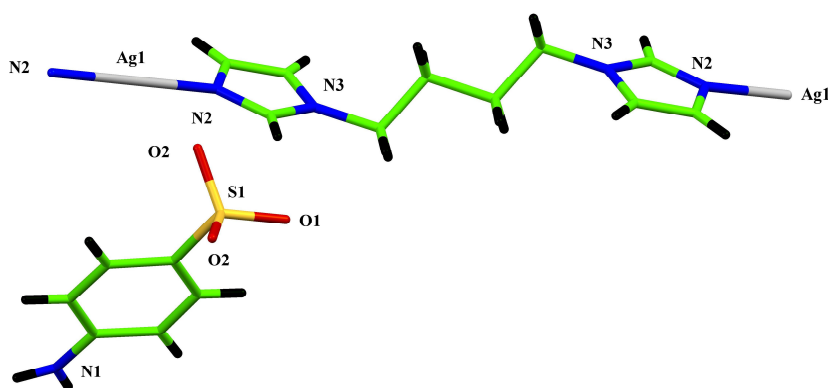


**Figure 19.** Molecular structure of  $AgL_2(biim)$ . (Li *et al.*, 2010)

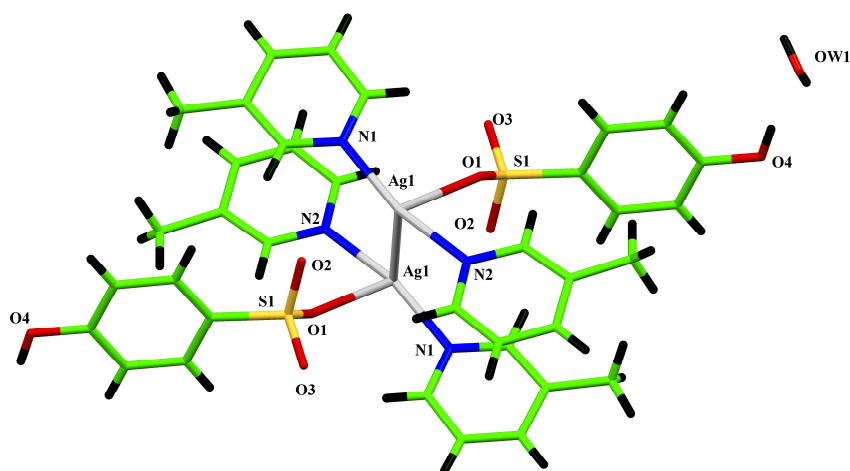


**Figure 20.** Molecular structure of  $[\text{Ag}(\text{HL}_3)(\text{Pic})_2] \cdot \text{H}_2\text{O}$ . (Li *et al.*, 2010)

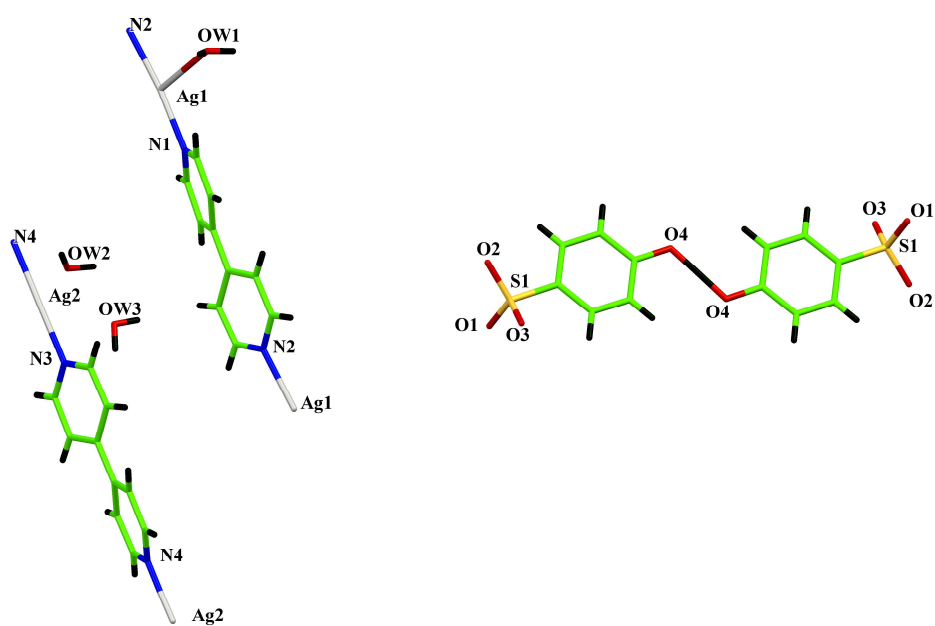


**Figure 21.** Molecular structure of  $[\text{Ag}_3(\text{L}_3)(\text{HL}_3)(4,4'\text{-bipy})_3(\text{H}_2\text{O})_2] \cdot 4\text{H}_2\text{O}$ .  
(Li *et al.*, 2010)



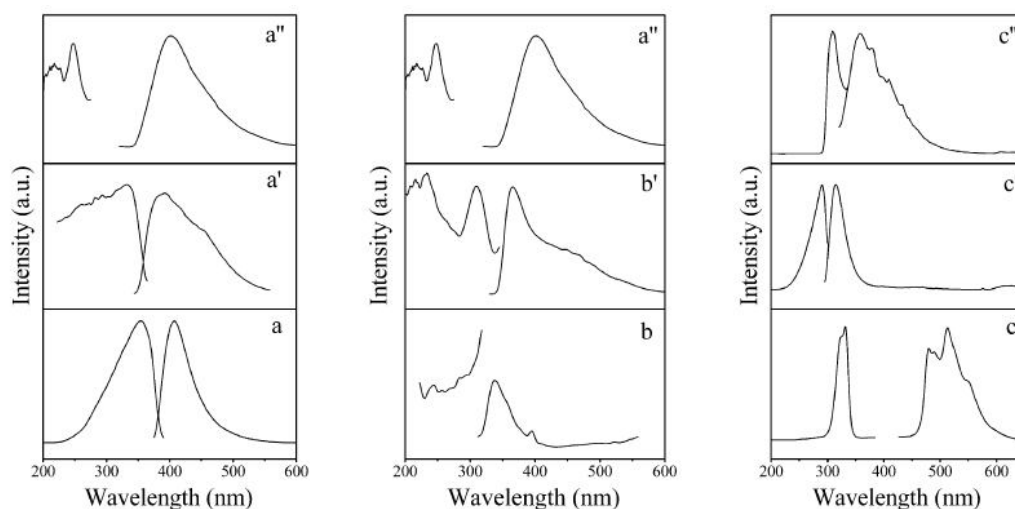


**Figure 22.** Solid-state photoluminescent spectra of **1** (a), **2** (b), and **3** (c) and free ligands [ $\text{H}_2\text{L1}$ (a'),  $\text{HL2}$ (b'),  $\text{H}_2\text{L3}$ (c'),  $\text{biim}$ (a''), and  $\text{Pic}$  (c'')] at room temperature. (Li *et al.*, 2010)

Liu *et al.* (2015) studied the synthesis of  $\{(\text{bmpp})[\text{Ag}_2\text{Br}_4]\}_n$  (**1**) and  $\{(\text{bmpp})[\text{Ag}_4\text{I}_6]\}_n$  (**2**) [ $\text{bmpp}$  = 1,3-bis(4-methylpyridine)]. All complexes were characterized by CHN analysis, IR, TGA, and X-ray crystallography. Complex (**1**) crystallized in orthorhombic system with space group  $\text{P2}_1\text{2}_1\text{2}$ . The coordination geometry around the Ag (I) ion was tetrahedral geometry by coordinating with 4 Br atoms (**Figure 23**). For complex (**2**) crystallized in monoclinic system with space group  $\text{C2/c}$ , the coordination geometry around the Ag(1) and Ag(2) ion are five-coordinated and three-coordinated, while Ag(3) was six-coordinated by I atoms (**Figure 24**). In this study the photocatalytic activity of two complexes were investigated. All complexes exhibited photocatalytic activity for methylene blue (MB) and Rhodamine B chloride (RhB) under UV irradiation of a 500 W high-pressure mercury lamp (**Figure 25**). The results indicated that MB decomposed by about 87% for complex (**1**) and 37% for complex (**2**) after magnetically stirring for 150 min and Rh B decomposed by about 90% for complex (**1**) and 53% for complex (**2**) after magnetically stirring for 150 min. The degradation rate of MB/RhB by complex (**1**) was higher than complex (**2**) which was explained based on the band gaps energy of complexes.

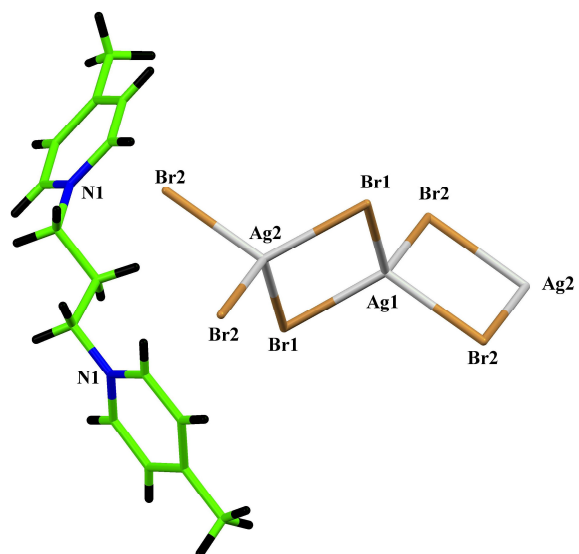


**Figure 23.** Molecular structure of  $\{(bmpp)[Ag_2Br_4]\}_n$ . (Liu *et al.*, 2015)

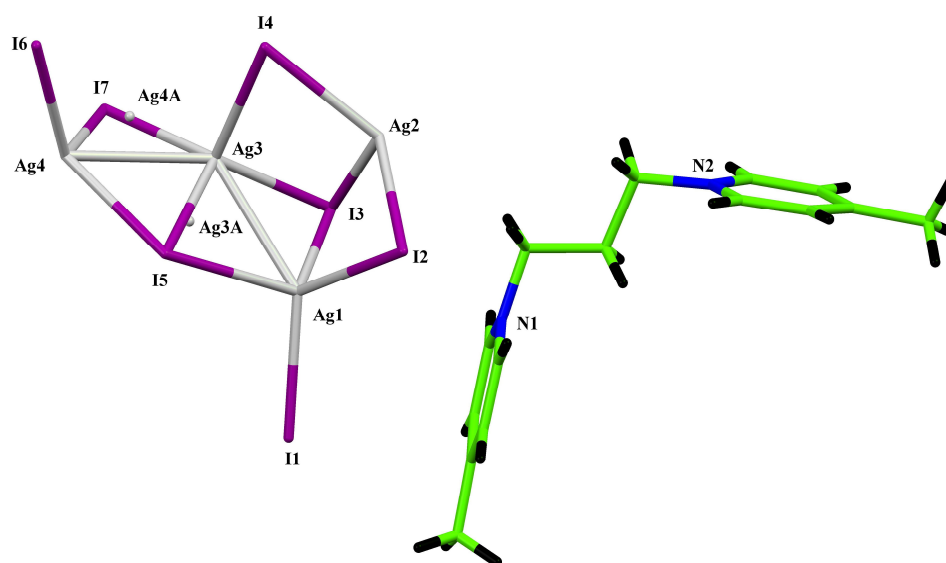


**Figure 24.** Molecular structure of  $\{(bmpp)[Ag_4I_6]\}_n$  (Liu *et al.*, 2015)

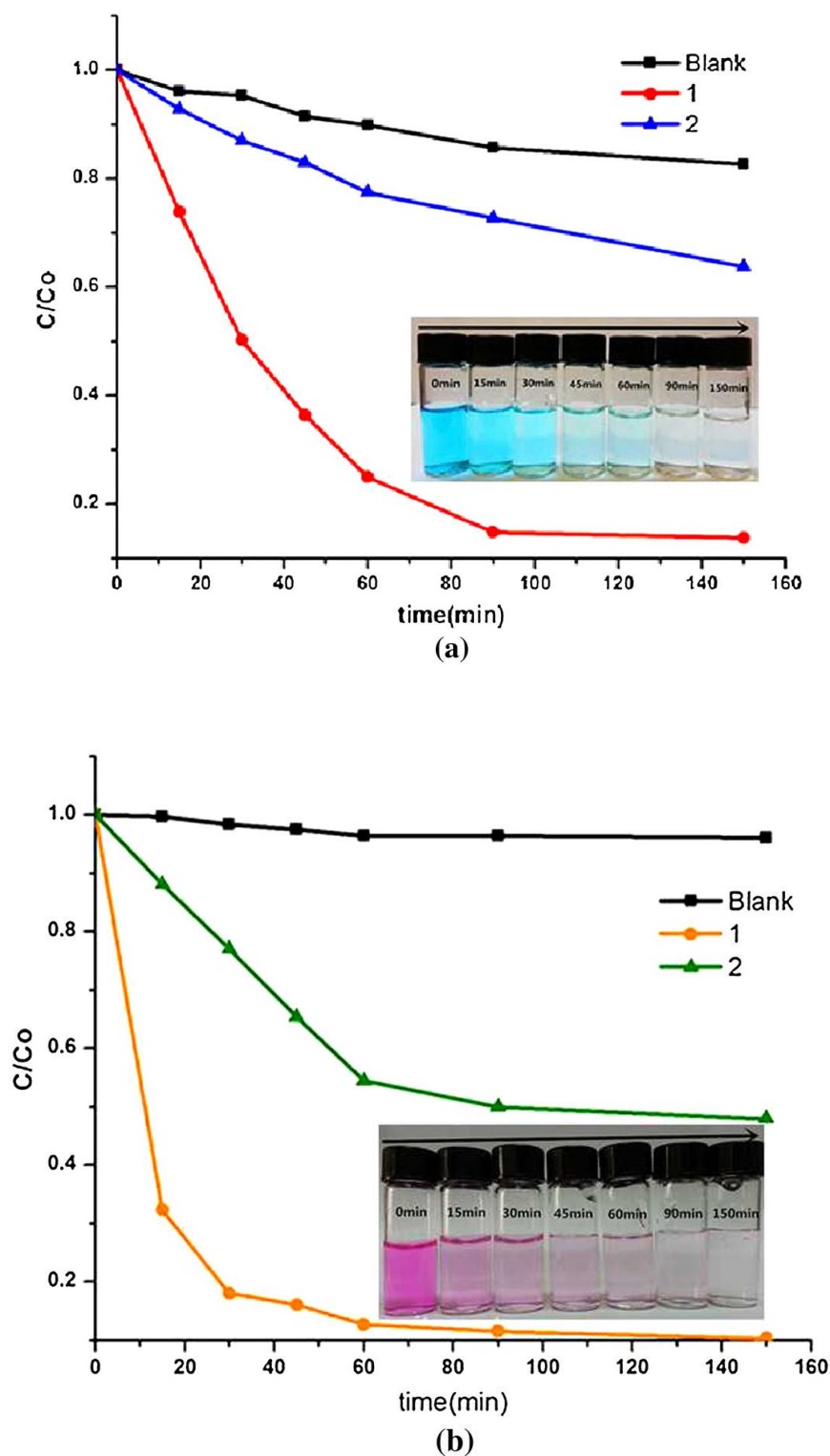


**Figure 25.** Photocatalytic decomposition of MB solution (a), RhB solution (b) under UV light irradiation with the use of complexes 1–2 and the control experiment without any catalyst under the same conditions. (Liu *et al.*, 2015)

Zhang *et al.* (2016) synthesized  $[\text{Ag}_4(\text{dpe})_4] \cdot (\text{btec})$  (1) and  $[\text{Ag}_4(\text{bpy})_4] \cdot (\text{btec}) \cdot 12\text{H}_2\text{O}$  (2) (dpe = 1,2-di(4-pyridyl)ethylene, bpy = 4,4'-bipyridine,  $\text{H}_4\text{btec}$  = 1,2,4,5-benzenetetracarboxylic acid) by slow evaporation at room temperature. The obtained complex was characterized by elemental analysis, single-crystal X-ray diffraction, FT-IR, UV-Vis, and luminescence spectroscopies. Single crystal X-ray diffraction analysis showed that complex (1) and complex (2) crystallized in triclinic system space group  $P\bar{1}$ . Molecular structure of complex (1) was one dimension polymer containing  $[\text{Ag}_4(\text{dpe})_4]$  chains with btec as counter-ions. The coordination geometry of Ag(I) atom was linear with Ag atom being coordinated by two nitrogen atoms from dpe ligands as shown in **Figure 26**. Molecular structure of complex (2) was one dimension polymer containing  $[\text{Ag}_4(\text{bpy})_4]$  chains, btec counter-ions, and twelve lattice water molecules. The coordination geometry around of Ag(I) atom was linear with Ag atom being coordinated by two nitrogen atoms from bpy ligands as shown in **Figure 27**.

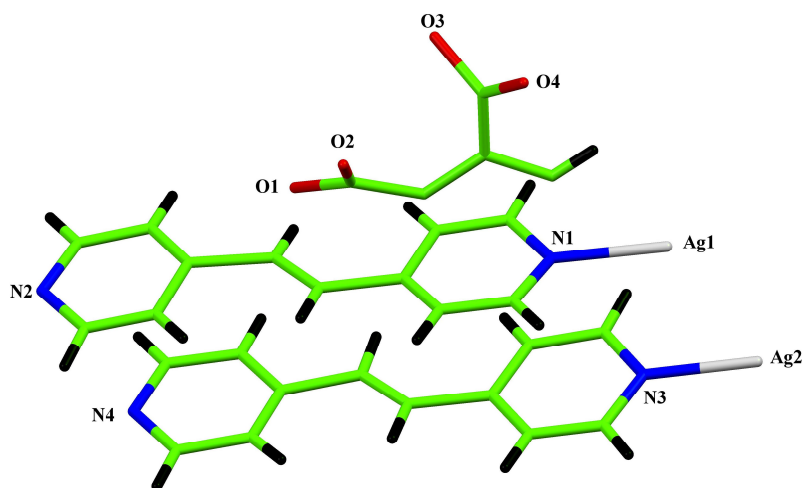


**Figure 26.** Molecular structure of  $[\text{Ag}_4(\text{dpe})_4] \cdot (\text{btec})$ . (Zhang *et al.*, 2016)

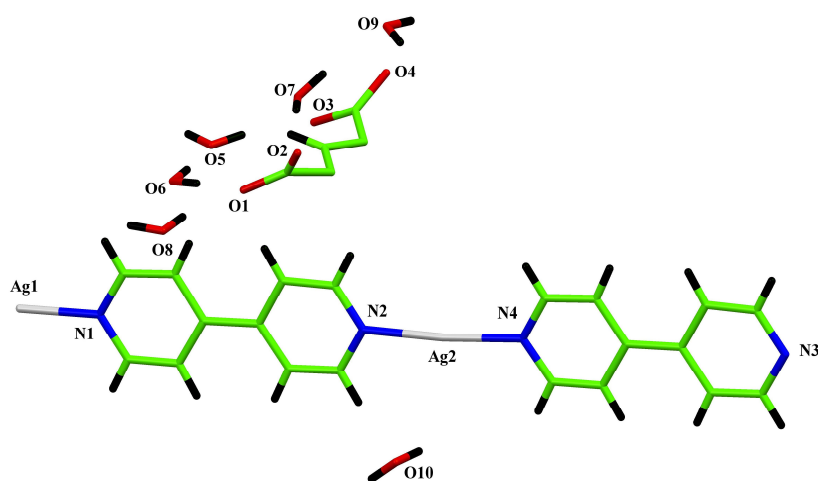


**Figure 27.** Molecular structure of  $[Ag_4(bpy)_4] \cdot (btec) \cdot 12H_2O$ . (Zhang *et al.*, 2016)

Furthermore, the two complexes showed photocatalytic activity for the degradation of methyl orange under Hg lamp irradiation for 120 min as shown in **Figure 28**. The results indicated that MO degradation proceeded by about 52.3% for complex (1) and 26.5% for complex (2) after magnetically stirring for 120 min.

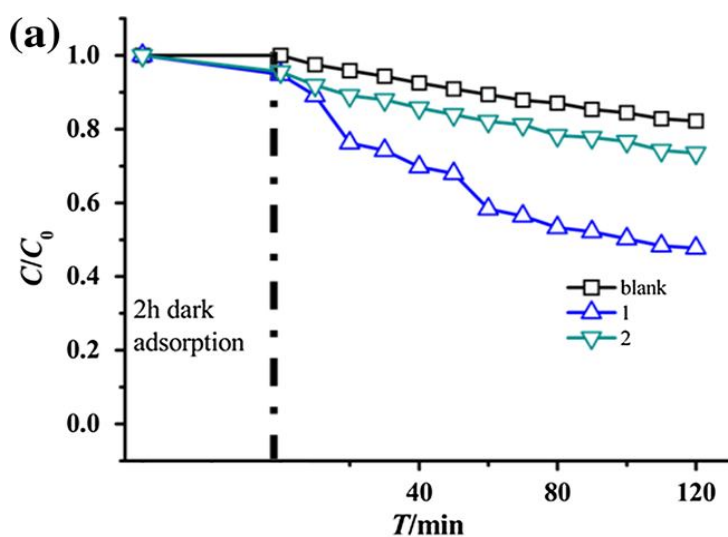


**Figure 28.** MO concentration versus irradiation time in the dark and under irradiation by Hg lamp in the presence of complexes 1 and 2. (Zhang *et al.*, 2016)

Huan *et al.* (2016) reported the synthesis and characterization of coordination polymers,  $\{\text{Co}(\text{btbb})_{0.5}(\text{ndc})(\text{H}_2\text{O})\}_n$  (1),  $\{[\text{Co}(\text{btbb})(\text{bpdc})]\cdot 1.5\text{H}_2\text{O}\}_n$  (2), and  $\{[\text{Co}(\text{btbp})_2(3\text{-npa})]\cdot 2\text{H}_2\text{O}\}_n$  (3) (btbb = 1,4-bis(thiabendazole)butane, btbp = 1,3-bis(thiabendazole)propane,  $\text{H}_2\text{ndc}$  = 2,6-naphthalenedicarboxylic acid,  $\text{H}_2\text{-bpdc}$  = 4,4'-biphenyldicarboxylic acid and 3- $\text{H}_2\text{npa}$  = 3-nitrophthalic acid) by hydrothermal methods. X-ray crystallographic data revealed that all complexes crystallized in the triclinic space group  $P\bar{1}$ . Molecular of complex (1) is shown in **Figure 29**. Co atom in complex (1) adopted a distorted octahedron coordination geometry provided with three oxygen atoms from two ndc ligands, one oxygen atom from coordinated water molecule, and two nitrogen atoms from one btbb ligand. For complex (2), the Co atom was six-coordinated binding to four nitrogen atoms from two btbb ligands and two oxygen atoms (**Figure 30**). Complex (3), Co center was in an octahedral geometry, with four-coordinated by two oxygen atoms from 3-npa ligand and and four nitrogen atoms from btbp ligand (**Figure 31**).

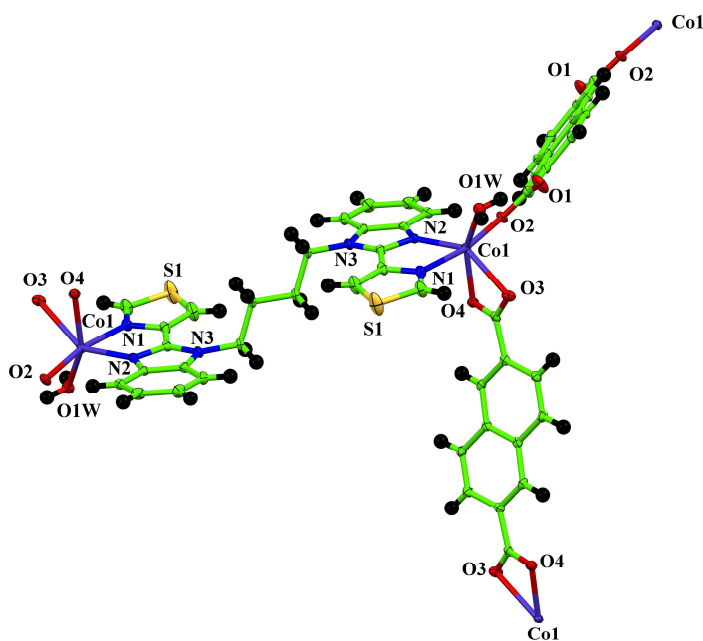


**Figure 29.** Molecular structure of  $\{\text{Co}(\text{btbb})_{0.5}(\text{ndc})(\text{H}_2\text{O})\}_n$ . (Huan *et al.*, 2016)

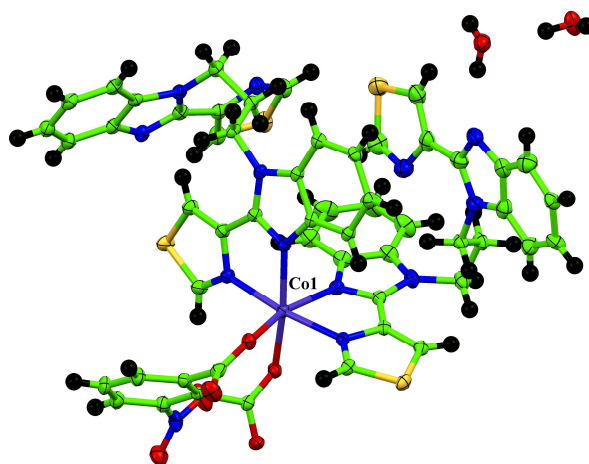


**Figure 30.** Molecular structure of  $\{[\text{Co}(\text{btbp})_2(3\text{-npa})]\cdot 2\text{H}_2\text{O}\}_n$ . (Huan *et al.*, 2016)

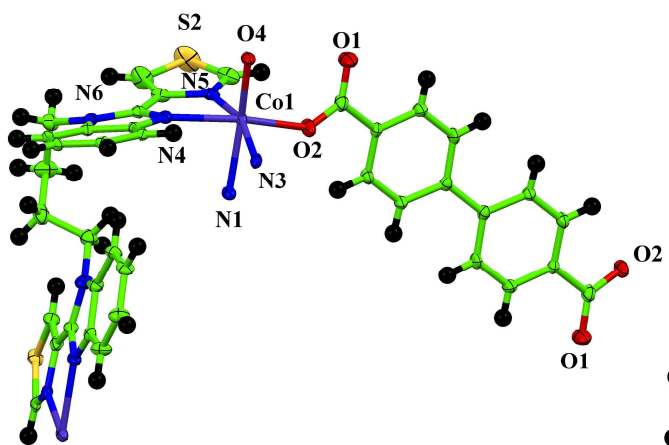


**Figure 31.** Molecular structure of  $\{[\text{Co}(\text{btbb})(\text{bpdc})]\cdot 1.5\text{H}_2\text{O}\}_n$ . (Huan *et al.*, 2016)

Furthermore, photocatalytic properties of all complexes were studied for degradation of methyl orange dye in the presence of  $\text{H}_2\text{O}_2$  as oxidant under simulated natural sunlight (**Figures 32 - 33**). The degradation efficiency of control (without catalyst) was about 14.9 % while in the presence of each catalyst was 98.5 % for complex (1), 93.3 % for complex (2), and 75.3 % for complex (3), after 120 min of irradiation.

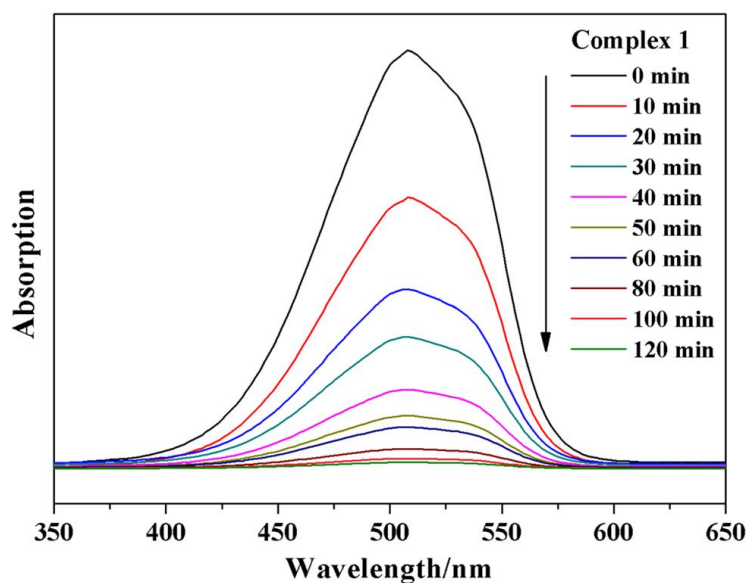


**Figure 32.** Absorption spectra of the MO solution during decomposition reaction under simulated natural sunlight irradiation in the presence of complex 1.

(Huan *et al.*, 2016)

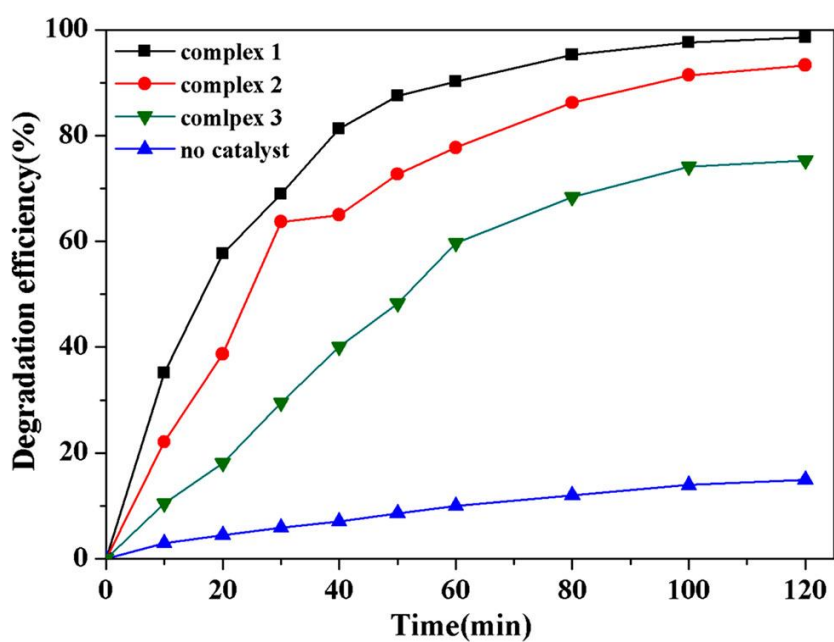


**Figure 33.** Decomposition of MO solution in a photocatalytic process.

(Huan *et al.*, 2016)

Ye *et al.* (2016) reported the synthesis of  $[\text{Zn}(\text{PAM})(\text{en})]$  (1) (PAM = 4,4'-methylene bis(3-hydroxy-2-naphthalenecarboxylate), en = 1,2-ethanediamine) by



hydrothermal condition, at 160 °C for 72 h. The obtained complex was characterized by Fourier-transformed infrared spectroscopy (FT-IR), single crystal x-ray diffraction (SCXRD), elemental analysis, and thermogravimetric analysis (TGA). Single-crystal X-ray diffraction showed that the obtained complex crystallized in triclinic space group P-1. Zn atom was coordinated by two oxygen atom from PAM ligands and two nitrogen atoms of en ligand forming  $ZnO_2N_2$  distorted tetrahedral. Complex (1) in dimethylsulfoxide solution showed fluorescent emission peak about 503 nm upon excitation at 371 nm which could be assigned to aromatic rings  $\pi-\pi^*$  transition. The strong emission of complex (1) was quenched efficiently by adding 2,4,6-trinitrophenol (TNP) for detecting trace quantity of nitroaromatic explosives compounds such as 4-nitrophenol, 2,6-dinitrotoluene, 2,4-dinitrotoluene, nitrobenzene, 1,3-dinitrobenzene, hydroquinone, dimethylbenzene, and bromobenzene (**Figure 34**).

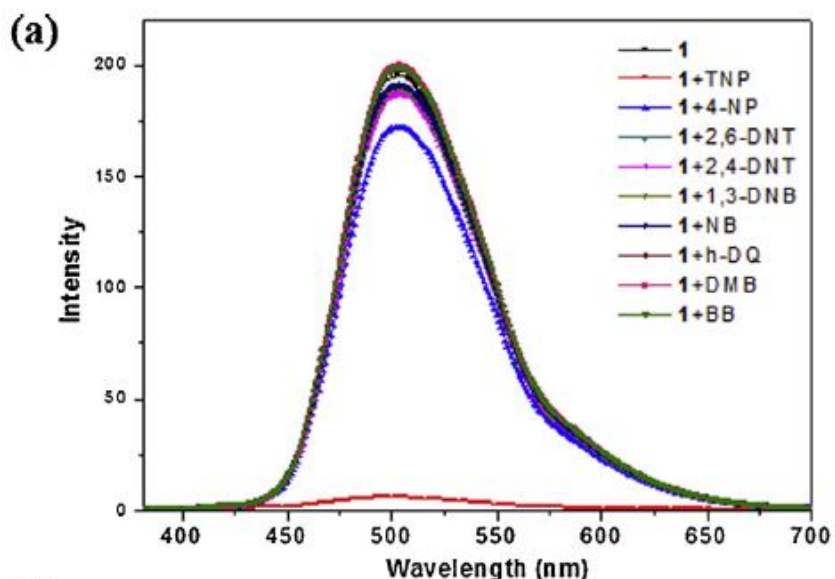


**Figure 34.** The fluorescence emission spectra of 1 in the DMSO in the presence of various contents of analytes ( $\lambda_{ex} = 371$  nm). (Ye *et al.*, 2016)

Wang *et al.* (2014) reported the synthesis and characterization of  $[M(H_2TTTA)_2(4,4'-bpy)_2]$  [ $M = Co$  for complex(1),  $Ni$  for complex(2),  $Mn$  for complex(3),  $Cd$  for complex(4), and  $Cu$  for complex(5)] ( $H_3TTTA = 2,2', 2''$ -[1,3,5-triazine-2,4,6-triyltris(thio)]tris-acetic acid,  $4,4'$ -bpy = 4,4'-dipyridine) by

hydrothermal condition. Single-crystal X-ray data of complexes (1) – (5) revealed that all complexes were isostructural. The geometry around metal atom of all complexes were disordered octahedral formed by the coordinated two nitrogen atoms from the 4,4'-bpy ligands in axial positions and the equatorial positions are occupied by four oxygen atoms from the H<sub>2</sub>TTTA ligands (**Figure 35**).

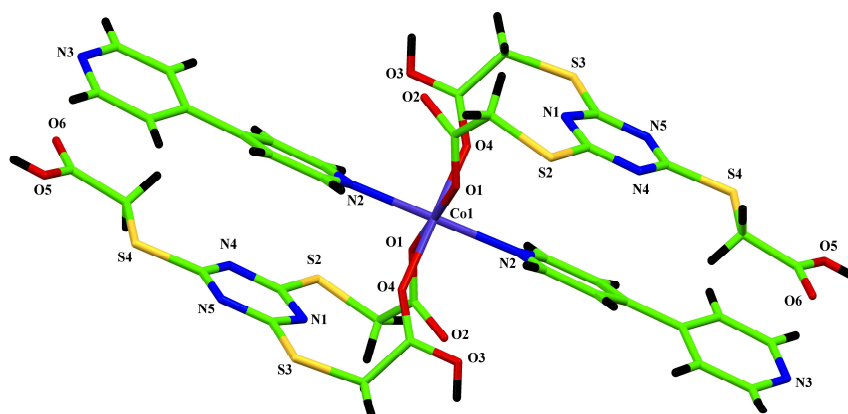


**Figure 35.** Molecular structure of [Co(H<sub>2</sub>TTTA)<sub>2</sub>(4,4'-bpy)<sub>2</sub>]. (Wang *et al.*, 2014)

Photoluminescence properties of the H<sub>3</sub>TTTA ligand and all complexes are shown in **Figure 36**. From the data, the Cd complex showed a stronger emission spectrum than the other complexes.

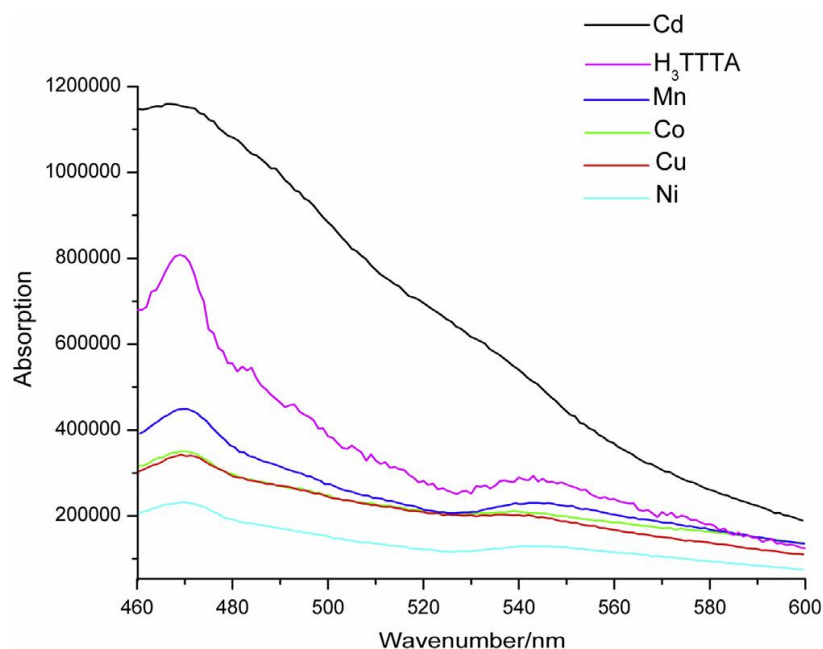


**Figure 36.** Solid state photoluminescence properties of the free H<sub>3</sub>TTTA ligand and all complexes. (Wang *et al.*, 2014)

Furthermore, all complexes were also been tested of catalytic properties in cyanosilylation of benzaldehyde and acetophenone at room temperature (Table 2). The data indicated that all complexes showed good catalytic activities for the cyanosilylation of benzaldehyde. However, a catalytic property of complex (3) was higher than the other complexes due to the stronger lewis acidity of complex (3).

**Table 2.** The catalytic activity for complexes 1-5 in the cyanosilylation of benzaldehyde and acetophenone with 3 h of reaction time. (Wang *et al.*, 2014)

Cyanosilylation	Entry	complex	Yield(%) <sup>a</sup>	TOF (h <sup>-1</sup> ) <sup>b</sup>
Benzaldehyde	1	1	93.3	12.6
	2	2	79.8	10.6
	3	3	98	13.1
	4	4	89.6	11.9
	5	5	94.5	12.6
Acetophenone	6	1	7.6	1.0
	7	2	5.7	0.8
	8	3	69.6	9.3
	9	4	2.8	0.4
	10	5	2.6	0.3

<sup>a</sup> Yield determination by GC-MS.

<sup>b</sup> TOF = (Yield)/(mol%cat)/t

Wang *et al.* (2016) reported new metal coordination complexes, namely [Co(BPY)<sub>2</sub>(H<sub>2</sub>O)<sub>2</sub>](BPY)(BS)<sub>2</sub>(H<sub>2</sub>O)<sub>4</sub> (1), [Co(BPY)<sub>2</sub>(H<sub>2</sub>O)<sub>4</sub>](ABS)<sub>2</sub>(H<sub>2</sub>O)<sub>2</sub> (2) and [Co(BPY)(H<sub>2</sub>O)<sub>4</sub>](MBS)<sub>2</sub> (3) (BPY = 4,4'-bipyridine, BS = phenylsulfonic acid, ABS = *p*-aminobenzenesulfonic acid, MBS = *p*-methylbenzenesulfonic acid). Complexes (1) – (3) were characterized by single-crystal X-ray diffraction and infrared spectroscopy. Single-crystal X-ray diffraction showed that the obtained complex crystallized in monoclinic system. For complex (1), a two-dimensional (2D) polymeric structure, the coordination geometry around Co atom was a distorted octahedral environment by coordination with four nitrogen atoms from BPY ligands and two oxygen atoms from water molecules as shown in **Figure 37**. Both complexes (2) and (3) were a one-dimensional (1D) chain structure with a distorted octahedral

environment around Co atom, coordinated by two nitrogen atoms from BPY ligands and four oxygen atoms from water molecules as shown in **Figures 38 - 39**.

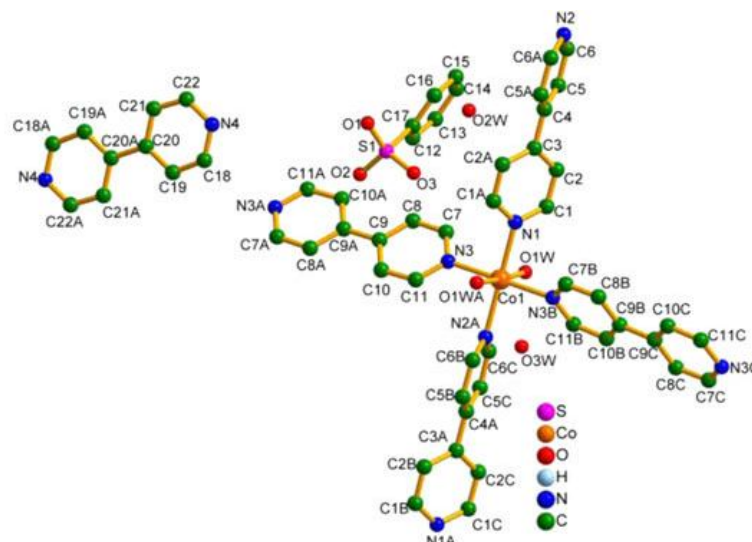


**Figure 37.** Molecular structure of  $[\text{Co}(\text{BPY})_2(\text{H}_2\text{O})_2](\text{BPY})(\text{BS})_2(\text{H}_2\text{O})_4$ .  
(Wang *et al.*, 2016)

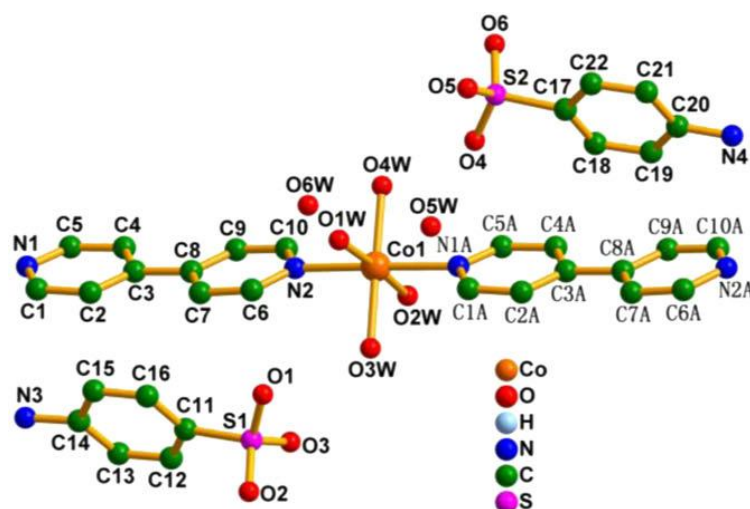


**Figure 38.** Molecular structure of  $[\text{Co}(\text{BPY})_2(\text{H}_2\text{O})_4](\text{ABS})_2(\text{H}_2\text{O})_2$   
(Wang *et al.*, 2016)

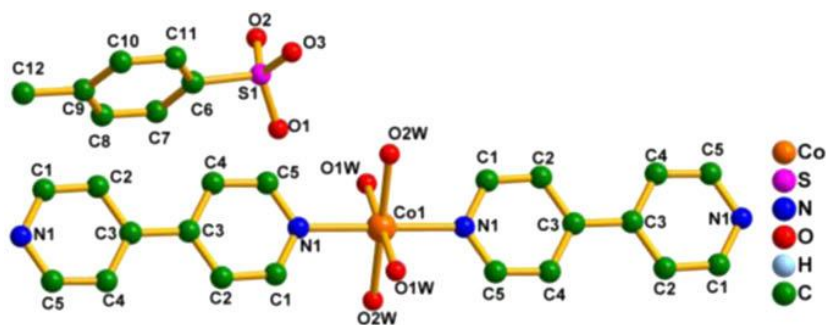


**Figure 39.** Molecular structure of  $[\text{Co}(\text{BPY})(\text{H}_2\text{O})_4](\text{MBS})_2$ . (Wang *et al.*, 2016)

All complexes were used as catalysts in synthesis of 3,4-dihydropyrimidin-2(1H)-ones under solvent-free conditions by Biginelli reactions. Catalysts 1–3 showed good efficiency for the desired product and the catalytic efficiency was in the order:  $2 > 1 \approx 3$ , which could be ascribed to the hydrophobic interactions of different phenylsulfonate groups.

Wang *et al.* (2015) synthesized  $\{[\text{Cu}_3(\text{btb})_3(\text{nbta})_2] \cdot (\text{H}_2\text{O})_2\}_n$  (btb = 4,4'-bis(1,2,4-triazolyl-1-yl)-biphenyl,  $\text{H}_3\text{nbta}$  = 5-nitro-1,2,3-benzenetricarboxylic acid) under hydrothermal condition. This complex has been characterized by IR, elemental analysis, thermogravimetric, fluorescence properties and single-crystal X-ray diffraction. The X-ray analyses revealed that the complex was a 3D framework and crystallized in triclinic, space group  $P\bar{1}$ . The coordination geometry was distorted square pyramidal for Cu1, coordinated by two nitrogen atoms of btb ligands and three oxygen atoms from btb ligand while Cu2 was distorted octahedral geometry, coordinated by four oxygen atoms from btb ligand, two nitrogen atoms of btb ligands (**Figure 40**). The complex displayed the emission band at 373 nm ( $\lambda_{\text{ex}} = 290$  nm) which was a blue-shift compared with free btb ligand due to increasing the ligand conformational rigidity (**Figure 41**).

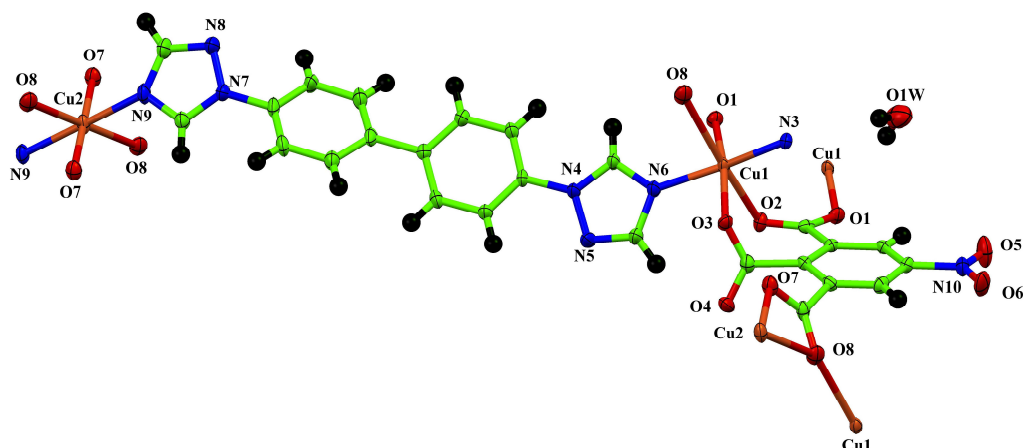


**Figure 40.** Molecular structure of  $\{[Cu_3(btb)_3(nbta)_2] \cdot (H_2O)_2\}_n$ . (Wang *et al.*, 2015)

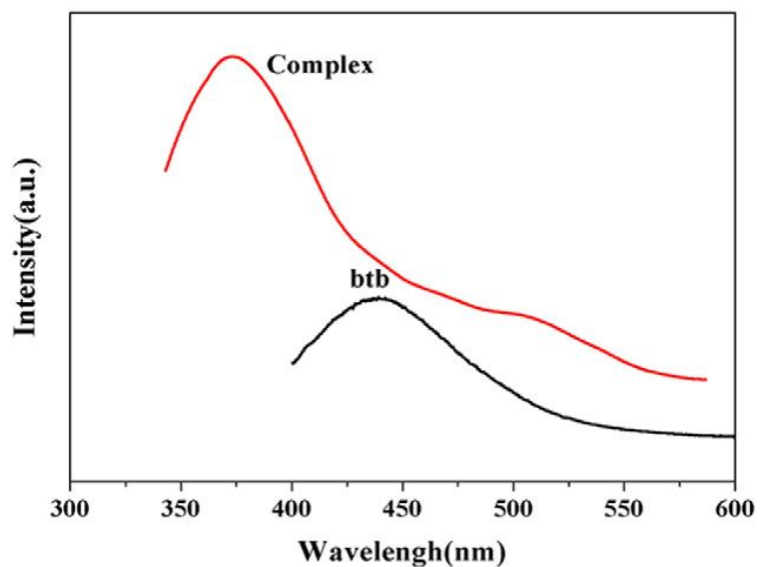


**Figure 41.** Solid-state fluorescence spectra of free btb and the complex.  
(Wang *et al.*, 2015)

Moreover, the complex showed high adsorption capacities for azo dye, congo red which the adsorbate congo red keeps increasing versus time (**Figure 42**). The maximum adsorption capacities of the Cu complex was 656 mg/g when  $C_0$  being 200 mg/L. The attractive forces between complex and congo red dye was described as a  $\pi$ - $\pi$  stacking interaction.

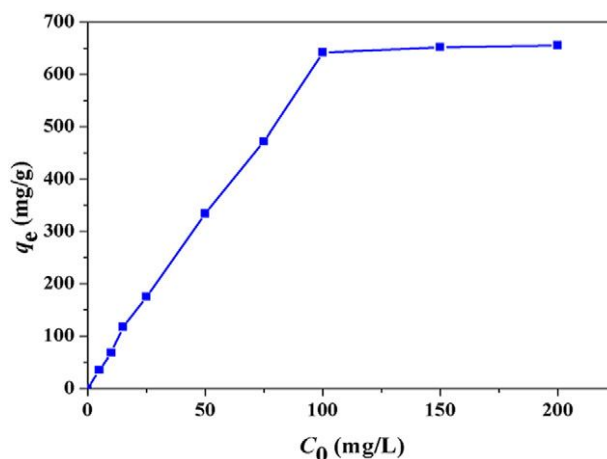


**Figure 42.** Adsorption result of congo red over the complex. (Wang *et al.*, 2015)

Xiao *et al.*, (2013) studied the synthesis of  $[\text{Co}(\text{L}_1)(\text{tp})]_n$  (1) and  $[\text{Co}(\text{L}_2)(\text{Htp})(\text{tp})_{0.5}]_n$  (2) ( $\text{L}_1 = 1,3\text{-bis}(5,6\text{-dimethylbenzimidazole})\text{propane}$ ;  $\text{L}_2 = 1,2\text{-bis}(5,6\text{-dimethylbenzimidazole-1-ylmethyl})\text{benzene}$ ;  $\text{tp} = \text{terephthalate}$ ) by hydrothermal method at  $140^\circ\text{C}$  for 3 days. Two complexes were characterized by SCXRD, TGA, IR, elemental analysis, and fluorescence properties. The Co atom of complex (1) was in a tetrahedral environment formed by two oxygen atoms from tp ligands and two nitrogen atoms from L1 ligand. For complex (2) Co atom was surrounded by two nitrogen atoms from L2 ligand and three oxygen atoms from tp ligand forming to a distorted trigonal bipyramidal geometry (**Figure 43**).

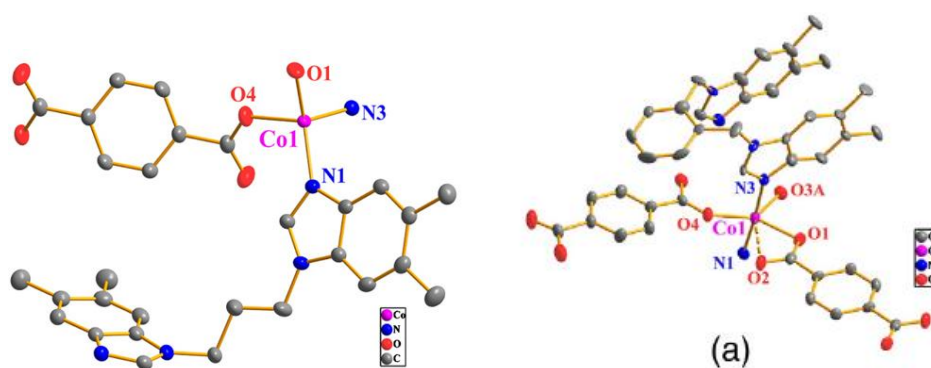


**Figure 43.** Molecular structure of  $[\text{Co}(\text{L}_1)(\text{tp})]_n$ (1) and  $[\text{Co}(\text{L}_2)(\text{Htp})(\text{tp})_{0.5}]_n$ (2). (Xiao *et al.*, 2013)

The emission spectra of complex (1) and (2) are shown in **Figure 44**, complex 1 exhibited weak emissions at 383 nm ( $\lambda_{\text{ex}} = 285$  nm) and at 390 nm ( $\lambda_{\text{ex}} = 305$  nm) for 2 while L1 showed maximum emission peak at 367 nm ( $\lambda_{\text{ex}} = 312$  nm) and at 346 nm ( $\lambda_{\text{ex}} = 300$  nm) for L(2). The emission band of all complexes assigned to  $\pi-\pi^*$  transition of coordinated N-containing ligands.

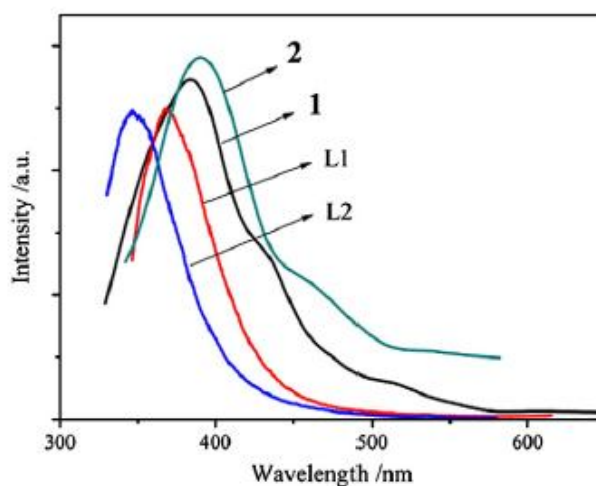


**Figure 44.** Emission spectra of complexes 1, 2 and free ligands in the solid state at room temperature. (Xiao *et al.*, 2013)

In addition, they found that both complexes could be used as adsorbents for congo red dye removal (**Figure 45**). The maximum adsorption capacities when  $C_0$  being 200 mg/L were 952.3 and 653.8 mg/g for 1 and 2, respectively.

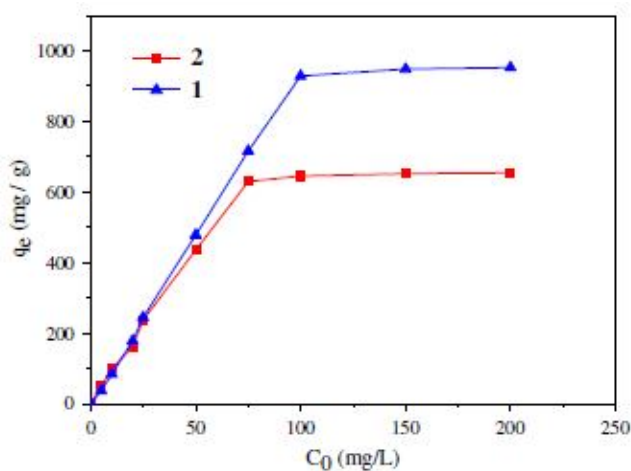


**Figure 45.** Adsorption results of congo red over complexes 1 and 2. (Xiao *et al.*, 2013)



Zhao *et al.* (2011) synthesized coordination polymer,  $\text{Mn}_3(\text{btdc})_3(\text{DMF})_4$  (1),  $\text{Co}(\text{btdc})(\text{DMF})_3$  (2),  $\text{Zn}(\text{btdc})(\text{DMF})_3$  (3), and  $\text{Zn}(\text{btdc})(4,4'\text{-bpy})_{0.5}$  (4), where  $\text{H}_2\text{btdc}$  = 2,2'-bithiophene-5,5'-dicarboxylic acid, DMF = N,N'-dimethylformamide, and 4,4'-bpy = 4,4'-bipyridine by hydrothermal method. All complexes were characterized by SCXRD, TGA, FT-IR, CHN analysis, and fluorescence property. X-ray analysis revealed that all complex crystallized in monoclinic system space group C 2/c for complex (1) and (4) and  $\text{P}2_1/\text{c}$  for complex (2) and (3). Molecular structure of all complexes are shown in **Figures 46-49**. In complex (1) each Mn ion was six-coordinate by bonding to six oxygen atoms from btdc ligand forming to distorted octahedral geometry. Complex (2) and complex (3) were isostructural with metal ion coordinated to two oxygen atoms from DMF ligand and three oxygen atoms from btdc ligand. Complex (4) had each zinc ion in square-pyramidally coordinated by four carboxylate oxygen atoms from btdc ligand at the equatorial positions and one nitrogen atom of 4,4'-bpy at the axial position. The luminescent properties of all complexes were investigated at room temperature in the solid state (**Figure 50**). Strong emission spectra of complexes (3) and (4) were observed at wavelengths about 490 nm ( $\lambda_{\text{ex}} = 420$  nm).

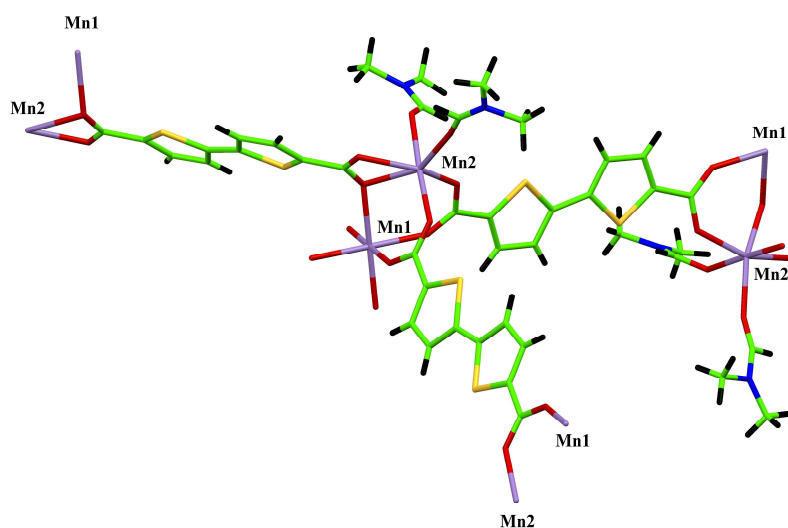


**Figure 46.** Molecular structure of  $\text{Mn}_3(\text{btdc})_3(\text{DMF})_4$ . (Zhao *et al.*, 2011)

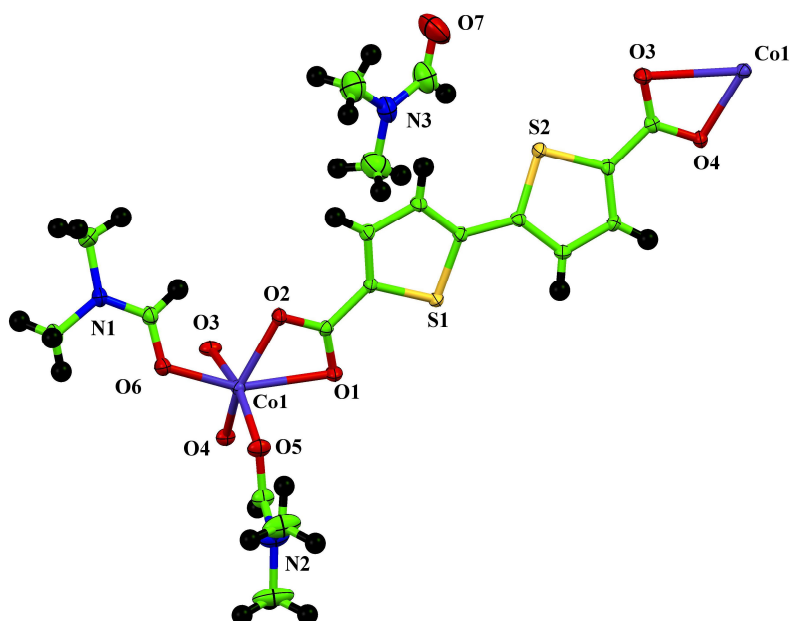


**Figure 47.** Molecular structure of  $\text{Co}(\text{btcd})(\text{DMF})_3$  (Zhao *et al.*, 2011)

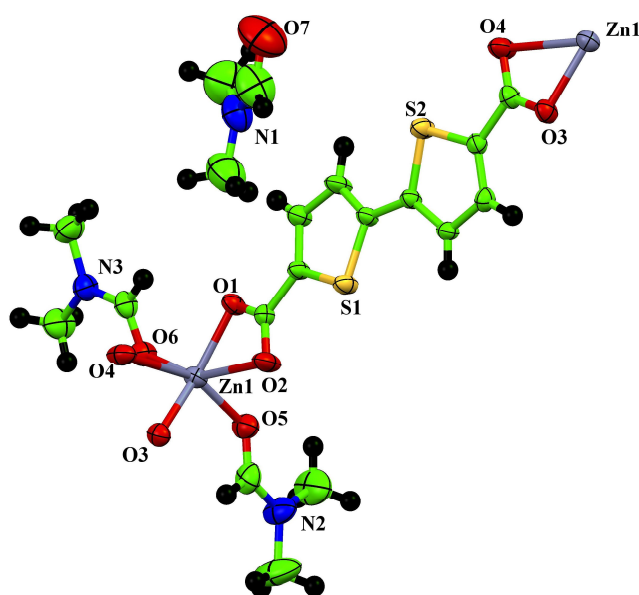


**Figure 48.** Molecular structure of  $\text{Zn}(\text{btcd})(\text{DMF})_3$ . (Zhao *et al.*, 2011)

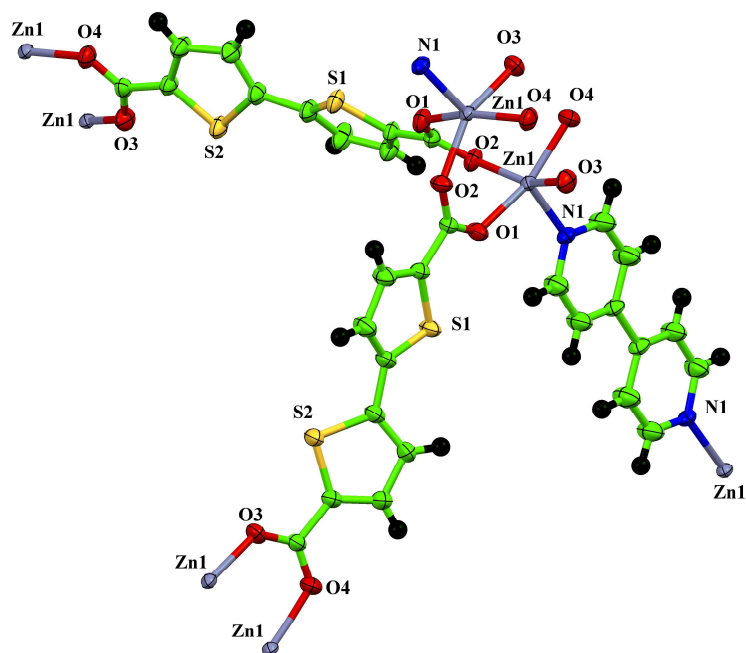


**Figure 49.** Molecular structure of  $\text{Zn}(\text{btdc})(4,4'\text{-bpy})_{0.5}$ . (Zhao *et al.*, 2011)

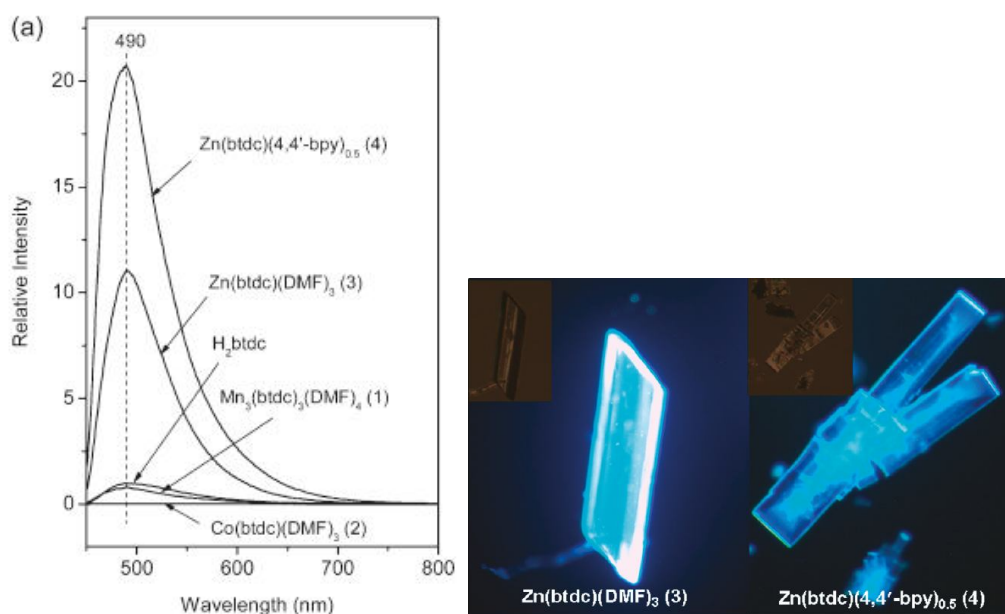


**Figure 50.** (a) Fluorescent emission spectra of the  $\text{H}_2\text{btdc}$  ligand and crystals 1-4 in the solid state at room temperature and fluorescent images of complexes 3 and 4. (Zhao *et al.*, 2011)

## Dye

In recent years organic dyes have been widely used in textile, plastics, printing, cosmetic and food industries and have become a source of wastewaters. Most of dyes cause to be toxic mutagenic, and carcinogenic on humans (Sachin *et al.*, 2011).

### Methylene blue

Methylene blue (MB) or methylothioninium chloride is an aromatic heterocyclic compound with the formula  $C_{16}H_{18}N_3SCl$ . It is used in biology (as bacteriologic stain) and chemistry (indicator).

At room temperature, methylene blue appears as dark green powder, when this compound dissolved in water or alcohol it appears as blue solution. In solution, it breaks up to the positive ion (methylene blue) and the negative ion (chloride).

In addition, MB is one of the high consuming materials in dyeing cottons. MB is a cationic basic thiazine dye. The maximum absorbance of MB dye is found about 664 nm. MB can cause health problems (nausea, increased heart rate, cyanosis, jaundice and necrosis) in humans after respiration (Shahryari *et al.*, 2010).

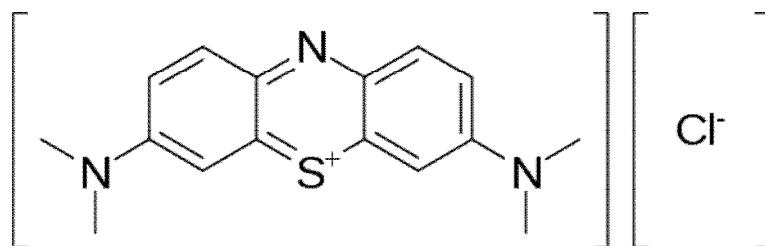


**Figure 51.** Molecular structure of methylene blue. (Adriana *et al.*, 2010)

### Rhodamine B (RhB)

Rhodamine B, (IUPAC Name [9-(2-carboxyphenyl)-6-diethylamino-3-xanthenylidene]-diethylammonium chloride) is a cationic dye with the formula  $C_{28}H_{31}N_2O_3Cl$ , MW 479.02  $gmol^{-1}$ . Molecular structure of Rhodamine B is illustrated in **Figure 52**. The maximum absorbance of RhB dye is found at 554 nm. RhB is a highly toxic dye which it is used in industries such as paper printing, food stuff and textile. RhB is highly carcinogenic, and cause irritation, redness and pain in eyes and

skin. When gets into the body by inhalation or eating, it may cause irritation in respiratory tract and gastrointestinal tract. (Khan *et al.*, 2011)

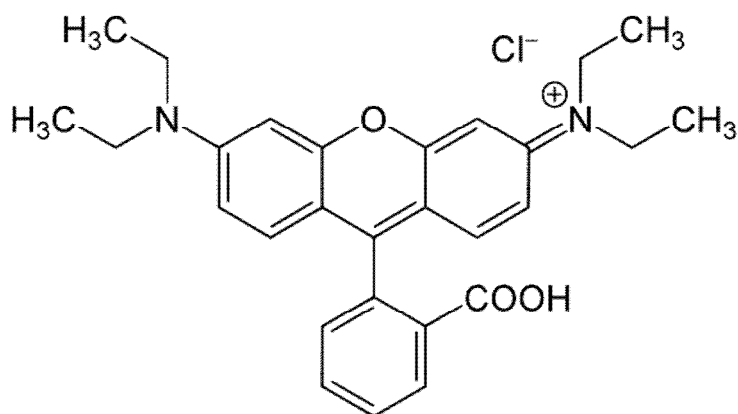


**Figure 52.** Molecular structure of Rhodamine B. (Mahasin *et al.*, 2011)

### Orange G

Orange G (OG) or Acid Orange 10 [IUPAC 7-Hydroxy-8-(phenylazo)-1,3-naphthalenedisulfonic acid disodium salt] is an anionic dye with the formula  $C_{16}H_{10}N_2Na_2O_7S_2$ , MW  $452.38 \text{ gmol}^{-1}$ . Molecular structure of OG is illustrated in **Figure 53**. The maximum absorbance of OG dye is found at 490 nm. OG is used mostly in dyeing the textile fabrics industry. OG can be carcinogenic and toxic for human.

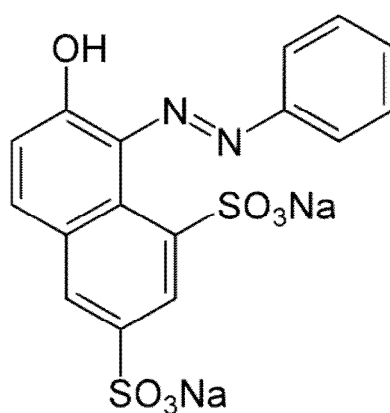
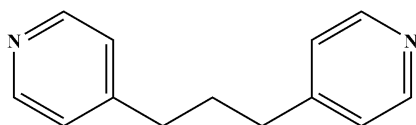


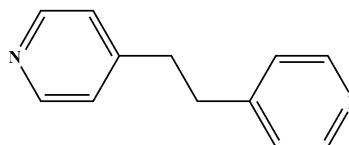
**Figure 53.** Molecular structure of Orange G. (Chenini *et al.*, 2011)

### Ligands used in this thesis.

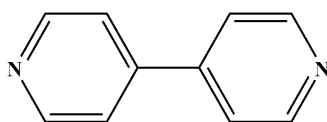
In this work, the researcher used N- and O-donor ligands for the syntheses of various complexes. Molecular structures of all ligands are illustrated in **Figure 54**.



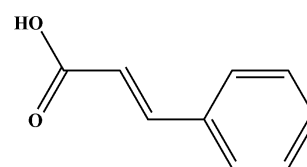
1,3-bis(4-pyridyl)propane



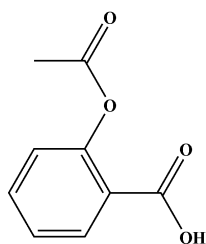
1,2-bis(4-pyridyl)ethane



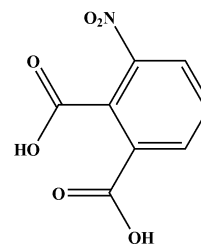
4,4'-bipyridine



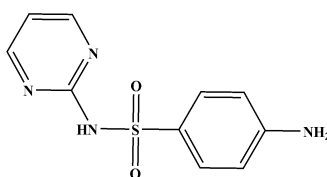
Cinnamic acid



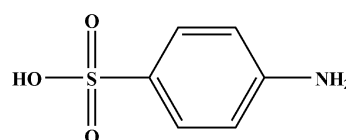
Aspirin



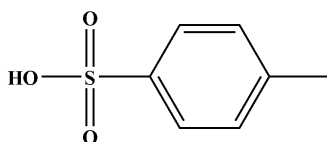
3-Nitrophthalic acid



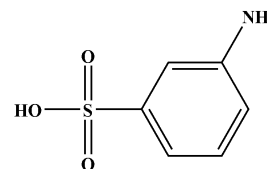
Sulfadiazine



Sulfanilic acid



*p*-Toluenesulfonic acid



3-aminobenzenesulfonic acid

**Figure 54.** Molecular structures of N- and O-donor ligands.

**Objectives**

★ To synthesize the supramolecular complexes with O-donor and N-donor ligands by suitable conditions.

★ To characterize structures of the as-synthesized supramolecular complexes by single-crystal X-ray diffraction analysis, infrared spectroscopy, elemental analysis, thermogravimetric analysis, UV-Visible spectroscopy, proton nuclear magnetic resonance, and powder X-ray diffraction.

★ To study photoluminescence properties of  $d^{10}$  complexes.

★ To study their possible applications of supramolecular complexes such as adsorption property, photocatalytic property, fluorescence sensing for metal ions property, and antibacterial activity.

## CHAPTER 2

### MATERIALS AND METHODS

#### 2.1 Chemicals

2.1.1 Cadmium(II) acetate dehydrate ( $\text{Cd}(\text{CH}_3\text{COO})_2 \cdot 2\text{H}_2\text{O}$ ), Analytical reagent, Univar, Ajax Finechem, Australia.

2.1.2 Zinc(II) acetate dehydrate ( $\text{Zn}(\text{CH}_3\text{COO})_2 \cdot 2\text{H}_2\text{O}$ ), Analytical reagent, Univar, Ajax Finechem, Australia.

2.1.3 Manganese(II) chloride tetrahydrate ( $\text{MnCl}_2 \cdot 4\text{H}_2\text{O}$ ), Laboratory reagent, BHD, England.

2.1.4 Cobalt(II) nitrate hexahydrate ( $\text{Co}(\text{NO}_3)_2 \cdot 6\text{H}_2\text{O}$ ), Analytical reagent, Univar, Ajax Finechem, Australia.

2.1.5 Nickel(II) nitrate hexahydrate ( $\text{Ni}(\text{NO}_3)_2 \cdot 6\text{H}_2\text{O}$ ), Analytical reagent, Univar, Ajax Finechem, Australia.

2.1.6 Zinc(II) nitrate hexahydrate ( $\text{Zn}(\text{NO}_3)_2 \cdot 6\text{H}_2\text{O}$ ), Analytical reagent, Univar, Ajax Finechem, Australia.

2.1.7 Silver nitrate ( $\text{AgNO}_3$ ), Analytical reagent, Fluka, USA.

2.1.8 Cadmium(II) nitrate tetrahydrate ( $\text{Cd}(\text{NO}_3)_2 \cdot 6\text{H}_2\text{O}$ ), Analytical reagent, Univar, Ajax Finechem, Australia.

2.1.9 4,4'-Bipyridine ( $\text{C}_{10}\text{H}_8\text{N}_2$ ), Analytical reagent, Sigma-Aldrich, USA.

2.1.10 1,3-bis(4-pyridyl)propane ( $\text{C}_{13}\text{H}_{14}\text{N}_2$ ), Analytical reagent, Sigma Aldrich, USA.

2.1.11 1,2-bis(4-pyridyl)ethane ( $\text{C}_{12}\text{H}_{12}\text{N}_2$ ), Analytical reagent, Sigma Aldrich, USA.

2.1.12 Cinnamic acid ( $\text{C}_9\text{H}_8\text{O}_2$ ), Analytical reagent, Fluka, USA.

2.1.13 3-Nitrophthalic acid ( $\text{C}_8\text{H}_5\text{NO}_6$ ), Analytical reagent, Fluka, USA.

2.1.14 Sulfanilic acid ( $\text{C}_7\text{H}_8\text{O}_3\text{S}$ ), Analytical reagent, Sigma-Aldrich, USA.

2.1.15 Sulfadiazine ( $\text{C}_{10}\text{H}_{10}\text{N}_4\text{O}_2\text{S}$ ), Analytical reagent, Sigma-Aldrich, USA.

2.1.16 3-aminobenzinesulfonic acid ( $\text{C}_6\text{H}_7\text{NO}_3\text{S}$ ), Analytical reagent, Sigma-Aldrich, USA.

2.1.17 *p*-Toluenesulfonic acid ( $\text{C}_7\text{H}_8\text{O}_3\text{S}$ ), Analytical reagent, Sigma-Aldrich, USA.



2.1.18 Ethanol (99.9%, C<sub>2</sub>H<sub>6</sub>O), American Chemical Society (ACS) reagent, Merck, Germany.

2.1.19 Methanol (99.9%, CH<sub>4</sub>O), American Chemical Society (ACS) reagent, Merck, Germany.

2.1.20 Aspirin (C<sub>9</sub>H<sub>8</sub>O<sub>4</sub>), Analytical reagent, Sigma-Aldrich, USA.

## 2.2 Synthesis

### Syntheses of the complexes with N-donor ligand and carboxylate ligand

#### Synthesis of [Cd(Cin)<sub>2</sub>(H<sub>2</sub>O)<sub>2</sub>] (1)

Cd(NO<sub>3</sub>)<sub>2</sub>·4H<sub>2</sub>O (0.3084 g, 1 mmol) was dissolved in 10 mL of water in a round bottom flask. Hexamethylenetetramine (0.2802 g, 2 mmol) in 5 mL of water was added. The mixture was stirred for 30 min to give a colorless solution. Then, cinnamic acid (0.2962 g, 2 mmol) in 20 mL of ethanol was added to give a colorless solution. The pH was adjusted to 7 with 1 M NaOH. The solution was stirred at room temperature for 6 h and filtered and then left to evaporate at room temperature. After several days, colorless needle shaped crystals suitable for X-ray analyses were obtained in 75% yield.

#### Synthesis of [Zn(4,4'-bpy)<sub>0.5</sub>(Cin)<sub>2</sub>]<sub>n</sub> (2)

Zn(CH<sub>3</sub>COO)<sub>2</sub>·2H<sub>2</sub>O (0.2195 g, 1 mmol), 4,4'-bipyridine (0.3132 g, 2 mmol) and cinnamic acid (0.2962 g, 2 mmol) were dissolved in 30 mL of water in a round bottom flask to a colorless solution. The pH was adjusted to 7 with 1 M NaOH. The solution was stirred at room temperature for 1 h, and then was added to a Parr Teflon-lined stainless steel vessel and heated for 3 days at 150 °C at rate of 5 °C/s and then cooled to room temperature. Colorless needle crystals were obtained in 45% yield.

#### Synthesis of [Cd<sub>3</sub>(4,4'-bpy)<sub>2</sub>(cin)<sub>6</sub>(H<sub>2</sub>O)<sub>2</sub>]<sub>n</sub> (3)

Complex (3) was obtained under the similar condition as that for preparation of complex (2) except for Zn(CH<sub>3</sub>COO)<sub>2</sub>·2H<sub>2</sub>O was replaced with Cd(CH<sub>3</sub>COO)<sub>2</sub>·2H<sub>2</sub>O. After several days, colorless needle crystals were obtained in 46% yield.

**Synthesis of [Cd(4,4'-bpy)(3-Npt)(H<sub>2</sub>O)]<sub>n</sub> (4)**

Cd(CH<sub>3</sub>COO)<sub>2</sub>·2H<sub>2</sub>O (0.2665 g, 1 mmol) was dissolved in 15 mL of water in a round bottom flask. 4,4'-bipyridine (0.3132 g, 2 mmol) in 10 mL of ethanol was added. The mixture was stirred for 30 min to a colorless solution. Then, 3-nitrophthalic acid (0.4222 g, 2 mmol) in 15 mL of ethanol was added to give a colorless solution. The pH was adjusted to 7 with 1 M NaOH. The solution was stirred at room temperature for 30 min, and then was added to a Parr Teflon-lined stainless steel vessel and heated for 3 days at 130 °C at rate of 5 °C/s and then cooled to room temperature. Colorless block crystals were obtained in 25% yield.

**Synthesis of [Mn<sub>2</sub>(bpp)(3-Npt)<sub>2</sub>(H<sub>2</sub>O)<sub>2</sub>]<sub>n</sub> (5)**

MnCl<sub>2</sub>·4H<sub>2</sub>O (0.1979 g, 1 mmol) was dissolved in 10 mL of water in a round bottom flask. 1,3-bis(4-pyridyl)propane (0.3963 g, 2 mmol) in 5 mL of water was added. The mixture was stirred for 30 min to a yellow solution. Then, 3-nitrophthalic acid (0.4222 g, 2 mmol) in 20 mL of ethanol was added to a yellow solution. The pH was adjusted to 7 with 1 M NaOH. The solution was stirred at room temperature for 6 h, was filtered and then left to evaporate at room temperature. After several days, colorless block crystals were obtained in 71% yield.

**Synthesis of [Ni(bpp)(3-Npt)(H<sub>2</sub>O)]<sub>n</sub> (6)**

Ni(NO<sub>3</sub>)<sub>2</sub>·4H<sub>2</sub>O (0.2907 g, 1 mmol) was dissolved in 15 mL of water in a round bottom flask. 1,3-bis(4-pyridyl)propane (0.3963 g, 2 mmol) in 5 mL of ethanol was added. The mixture was stirred for 15 min to give a green solution. Then, 3-nitrophthalic acid (0.4222 g, 2 mmol) in 15 mL of ethanol was added to a green solution. The pH was adjusted to 6 with 1 M NaOH. The solution was stirred at room temperature for 30 min, and then was added to a Parr Teflon-lined stainless steel vessel and heated for 3 days at 120 °C at rate of 5 °C/s and then cooled to room temperature. Green plate crystals were obtained in 41% yield.

### Synthesis of $\{[\text{Ag}_2(\text{bpp})_2] \cdot (4\text{H}_2\text{O}) \cdot (3\text{-Npt})\}_n$ (7)

$\text{AgNO}_3$  (0.1698g, 1 mmol) was dissolved in 20 mL of water in a round bottom flask. 1,3-bis(4-pyridyl)propane (0.3963 g, 2 mmol) in 15 mL of ethanol was added. The mixture was stirred for 30 min to give a colorless solution. Then, 3-nitrophthalic acid (0.2111 g, 1 mmol) in 10 mL of ethanol was added to a colorless solution. The pH was adjusted to 7 with 2 M  $\text{NH}_4\text{OH}$ . The solution was stirred at 80 °C for 120 min, was filtered and then left to evaporate at room temperature. After several days, colorless needle shaped crystals suitable for X-ray analysis was obtained in 75% yield.

### Synthesis of $\{[\text{Ag}_2(\text{bpe})_2(3\text{-Npt})] \cdot 7\text{H}_2\text{O}\}_n$ (8)

Complex (8) was obtained under the similar condition as that for preparation of complex (7) except for 1,3-bis(4-pyridyl)propane (0.3963 g, 2 mmol) was replaced with 1,2-bis(4-pyridyl)ethane (0.1842 g, 1 mmol). After several days, colorless needle crystals were obtained in 75% yield.

### Synthesis of $[\text{Zn}(\text{bpp})_2(\text{Sal})_2]_n$ (9)

$\text{Zn}(\text{CH}_3\text{COO})_2 \cdot 2\text{H}_2\text{O}$  (0.2195 g, 1 mmol) was dissolved in 15 mL of water in a round bottom flask. 1,3-bis(4-pyridyl)propane (0.1982 g, 1 mmol) in 10 mL of ethanol was added. The mixture was stirred for 15 min to give a colorless solution. Then, Aspirin (0.3602 g, 2 mmol) in 15 mL of ethanol was added to a give a colorless solution. The pH was adjusted to 7 with 1 M  $\text{NaOH}$ . The solution was stirred at room temperature for 30 min and then was added to a Parr Teflon-lined stainless steel vessel and heated for 3 days at 120 °C at rate of 5 °C/s and then cooled to room temperature. Block crystals were obtained in 83% yield.

### Synthesis of $[\text{Zn}_2(\text{bpe})_2(\text{Sal})_4]$ (10)

Complex (10) was obtained under the similar condition as that for preparation of complex (9) except for 1,3-bis(4-pyridyl)propane was replace with 1,2-bis(4-pyridyl)ethane. After several days, colorless needle crystals were obtained in 32% yield.

## Syntheses of the complexes with N-donor ligand and sulfanate ligand

### Synthesis of $\{[\text{Co}(\text{bpp})_2(\text{H}_2\text{O})_2](4\text{-abs})_2 \cdot \text{H}_2\text{O}\}_n$ (11)

$\text{Co}(\text{NO}_3)_2 \cdot 6\text{H}_2\text{O}$  (0.2910 g, 1 mmol) was dissolved in 10 mL of water in a round bottom flask. 1,3-bis(4-pyridyl)propane (0.1982 g, 1 mmol) in 5 mL of ethanol was added. The mixture was stirred for 30 min to give a pink solution. Then, 4-aminobenzenesulfonic acid (2 mmol, 0.3462 g) in 20 mL of water was added to give a pink solution. The pH was adjusted to 6 with 1 M NaOH. The solution was stirred at room temperature for 4 h, was filtered and then left to evaporate at room temperature. After several days, pink block crystals were obtained in 66% yield.

### Synthesis of $[\text{Mn}_{0.5}(\text{bpp})(\text{H}_2\text{O})_2] \cdot (4\text{-abs})$ (12)

Complex (12) was obtained under the similar condition as that for preparation of complex (11) except for  $\text{Co}(\text{NO}_3)_2 \cdot 6\text{H}_2\text{O}$  was replaced with  $\text{MnCl}_2 \cdot 4\text{H}_2\text{O}$ . After several days, colorless block crystals were obtained in 50% yield.

### Synthesis of $\{[\text{Cd}_{0.5}(\text{bpp})(4\text{-abs})] \cdot (\text{H}_2\text{O})\}_n$ (13)

Complex (13) was obtained under the similar condition as that for preparation of complex (11) except for  $\text{Co}(\text{NO}_3)_2 \cdot 6\text{H}_2\text{O}$  was replaced with  $\text{Cd}(\text{NO}_3)_2 \cdot 4\text{H}_2\text{O}$ . After several days, colorless block crystals were obtained in 46% yield.

### Synthesis of $[\text{Zn}_{0.5}(\text{bpp})(\text{H}_2\text{O})_2] \cdot (4\text{-abs})$ (14)

Complex (14) was obtained under the similar condition as that for preparation of complex (11) except for  $\text{Co}(\text{NO}_3)_2 \cdot 6\text{H}_2\text{O}$  was replaced with  $\text{Zn}(\text{CH}_3\text{COO})_2 \cdot 2\text{H}_2\text{O}$ . After several days, colorless block crystals were obtained in 40% yield.

### Synthesis of $\{[\text{Zn}(4,4'\text{-bpy})(\text{H}_2\text{O})_4] \cdot (4\text{-abs})_2 \cdot 2\text{H}_2\text{O}\}_n$ (15)

Complex (15) was obtained under the similar condition as that for preparation of complex (11) except for  $\text{Co}(\text{NO}_3)_2 \cdot 6\text{H}_2\text{O}$  and 1,3-bis(4-pyridyl)propane were replaced with  $\text{Zn}(\text{CH}_3\text{COO})_2 \cdot 2\text{H}_2\text{O}$  and 4,4'-bipyridine. After several days, colorless block crystals were obtained in 56% yield based on Zn.

### Synthesis of $\{[\text{Cd}(\text{4,4}'\text{-bpy})_{1.5}(\text{H}_2\text{O})_3] \cdot (\text{4,4}'\text{-bpy}) \cdot (\text{4-abs}) \cdot (\text{H}_2\text{O}) \cdot \text{NO}_3\}_n$ (16)

Complex (16) was obtained under the similar condition as that for preparation of complex (11) except for  $\text{Co}(\text{NO}_3)_2 \cdot 6\text{H}_2\text{O}$  and 1,3-bis(4-pyridyl)propane were replaced with  $\text{Cd}(\text{NO}_3)_2 \cdot 4\text{H}_2\text{O}$  and 4,4'-bipyridine. After several days, block crystals were obtained in 30% yield.

### Synthesis of $\{[\text{Cd}_{0.5}(\text{bpe})(\text{4-abs})] \cdot \text{H}_2\text{O}\}_n$ (17)

Complex (17) was obtained under the similar condition as that for preparation of complex (11) except for  $\text{Co}(\text{NO}_3)_2 \cdot 6\text{H}_2\text{O}$  and 1,3-bis(4-pyridyl)propane were replaced with  $\text{Cd}(\text{NO}_3)_2 \cdot 4\text{H}_2\text{O}$  and 1,2-bis(4-pyridyl)ethane. After several days, block crystals were obtained in 47% yield.

### Synthesis of $\{[\text{Cd}(\text{bpp})_2(\text{H}_2\text{O})_4] \cdot (\text{3-abs})_2 \cdot 2\text{H}_2\text{O}\}_n$ (18)

Complex (18) was obtained under the similar condition as that for preparation of complex (11) except for  $\text{Co}(\text{NO}_3)_2 \cdot 6\text{H}_2\text{O}$  and 4-aminobenzenesulfonic acid were replaced with  $\text{Cd}(\text{NO}_3)_2 \cdot 4\text{H}_2\text{O}$  and 3-aminobenzinesulfonic acid. After several days, block crystals were obtained in 64% yield.

### Synthesis of $[\text{Zn}(\text{bpp})_2(\text{Mbs})_2]_n$ (19)

$\text{Zn}(\text{CH}_3\text{COO})_2 \cdot 2\text{H}_2\text{O}$  (0.2195 g, 1 mmol) was dissolved in 10 mL of water in a round bottom flask. 1,3-bis(4-pyridyl)propane (0.1982 g, 1 mmol) in 5 mL of ethanol was added. The mixture was stirred for 30 min to give a yellow solution. Then, 4-methylbenzenesulfonic acid (2 mmol, 0.3462 g) in 20 mL of water was added to give a yellow solution. The pH was adjusted to 6 with 1 M NaOH. The solution was stirred for 180 min at 80 °C, was filtered and then left to evaporate at room temperature. After several days, colorless block crystals were obtained in 55% yield.

### Synthesis of $[\text{Cd}(\text{bpp})_2(\text{Mbs})_2]_n$ (20)

Complex (16) was obtained under the similar condition as that for preparation of complex (15) except for  $\text{Zn}(\text{CH}_3\text{COO})_2 \cdot 2\text{H}_2\text{O}$  was replaced with  $\text{Cd}(\text{NO}_3)_2 \cdot 4\text{H}_2\text{O}$ . After several days, block crystals were obtained in 50% yield.

### Synthesis of $\{[\text{Cd}(\text{bpp})(\text{sdz})_2] \cdot 2\text{H}_2\text{O}\}_n$ (21)

$\text{Cd}(\text{NO}_3)_2 \cdot 4\text{H}_2\text{O}$  (0.2665 g, 1 mmol) was dissolved in 15 mL of water in a round bottom flask. 1,3-bis(4-pyridyl)propane (0.1982 g, 1 mmol) in 10 mL of methanol was added. The mixture was stirred for 15 min to give a colorless solution. Then, sulfadiazine (0.5004 g, 2 mmol) in 15 mL of methanol was added to give a colorless solution. The pH was adjusted to 8 with 1 M KOH. The solution was stirred at room temperature for 30 min and then, the resultant solution was added to a Parr Teflon-lined stainless steel vessel and heated for 4 days at 140 °C at rate of 5 °C/s and then cooled to room temperature. Colorless block crystals were obtained in 32% yield.

### Synthesis of $\{[\text{Zn}(\text{bpe})(\text{sdz})(\text{ac})] \cdot \text{H}_2\text{O}\}_n$ (22)

Complex (22) was obtained under the similar condition as that for preparation of complex (21) except for  $\text{Cd}(\text{NO}_3)_2 \cdot 4\text{H}_2\text{O}$  and 1,3-bis(4-pyridyl)propane were replaced with  $\text{Zn}(\text{CH}_3\text{COO})_2 \cdot 2\text{H}_2\text{O}$  and 1,2-bis(4-pyridyl)ethane. Colorless block crystals were obtained in 32% yield.

## 2.3 Instrument

### 2.3.1 Fourier-transformed infrared spectrophotometer

FT-IR spectra were obtained using KBr pellet on a Perkin-Elmer Spectrum One Fourier-transformed infrared spectrophotometer between 4000 – 400  $\text{cm}^{-1}$ . The infrared spectra of all complexes are shown in Appendix.

### 2.3.2 Thermogravimetric analyses

Thermogravimetric analyses (TGA) were carried out on a Perkin Elmer TGA7 in the range 50 – 1000 °C with a heating rate of 10 °C/ min under  $\text{N}_2$  atmosphere. The thermograms of all complexes are shown in Appendix.

### 2.3.3 Elemental analyser

Elemental analysis for carbon, hydrogen, and nitrogen were performed on a Perkin-Elmer 240 elemental analyzer.

### 2.3.4 Powder X-ray diffractometer

Powder X-ray diffraction measurements were carried out using a X'Pert MPD PHILIPS X-ray diffractometer with Cu K $\alpha$  radiation in the  $2\theta$  range of 5–50° at room temperature.

### 2.3.5 Luminescence spectrometer

Fluorescence spectra were recorded on a Perkin Elmer LS55 Luminescence spectrometer with excitation and emission slit width 10 nm and scans rate 400 nm/min at room temperature.

### 2.3.6 Single crystal X-ray diffractometer

Suitable single crystal of [Cd(Cin)<sub>2</sub>(H<sub>2</sub>O)<sub>2</sub>] (**1**), [Zn(4,4'-bpy)<sub>0.5</sub>(Cin)<sub>2</sub>]<sub>n</sub> (**2**), [Cd<sub>3</sub>(4,4'-bpy)<sub>2</sub>(cin)<sub>6</sub>(H<sub>2</sub>O)<sub>2</sub>]<sub>n</sub> (**3**), [Cd(4,4'-bpy)(3-Npt)(H<sub>2</sub>O)]<sub>n</sub> (**4**), [Mn<sub>2</sub>(bpp)(3-Npt)<sub>2</sub>(H<sub>2</sub>O)<sub>2</sub>]<sub>n</sub> (**5**), and [Ni(bpp)(3-Npt)(H<sub>2</sub>O)]<sub>n</sub> (**6**) were collected and mounted on a Bruker Smart APEX II CCD diffractometer at Youngstown State University. Absorption corrections were based on symmetry equivalent reflections using the SADABS program. The molecular structure was solved by direct method and refined by full-matrix least squares on  $F^2$  using SHELXS-97 and SHELXL-2013.

For suitable single crystal of {[Ag<sub>2</sub>(bpp)]·(4H<sub>2</sub>O)·(3-Npt)}<sub>n</sub> (**7**), {[Ag<sub>2</sub>(bpe)<sub>2</sub>(3-Npt)]·7H<sub>2</sub>O}<sub>n</sub> (**8**), [Zn(bpp)<sub>2</sub>(sal)<sub>2</sub>]<sub>n</sub> (**9**), [Zn<sub>2</sub>(bpe)<sub>2</sub>(sal)<sub>4</sub>] (**10**), {[Co(bpp)<sub>2</sub>(H<sub>2</sub>O)<sub>2</sub>](4-abs)<sub>2</sub>·H<sub>2</sub>O}<sub>n</sub> (**11**), [Mn<sub>0.5</sub>(bpp)(H<sub>2</sub>O)<sub>2</sub>](4-abs) (**12**), {[Cd<sub>0.5</sub>(bpp)(4-abs)]·(H<sub>2</sub>O)}<sub>n</sub> (**13**), [Zn<sub>0.5</sub>(bpp)(H<sub>2</sub>O)<sub>2</sub>](4-abs) (**14**), {[Zn(4,4'-bpy)(H<sub>2</sub>O)<sub>4</sub>](4-abs)<sub>2</sub>·2H<sub>2</sub>O}<sub>n</sub> (**15**), {[Cd(4,4'-bpy)<sub>1.5</sub>(H<sub>2</sub>O)<sub>3</sub>](4-abs)·(4,4'-bpy)·(H<sub>2</sub>O)·NO<sub>3</sub>}<sub>n</sub> (**16**), {[Cd(bpe)<sub>2</sub>(4-abs)<sub>2</sub>]·H<sub>2</sub>O}<sub>n</sub> (**17**), {[Cd(bpp)<sub>2</sub>(H<sub>2</sub>O)<sub>4</sub>](3-abs)<sub>2</sub>·2H<sub>2</sub>O}<sub>n</sub> (**18**), [Zn(bpp)<sub>2</sub>(Mbs)<sub>2</sub>]<sub>n</sub> (**19**), [Cd(bpp)<sub>2</sub>(Mbs)<sub>2</sub>]<sub>n</sub> (**20**), {[Cd(bpp)(sdz)<sub>2</sub>]·2H<sub>2</sub>O}<sub>n</sub> (**21**), and {[Zn(bpe)(sdz)(ac)]·H<sub>2</sub>O}<sub>n</sub> (**22**) were collected and mounted on a Bruker Smart APEX II CCD diffractometer at 296 K with Mo-K $\alpha$  radiation ( $\lambda = 0.71073 \text{ \AA}$ ) at Department of Physics, Faculty of Science and Technology, Thammasart University. Absorption corrections were based on symmetry equivalent reflections using the SADABS program. The structure were solved with direct methods using *Olex2* program and refined with the full-matrix least-squares technique on  $F^2$ . All non-hydrogen atoms were refined using anisotropic

thermal parameters. The hydrogen atoms of the organic ligands were located in difference Fourier maps.

The molecular structure, packing diagrams and hydrogen bonding interaction of all complexes were produced using the Mercury 3.8 software program.

### 2.3.7 Nuclear magnetic resonance

$^1\text{H}$  NMR spectra were recorded on a Bruker 400 MHz Spectrometer in Dimethyl sulfoxide- $d_6$  using TMS as an internal reference.

### 2.3.8 UV-Visible spectrophotometer

Electronic spectra of the complexes in solution were recorded on SHIMADZU UV-2600 UV-visible spectrophotometer.

### 2.3.9 UV-Visible diffused reflectance spectrophotometer

Solid state UV-Vis diffused reflectance spectra were recorded with a Shimadzu 2450 PC UV-Vis recording spectrophotometer at room temperature with  $\text{BaSO}_4$  as the background.

## 2.4 Photocatalytic experiments

In the photocatalytic studies of the  $\{[\text{Ag}_2(\text{bpp})]\cdot(4\text{H}_2\text{O})\cdot(3\text{-Npt})\}_n$  (**7**) and  $\{[\text{Ag}_2(\text{bpe})_2(3\text{-Npt})]\cdot 7\text{H}_2\text{O}\}_n$  (**8**) to investigate the degradation of Rhodamine B (RhB) and Methylene blue (MB) dye under UV light and visible irradiation the experimental set up were as follows: 0.100 g of the samples were mixed with RhB solution (5 ppm, 100 mL) (or methylene blue aqueous solution (5 ppm, 100 mL)) in a 250 mL breaker, respectively. And then, the solution was stirred for 1 hr. in the dark to reach the adsorption equilibrium in tightly closed photoreaction compartment (90 cm  $\times$  90 cm  $\times$  90 cm for UV light and 70 cm  $\times$  70 cm  $\times$  70 cm for visible light) to avoid light from ambient light. Afterward, under 100 W mercury lamps for UV light and 90 W for visible light were used as radiation sources for photocatalytic process, the solution was kept continuously stirring with magnetic stirrer. The solution of dye sample was taken out and centrifuged (5000 rpm for 3 min) to remove the residual catalyst for analysis by UV-visible spectrophotometer every 30 min. The control experimental was prepared without catalyst. The degradation efficiency (%) of dyes is defined as equation:



$$\text{Degradation efficiency (\%)} = \left( \frac{C_0 - C_t}{C_0} \right) \times 100$$

where  $C_0$  (ppm) is the initial concentration of dyes, and  $C_t$  (ppm) is the concentration of dyes at reaction time  $t$  (min).

## 2.5 Metal ions sensing experiments

Complexes  $[\text{Zn}(\text{bpp})_2(\text{Sal})_2]_n$  (**9**) and  $[\text{Zn}_2(\text{bpe})_2(\text{Sal})_4]$  (**10**) were tested for metal ion sensing property. Different volumes of metal ions ( $M = \text{Cd}^{2+}$ ,  $\text{Mn}^{2+}$ ,  $\text{Sr}^{2+}$ ,  $\text{K}^+$ ,  $\text{Na}^+$ ,  $\text{Ni}^{2+}$ ,  $\text{Co}^{2+}$ ,  $\text{Ca}^{2+}$ ,  $\text{Cu}^{2+}$ ) in aqueous solution (0.5 mM) was added to the DMSO solution of complexes (**9**) and (**10**) (0.005 mM, 4 mL). The solution was stirred for 10 min and was taken for analysis by LS55 Luminescence spectrometry. The quenching efficiency (%) is defined as equation:

$$\text{Quenching efficiency (\%)} = \left( \frac{F_0 - F}{F_0} \right) \times 100$$

where  $F_0$  is the maximum fluorescence intensity of complexes and  $F$  is the maximum fluorescence intensity after adding metal ions.

## 2.6 Antibacterial activity

The complexes  $[\text{Zn}(\text{bpp})_2(\text{Sal})_2]_n$  (**9**) and  $[\text{Zn}_2(\text{bpe})_2(\text{Sal})_4]$  (**10**) were screened for their antibacterial activity against *Staphylococcus aureus* (*S. aureus*) ATCC 25923, *Escherichia coli* (*E. coli*) ATCC 25922, and *Pseudomonas aeruginosa* (*P. aeruginosa*) ATCC 27853, and Penicillin (20  $\mu\text{g}/\text{disc}$ ) and Gentamicin were used as a standard. Antibacterial activity was tested at Scientific Equipment Center, Faculty of Science, King Mongkut's Institute of Technology Ladkrabang, Bangkok. The complexes (**9**) and (**10**) were dissolved in DMSO for a concentration of 1 mg/mL. The inoculums were prepared using a liquid broth of bacterial and adjusted to a turbidity equivalent to a 0.5 McFarland standard containing approximately  $10^4$ - $10^6$  CFU/mL. A cotton buds was dipped into the inoculums and the surface area of the nutrient agar (NA) was inoculated by streaking the sterile cotton swab. The paper disks impregnated with the test complexes were placed on nutrient agar. The plates

inoculated with bacteria at 37 °C for 24 h. The antibacterial activity was evaluated by measuring growth inhibition zone diameter (mm).

## 2.7 Adsorption experiment procedure

In the adsorption studies of the  $\{[Ag_2(bpp)] \cdot (4H_2O) \cdot (3-Npt)\}_n$  (7) to investigate the adsorption of dye.

### Preparation of calibration graph of orange G

Orange G (OG) was selected to represent organic pollutants. The standard calibration graph was used to find the concentration of OG. The concentration of OG solutions for the calibration graph was prepared in the range  $1 \times 10^{-5}$  mol/L to  $5 \times 10^{-5}$  mol/L.

### The optimum condition experiments

The adsorption capacity of dye, orange G, was carried out by varying dosage of complex (0.005–0.04 g), contact time (1–60 min), and initial dye concentration ( $5 \times 10^{-5}$  -  $2.5 \times 10^{-4}$  mol/L). Adsorption was achieved by adding complex (7) into 100 mL of OG solution of known concentration in a 250 mL beaker and was stirred at 5000 rpm/min. The solution of dye sample was taken and centrifuged (5000 rpm for 3 min) to remove the residual and analysed by UV-visible spectrophotometry to obtain the concentration of OG dye in the solution.

The adsorption efficiency (%) of complex (7) adsorbent to OG dye is defined as

$$\text{Adsorption efficiency (\%)} = \left( \frac{C_0 - C_t}{C_0} \right) \times 100$$

where  $C_0$  is the initial concentration of OG dye solution and  $C_t$  is the concentration of OG dye solution at reaction time  $t$  (min) was collected.

### Adsorption isotherms

The adsorption isotherms of Langmuir and Freundlich are widely used to test and compare the adsorption execution of adsorbents. In this work, the initial concentration of OG dye solution was prepared from  $5 \times 10^{-5}$  -  $4 \times 10^{-4}$  mol/L. 0.03 g of complex (7) was added to 100 mL of OG dye solution in a 250 mL beaker and stirred with 300 rpm for 60 min under dark environment at room temperature to avoid

interference from ambient light. The aqueous phase of dye was separated from complex by centrifugation for analysis by UV-visible spectrophotometry to obtain concentration of OG dye in the solution. The amount of equilibrium adsorption was calculated using the equation;

$$q_e = \frac{(C_0 - C_e) \cdot V}{W}$$

W is the mass of dry adsorbent (g)  $C_0$  is the initial concentration of OG dye solution,  $C_e$  is the concentration of OG dye solution in equilibrium, and V is the volume of the dye solution (L).

## CHAPTER 3

## RESULTS AND DISCUSSTION

In this work, the complexes containing N-donor ligand and carboxylate ligand or sulfonate ligand were prepared at the appropriate temperature by using metal salt (Ni(II), Co(II), Mn(II), Zn(II), Ag(I), and Cd(II)), N-donor ligand (4,4'-bipyridine (bpy), 1,3-bis(4-pyridyl)propane (bpp), 1,2-bis(4-pyridyl)ethane (bpe)) and O-donor ligand from carboxylate ligand (Cinnamic acid, 3-Nitroptalic acid and Aspirin) or sulfonate ligand (Sulfanilic acid, Sulfadiazine, 3-aminobenzinesulfonic acid, and *p*-Toluenesulfonic acid) as starting materials. The syntheses data are summarized in **Table 3** and the solubilities of all complexes are summarized in **Table 4**.

**Table 3.** The preparation of complexes.

Reactants	Mole ratio	Solvent	Temp. (°C)	Complexes
Cd(NO <sub>3</sub> ) <sub>2</sub> ·4H <sub>2</sub> O: hmt : cin.	1:2:2	EtOH- H <sub>2</sub> O	rt.	[Cd(Cin) <sub>2</sub> (H <sub>2</sub> O) <sub>2</sub> ] (1) (Mononuclear)
Zn(Ac) <sub>2</sub> ·2H <sub>2</sub> O: 4,4'-bpy:cin	1:2:2	EtOH- H <sub>2</sub> O	150	[Zn(4,4'-bpy) <sub>0.5</sub> (Cin) <sub>2</sub> ] <sub>n</sub> (2) (3-D polymer)
Cd(Ac) <sub>2</sub> ·2H <sub>2</sub> O: 4,4'-bpy:cin	1:2:2	EtOH- H <sub>2</sub> O	150	[Cd <sub>3</sub> (4,4'-bpy) <sub>2</sub> (cin) <sub>6</sub> (H <sub>2</sub> O) <sub>2</sub> ] <sub>n</sub> (3) (2-D polymer)
Cd(Ac) <sub>2</sub> ·2H <sub>2</sub> O: 4,4'-bpy:Npt	1:2:2	EtOH- H <sub>2</sub> O	130	[Cd(4,4'-bpy)(3-Npt)(H <sub>2</sub> O)] <sub>n</sub> (4) (2-D polymer)
MnCl <sub>2</sub> ·4H <sub>2</sub> O: bpp :Npt	1:2:2	EtOH- H <sub>2</sub> O	rt.	[Mn <sub>2</sub> (bpp)(3-Npt) <sub>2</sub> (H <sub>2</sub> O) <sub>2</sub> ] <sub>n</sub> (5) (2-D polymer)
Ni(NO <sub>3</sub> ) <sub>2</sub> ·4H <sub>2</sub> O: bpp :Npt	1:2:2	EtOH- H <sub>2</sub> O	120	[Ni(bpp)(3-Npt)(H <sub>2</sub> O)] <sub>n</sub> (6) (1-D polymer)
AgNO <sub>3</sub> : bpp :Npt	1:2:1	EtOH- H <sub>2</sub> O	80	{[Ag <sub>2</sub> (bpp)]·(4H <sub>2</sub> O)·(3-Npt)} <sub>n</sub> (7) (1-D polymer)
AgNO <sub>3</sub> : bpe :Npt	1:1:1	EtOH- H <sub>2</sub> O	80	{[Ag <sub>2</sub> (bpe) <sub>2</sub> (3-Npt)]·7H <sub>2</sub> O} <sub>n</sub> (8) (1-D polymer)
Zn(Ac) <sub>2</sub> ·2H <sub>2</sub> O: bpp:Aps	1:1:2	EtOH- H <sub>2</sub> O	120	[Zn(bpp) <sub>2</sub> (Sal) <sub>2</sub> ] <sub>n</sub> (9) (1-D polymer)
Zn(Ac) <sub>2</sub> ·2H <sub>2</sub> O: bpe:Aps	1:1:2	EtOH- H <sub>2</sub> O	120	[Zn <sub>2</sub> (bpe) <sub>2</sub> (Sal) <sub>4</sub> ] (10) (Dinuclear)
Co(NO <sub>3</sub> ) <sub>2</sub> ·6H <sub>2</sub> O: bpp :Abs	1:1:2	EtOH- H <sub>2</sub> O	rt.	{[Co(bpp) <sub>2</sub> (H <sub>2</sub> O) <sub>2</sub> ](4- abs) <sub>2</sub> ·H <sub>2</sub> O} <sub>n</sub> (11) (1-D polymer)

**Table 3.** The preparation of complexes (continued).

Reactant	Mole ratio	Solvent	Temp. (°C)	Complexes
MnCl <sub>2</sub> ·4H <sub>2</sub> O: bpp :Abs	1:1:2	EtOH- H <sub>2</sub> O	rt.	[Mn <sub>0.5</sub> (bpp)(H <sub>2</sub> O) <sub>2</sub> ]·(4-abs) ( <b>12</b> ) (Mononuclear)
Cd(NO <sub>3</sub> ) <sub>2</sub> ·4H <sub>2</sub> O: bpp :Abs	1:1:2	EtOH- H <sub>2</sub> O	rt.	{[Cd <sub>0.5</sub> (bpp)(4-abs)]·(H <sub>2</sub> O)} <sub>n</sub> ( <b>13</b> ) (1-D polymer)
Zn(Ac) <sub>2</sub> ·2H <sub>2</sub> O: bpp:Abs	1:1:2	EtOH- H <sub>2</sub> O	rt.	[Zn <sub>0.5</sub> (bpp)(H <sub>2</sub> O) <sub>2</sub> ]·(4-abs) ( <b>14</b> ) (Mononuclear)
Zn(Ac) <sub>2</sub> ·2H <sub>2</sub> O: 4,4'-bpy:Abs	1:1:2	EtOH- H <sub>2</sub> O	80	{[Zn(4,4'-bpy)(H <sub>2</sub> O) <sub>4</sub> ](4- abs) <sub>2</sub> ·2H <sub>2</sub> O} <sub>n</sub> ( <b>15</b> ) (1-D polymer)
Cd(NO <sub>3</sub> ) <sub>2</sub> ·4H <sub>2</sub> O: 4,4'-bpy:Abs	1:1:2	EtOH- H <sub>2</sub> O	80	{[Cd(4,4'-bpy) <sub>1.5</sub> (H <sub>2</sub> O) <sub>3</sub> ]·(4- abs)(4,4'-bpy)·(H <sub>2</sub> O)·NO <sub>3</sub> } <sub>n</sub> ( <b>16</b> ) (2-D polymer)
Cd(NO <sub>3</sub> ) <sub>2</sub> ·4H <sub>2</sub> O: bpe:Abs	1:1:2	EtOH- H <sub>2</sub> O	80	{[Cd(bpe) <sub>2</sub> (4-abs) <sub>2</sub> ]·H <sub>2</sub> O} <sub>n</sub> ( <b>17</b> ) (2-D polymer)
Cd(NO <sub>3</sub> ) <sub>2</sub> ·4H <sub>2</sub> O: bpp:3-Abs	1:1:2	EtOH- H <sub>2</sub> O	80	{[Cd(bpp) <sub>2</sub> (H <sub>2</sub> O) <sub>4</sub> ]·(3-abs) <sub>2</sub> 2H <sub>2</sub> O} <sub>n</sub> ( <b>18</b> ) (2-D polymer)
Zn(Ac) <sub>2</sub> ·2H <sub>2</sub> O: bpp:Mbs	1:1:2	EtOH- H <sub>2</sub> O	80	[Zn(bpp) <sub>2</sub> (Mbs) <sub>2</sub> ] <sub>n</sub> ( <b>19</b> ) (2-D polymer)
Cd(NO <sub>3</sub> ) <sub>2</sub> ·4H <sub>2</sub> O: bpp:Mbs	1:1:2	EtOH- H <sub>2</sub> O	80	[Cd(bpp) <sub>2</sub> (Mbs) <sub>2</sub> ] <sub>n</sub> ( <b>20</b> ) (2-D polymer)
Cd(NO <sub>3</sub> ) <sub>2</sub> ·4H <sub>2</sub> O: bpp:Sdz	1:1:2	MeOH- H <sub>2</sub> O	140	{[Cd(bpp)(sdz) <sub>2</sub> ]·2H <sub>2</sub> O} <sub>n</sub> ( <b>21</b> ) (1-D polymer)
Zn(Ac) <sub>2</sub> ·2H <sub>2</sub> O: bpe:Sdz	1:1:2	MeOH- H <sub>2</sub> O	140	{[Zn(bpe)(sdz)(ac)]·H <sub>2</sub> O} <sub>n</sub> ( <b>22</b> ) (1-D polymer)

**Table 4.** The solubilities of all complexes.

Complexes	Solubility						
	EtOH	MeOH	H <sub>2</sub> O	Acetonitrile	DMF	DMSO	Chloroform
[Cd(Cin) <sub>2</sub> (H <sub>2</sub> O) <sub>2</sub> ] ( <b>1</b> )	×	×	×	×	×	×	×
[Zn(4,4'-bpy) <sub>0.5</sub> (Cin) <sub>2</sub> ] <sub>n</sub> ( <b>2</b> )	×	×	×	×	×	×	×
[Cd <sub>3</sub> (4,4'-bpy) <sub>2</sub> (cin) <sub>6</sub> (H <sub>2</sub> O) <sub>2</sub> ] <sub>n</sub> ( <b>3</b> )	×	×	×	×	×	×	×
[Cd(4,4'-bpy)(3-Npt)(H <sub>2</sub> O)] <sub>n</sub> ( <b>4</b> )	×	×	×	×	×	×	×
[Mn <sub>2</sub> (bpp)(3-Npt) <sub>2</sub> (H <sub>2</sub> O) <sub>2</sub> ] <sub>n</sub> ( <b>5</b> )	×	×	√	×	×	×	×

**Table 4.** The solubilities of all complexes (continued).

Complexes	Solubility						
	EtOH	MeOH	H <sub>2</sub> O	Acetonitrile	DMF	DMSO	Chloroform
[Ni(bpp)(3-Npt)(H <sub>2</sub> O)] <sub>n</sub> ( <b>6</b> )	×	×	×	×	×	×	×
{[Ag <sub>2</sub> (bpp)]·(4H <sub>2</sub> O)·(3-Npt)} <sub>n</sub> ( <b>7</b> )	×	×	×	×	×	×	×
{[Ag <sub>2</sub> (bpe) <sub>2</sub> (3-Npt)]·7H <sub>2</sub> O} <sub>n</sub> ( <b>8</b> )	×	×	×	×	×	×	×
[Zn(bpp) <sub>2</sub> (Sal) <sub>2</sub> ] <sub>n</sub> ( <b>9</b> )	×	×	×	×	×	√	×
[Zn <sub>2</sub> (bpe) <sub>2</sub> (Sal) <sub>4</sub> ] ( <b>10</b> )	×	×	×	×	×	√	×
{[Co(bpp) <sub>2</sub> (H <sub>2</sub> O) <sub>2</sub> ]·(4-abs) <sub>2</sub> ·H <sub>2</sub> O} <sub>n</sub> ( <b>11</b> )	×	×	×	×	×	√	×
[Mn <sub>0.5</sub> (bpp)(H <sub>2</sub> O) <sub>2</sub> ]·(4-abs) ( <b>12</b> )	×	×	×	×	×	×	×
{[Cd <sub>0.5</sub> (bpp)(4-abs)]·(H <sub>2</sub> O)} <sub>n</sub> ( <b>13</b> )	×	×	×	×	×	×	×
[Zn <sub>0.5</sub> (bpp)(H <sub>2</sub> O) <sub>2</sub> ]·(4-abs) ( <b>14</b> )	×	×	×	×	×	×	×
{[Zn(4,4'-bpy)(H <sub>2</sub> O) <sub>4</sub> ]·(4-abs) <sub>2</sub> ·2H <sub>2</sub> O} <sub>n</sub> ( <b>15</b> )	×	×	×	×	×	×	×
{[Cd(4,4'-bpy) <sub>1.5</sub> (H <sub>2</sub> O) <sub>3</sub> ]·(4-abs)·(4,4'-bpy)·(H <sub>2</sub> O)·NO <sub>3</sub> } <sub>n</sub> ( <b>16</b> )	×	×	×	×	×	×	×
{[Cd <sub>0.5</sub> (bpe)(4-abs)]·H <sub>2</sub> O} <sub>n</sub> ( <b>17</b> )	×	×	×	×	×	×	×
{[Cd(bpp) <sub>2</sub> (H <sub>2</sub> O) <sub>4</sub> ]·(3-abs) <sub>2</sub> ·2H <sub>2</sub> O} <sub>n</sub> ( <b>18</b> )	×	×	×	×	×	×	×
[Zn(bpp) <sub>2</sub> (Mbs) <sub>2</sub> ] <sub>n</sub> ( <b>19</b> )	×	×	×	×	×	×	×
[Cd(bpp) <sub>2</sub> (Mbs) <sub>2</sub> ] <sub>n</sub> ( <b>20</b> )	×	×	×	×	×	×	×
{[Cd(bpp)(sdz) <sub>2</sub> ]·2H <sub>2</sub> O} <sub>n</sub> ( <b>21</b> )	×	×	×	×	×	×	×
{[Zn(bpe)(sdz)(ac)]·H <sub>2</sub> O} <sub>n</sub> ( <b>22</b> )	×	×	×	×	×	×	×

### 3.1 Characterization

#### 3.1.1 Single crystal X-ray diffraction

##### Structural description of $[\text{Cd}(\text{Cin})_2(\text{H}_2\text{O})_2]$ (**1**)

X-ray crystallographic analyses showed that complex (**1**) crystallized in monoclinic crystal system of space group  $C2$ . The complex was obtained as an accidental product of the reaction of cadmium nitrate with hexamethylenetetramine and cinnamic acid in ethanol solution. Molecular structure showed that complex contained one Cd atom, two cinnamate ligands, two water molecules and no hexamethylenetetramine. Cd ion was coordinated by four oxygen atoms from two cinnamate ligands and two water molecules giving rise to a distorted octahedral geometry (**Figure 55**).

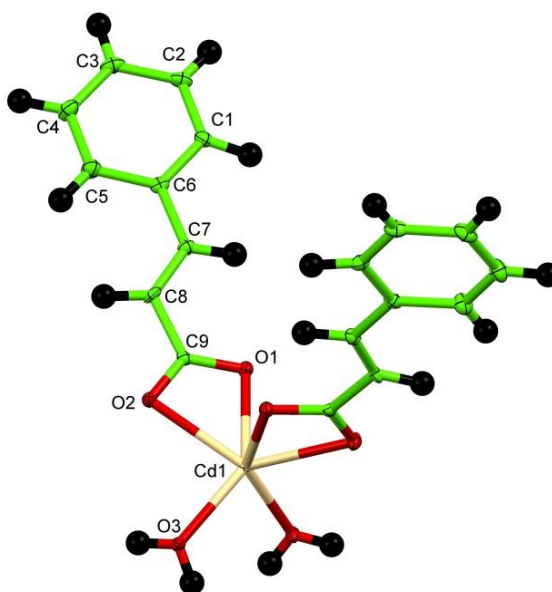


**Figure 55.** Molecular structure of  $\text{Cd}(\text{Cin})_2(\text{H}_2\text{O})_2$  (ellipsoid probability at 50%).

The completely deprotonated carboxylate groups of cinnamate ligands were bidentate-chelating, the water molecules as monodentate, resulting in a mononuclear complex. The Cd—O bond distances were in the expected ranges. The bonds involving the water O atoms were 2.208 (2) Å similar to the other Cd complexes (Mondal *et al.*, 2016) but the Cd—O bond distances of carboxylate group were longer than Cd—O of water molecules due to the chelating coordination mode of the

cinnamate ligand. The selected bond distances and angles are shown in **Table 5**. The molecular packing of complex plotted along the b axis are shown in **Figure 56**.

**Table 5.** Selected bond distances and angles of  $[\text{Cd}(\text{Cin})_2(\text{H}_2\text{O})_2]$  (**1**).

Bond lengths (Å)		Bond angles (°)	
Cd1—O3 <sup>1</sup>	2.2083(15)	O3 <sup>1</sup> —Cd1—O3	92.86(8)
Cd1—O3	2.2083(15)	O3—Cd1—O1 <sup>1</sup>	99.10(6)
Cd1—O1 <sup>1</sup>	2.3301(15)	O3—Cd1—O1	141.89(5)
Cd1—O2 <sup>1</sup>	2.3752(15)	O3 <sup>1</sup> —Cd1—O1 <sup>1</sup>	141.89(5)
Cd1—O2	2.3753(15)	O3 <sup>1</sup> —Cd1—O1	99.10(6)
		O3—Cd1—O2 <sup>1</sup>	126.04(6)
		O3—Cd1—O2	87.88(5)
		O3 <sup>1</sup> —Cd1—O2	126.04(6)
		O3 <sup>1</sup> —Cd1—O2 <sup>1</sup>	87.88(5)

Symmetry codes: <sup>1</sup>2-x,-1+y,2-z

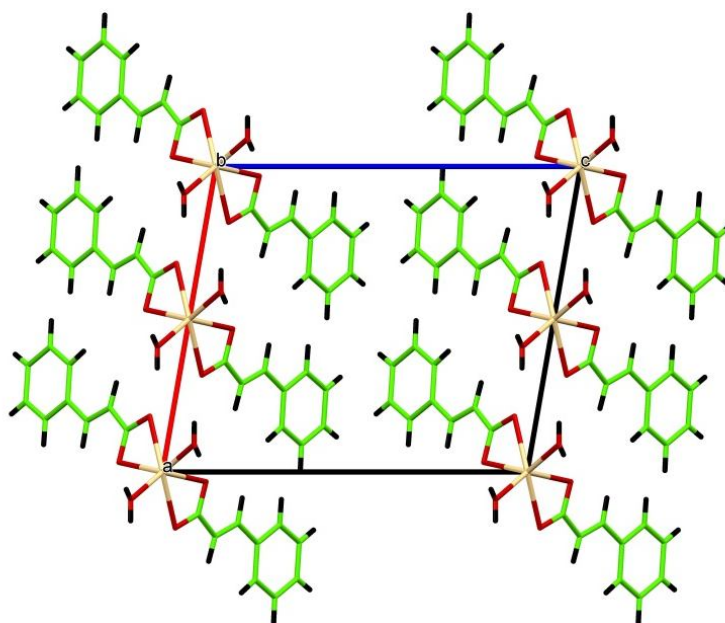


**Figure 56.** Packing diagram of  $\text{Cd}(\text{Cin})_2(\text{H}_2\text{O})_2$  plotted down b axis.

In the crystal structure strong hydrogen bonding interactions O—H...O between hydrogen atom of the coordinated water and an oxygen atom of the cinnamate ligand O3—H3A...O1<sup>1</sup>, O3—H3B...O2<sup>2</sup> and O8—H8...O3<sup>3</sup> (<sup>1</sup>2-x,-1+y,2-z; <sup>2</sup>3/2-x,-1/2+y,2-z; <sup>3</sup>3/2-x,1/2+y,2-z) were observed to form the one dimensional supramolecular chain (**Figure 57**).



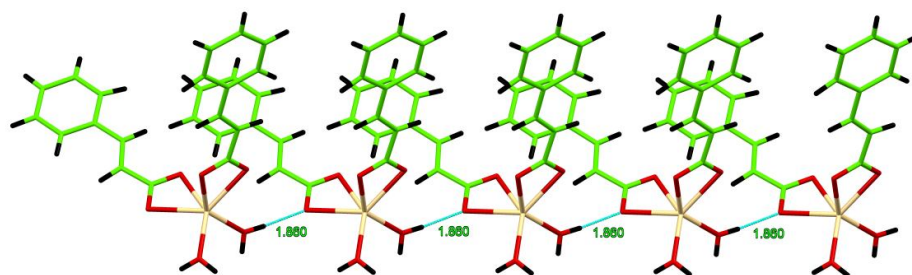


**Figure 57.** View of the supramolecular network via O–H...O interactions.

### Structural description of $[\text{Zn}(4,4'\text{-bpy})_{0.5}(\text{Cin})_2]_n$ (**2**)

X-ray analysis revealed that complex crystallized in the trigonal system, space group  $R\bar{3}$ . The structure of complex exhibited a 3-D network when taking the zinc(II) atoms as connected nodes and the bpy and deprotonated Cin ligands as linkers. The coordination environment of Zn center is shown in **Figure 58**. The coordination mode of carboxylate group from cin anion was monodentate bridging and bidentate chelating. Each Zn(II) atom was five-coordinate by one nitrogen atom from 4,4'-bpy ligand, four oxygen atoms from three cinnamate anions to form a distorted square-pyramidal coordination geometry.

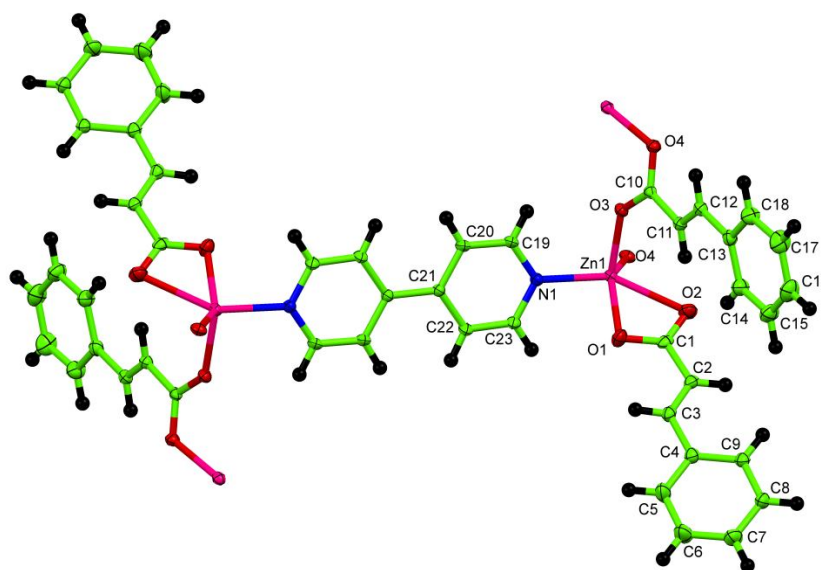


**Figure 58.** Molecular structure of  $[\text{Zn}(4,4'\text{-bpy})_{0.5}(\text{Cin})_2]_n$  (ellipsoid probability at 50%).

The coordinating bond lengths of complex varied from 1.9717(11) to 2.3549(14) for Zn-O and 2.0711(13) Å for Zn-N; the coordinating bond angles around Zn ion were in the range 59.23(5) - 134.09(5)° (**Table 6**) similar to those found in  $[\text{Zn}_2(\text{L})(\text{HCOO})(\text{bpy})_2]\cdot\text{H}_2\text{O}$  (Kuai *et al.*, 2013). The molecular packing of complex plotted along the c axis is shown in **Figure 59**.

**Table 6.** Selected bond distances and angles of  $[\text{Zn}(4,4'\text{-bpy})_{0.5}(\text{Cin})_2]_n$ .

Bond lengths (Å)		Bond angles (°)	
Zn1 — O1	2.0247(13)	O1 — Zn1 — O2	59.23(5)
Zn1 — O2	2.3549(14)	O1 — Zn1 — N1	89.97(5)
Zn1 — O3	1.9892(11)	O3 — Zn1 — O1	123.41(5)
Zn1 — O4 <sup>1</sup>	1.9717(11)	O3 — Zn1 — O2	101.65(5)
Zn1 — N1	2.0711(13)	O3 — Zn1 — N1	97.61(5)
		O4 <sup>1</sup> — Zn1 — O1	134.09(5)
		O4 <sup>1</sup> — Zn1 — O2	90.09(5)
		O4 <sup>1</sup> — Zn1 — O3	93.82(5)
		O4 <sup>1</sup> — Zn1 — N1	112.60(5)

Symmetry codes:  $^12/3-y, -2/3+x-y, 1/3+z$

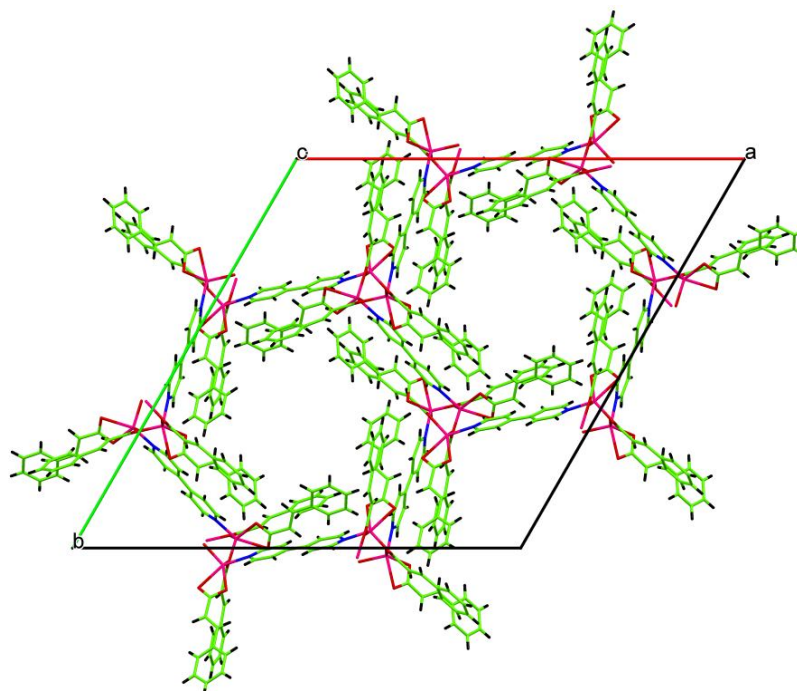


**Figure 59.** Packing diagram of  $[\text{Zn}(4,4'\text{-bpy})_{0.5}(\text{Cin})_2]$  plotted down c axis.

Moreover, the existing  $\pi$ - $\pi$  interactions between aromatic rings of 4,4'-bpy and Cin ligand with centroid-to-centroid distance of 3.684 Å (**Figure 60**) indicated strong  $\pi$ - $\pi$  stacking interactions in these 3D network, which gave advantage for the thermal stability of the complex.

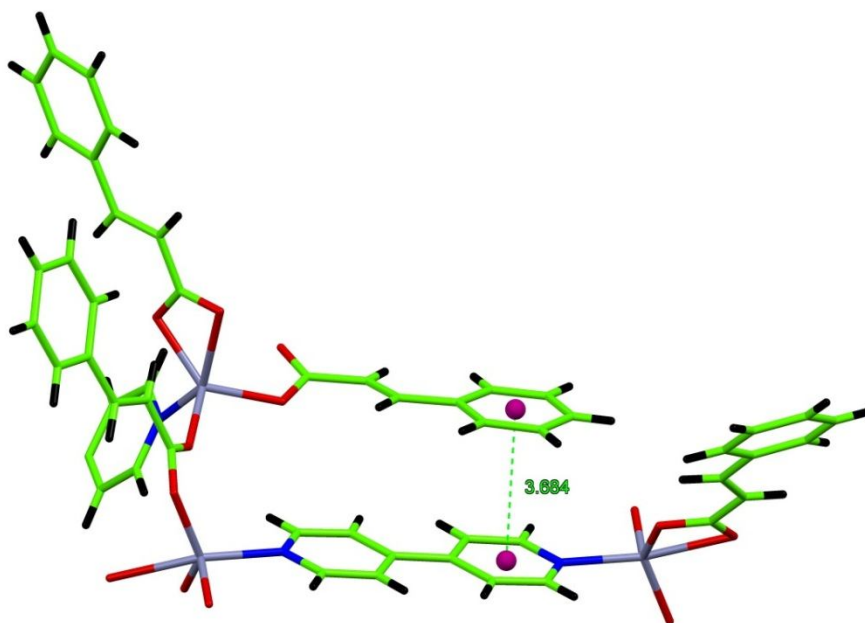


**Figure 60.** The  $\pi$ - $\pi$  interactions between aromatic rings of 4,4'-bpy and Cin ligand.

### Structural description of $[\text{Cd}_3(4,4'\text{-bpy})_2(\text{cin})_6(\text{H}_2\text{O})_2]_n$ (**3**)

Single crystal X-ray diffraction analyses showed that complex crystallized in the triclinic system, space group  $P\bar{1}$ . The cadmium atoms exhibited two different coordination modes; Cd(1) was seven-coordinated with a distorted pentagonal bipyramidal geometry defined by five oxygen atom from carboxylate group of cinnamate ligand locate at the equatorial plane and two nitrogen atom from 4,4'-bpy ligand locate at the axial position. The 4,4'-bpy and cinnamate ligand acted as a bridging ligands to join center Cd(II) atom into 2-D infinite layer. The Cd(2) coordinated to four oxygen atoms from four cinnamate units and two oxygen atoms from two coordinated water molecule forming a distorted octahedral geometry (**Figure 61**). The carboxylate group of cinnamate containing O6 and O6a were monodentate ligand and the other carboxylate group containing O4 and O4a acted as a bridging ligand linking the adjacent Cd(II) ions. The Cd(1)-O bond associated with

the chelating and bridging lengths are 2.231(2) - 2.500(2) Å and Cd(1)–N bond lengths was 2.269(2) Å similar to those observed in  $\{\text{Cd}(\text{L})_{0.5}(\text{pydc})\cdot 0.5\text{H}_2\text{O}\}_n$  (Ge *et al.*, 2014). The Cd(2)–O bond lengths were 2.284(3) - 2.358(2) Å. The Selected bond lengths and bond angles are given in **Table 7** and molecular packing of complex plotted along the b axis is shown in **Figure 62**.

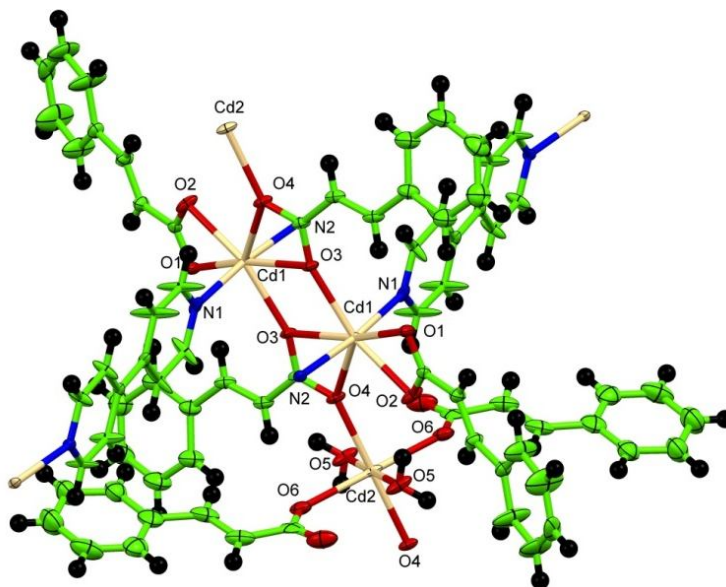


**Figure 61.** Molecular structure of  $[\text{Cd}_3(4,4'\text{-bpy})_2(\text{cin})_6(\text{H}_2\text{O})_2]_n$  (ellipsoid probability at 50%).

**Table 7.** Selected bond distances and angles of  $[\text{Cd}_3(4,4'\text{-bpy})_2(\text{cin})_6(\text{H}_2\text{O})_2]_n$  (**3**).

Bond lengths (Å)		Bond angles (°)	
Cd1—O1	2.423(3)	O1—Cd1—O3 <sup>1</sup>	167.22(8)
Cd1—O2	2.321(2)	O1—Cd1—O4 <sup>1</sup>	138.33(7)
Cd1—O3 <sup>1</sup>	2.500(2)	O2—Cd1—O1	54.96(8)
Cd1—O3	2.354(2)	O2—Cd1—O3	149.16(8)
Cd1—O4 <sup>1</sup>	2.434(2)	O2—Cd1—O3 <sup>1</sup>	136.09(8)
Cd1—N1	2.269(2)	O2—Cd1—O4 <sup>1</sup>	83.54(8)
Cd2—O4 <sup>3</sup>	2.358(2)	O3—Cd1—O1	94.50(8)
Cd2—O4	2.358(2)	N1—Cd1—O1	96.31(11)
Cd2—O6	2.284(3)	N1—Cd1—O2	98.17(9)
Cd2—O6 <sup>3</sup>	2.284(3)	O4 <sup>3</sup> —Cd2—O4	180.0
		O5 <sup>3</sup> —Cd2—O4 <sup>3</sup>	89.30(8)
		O5—Cd2—O4 <sup>3</sup>	90.70(8)
		O5 <sup>3</sup> —Cd2—O6	92.71(11)
		O5 <sup>3</sup> —Cd2—O6 <sup>3</sup>	87.29(11)
		O6—Cd2—O6 <sup>3</sup>	180.00(12)
		O6—Cd2—O4	86.24(8)

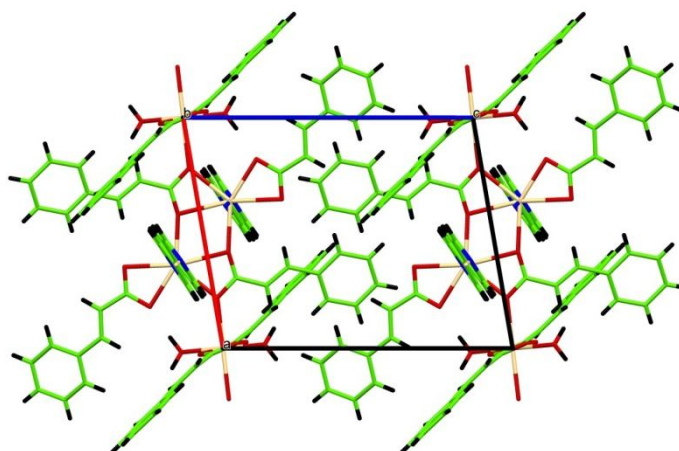


**Figure 62.** Packing diagram of  $[\text{Cd}_3(4,4'\text{-bpy})_2(\text{cin})_6(\text{H}_2\text{O})_2]_n$  plotted down  $b$  axis.

In addition, O–H ... O hydrogen bond (**Table 8**) was generated by hydrogen atom of water molecule and oxygen atom of chelating cinnamate ligand (**Figure 63**).

**Table 8.** Hydrogen-bond geometry ( $\text{\AA}$ ,  $^\circ$ ) of  $[\text{Cd}_3(4,4'\text{-bpy})_2(\text{cin})_6(\text{H}_2\text{O})_2]_n$  (**3**).

$D\text{---}H\cdots A$	$D\text{---}H$	$H\cdots A$	$D\cdots A$	$D\text{---}H\cdots A$
$\text{O5---H5A}\cdots\text{O2}^1$	0.87	1.82	2.682(4)	169.5

Symmetry codes:  $^11-x, 1-y, -z$

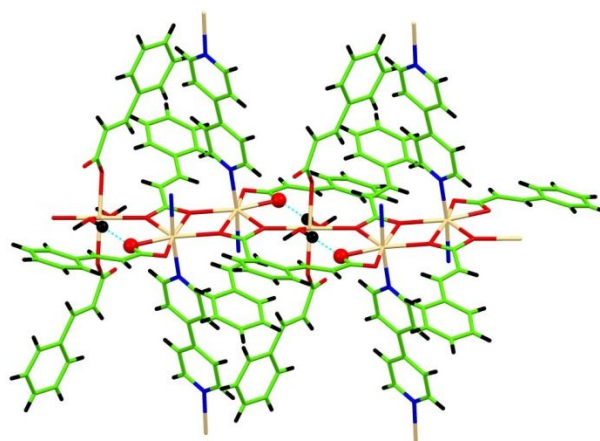


**Figure 63.** O–H ... O hydrogen bond between hydrogen atom of water molecule and oxygen atom of cinnamate ligand.

### Structural description of $[\text{Cd}(4,4'\text{-bpy})(3\text{-Npt})(\text{H}_2\text{O})]_n$ (**4**)

The crystal structure determination showed that complex (**4**) crystallized in monoclinic crystal system of space group  $P2_1/n$ . Molecular structure of the complex is shown in **Figure 64**. The asymmetric unit contained one Cd(II) cation, one 4,4'-bipyridine ligand, one deprotonated 3-Nitroptalic acid, and one coordinated water molecule. The coordination geometry of Cd(II) atom was distorted octahedral environment to three oxygen atoms from two 3-Npt anions, one oxygen atom from coordination water molecule, and two N atoms from two 4,4'-bpy ligands.

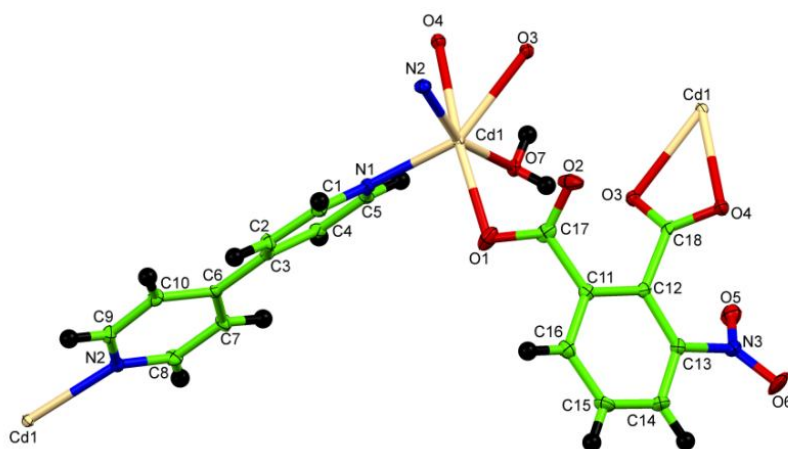


**Figure 64.** Molecular structure of  $[\text{Cd}(4,4'\text{-bpy})(3\text{-Npt})_2(\text{H}_2\text{O})]_n$  (ellipsoid probability at 50%).

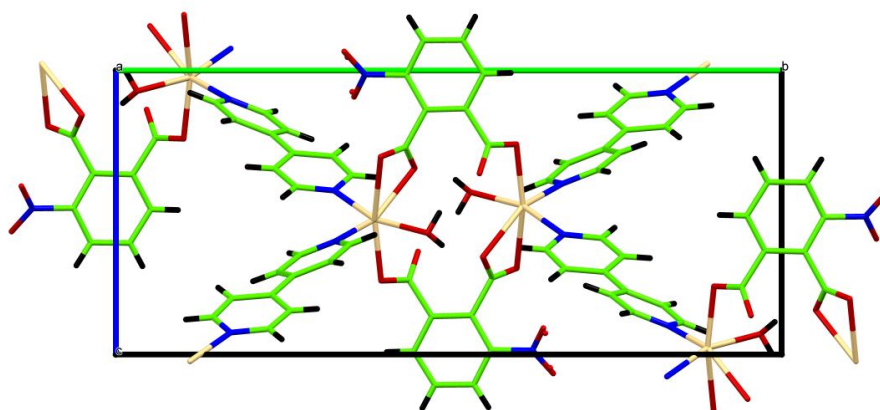
The Cd–O bond distances were in the range of 2.283(3)–2.496(3)Å, and the Cd–N bond distances range from 2.286(3)–2.316(3)Å similar to those found in other Cd(II) compounds (Cha *et al.*, 2013). The molecular packing of complex plotted along the a axis is shown in **Figure 65**. Two adjacent Cd(II) atom were firstly coordinated together by a pair of 3-Npt anions with the bidentate bridging and monodentate coordination modes and 4,4'-bpy ligand acted as a typical bis-monodentate linkers to join Cd(II) atom into two-dimensional layers propagating along the a axis. The selected bond lengths and bond angles are given in **Table 9**.



**Table 9.** Selected bond distances and angles of  $[\text{Cd}(4,4'\text{-bpy})(3\text{-Npt})(\text{H}_2\text{O})]_n$  (**4**).

Bond lengths (Å)		Bond angles (°)	
Cd1 — O1	2.2832(17)	O1 — Cd1 — N1	88.78(6)
Cd1 — N1	2.2864(17)	O1 — Cd1 — N2 <sup>1</sup>	104.41(6)
Cd1 — N2 <sup>1</sup>	2.3165(17)	N1 — Cd1 — N2 <sup>1</sup>	104.69(7)
Cd1 — O7	2.3478(14)	O1 — Cd1 — O7	85.27(5)
Cd1 — O3 <sup>2</sup>	2.3528(14)	N1 — Cd1 — O7	89.39(6)
Cd1 — O4 <sup>2</sup>	2.4969(15)	N2 <sup>1</sup> — Cd1 — O7	162.87(6)
		O1 — Cd1 — O3 <sup>2</sup>	124.54(6)
		N1 — Cd1 — O3 <sup>2</sup>	143.77(6)
		N2 <sup>1</sup> — Cd1 — O3 <sup>2</sup>	82.18(6)

Symmetry codes: <sup>1</sup>-x,1-y,1-z; <sup>2</sup>1+x,3/2-y,-1/2+z; <sup>3</sup>-1+x,3/2-y,1/2+z

**Figure 65.** Packing diagram of  $[\text{Cd}(4,4'\text{-bpy})(3\text{-Npt})_2(\text{H}_2\text{O})]_n$  plotted down a axis.

The intramolecular hydrogen bonds interaction (**Table 10**) between hydrogen atoms of water molecule and carboxylate oxygen atoms are shown in **Figure 66**.

**Table 10.** Hydrogen-bond geometry (Å, °) of  $[\text{Cd}(4,4'\text{-bpy})(3\text{-Npt})(\text{H}_2\text{O})]_n$  (**4**).

$D\text{—}H\cdots A$	$D\text{—}H$	$H\cdots A$	$D\cdots A$	$D\text{—}H\cdots A$
O7—H7A $\cdots$ O2 <sup>1</sup>	0.82	1.98	2.761(2)	158.9
O7—H7B $\cdots$ O3	0.81	1.91	2.690(2)	161.0

Symmetry codes: <sup>1</sup>-x,1-y,1-z

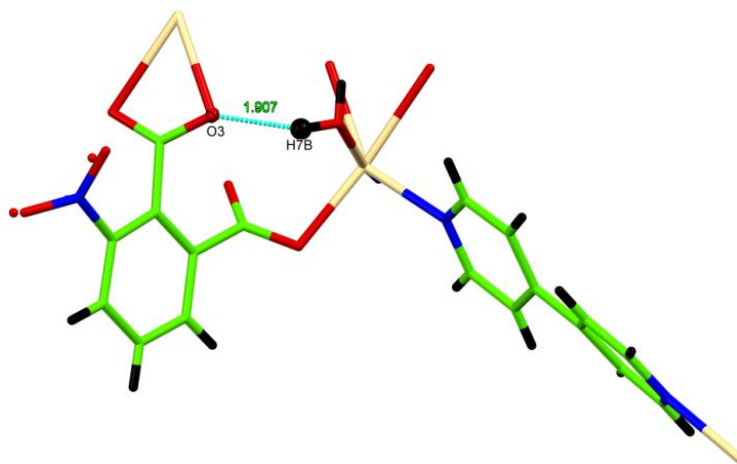


**Figure 66.** Intramolecular hydrogen bond interaction of  $[\text{Cd}(4,4'\text{-bpy})(3\text{-Npt})(\text{H}_2\text{O})]_n$ .

#### Structural description of $[\text{Mn}_2(\text{bpp})(3\text{-Npt})_2(\text{H}_2\text{O})_2]_n$ (**5**)

From X-ray crystallographic data of complex (**5**), the complex crystallized in a non-centrosymmetric in the orthorhombic system space group *Aba2*. The molecular structure of complex contained dinuclear manganese(II) as metal center while bpp and 3-Npt dianion acted as the linkers leading to two-dimensional coordination polymer. Both  $\text{Mn}^{2+}$  ions were coordinated by three oxygen atoms from two 3-Npt ligands and two oxygen atoms from two water molecules, and one nitrogen atom from a pyridine ring of bpp ligand (**Figure 67**).

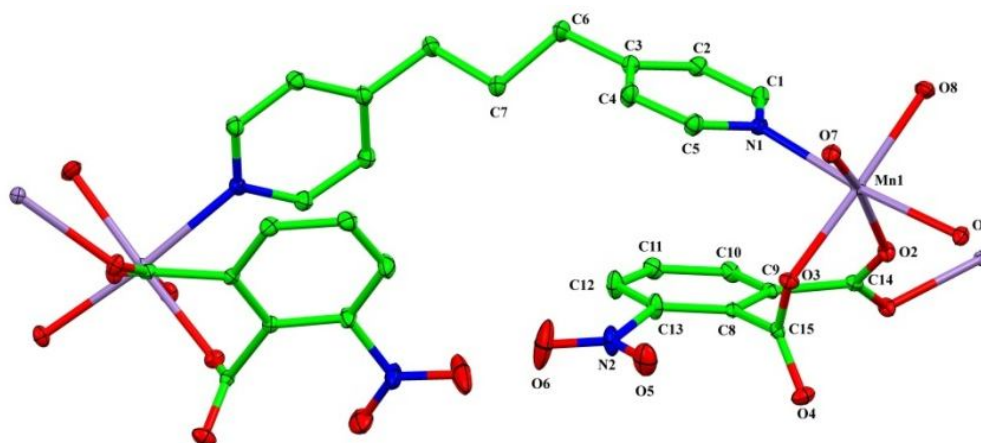


**Figure 67.** Molecular structure of  $[\text{Mn}_2(\text{bpp})(3\text{-Npt})_2(\text{H}_2\text{O})_2]_n$  (ellipsoid probability at 50%).



The Mn-O distances connected with the chelating/bridging 3-Npt ligands ranged from 2.1397 (17) to 2.2248 (15) Å and Mn-N distance 2.2539 (19) Å similar to those found in [Mn(H<sub>2</sub>O)<sub>2</sub>(3-nitrophthalate)](Yu *et al.*, 2014). The bond angles subtended at the Mn<sup>2+</sup> ions in the range of 164.81 (7)°- 177.99 (7)° and 82.61 (7)°- 96.73 (7)° (**Table 11**), respectively, giving a slight distorted octahedral geometry. One of the two carboxylate groups of 3-Npt adopted terminal monodentate bonding mode and Mn<sup>2+</sup> ion was linked to two adjacent ions through syn-anti mode from carboxylates of 3-Npt ligands, while the other bridged to neighboring Mn to form 2D polymer. In the molecular structure, bpp ligand adopted a TT (*trans-trans*) conformation with the N---N distance of 10.768 Å, similar to those reported in the literatures. The nitro group on 3-nitrophthalate ligand (N2, O5, O6) were found disordered over two positions with an occupancy ratio of 0.344(5) : 0.656(5).

**Table 11.** Selected bond distances and angles of [Mn<sub>2</sub>(bpp)(3-Npt)<sub>2</sub>(H<sub>2</sub>O)<sub>2</sub>]<sub>n</sub> (**5**).

Bond lengths (Å)		Bond angles (°)	
Mn1—O3	2.1397 (17)	O3—Mn1—O7	82.61 (7)
Mn1—O7	2.1640 (14)	O3—Mn1—O8	177.99 (7)
Mn1—O8	2.1703 (18)	O7—Mn1—O8	96.73 (7)
Mn1—O1 <sup>i</sup>	2.2068 (15)	O3—Mn1—O1 <sup>i</sup>	95.02 (7)
Mn1—O2	2.2248 (15)	O7—Mn1—O1 <sup>i</sup>	86.26 (6)
Mn1—N1	2.2539 (19)	O8—Mn1—O1 <sup>i</sup>	86.82 (7)
O1—Mn1 <sup>ii</sup>	2.2069 (15)	O3—Mn1—O2	85.36 (6)
		O7—Mn1—O2	164.81 (7)
		O8—Mn1—O2	95.59 (6)
		O1 <sup>i</sup> —Mn1—O2	85.59 (6)
		O3—Mn1—N1	90.51 (7)

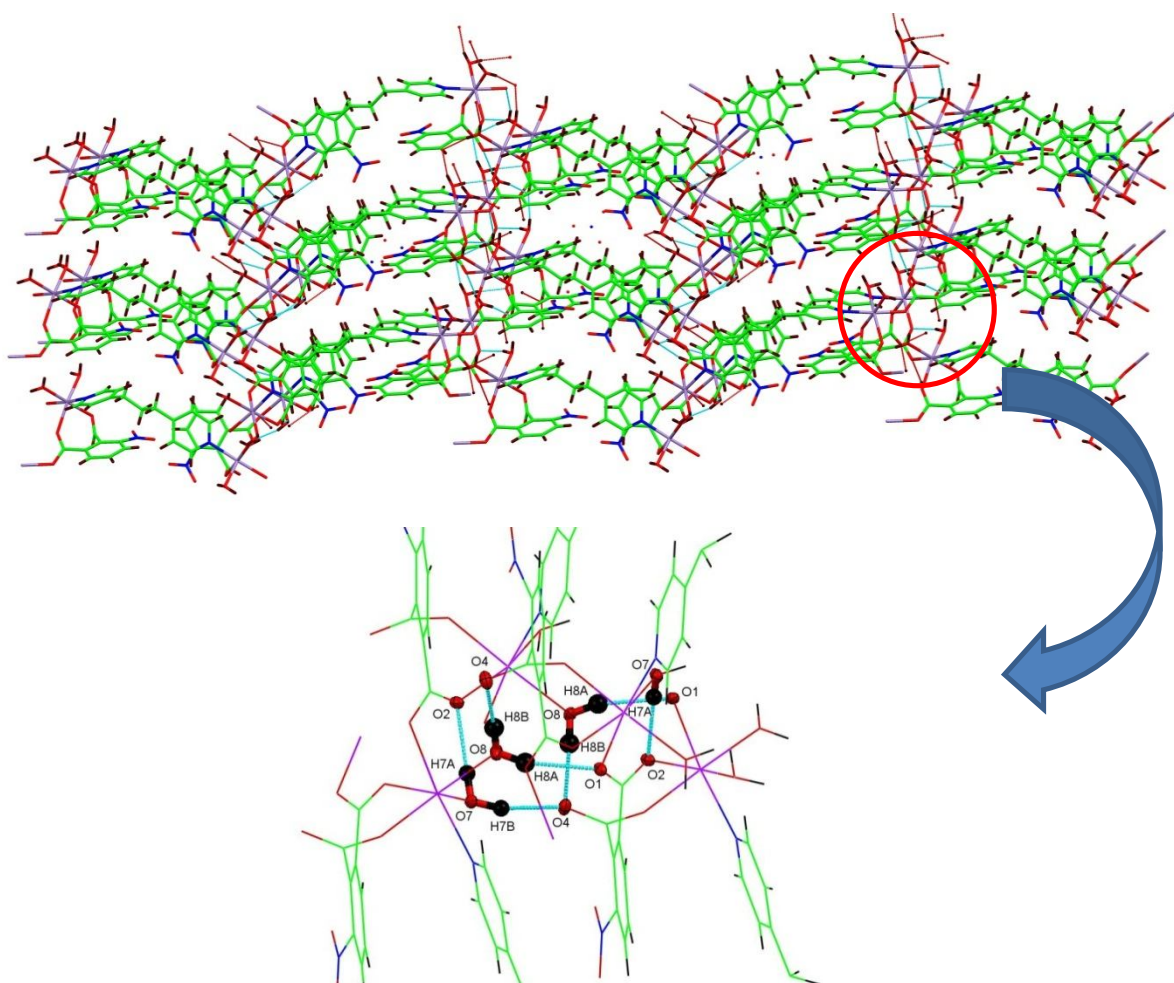
Symmetry codes: (i)  $-x+1/2, y+1/2, z$ ; (ii)  $-x+1/2, y-1/2, z$ .

Hydrogen bonds interaction (**Table 12**) between hydrogen of the coordinated water molecules and the oxygen atoms of the carboxylates were O7—H7A···O2<sup>i</sup>, O7—H7B···O4<sup>iv</sup>, O8—H8A···O1<sup>iv</sup>, and O8—H8B···O4<sup>v</sup> ((i)  $-x+1/2, y+1/2, z$ ; (iv)  $x, y+1/2, z+1/2$ ; (v)  $-x+1/2, y, z+1/2$ .) generating a 3-D supramolecular network as shown in **Figure 68**.

**Table 12.** Hydrogen-bond geometry (Å, °) of  $[\text{Mn}_2(\text{bpp})(3\text{-Npt})_2(\text{H}_2\text{O})_2]_n$  (**5**).

$D\text{---}H\cdots A$	$D\text{---}H$	$H\cdots A$	$D\cdots A$	$D\text{---}H\cdots A$
$\text{O7---H7A}\cdots\text{O2}^{\text{i}}$	0.84	1.95	2.769 (2)	163
$\text{O7---H7B}\cdots\text{O4}^{\text{iv}}$	0.84	1.81	2.623 (2)	162
$\text{O8---H8A}\cdots\text{O1}^{\text{iv}}$	0.83	2.09	2.898 (2)	165
$\text{O8---H8B}\cdots\text{O4}^{\text{v}}$	0.82	1.88	2.693 (2)	169

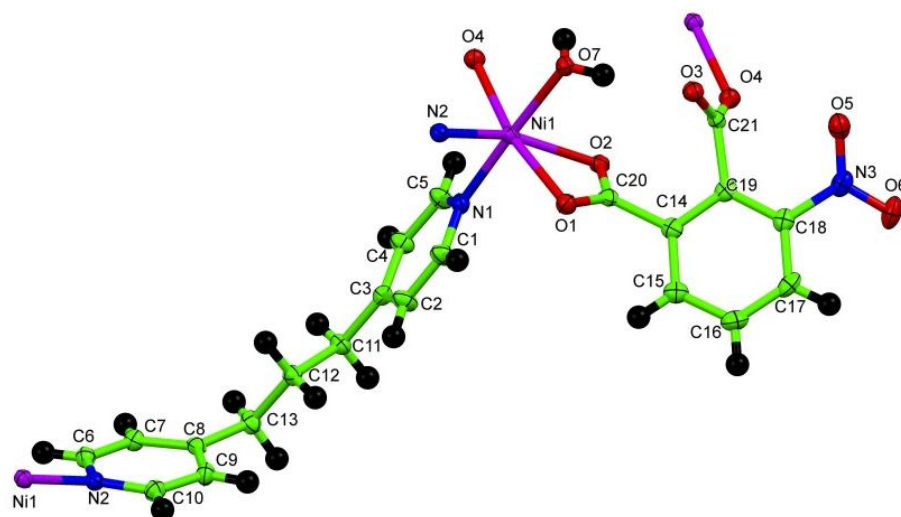
Symmetry codes: (i)  $-x+1/2, y+1/2, z$ ; (iv)  $x, y+1/2, z+1/2$ ; (v)  $-x+1/2, y, z+1/2$ .

**Figure 68.** View of the 3D supramolecular network via O—H---O interactions.

### Structural description of $[\text{Ni}(\text{bpp})(3\text{-Npt})(\text{H}_2\text{O})]_n$ (**6**)

Single-crystal X-ray analysis of complex (**6**) showed that the complex crystallized in a monoclinic system with space group,  $P2_1/n$ . Molecular structure of the complex is shown in **Figure 69**. In the asymmetric unit, the complex was

constructed from a 1D chain contains one Ni(II) ion, one bpp ligand, one 3-nitrophenolate anion and one coordinated water molecule. As shown in **Figure 69**, the Ni(II) ion is six coordinated by bonding to three oxygen atom from two 3-Npt anions, one oxygen atom from water molecule and two nitrogen atom from bpp ligand into a distorted octahedral geometry.

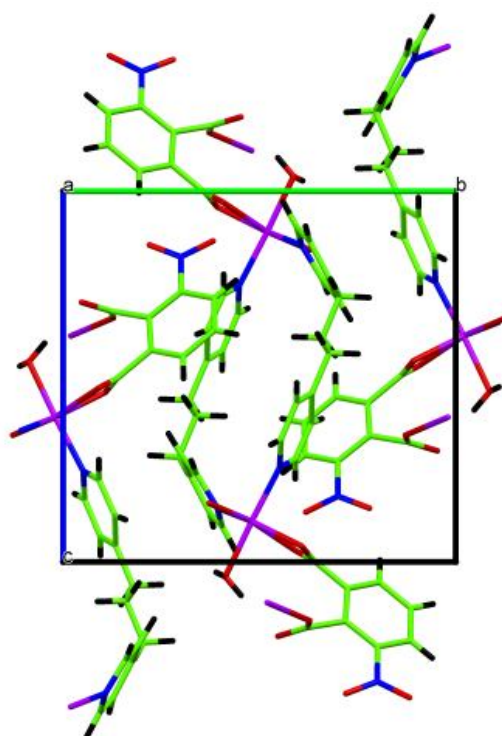


**Figure 69.** Molecular structure of  $[\text{Ni}(\text{bpp})(3\text{-Npt})_2(\text{H}_2\text{O})]_n$  (ellipsoid probability at 50%).

The Ni–O bond distances associated with the chelate and monodentate of 3-Npt ligands range from 2.0250 to 2.1734 Å and Ni – N bond distances range from 2.046 to 2.073 Å were in good agreement with the literature reports (Sanram *et al.*, 2016). The transoid and cisoid angles subtended at the Ni<sup>2+</sup> ions fit in the range of 168.13 (8)°- 177.05 (8)° and 82.95 (8)°- 97.33 (8)° (**Table 13**), respectively, exhibiting slight departure from the corresponding value expected for a regular octahedron geometry (theoretical values: 180° and 90°). In the crystal structure, bpp ligand adopted a TT (trans–trans) conformation with the N---N distance of 9.795 Å, similar to those reported in the literatures (Li *et al.*, 2015). The molecular packing of complex plotted along the a axis is shown in **Figure 70**.

**Table 13.** Selected bond distances and angles of  $[\text{Ni}(\text{bpp})(3\text{-Npt})(\text{H}_2\text{O})]_n(\mathbf{6})$ .

Bond lengths (Å)		Bond angles (°)	
Ni1 — N1	2.073(2)	O4 <sup>1</sup> — Ni1 — N2	91.67(8)
Ni1 — O1	2.1420(18)	O4 <sup>1</sup> — Ni1 — N1	97.33(8)
Ni1 — O4 <sup>1</sup>	2.0250(18)	N2 — Ni1 — N1	88.81(9)
Ni1 — N2	2.046(2)	O4 <sup>1</sup> — Ni1 — O7	82.95(8)
Ni1 — O7	2.1062(19)	N2 — Ni1 — O7	94.12(8)
Ni1 — O2	2.1734(18)	N1 — Ni1 — O7	177.05(8)
		O4 <sup>1</sup> — Ni1 — O1	168.13(8)
		N2 — Ni1 — O1	95.61(8)
		N1 — Ni1 — O1	92.19(8)

**Figure 70.** Packing diagram of  $[\text{Ni}(\text{bpp})(3\text{-Npt})_2(\text{H}_2\text{O})]_n$  plotted down *a* axis.

In addition, there are intramolecular strong hydrogen bonds interaction between the hydrogen atom of water molecule and oxygen atom of carboxylate group from 3-Npt ligand (**Figure 71**).

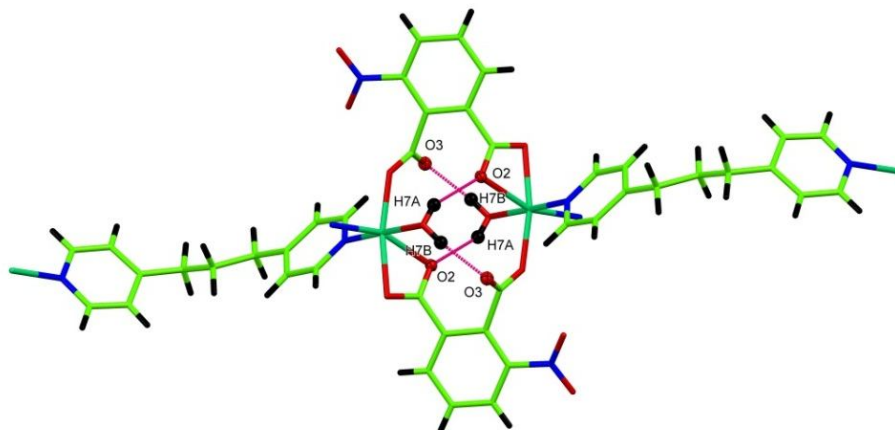


**Figure 71.** View of the hydrogen bonds interaction via strong O–H...O.

### Structural description of $\{[Ag_2(bpp)_2] \cdot (3-Npt)\}_n$ (7)

Single crystal X-ray diffraction analyses showed that complex crystallized in the orthorhombic system, space group  $Pnma$ . The asymmetric unit contained two Ag atoms, one 3-Npt dianion, two bpp ligands, and four crystallization water molecules. The lattice water molecules in complex could not be located due to disorder and was thus removed by using Olex solvent mask (**Figure 72**). Each Ag atoms was linked by nitrogen atoms from bpp ligand to form 1-D chain polymer.

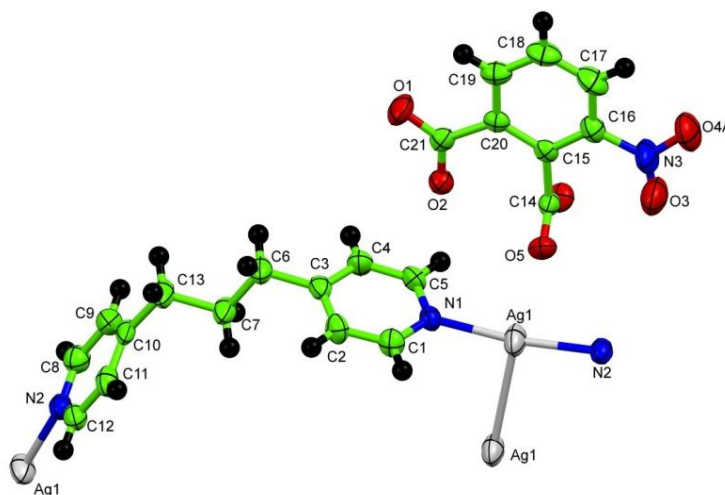


**Figure 72.** ORTEP representation of the asymmetric unit of  $\{[Ag_2(bpp)_2] \cdot (3-Npt)\}_n$  (Thermal ellipsoids are drawn at 40% probability).

The N–Ag–N bond angle was 170.99(8)°, and Ag–N distances ranging from 2.124(2) to 2.129(2) Å (**Table 14**), similar to those reported in the similar coordination complex of Ag (Jia *et al.*, 2016). The carboxylate groups of 3-Npt anion were terminal and not coordinated to the Ag atom, i.e. it acted as a counter-anion to compensate the charge of the  $[\text{Ag}_2(\text{bpp})_2]^{2+}$ . Interestingly, the Ag⋯Ag distance was 3.0153(5) Å, which was shorter than the sum of the van der Waals radii of silver 3.44 Å, indicating a weak Ag⋯Ag interactions. The coordination environment around Ag(I) ion was a linear geometry. The molecular packing of complex plotted along the b axis is shown in **Figure 73**.

**Table 14.** Selected bond distances and angles of  $\{[\text{Ag}_2(\text{bpp})_2]\cdot 3\text{-Npt}\}_n$  (**7**).

Bond lengths (Å)		Bond angles (°)	
Ag1 — Ag1 <sup>1</sup>	3.0153(5)	N1 — Ag1—Ag1 <sup>1</sup>	91.11(6)
Ag1 — N1	2.124(2)	N1 — Ag1—N2	170.99(8)
Ag1 — N2	2.129(2)	N2 — Ag1—Ag1 <sup>1</sup>	97.71(6)

Symmetry codes: <sup>1</sup>2-x,-y,1-z

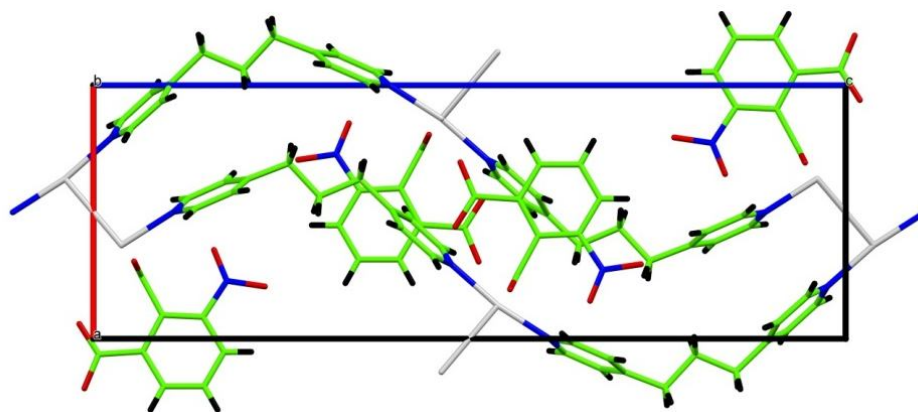


**Figure 73.** Packing diagram of  $\{[\text{Ag}_2(\text{bpp})_2]\cdot 3\text{-Npt}\}_n$  plotted down b axis.

The supramolecular sandwich-like structure was constructed by  $\pi$ — $\pi$  stacking interactions (**Figure 74**) with centroid–centroid distances of 3.759 Å between benzene ring from bpp ligand of 1D cationic chains  $[\text{Ag}(\text{bpp})]^{1+}$ .

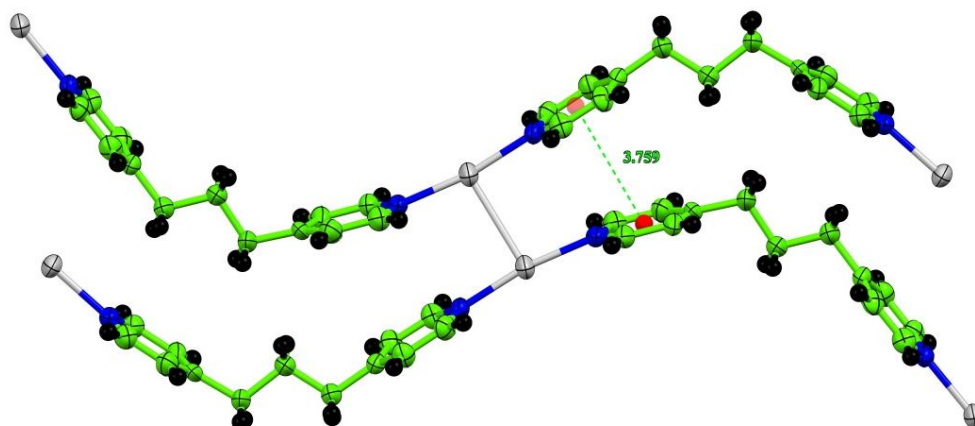


**Figure 74.**  $\pi$ — $\pi$  Stacking interactions of  $\{[Ag_2(bpp)_2] \cdot 3-Npt\}_n$ .

#### **Structural description of $\{[Ag_2(bpe)_2(3-Npt)] \cdot 7H_2O\}_n$ (8)**

Single crystal X-ray diffraction analyses showed that complex crystallized in the triclinic system, space group  $P\bar{1}$ . The asymmetric unit contained two Ag atoms, one 3-Npt ligand, two bpp ligands, and seven two crystallization water molecules. Molecular structure of the complex is shown in **Figure 75**. In the complex, the bpe ligand adopted a anti conformation, providing an N-to-N distance of 9.232 Å. The 3-Npt anion ligands linked each Ag atoms by oxygen donor atom of two carboxylate group from one 3-Npt. The Ag atom center had T-shaped coordination geometry, where each Ag atom were linked by nitrogen atoms from bpe ligand to form 1-D and further linked by oxygen atoms from 3-Npt ligand to form 2-D sheets.



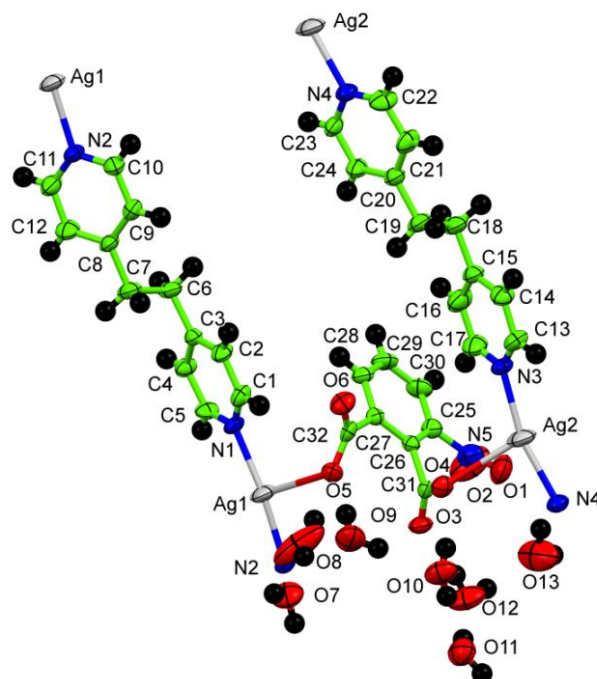


**Figure 75.** ORTEP representation of the asymmetric unit of  $\{[Ag_2(bpe)_2(3-Npt)] \cdot 7H_2O\}_n$  (Thermal ellipsoids are drawn at 50% probability).

The Ag–N bond distances ranged from 2.143(4) and 2.148(4) Å (**Table 15**), and N–Ag–N bond angles were 165.72° to 169.99°, The Ag...O bond lengths were 2.678 Å for Ag1 and 2.711 Å for Ag2 similar to those observed in similar complexes (Min *et al.*, 2015). The molecular packing of complex plotted along the *a* axis is shown in **Figure 76**.

**Table 15.** Selected bond distances and angles of  $\{[Ag_2(bpe)_2(3-Npt)] \cdot 7H_2O\}_n$  (**8**).

Bond lengths (Å)		Bond angles (°)	
Ag1 — N1	2.143(4)	N1 — Ag1 — N2 <sup>1</sup>	169.99(16)
Ag1 — N2 <sup>1</sup>	2.148(4)	N3 — Ag2 — N4 <sup>1</sup>	165.72(15)

Symmetry codes: <sup>1</sup>1+x,-1+y,+z



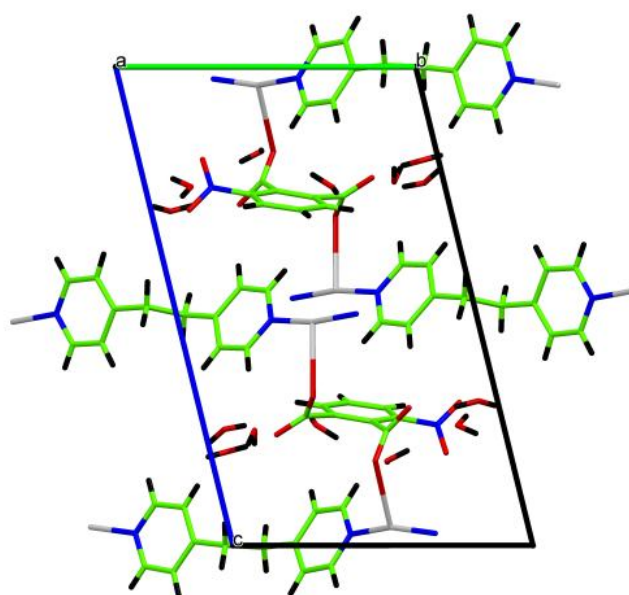


**Figure 76.** Packing diagram of  $\{[Ag_2(bpe)_2(3-Npt)] \cdot 7H_2O\}_n$  plotted down a axis.

Strong hydrogen bonding interactions  $O-H \cdots O$  between hydrogen atom of the crystallization water molecules and an oxygen atom of the 3-Npt anion ligand [ $O7-H7D \cdots O6^1$ ,  $O9-H9B \cdots O5$ ,  $O12-H12A \cdots O3$  and  $O13-H13A \cdots O6^2$  ( $^11+x,y,z$ ;  $^2+x,-1+y,z$ )] and between the crystallization water and water molecules [ $O8-H8B \cdots O7$ ,  $O9-H9A \cdots O10$ ,  $O12-H12B \cdots O13$ ,  $O11-H11A \cdots O7^2$ ,  $O11-H11B \cdots O12$  and  $O10-H10A \cdots O4$  ( $^2+x,-1+y,z$ )] were observed (**Figure 77**), which help support them into the three dimensional supramolecular network as well as help the molecular structure more stable.

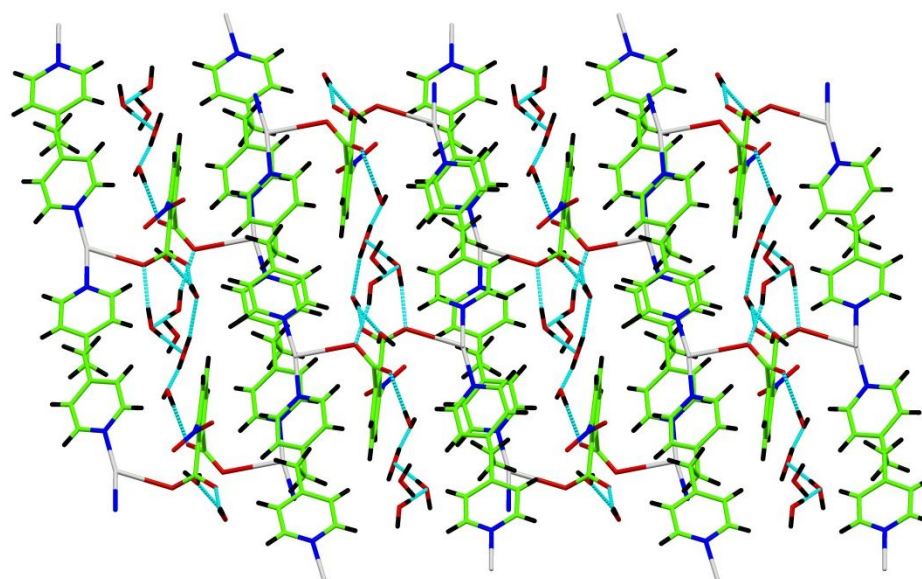


**Figure 77.** 3-D supramolecular network by hydrogen bonding.

### Structural description of $[\text{Zn}(\text{bpp})_2(\text{Sal})_2]_n$ (**9**)

Single crystal X-ray diffraction analyses showed that complex (**9**) crystallized in the monoclinic space group  $P2_1/n$ . The 1-D coordination polymer was formed by the reaction between  $\text{Zn}(\text{ac})_2 \cdot 2\text{H}_2\text{O}$ , bpp, and aspirin in mixtures of methanol and water solution. In the reaction, acetoxy group of aspirin underwent cleavage of the covalent bond in a molecule by reaction with water and base (hydrolysis process) to give the salicylate ligand. The asymmetric unit contained one Zn(II), one bpp ligand and two salicylate anions as shown in **Figure 78**. The Zn center adopted tetrahedral geometry by coordinating to two oxygen atoms from two monodentate salicylate anions and two nitrogen atoms from two bpp ligands. The distortion of the tetrahedron was detected by the calculated value of the  $\tau_4$  parameter to describe the geometry around metal center. From the equation  $\tau_4 = \frac{360 - (\alpha + \beta)}{360 - 2\theta}$  where  $\alpha$  and  $\beta$  are the largest angles around the metal centers of perfect tetrahedral geometry ( $\tau_4 = 1$ ) and perfect square-planar geometry ( $\tau_4 = 0$ ) (Di *et al*, 2010). The value of the  $\tau_4$  of complex (**9**) was 0.84 indicating the coordination geometry around Zn ion was distorted tetrahedral.

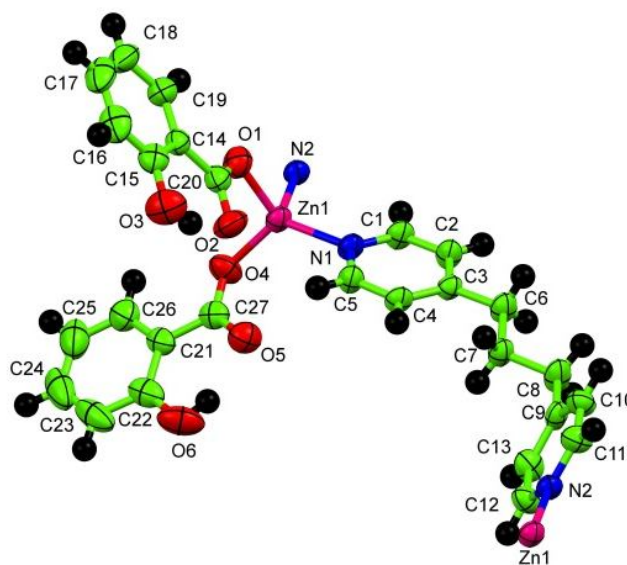


**Figure 78.** ORTEP representation of the asymmetric unit of  $[\text{Zn}(\text{bpp})_2(\text{Sal})_2]_n$  (Thermal ellipsoids are drawn at 50% probability).

The selected bond lengths and bond angles are given in **Table 16**. Zn metal centers were bridged by bpp ligands to generate 1D chain. The Zn-O bond distances ranged from 1.9275(18) and 1.9453(17) Å, and the Zn-N bond lengths were 2.0098 and 2.0589 Å similar to that found in  $[\text{Zn}(\text{imbz})(\mu_2\text{-OH})]_n$  (Xu *et al.*, 2009). In this structure, bpp molecule adopted a TT (*trans-trans*) conformation with the N-to-N distance of 9.866 Å, similar to those reported in the literatures (Lucia *et al.*, 2002). The molecular packing of complex plotted along the *a* axis is shown in **Figure 79**.

**Table 16.** Selected bond distances and angles of  $[\text{Zn}(\text{bpp})_2(\text{Sal})_2]_n$  (**9**).

Bond lengths (Å)		Bond angles (°)	
Zn1 — O1	1.9453(17)	O1 — Zn1 — N1	119.58(8)
Zn1 — O4	1.9272(18)	O1 — Zn1 — N2 <sup>1</sup>	96.91(8)
Zn1 — N1	2.0098(18)	O4 — Zn1 — O1	107.73(8)
Zn1 — N2 <sup>1</sup>	2.0589(17)	O4 — Zn1 — N1	121.32(8)
		O4 — Zn1 — N2 <sup>1</sup>	98.91(7)
		N1 — Zn1 — N2 <sup>1</sup>	107.22(7)

Symmetry codes: <sup>1</sup>1+x,+y,+z

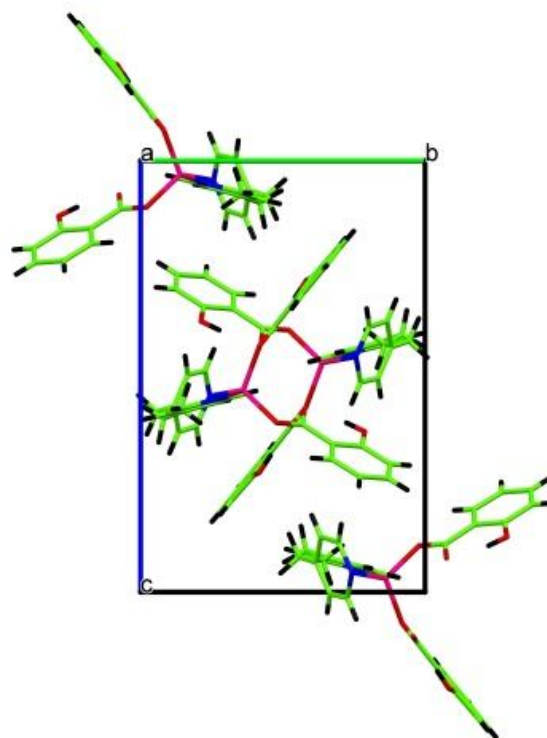


**Figure 79.** Packing diagram of  $[\text{Zn}(\text{bpp})_2(\text{Sal})_2]_n$  plotted down *a* axis.

The strong hydrogen bonds showed intramolecular interaction between the hydrogen atom of hydroxyl group and oxygen atom of carboxylate group from sal ligand as shown in **Figure 80**. The molecular structure of complex was stabilized intermolecular  $\text{O}-\text{H}\cdots\text{O}$ . The details of the intramolecular H-bonding are listed in **Table 17**.

**Table 17.** Hydrogen-bond geometry ( $\text{\AA}$ ,  $^\circ$ ) of  $[\text{Zn}(\text{bpp})_2(\text{Sal})_2]_n$  (**9**).

$D-\text{H}\cdots A$	$D-\text{H}$	$\text{H}\cdots A$	$D\cdots A$	$D-\text{H}\cdots A$
$\text{O}3-\text{H}3\cdots\text{O}2$	0.82	1.82	2.547(3)	146.8
$\text{O}6-\text{H}6\cdots\text{O}5$	0.82	1.81	2.540(3)	147.2

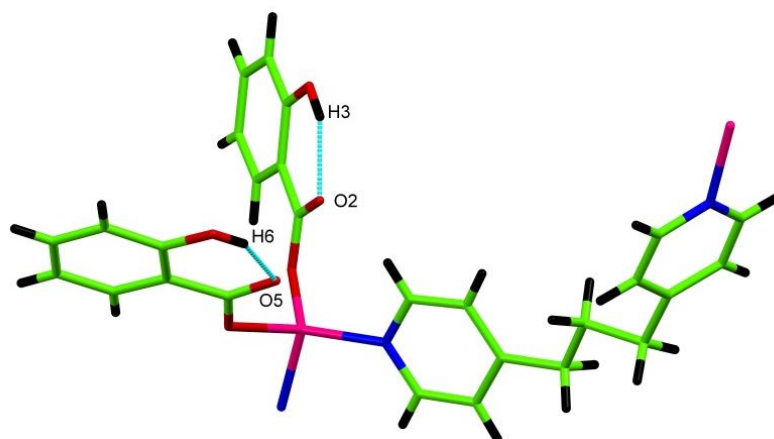


**Figure 80.** Intramolecular interaction via strong O–H---O interactions.

### Structural description of $[\text{Zn}_2(\text{bpe})_2(\text{Sal})_4]$ (10)

Single crystal X-ray diffraction analyses showed that complex crystallized in the triclinic space group  $P\bar{1}$ . The selected bond lengths and bond angles are given in **Table 18**. Molecular structure of the complex is shown in **Figure 81**. In the structure, aspirin was hydrolyzed to salicylic acid similar to complex (9). The two  $\text{Zn}^{\text{II}}$  ions coordinated to two oxygen atoms each one from a monodentate salicylate ligands, and two nitrogen atoms of bpe ligands.

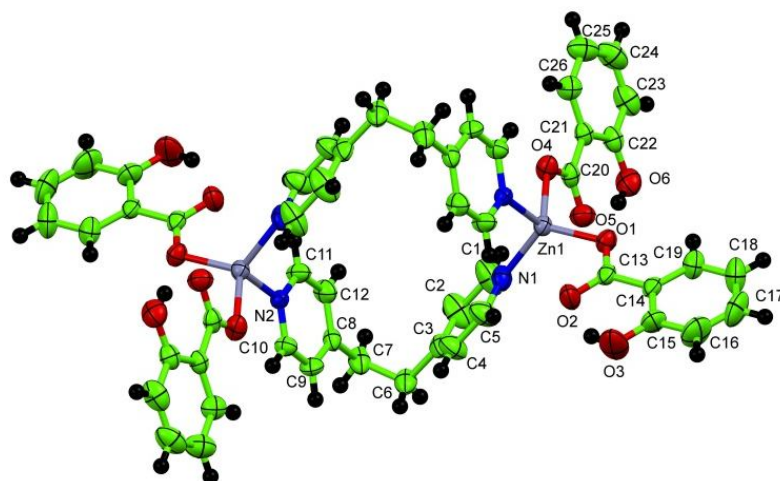


**Figure 81.** ORTEP representation of the asymmetric unit of  $[\text{Zn}_2(\text{bpe})_2(\text{Sal})_4]$  (Thermal ellipsoids are drawn at 50% probability).

The zinc centers were connected by the bpe ligands into Zn-bpe-Zn dinuclear, N-to-N distance of bpe ligands was 6.435 Å providing a Zn···Zn separation of 8.867 Å. The bpe ligand adopted a gauche-conformation with the C-CH<sub>2</sub>-CH<sub>2</sub>-C torsion angle of 62.45°. The Zn—N distances were 2.052(2) and 2.052(3), while the O—Zn—O, O—Zn—N and N—Zn—N angle were in a range 108.12(9), 96.29(9) - 119.51(10) and 106.07(9), respectively. The bond lengths and bond angles indicating that coordination geometry around Zn atoms were slight distorted tetrahedral. The molecular packing of complex plotted along the b axis is shown in **Figure 82**.

**Table 18.** Selected bond distances and angles of [Zn<sub>2</sub>(bpe)<sub>2</sub>(Sal)<sub>4</sub>] (**10**).

Bond lengths (Å)		Bond angles (°)	
Zn1 — O1	1.9574(19)	O1 — Zn1 — O4	108.12(9)
Zn1 — O4	1.971(2)	O1 — Zn1 — N1	119.51(10)
Zn1 — N1	2.052(3)	O1 — Zn1 — N2 <sup>1</sup>	110.38(9)
Zn1 — N2 <sup>1</sup>	2.052(2)	O4 — Zn1 — N1	113.94(10)
		O4 — Zn1 — N2 <sup>1</sup>	96.29(9)
		N1 — Zn1 — N2 <sup>1</sup>	106.07(9)

Symmetry codes: <sup>1</sup>1-x,-y,1-z

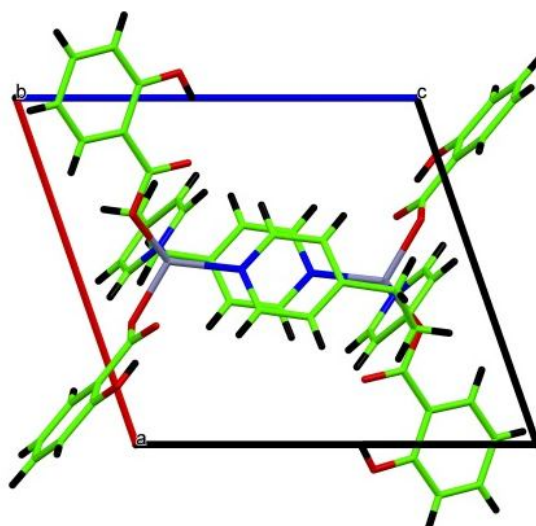


**Figure 82.** Packing diagram of [Zn<sub>2</sub>(bpe)<sub>2</sub>(Sal)<sub>4</sub>] plotted down b axis.

In addition, the strong hydrogen bonds (O—H···O) showed intramolecular interaction between the hydrogen atom of hydroxyl group and oxygen atom (acceptor)

of carboxylate group from sal ligand as shown in **Figure 83**. The details of the hydrogen bond are listed in **Table 19**.

**Table 19.** Hydrogen-bond geometry (Å, °) of  $[\text{Zn}_2(\text{bpe})_2(\text{Sal})_4]$  (**10**).

$D-H\cdots A$	$D-H$	$H\cdots A$	$D\cdots A$	$D-H\cdots A$
$\text{O3}-\text{H3}\cdots\text{O2}$	0.82	1.82	2.545(4)	146.6
$\text{O6}-\text{H6}\cdots\text{O5}$	0.82	1.81	2.545(3)	147.8
$\text{C1}-\text{H1}\cdots\text{O5}$	0.93	2.55	3.198(4)	127.2
$\text{C5}-\text{H5}\cdots\text{O2}$	0.93	2.45	3.109(4)	128.2
$\text{C11}-\text{H11}\cdots\text{O3}^{\dagger}$	0.93	2.35	3.111(4)	139.0

Symmetry codes: 1-1+x,+y,+z

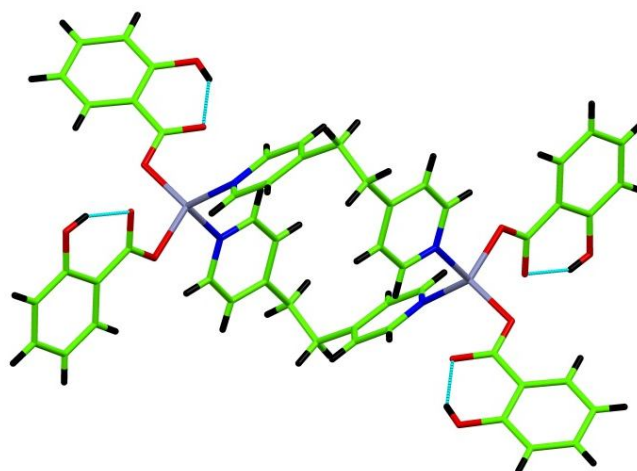


**Figure 83.** View of the hydrogen bond via strong O-H---O interactions.

#### Structural description of $\{[\text{Co}(\text{bpp})_2(\text{H}_2\text{O})_2]\cdot(4\text{-abs})_2\cdot\text{H}_2\text{O}\}_n$ (**11**)

Single crystal X-ray diffraction analyses showed that complex crystallized in the triclinic system, space group  $P\bar{1}$ . The asymmetric unit contained one Co(II) atom, two bpp ligands, two coordinated water molecule, one crystallization water molecule, and two uncoordinated Abs anions. The central Co atom was surrounded by an octahedral environment composed of four nitrogen atoms of two four bpp ligands in the equatorial position and coordinated by two oxygen atom of two water molecule in the axial position (**Figure 84**). The molecular packing of complex plotted along the  $a$  axis is shown in **Figure 85**.



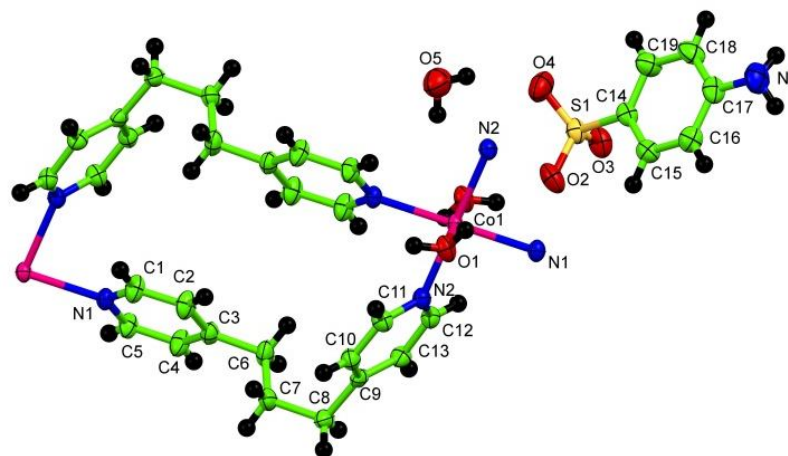


**Figure 84.** Molecular structure of  $\{[\text{Co}(\text{bpp})_2(\text{H}_2\text{O})_2]\cdot(4\text{-abs})_2\cdot\text{H}_2\text{O}\}_n$  (ellipsoid probability at 50%).

The Co–O bond length was 2.0906(12) Å and Co–N bond lengths ranged from 2.2035(14) - 2.2247(14) Å (**Table 20**) similar to those found in  $[\text{Co}(4,4'\text{-bipy})(\text{H}_2\text{O})_4](4\text{-abs})_2\cdot\text{H}_2\text{O}$  (Wang *et al.*, 2002). The bpp ligand acted as a typical N,N'-bipyridine ligands to join Co(II) atom into 1-D infinite chains. The bpp ligand adopted a GG' conformation, providing an N-to-N distance of 8.720 Å (Carlucci *et al.*, 2002).

**Table 20.** Selected bond distances and angles of  $\{[\text{Co}(\text{bpp})_2(\text{H}_2\text{O})_2]\cdot(4\text{-abs})_2\cdot\text{H}_2\text{O}\}_n$ .

Bond lengths (Å)		Bond angles (°)	
Co1—O1	2.0906(12)	O1—Co1—O1 <sup>1</sup>	180.000(1)
Co1—O1 <sup>1</sup>	2.0906(12)	O1 <sup>1</sup> —Co1—N1	91.89(5)
Co1—N1 <sup>1</sup>	2.2035(14)	O1—Co1—N1	88.11(5)
Co1—N1	2.2036(14)	O1 <sup>1</sup> —Co1—N1 <sup>1</sup>	88.10(5)
Co1—N2 <sup>2</sup>	2.2247(14)	O1—Co1—N1 <sup>1</sup>	91.90(5)
Co1—N2 <sup>3</sup>	2.2247(14)	O1 <sup>1</sup> —Co1—N2 <sup>2</sup>	88.65(5)
		O1—Co1—N2 <sup>2</sup>	91.35(5)
		O1—Co1—N2 <sup>3</sup>	88.65(5)
		O1 <sup>1</sup> —Co1—N2 <sup>3</sup>	91.35(5)
		N1 <sup>1</sup> —Co1—N1	179.999(2)
		N1—Co1—N2 <sup>3</sup>	83.75(5)
		N1 <sup>1</sup> —Co1—N2 <sup>3</sup>	96.25(5)
		N1—Co1—N2 <sup>2</sup>	96.25(5)

Symmetry codes: <sup>1</sup>2-x,2-y,1-z; <sup>2</sup>2-x,2-y,2-z; <sup>3</sup>+x,+y,1+z



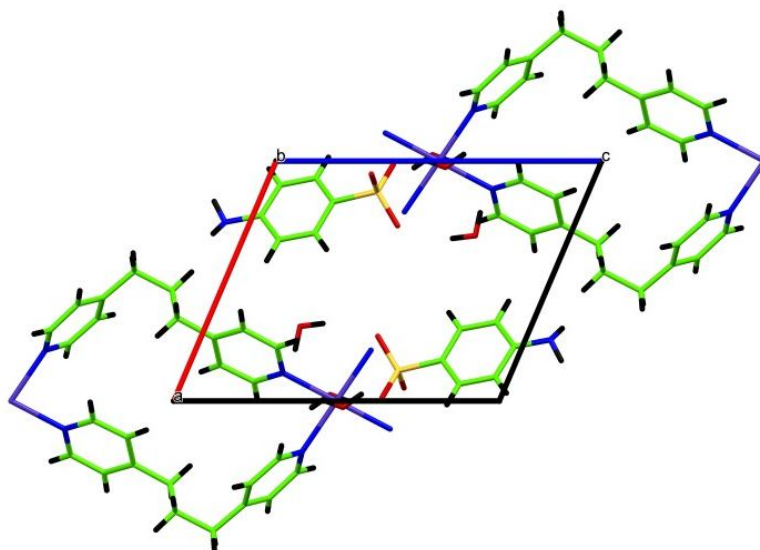


**Figure 85.** Packing diagram of  $\{[\text{Co}(\text{bpp})_2(\text{H}_2\text{O})_2]\cdot(4\text{-abs})_2\cdot\text{H}_2\text{O}\}_n$  plotted down *b* axis.

The cations and anionic were linked by intra- and inter-molecular hydrogen bonds (**Table 21**) formed between hydrogen atoms from coordinated water molecule in the  $[\text{Co}(\text{bpp})_2(\text{H}_2\text{O})_2]^{2+}$  chain and oxygen atom from 4-abs anions, thus forming an infinite 3-D supramolecular architecture (**Figure 86**).

**Table 21.** Hydrogen-bond geometry (Å, °) of  $\{[\text{Co}(\text{bpp})_2(\text{H}_2\text{O})_2]\cdot(4\text{-abs})_2\cdot\text{H}_2\text{O}\}_n$  (**11**).

<i>D—H</i> ⋯ <i>A</i>	<i>D—H</i>	<i>H</i> ⋯ <i>A</i>	<i>D</i> ⋯ <i>A</i>	<i>D—H</i> ⋯ <i>A</i>
O1—H1A⋯O3 <sup>1</sup>	0.86	2.01	2.7832(16)	149.5
O1—H1B⋯O2	0.86	1.89	2.6624(17)	149.0
N3—H3A⋯O3 <sup>2</sup>	0.86	2.29	3.145(3)	172.0
N3—H3B⋯O5 <sup>3</sup>	0.86	2.45	3.141(3)	137.2
O5—H5A⋯O2 <sup>1</sup>	0.85	2.04	2.883(2)	170.7
O5—H5B⋯O4	0.85	2.07	2.878(2)	159.8

Symmetry codes: <sup>1</sup>2-x,2-y,1-z; <sup>2</sup>2-x,2-y,2-z; <sup>3</sup>+x,+y,1+z

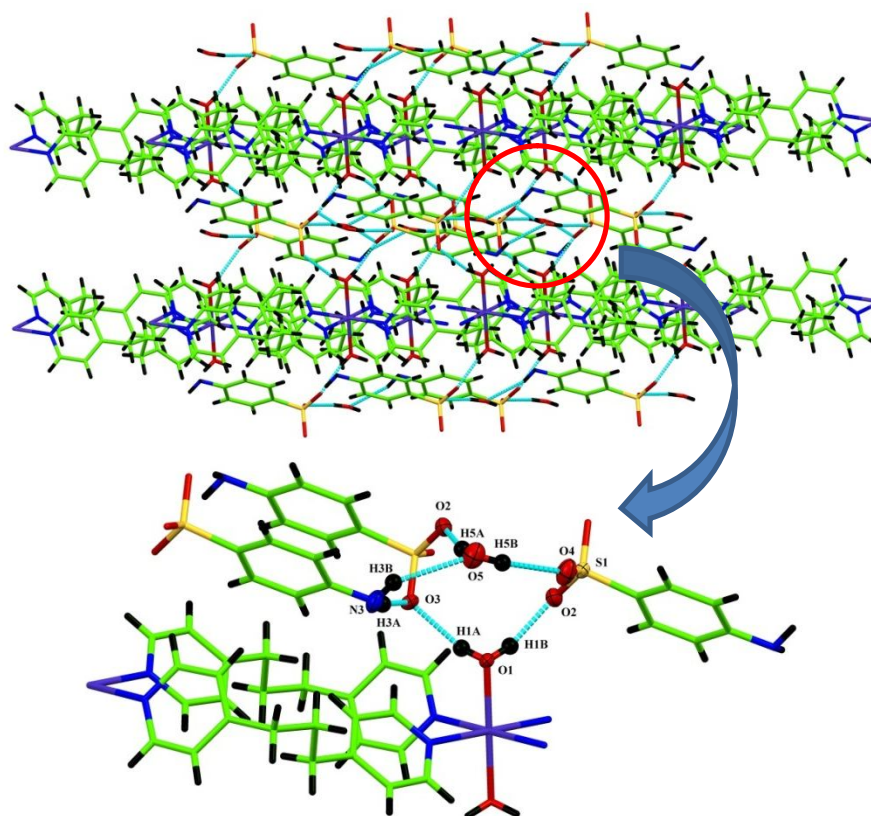


**Figure 86.** View of the 3D supramolecular network via O–H---O and N–H---O interactions.

### Structural description of $[M_{0.5}(\text{bpp})(\text{H}_2\text{O})_2](4\text{-abs})$ [ $M = \text{Mn(II)}(12)$ or $\text{Zn(II)}(14)$ ]

The single crystal X-ray diffraction analyses revealed that complexes **(12)** and **(14)** crystallized in the monoclinic system space group  $P2_1/n$ . Single-crystal X-ray analyses showed that the two complexes were isostructural. Both crystal structures of complexes composed of cationic molecule of  $[M_{0.5}(\text{bpp})(\text{H}_2\text{O})_2]^+$  and charge balanced by 4-abs<sup>-</sup> anions, as illustrated in **Figure 87**. In the cationic part of  $[M_{0.5}(\text{bpp})(\text{H}_2\text{O})_2]^+$  the metal atom (Mn or Zn) coordinated to two nitrogen atoms from bpp ligand, two oxygen atoms from coordinated water molecules in the equatorial plane and two oxygen atoms from coordinated water molecules in the axial positions to form a distorted octahedral geometry. The selected bond distances and angles are shown in **Table 22** for complex **(12)** and **Table 23** for complex **(14)** and molecular packing of complex plotted along the *a* axis is shown in **Figure 88**.

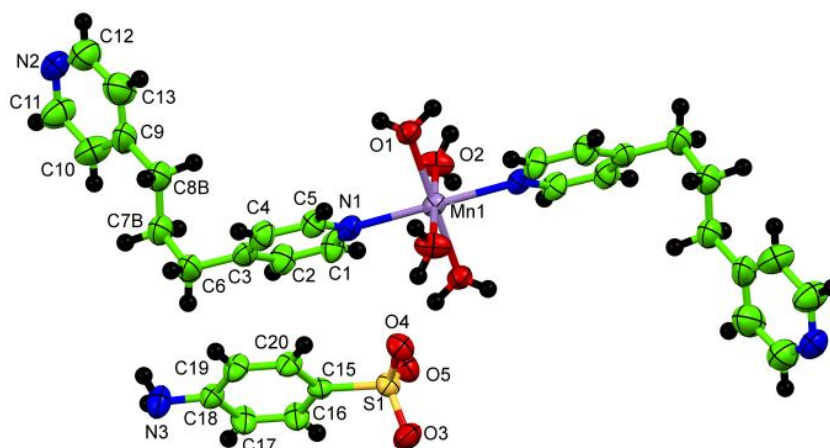


**Figure 87.** ORTEP representation of the asymmetric unit of  $[\text{Mn}_{0.5}(\text{bpp})(\text{H}_2\text{O})_2] \cdot (4\text{-abs})$  (Thermal ellipsoids are drawn at 50% probability).

**Table 22.** Selected bond distances and angles of  $[\text{Mn}_{0.5}(\text{bpp})(\text{H}_2\text{O})_2] \cdot (4\text{-abs})$ .

Bond lengths (Å)		Bond angles (°)	
Mn1—O1	2.1562(14)	O1 — Mn1—O1 <sup>1</sup>	180.00(8)
Mn1—O1 <sup>1</sup>	2.1562(14)	O1 <sup>1</sup> — Mn1—O2 <sup>1</sup>	92.96(6)
Mn1—O2	2.1853(15)	O1 — Mn1—O2 <sup>1</sup>	87.04(6)
Mn1—O2 <sup>1</sup>	2.1854(15)	O1 <sup>1</sup> — Mn1—O2	87.04(6)
Mn1—N1	2.2729(18)	O1 — Mn1—O2	92.96(6)
Mn1—N1 <sup>1</sup>	2.2729(18)	O1 — Mn1—N1	91.04(6)
		O2 — Mn1—N1	92.32(7)
		O2 — Mn1—N1 <sup>1</sup>	87.68(7)
		O2 <sup>1</sup> — Mn1—N1	87.68(7)

Symmetry codes: <sup>1</sup>2-x,2-y,1-z

**Table 23.** Selected bond distances and angles of  $[\text{Zn}_{0.5}(\text{bpp})(\text{H}_2\text{O})_2] \cdot (4\text{-abs})$ .

Bond lengths (Å)		Bond angles (°)	
Zn1 — O1 <sup>1</sup>	2.0863(15)	O1 <sup>1</sup> — Zn1 — O1	179.999(1)
Zn1 — O1	2.0863(15)	O1 — Zn1 — O2 <sup>1</sup>	92.53(7)
Zn1 — O2 <sup>1</sup>	2.1248(16)	O1 <sup>1</sup> — Zn1 — O2 <sup>1</sup>	87.48(7)
Zn1 — O2	2.1247(16)	O1 — Zn1 — O2	87.47(7)
Zn1 — N1	2.146(2)	O1 <sup>1</sup> — Zn1 — O2	92.52(7)
Zn1 — N1 <sup>1</sup>	2.146(2)	O1 <sup>1</sup> — Zn1 — N1	89.12(7)
		O1 — Zn1 — N1 <sup>1</sup>	89.12(7)
		O1 — Zn1 — N1	90.88(7)

Symmetry codes: <sup>1</sup>-x,-y,1-z

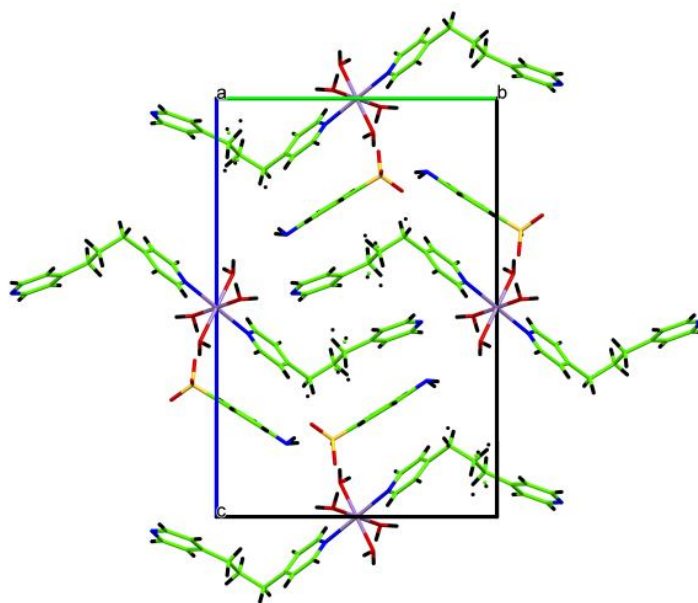


**Figure 88.** Packing diagram of  $[M_{0.5}(\text{bpp})(\text{H}_2\text{O})_2]\cdot(4\text{-abs})$  plotted down a axis.

The bpp carbon atoms of  $-\text{CH}_2-\text{CH}_2-\text{CH}_2-$  groups in Mn complex were found disordered over two positions with an occupancy ratio of 0.784(5) : 0.216(5). The cationic molecules were extended to form a 3D supramolecular layer by classical intermolecular  $\text{O}-\text{H}\cdots\text{O}$  hydrogen bonds between the hydrogen atom of cationic molecule and uncoordinated 4-aminobenzenesulfonate anions as shown in **Figure 89-90**. The Hydrogen-bond geometry of complexes **(12)** and **(14)** are listed in **Table 24-25**.

**Table 24.** Hydrogen-bond geometry ( $\text{\AA}$ ,  $^\circ$ ) of  $[\text{Mn}_{0.5}(\text{bpp})(\text{H}_2\text{O})_2]\cdot(4\text{-abs})$ .

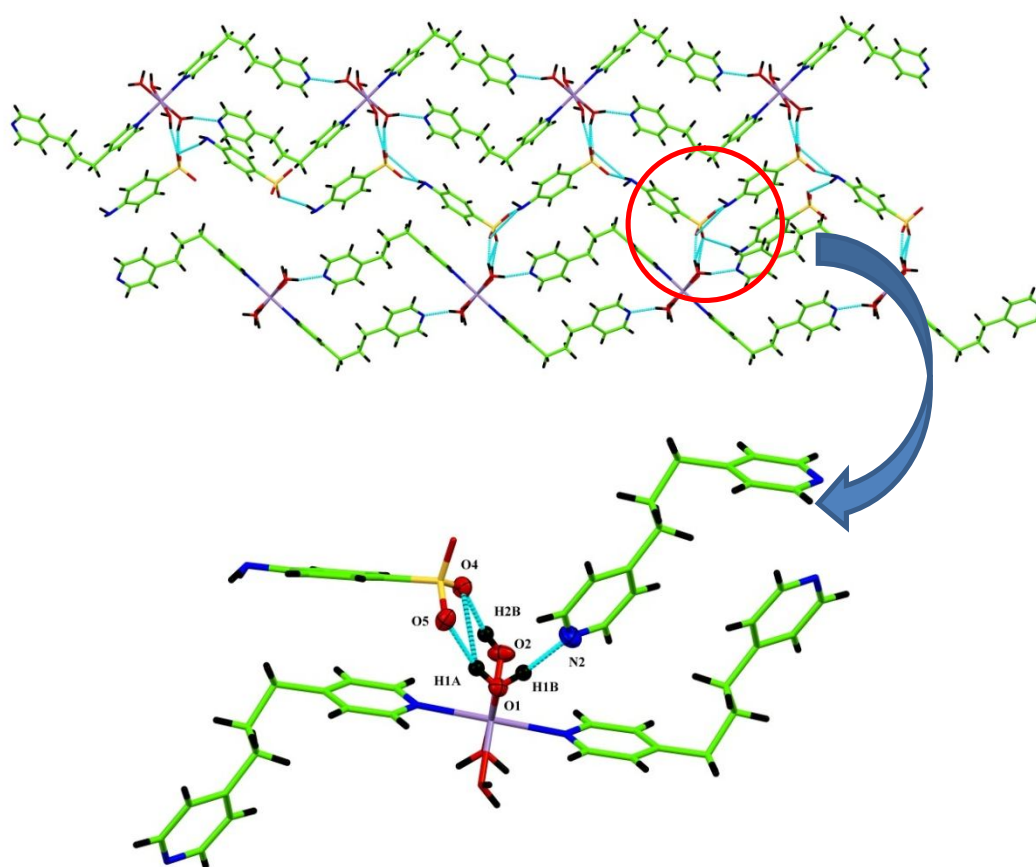
$D-\text{H}\cdots A$	$D-\text{H}$	$\text{H}\cdots A$	$D\cdots A$	$D-\text{H}\cdots A$
$\text{O1}-\text{H1A}\cdots\text{O5}$	0.88	1.85	2.692(2)	160.4
$\text{O1}-\text{H1B}\cdots\text{N2}^1$	0.88	1.89	2.736(3)	161.7
$\text{O2}-\text{H2A}\cdots\text{O5}^2$	0.87	2.12	2.731(2)	126.6
$\text{O2}-\text{H2B}\cdots\text{O4}^3$	0.87	1.89	2.744(2)	168.3

Symmetry codes:  $^1+x,1+y,+z$ ;  $^21-x,2-y,1-z$ ;  $^32-x,2-y,1-z$

**Table 25.** Hydrogen-bond geometry (Å, °) of  $[\text{Zn}_{0.5}(\text{bpp})(\text{H}_2\text{O})_2]\cdot(4\text{-abs})$ .

$D\text{---}H\cdots A$	$D\text{---}H$	$H\cdots A$	$D\cdots A$	$D\text{---}H\cdots A$
$\text{O1---H1A}\cdots\text{N2}^1$	0.89	1.88	2.744(3)	165.4
$\text{O1---H1B}\cdots\text{O4}$	0.89	1.84	2.694(3)	160.0
$\text{O2---H2A}\cdots\text{O4}^2$	0.87	2.01	2.727(2)	139.3
$\text{O2---H2B}\cdots\text{O3}$	0.87	1.88	2.739(3)	172.0

$^1+x,-1+y,+z; ^2-1+x,+y,+z$

**Figure 89.** View of the 3D supramolecular network via O–H---O and N–H---O interactions.

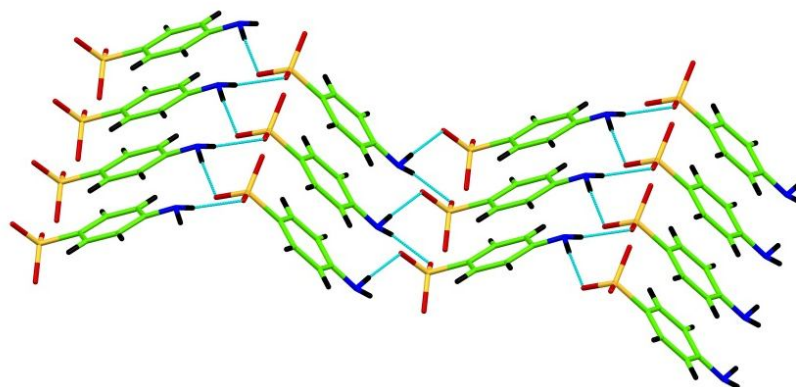


**Figure 90.** View of the 3D supramolecular network via N–H---O interactions.

### Structural description of $\{[\text{Cd}_{0.5}(\text{bpp})(4\text{-abs})]\cdot(\text{H}_2\text{O})\}_n$ (**13**)

Single crystal X-ray diffraction analyses showed that complex crystallized in the monoclinic system, space group  $P2_1/n$ . The molecular structure of complex contained one Cd(II) ion, two bpp ligands, two monodentate 4-abs ligands and one lattice water molecule. The crystal structure of complex (**13**) revealed a 1-D chain by bpp ligand acted as bridging to join each Cd(II) center. The Cd(II) atom, in an octahedral geometry, were coordinated by four nitrogen atom of bpp ligands occupying the equatorial positions and in the axial positions by two oxygen atom from deprotonated 4-abs ligands (**Figure 91**).

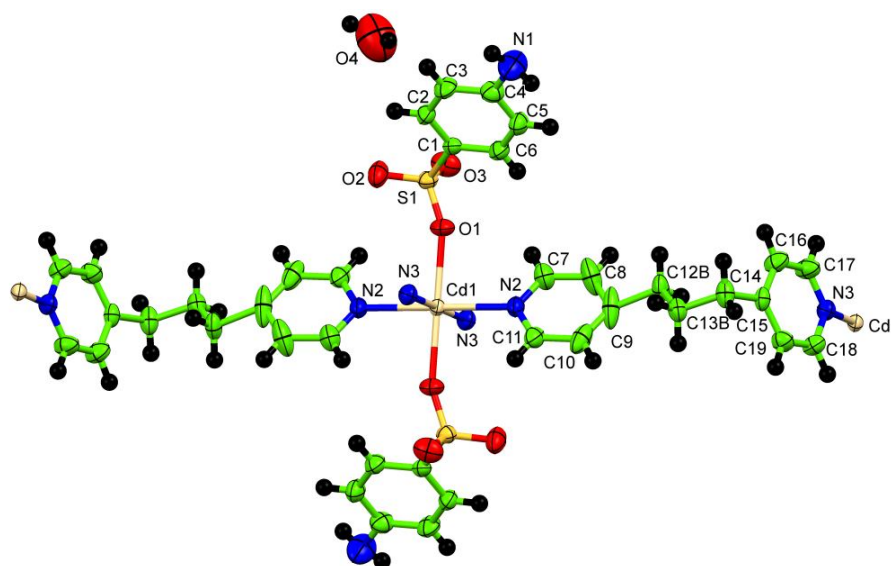


**Figure 91.** ORTEP representation of the asymmetric unit of  $\{[\text{Cd}_{0.5}(\text{bpp})(4\text{-abs})]\cdot(\text{H}_2\text{O})\}_n$  (Thermal ellipsoids are drawn at 50% probability).

In the equatorial plane, Cd–N bond distance ranged from 2.338(2) Å to 2.359(2) Å, bond angle ranged from 83.30(7) to 96.70(7)°. In the axial position, Cd–O bond distance was 2.3217(17) Å with bond angle 180.0°. From the bond lengths and bond angles (**Table 26**) surround metal atom, the Cd centered coordination octahedron was slightly distorted. In the molecular structure of complex, bpp ligand adopted a TG conformation with the N---N distance of 8.986 Å, similar to those reported in the literatures (Li *et al.*, 2015).

**Table 26.** Selected bond distances and angles of  $\{[\text{Cd}_{0.5}(\text{bpp})(4\text{-abs})]\cdot(\text{H}_2\text{O})\}_n$ .

Bond lengths (Å)		Bond angles (°)	
Cd1 — O1	2.3217(17)	O1 — Cd1 — O1 <sup>1</sup>	180.0
Cd1 — O1 <sup>1</sup>	2.3217(17)	O1 <sup>1</sup> — Cd1 — N2	92.07(7)
Cd1 — N2	2.338(2)	O1 — Cd1 — N2	87.93(7)
Cd1 — N2 <sup>1</sup>	2.338(2)	O1 <sup>1</sup> — Cd1 — N2 <sup>1</sup>	87.93(7)
Cd1 — N3 <sup>2</sup>	2.359(2)	O1 — Cd1 — N2 <sup>1</sup>	92.07(7)
Cd1 — N3 <sup>3</sup>	2.359(2)	O1 <sup>1</sup> — Cd1 — N3 <sup>2</sup>	90.11(7)
		O1 — Cd1 — N3 <sup>2</sup>	89.89(7)
		N2 <sup>1</sup> — Cd1 — N2	179.999(1)
		N2 <sup>1</sup> — Cd1 — N3 <sup>3</sup>	83.30(7)
		N2 <sup>1</sup> — Cd1 — N3 <sup>2</sup>	96.70(7)
		N2 — Cd1 — N3 <sup>2</sup>	83.30(7)
		N2 — Cd1 — N3 <sup>3</sup>	96.70(7)

Symmetry codes: <sup>1</sup>-x,1-y,-z; <sup>2</sup>1-x,1-y,1-z; <sup>3</sup>-1+x,+y,-1+z

Moreover, these 1D networks were connected into 2D frameworks through strong intermolecular hydrogen bonding (**Table 27**) occurred between the hydrogen of lattice water molecule and oxygen of monodentate 4-abs ligand [O4A—H4A•••O3<sup>1</sup>](**Figure 92**), which seemed to be effective in stabilizing the crystal structures.

**Table 27.** Hydrogen-bond geometry (Å, °) of  $\{[\text{Cd}_{0.5}(\text{bpp})(4\text{-abs})]\cdot(\text{H}_2\text{O})\}_n$  (**13**).

$D\text{---}H\cdots A$	$D\text{---}H$	$H\cdots A$	$D\cdots A$	$D\text{---}H\cdots A$
O4A—H4A•••O3 <sup>1</sup>	0.85	2.10	2.887(6)	153.8

Symmetry codes: <sup>1</sup>-1/2+x,3/2-y,-1/2+z



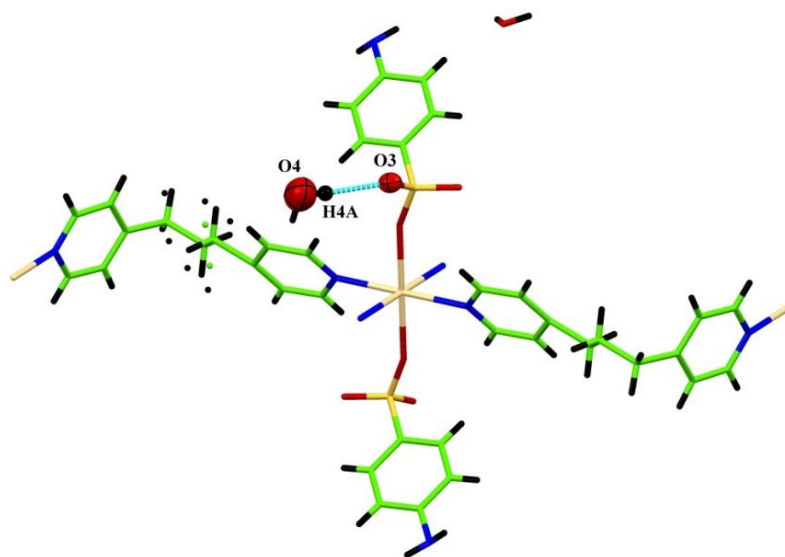


**Figure 92.** Intermolecular hydrogen bonding occurs between the hydrogen of lattice water molecule and oxygen of monodentate 4-abs ligand.

#### Structural description of $\{[\text{Zn}(4,4'\text{-bpy})(\text{H}_2\text{O})_4]\cdot(4\text{-abs})_2\cdot 2\text{H}_2\text{O}\}_n$ (15)

The crystal structure revealed that the complex (15) crystallized in monoclinic system of space group  $P2_1$ . The selected bond lengths and bond angles are given in **Table 28**. Molecular structure of the complex is shown in **Figure 93**. The molecular packing of complex plotted is shown in **Figure 94**. X-ray crystallography showed that the complex contained one-dimensional covalently bonded chains formed by 4,4'-bipyridine ligands connecting Zn(II) atoms, two crystallization water molecules, and 4-aminobenzenesulfonate counter-ions. The Zn(II) ion was coordinated by four oxygen atoms from four water molecules in the equatorial positions and two nitrogen atoms from 4,4'-bipyridine molecule in the axial positions forming a distorted octahedral geometry.



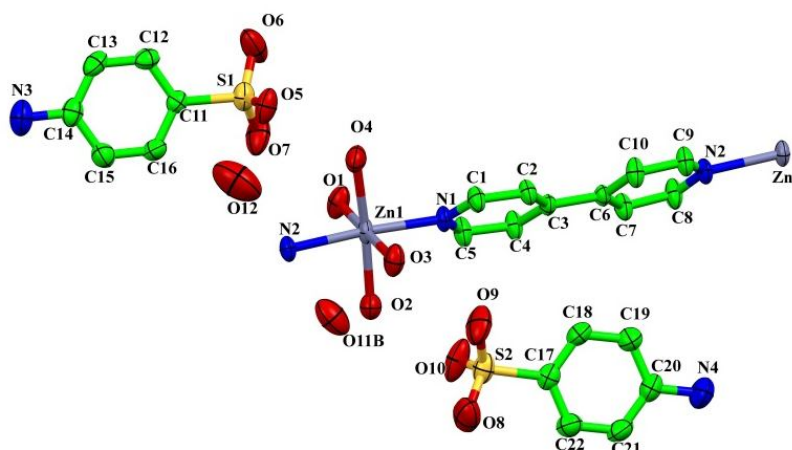


**Figure 93.** ORTEP representation of the asymmetric unit of  $\{[\text{Zn}(4,4'\text{-bpy})(\text{H}_2\text{O})_4]\cdot(4\text{-abs})_2\cdot 2\text{H}_2\text{O}\}_n$  (Thermal ellipsoids are drawn at 50% probability).

The Zn-O bond distances ranged from 2.093(3) to 2.149(3) Å, and the Zn-N bond lengths were 2.133-2.136 Å, these were in good agreement with the literature reports (Liu *et al.*, 2006). The 4,4'-bipy groups acted as a typical N,N'-bipyridine ligands to join Zn(II) atom into 1-D infinite chains. The 4-abs anions were not coordinated to Zn ion but hydrogen-bonded to  $[\text{Zn}(\text{bpy})(\text{H}_2\text{O})_4]^{2+}$  chain via hydrogen of coordinated water molecule and oxygen of sulfonate group.

**Table 28.** Selected bond distances and angles of  $\{[\text{Zn}(4,4'\text{-bpy})(\text{H}_2\text{O})_4]\cdot(4\text{-abs})_2\cdot 2\text{H}_2\text{O}\}_n$ .

Bond lengths (Å)		Bond angles (°)	
Zn1 — O1	2.093(3)	O1 — Zn1 — O2	91.73(12)
Zn1 — O2	2.123(3)	O1 — Zn1 — O3	179.48(11)
Zn1 — O3	2.149(3)	O1 — Zn1 — O4	91.02(12)
Zn1 — O4	2.104(2)	O1 — Zn1 — N1	92.70(12)
Zn1 — N1	2.133(2)	O1 — Zn1 — N2 <sup>1</sup>	87.40(12)
Zn1 — N2 <sup>1</sup>	2.136(2)	O2 — Zn1 — O3	88.36(11)
		O2 — Zn1 — N1	88.95(10)
		O4 — Zn1 — O3	88.93(11)
		O4 — Zn1 — N1	95.27(10)

Symmetry codes: <sup>1</sup>-1+x,+y,+z

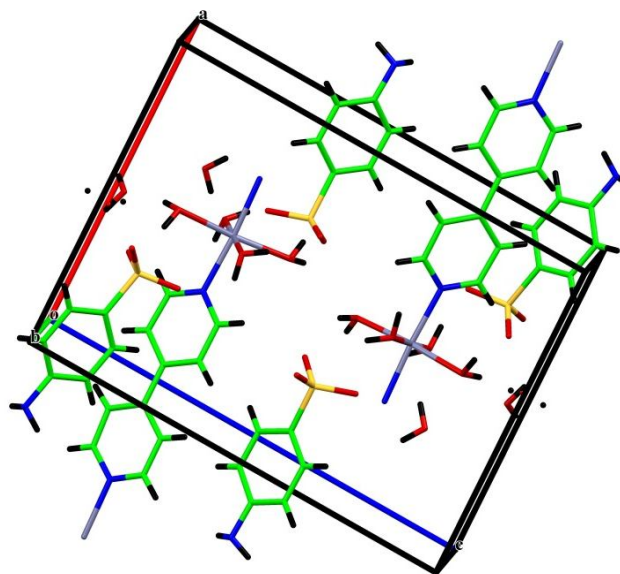


**Figure 94.** Packing diagram of  $\{[\text{Zn}(4,4'\text{-bpy})(\text{H}_2\text{O})_4]\cdot(4\text{-abs})_2\cdot 2\text{H}_2\text{O}\}_n$ .

In addition, there existed strong hydrogen bonding O—H $\cdots$ O interactions (**Table 29**) between the uncoordinated 4-aminobenzenesulfonate anions. That is, the NH<sub>2</sub> group of one 4-aminobenzenesulfonate anions served as a H-donor and interacted with the SO<sub>3</sub><sup>-</sup> group (H-acceptor) of another adjacent 4-aminobenzenesulfonate anion to form a 2-D honeycomb-like framework (**Figure 95-96**). The one lattice water molecule (O11) was modeled as a disordered group over two different orientations and was refined to give an occupancy ratio of 0.519(17) : 0.481(17).

**Table 29.** Hydrogen-bond geometry (Å, °) of  $\{[\text{Zn}(4,4'\text{-bpy})(\text{H}_2\text{O})_4](4\text{-abs})_2\cdot 2\text{H}_2\text{O}\}_n$  (**15**).

$D\text{—H}\cdots A$	$D\text{—H}$	$\text{H}\cdots A$	$D\cdots A$	$D\text{—H}\cdots A$
O1—H1B $\cdots$ O7	0.88	1.87	2.734(4)	164.9
O2—H2A $\cdots$ O10	0.87	1.83	2.689(4)	167.8
O2—H2B $\cdots$ O11B	0.87	1.79	2.610(16)	156.7
O2—H2B $\cdots$ O11A	0.87	1.83	2.677(18)	140.2
O3—H3B $\cdots$ O9	0.85	2.23	2.789(4)	123.0
O4—H4B $\cdots$ O5	0.87	1.90	2.752(4)	167.0
O11A—H11D $\cdots$ O8 <sup>1</sup>	0.81	0.85	2.77(2)	140.2

Symmetry codes: <sup>1</sup>-1+x,+y,+z

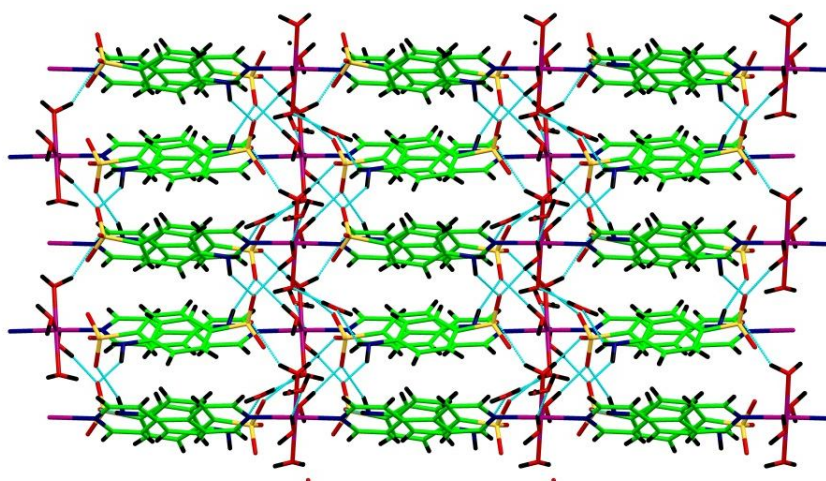


**Figure 95.** Three-dimensional supramolecular structure of  $\{[\text{Zn}(4,4'\text{-bpy})(\text{H}_2\text{O})_4]\cdot(4\text{-abs})_2\cdot 2\text{H}_2\text{O}\}_n$ .

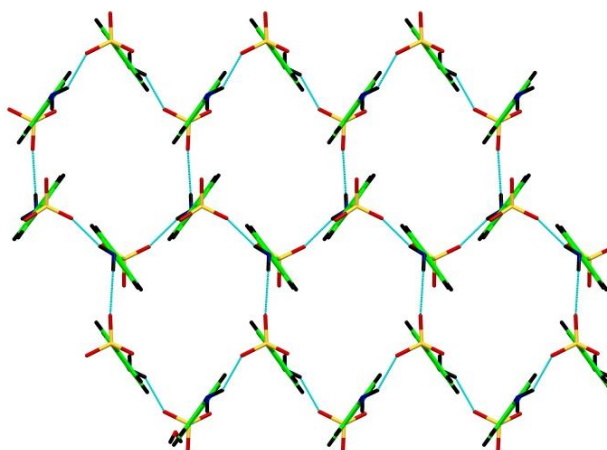


**Figure 96.** 2-D honeycomb-like supramolecular network in complex generated from the basic building blocks through hydrogen-bonding interactions.

**Structural description of  $\{[\text{Cd}(4,4'\text{-bpy})_{1.5}(\text{H}_2\text{O})_3](4,4'\text{bpy})(4\text{-abs})(\text{H}_2\text{O})\text{NO}_3\}_n$  (16)**

Single crystal X-ray diffraction analyses showed that complex crystallized in the monoclinic system, space group  $P2_1/c$ . In the crystal structure, one asymmetric unit consisted of one cadmium atom, one half of coordinated bpy ligand, three coordinated water molecules, one uncoordinated bpy molecule, one uncoordinated  $\text{NO}_3^-$  anion, one uncoordinated 4-abs anion, and one lattice water molecules (**Figure 97**). The Cd(II) center was six coordinate by bonding to three nitrogen atoms from 4,4'-bpy and three oxygen atoms from coordinated water molecules.

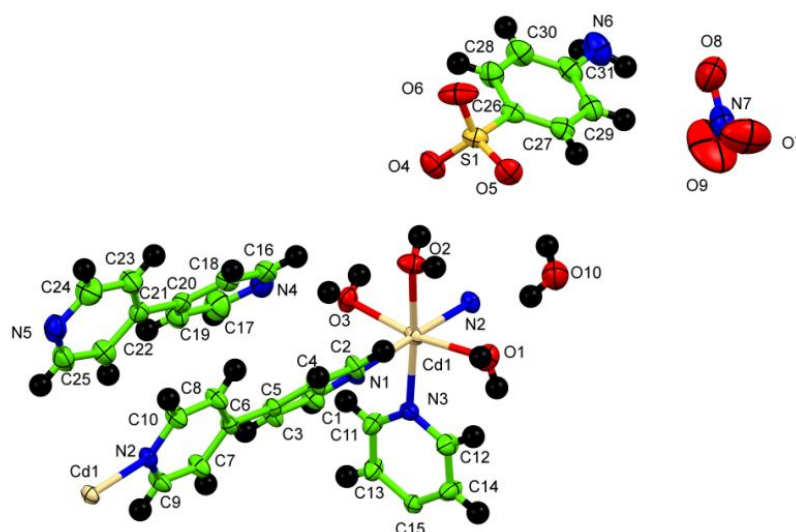


**Figure 97.** ORTEP representation of the asymmetric unit of  $\{[\text{Cd}(4,4'\text{-bpy})_{1.5}(\text{H}_2\text{O})_3] \cdot (4,4'\text{bpy}) \cdot (4\text{-abs}) \cdot (\text{H}_2\text{O}) \cdot \text{NO}_3\}_n$  (Thermal ellipsoids are drawn at 50% probability).

The Cd–N bond lengths (**Table 30**) were 2.330(2) Å, 2.365(2) and 2.374(2) Å and the Mn–O bond lengths were 2.278(2) Å, 2.316(2) and 2.318(2) Å. These values were in good agreement with the literature reports (Mei *et al.*, 2011). The bond angles around Cd(II) ion were in the range 169.86 (8)°–174.68 (8)° and 84.69(8)°–97.38 (8)° to give a slightly distorted octahedral geometry. The bpy ligands acted as a bridging ligand linking the adjacent Cd(II) ions to form 2D layers. The molecular packing of complex plotted down b axis is shown in **Figure 98**.

**Table 30.** Selected bond distances and angles of  $\{[\text{Cd}(4,4'\text{-bpy})_{1.5}(\text{H}_2\text{O})_3] \cdot (4,4'\text{bpy}) \cdot (4\text{-abs}) \cdot (\text{H}_2\text{O}) \cdot \text{NO}_3\}_n$ .

Bond lengths (Å)		Bond angles (°)	
Cd1 — O1	2.318(2)	O1 — Cd1 — N1	96.39(8)
Cd1 — O2	2.316(2)	O1 — Cd1 — N2 <sup>1</sup>	86.59(8)
Cd1 — O3	2.278(2)	O1 — Cd1 — N3	96.42(8)
Cd1 — N1	2.365(2)	O2 — Cd1 — O1	84.69(8)
Cd1 — N2 <sup>1</sup>	2.374(2)	O2 — Cd1 — N1	87.31(8)
		O2 — Cd1 — N3	174.38(8)
		O3 — Cd1 — O1	169.86(8)
		O3 — Cd1 — O2	87.73(9)
		O3 — Cd1 — N1	89.96(8)
		N3 — Cd1 — N1	87.09(8)

Symmetry codes: <sup>1</sup>1-x, -1/2+y, 3/2-z

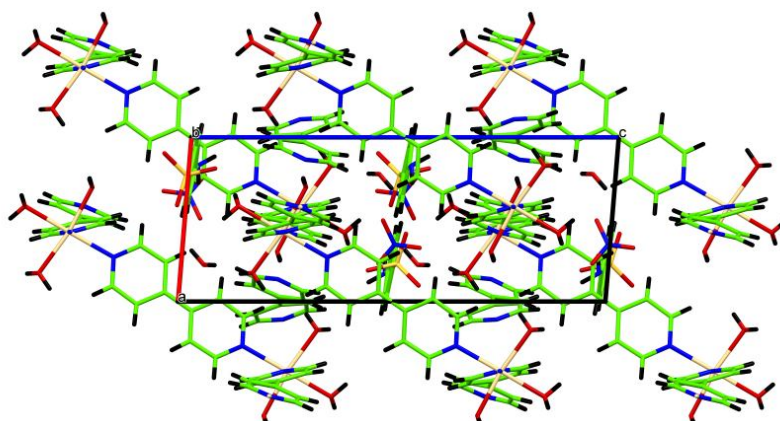


**Figure 98.** Packing diagram of  $\{[\text{Cd}(4,4'\text{-bpy})_{1.5}(\text{H}_2\text{O})_3] \cdot (4,4'\text{-bpy}) \cdot (4\text{-abs}) \cdot (\text{H}_2\text{O}) \cdot \text{NO}_3\}_n$  plotted down *b* axis.

The layers of the coordination polymer (**Table 31**) were further connected by hydrogen bonds between hydrogen atoms of water molecules and uncoordinated 4-abs anions [O1—H1B $\cdots$ O6<sup>1</sup>, O2—H2A $\cdots$ O4, O2—H2B $\cdots$ O5<sup>1</sup> and O3—H3A $\cdots$ O5<sup>2</sup>], oxygen atoms of coordinated water molecules and nitrogen atoms of lattice 4,4'-bpy [O3—H3B $\cdots$ N4] and hydrogen of coordinated water molecules and lattice water molecules [O10—H10A $\cdots$ O1] to form a 3D supramolecular network (**Figure 99**).

**Table 31.** Hydrogen-bond geometry (Å, °) of  $\{[\text{Cd}(4,4'\text{-bpy})_{1.5}(\text{H}_2\text{O})_3] \cdot (4,4'\text{-bpy}) \cdot (4\text{-abs}) \cdot (\text{H}_2\text{O}) \cdot \text{NO}_3\}_n$ .

<i>D</i> —H $\cdots$ <i>A</i>	<i>D</i> —H	H $\cdots$ <i>A</i>	<i>D</i> $\cdots$ <i>A</i>	<i>D</i> —H $\cdots$ <i>A</i>
O1—H1B $\cdots$ O6 <sup>1</sup>	0.85	1.99	2.793(3)	156.2
O2—H2A $\cdots$ O4	0.87	1.93	2.755(3)	159.2
O2—H2B $\cdots$ O5 <sup>1</sup>	0.87	2.02	2.782(3)	146.1
O3—H3A $\cdots$ O5 <sup>2</sup>	0.86	1.94	2.788(4)	167.7
O3—H3B $\cdots$ N4	0.62(3)	2.21(3)	2.815(4)	166(4)
O10—H10A $\cdots$ O1	0.85	2.01	2.798(4)	152.9

Symmetry codes: <sup>1</sup>1-x,1-y,1-z; <sup>2</sup>-x,-1/2+y,3/2-z

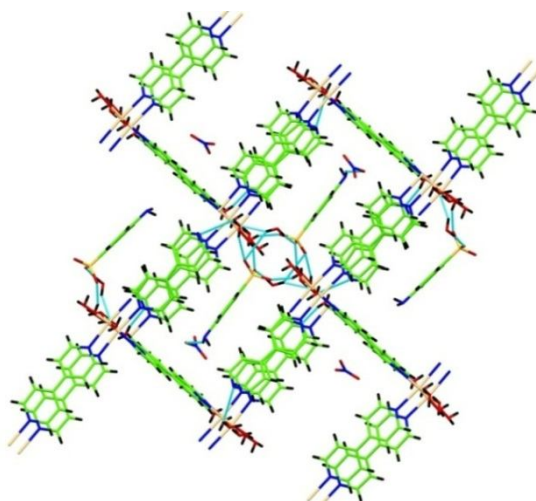


**Figure 99.** 3-D supramolecular network of  $\{[\text{Cd}(4,4'\text{-bpy})_{1.5}(\text{H}_2\text{O})_3]\cdot(4,4'\text{bpy})\cdot(4\text{-abs})\cdot(\text{H}_2\text{O})\cdot\text{NO}_3\}_n$ .

#### Structural description of $\{[\text{Cd}_{0.5}(\text{bpe})(4\text{-abs})]\cdot\text{H}_2\text{O}\}_n$ (17)

Single crystal X-ray diffraction analyses showed that the complex crystallized in the monoclinic system, space group  $C2/c$ . The structure of the complex was a one-dimensional polymer. One asymmetric unit consisted of half of cadmium atom, one bpe ligand and one 4-abs anion and one lattice water molecules (**Figure 100**). The Cd(II) ion acted as metal center while bpe acted as the linker leading to 1-D covalently bonded chains. The bpe ligand adopted a gauche-conformation with the C–CH<sub>2</sub>–CH<sub>2</sub>–C torsion angle of 80.91°.

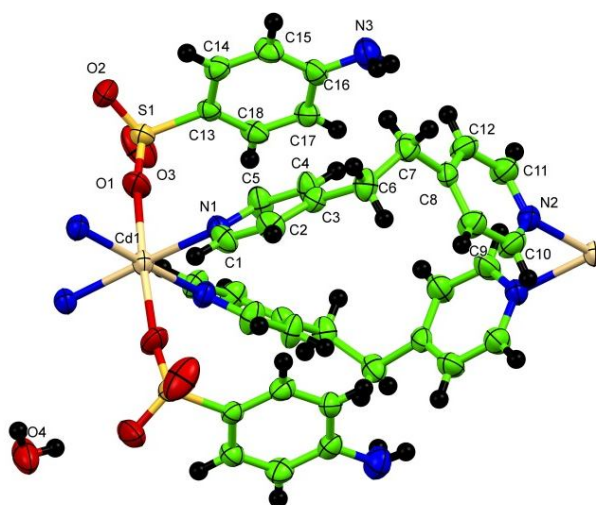


**Figure 100.** ORTEP representation of the asymmetric unit of  $\{[\text{Cd}_{0.5}(\text{bpe})(4\text{-abs})]\cdot\text{H}_2\text{O}\}_n$  (Thermal ellipsoids are drawn at 50% probability).



The cadmium atom was in an octahedral environment surrounded by four nitrogen atoms from bpe ligands [Cd–N = 2.341(2)- 2.344(2)] in equatorial plane, and bonded to two oxygen atoms from 4-abs anion ligands [Cd–O = 2.321(2)] in axial position. These bond lengths were in good agreement with the literature reports (Xiao *et al.*, 2013). The selected bond lengths and bond angles are given in **Table 32**. In the intra-chain Cd···Cd distances separated by bpe ligand was 11.001 Å. The molecular packing of complex plotted down c axis is shown in **Figure 101**.

**Table 32.** Selected bond distances and angles of  $\{[\text{Cd}_{0.5}(\text{bpe})(4\text{-abs})]\cdot\text{H}_2\text{O}\}_n$ .

Bond lengths (Å)		Bond angles (°)	
Cd1 — O1	2.321(2)	O1 — Cd1 — O1 <sup>1</sup>	176.78(10)
Cd1 — O1 <sup>1</sup>	2.321(2)	O1 — Cd1 — N1 <sup>1</sup>	84.32(8)
Cd1 — N1	2.344(2)	O1 <sup>1</sup> — Cd1 — N1 <sup>1</sup>	93.38(8)
Cd1 — N1 <sup>1</sup>	2.344(2)	O1 <sup>1</sup> — Cd1 — N1	84.32(8)
Cd1 — N2 <sup>2</sup>	2.341(2)	O1 — Cd1 — N1	93.38(8)
Cd1 — N2 <sup>3</sup>	2.341(2)	N1 — Cd1 — N1 <sup>1</sup>	89.06(11)
		N2 <sup>2</sup> — Cd1 — N1	175.36(8)
		N2 <sup>3</sup> — Cd1 — N1 <sup>1</sup>	175.36(8)
		N2 <sup>2</sup> — Cd1 — N2 <sup>3</sup>	84.11(11)

Symmetry codes: <sup>1</sup>1-x,+y,1/2-z; <sup>2</sup>1-x,-1+y,1/2-z; <sup>3</sup>+x,-1+y,+z

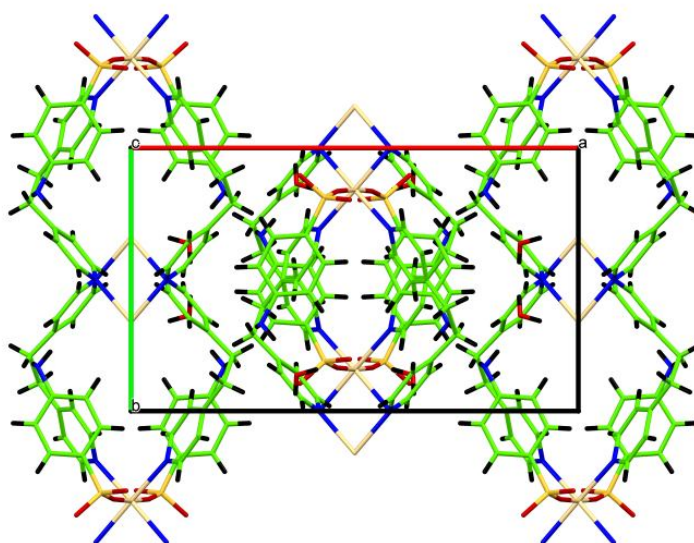


**Figure 101.** Packing diagram of  $\{[\text{Cd}_{0.5}(\text{bpe})(4\text{-abs})]\cdot\text{H}_2\text{O}\}_n$  plotted down c axis.

Each coordination polymer chain were linked by O–H...O (Table 33) intermolecular hydrogen bonding between oxygen atom of sulfonate group and hydrogen of water molecule resulting in a 2-D network supramolecular (Figure 102).

**Table 33.** Hydrogen-bond geometry (Å, °) of  $[\text{Cd}_{0.5}(\text{bpe})(4\text{-abs})]\cdot\text{H}_2\text{O}$ .

$D\text{---}H\cdots A$	$D\text{---}H$	$H\cdots A$	$D\cdots A$	$D\text{---}H\cdots A$
$\text{O4---H4A}\cdots\text{O3}^1$	0.85	1.91	2.755(3)	175.2
$\text{O4---H4B}\cdots\text{O2}$	0.85	1.91	2.728(3)	161.5

Symmetry codes: <sup>1</sup>1-x,-y,1-z

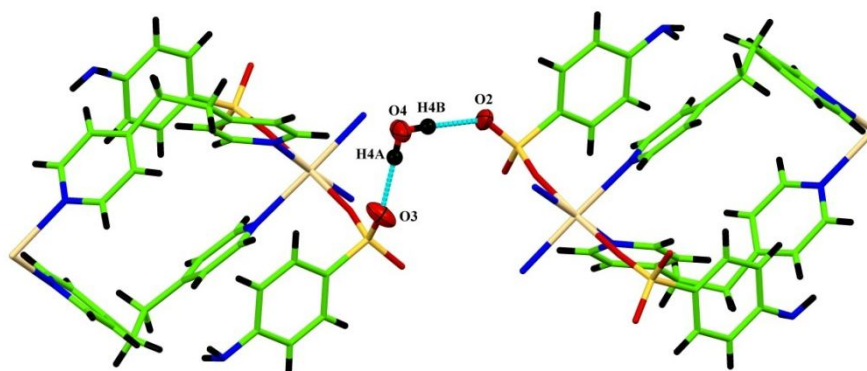


**Figure 102.** Hydrogen bonding of  $\{[\text{Cd}_{0.5}(\text{bpe})(4\text{-abs})]\cdot\text{H}_2\text{O}\}_n$  between water molecule and sulfonate ligands.

#### Structural description of $\{[\text{Cd}(\text{bpp})_2(\text{H}_2\text{O})_2]\cdot(3\text{-abs})_2\cdot 2\text{H}_2\text{O}\}_n$ (18)

Single crystal X-ray diffraction analyses showed that complex crystallized in the monoclinic system, space group  $C2/c$ . The asymmetric unit of complex contained one Cd atom, two bpp ligand, two coordinated water molecules, two uncoordinated 3-abs anions, and two lattice water molecules (Figure 103). The coordination environment of Cd(II) ion was a distorted octahedral geometry. The molecular packing of complex plotted down c axis is shown in Figure 104.



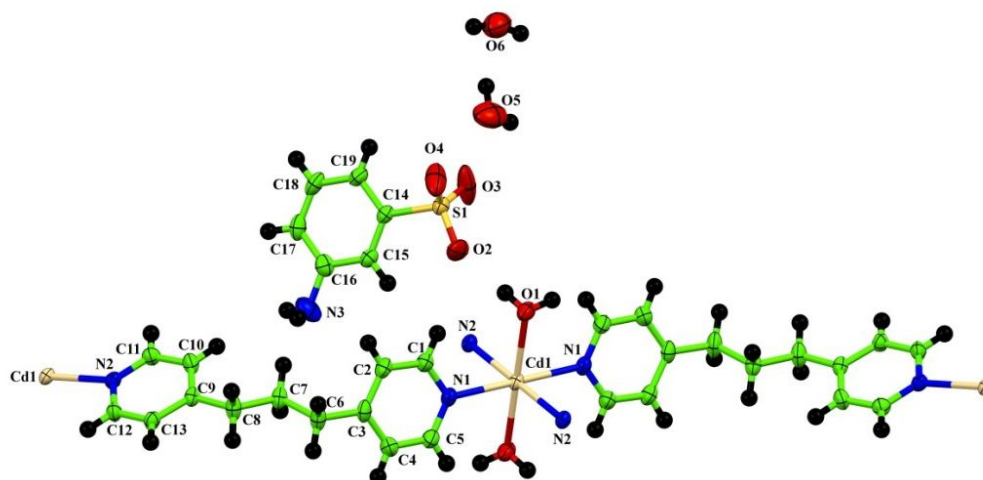


**Figure 103.** ORTEP representation of the asymmetric unit of  $\{[\text{Cd}(\text{bpp})_2(\text{H}_2\text{O})_2] \cdot (3\text{-abs})_2 \cdot 2\text{H}_2\text{O}\}_n$  (Thermal ellipsoids are drawn at 50% probability).

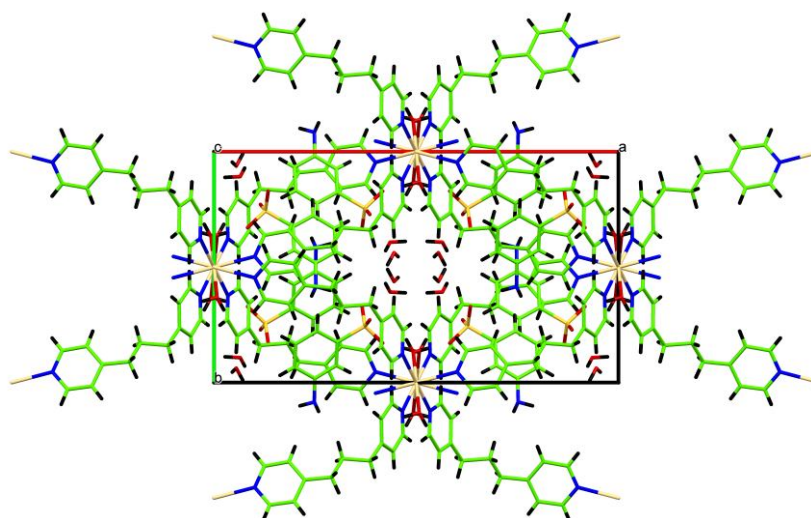


**Figure 104.** Packing diagram of  $\{[\text{Cd}(\text{bpp})_2(\text{H}_2\text{O})_2] \cdot (3\text{-abs})_2 \cdot 2\text{H}_2\text{O}\}_n$  plotted down *c*-axis.

The equatorial plane Cd–N bond distances ranged from 2.0785(18) Å to 2.163(2) Å and bond angles of N–Cd–N from 86.09(7) to 93.91(7)°. The axial Cd–O distances ranged from 2.071(2) Å to 2.1287(18) Å and bond angle of O–Cd–O was 179.999(1)° (**Table 34**). These bond distances and bond angles were similar to those

found in related complexes (Mei *et al.*, 2011). The bpp ligands acted as a bridging ligand linking the adjacent Cd(II) centers to form 2D sheet and bpp was in a TT (*trans-trans*) conformation with the N---N distance of 9.886 Å, similar to those reported in the literatures (Lucia *et al.*, 2002).

**Table 34.** Selected bond distances and angles of  $\{[\text{Cd}(\text{bpp})_2(\text{H}_2\text{O})_2]\cdot(3\text{-abs})_2\cdot 2\text{H}_2\text{O}\}_n$ .

Bond lengths (Å)		Bond angles (°)	
Cd1 — O1 <sup>1</sup>	2.1287(18)	O1 — Cd1 — O1 <sup>1</sup>	179.999(1)
Cd1 — O1	2.071(2)	N1 — Cd1 — O1	88.00(7)
Cd1 — N1 <sup>1</sup>	2.0785(18)	N1 <sup>1</sup> — Cd1 — O1	92.00(7)
Cd1 — N1	2.0902(18)	N1 — Cd1 — O1 <sup>1</sup>	92.00(7)
Cd1 — N2 <sup>2</sup>	2.154(2)	N1 <sup>1</sup> — Cd1 — O1 <sup>1</sup>	88.00(7)
Cd1 — N2 <sup>3</sup>	2.163(2)	N1 — Cd1 — N1 <sup>1</sup>	180.00(9)
		N1 — Cd1 — N2 <sup>2</sup>	93.91(7)
		N1 — Cd1 — N2 <sup>3</sup>	86.09(7)
		N1 <sup>1</sup> — Cd1 — N2 <sup>2</sup>	86.09(7)

Symmetry codes: <sup>1</sup>1-x,2-y,1-z; <sup>2</sup>-1/2+x,3/2-y,-1/2+z; <sup>3</sup>3/2-x,1/2+y,3/2-z; <sup>4</sup>3/2-x,-1/2+y,3/2-z

The crystal-packed structure revealed a 2-D supramolecular network (**Table 35**) formed by the O—H...O hydrogen bonds between the coordinated water molecules and the oxygen atoms of the sulfonate group. There existed hydrogen bonds between the lattice water molecules as well to generate a 2-D supramolecular network as shown in **Figure 105**.

**Table 35.** Hydrogen-bond geometry (Å, °) of  $\{[\text{Cd}(\text{bpp})_2(\text{H}_2\text{O})_2]\cdot(3\text{-abs})_2\cdot 2\text{H}_2\text{O}\}_n$ .

$D\text{---}H\cdots A$	$D\text{---}H$	$H\cdots A$	$D\cdots A$	$D\text{---}H\cdots A$
O1—H1A...O2	0.86	1.93	2.700(3)	149.9
O5—H5B...O6	0.85	2.02	2.785(5)	149.1
O6—H6C...O5 <sup>1</sup>	0.85	1.99	2.785(5)	154.5

Symmetry codes: <sup>1</sup>1-x,1-y,-z

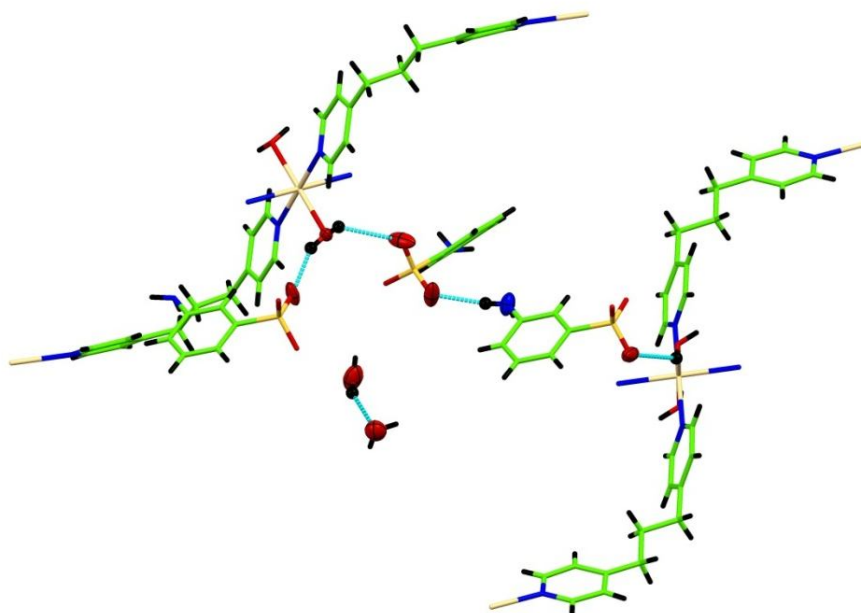


**Figure 105.** O–H···O hydrogen bonding of  $\{[\text{Cd}(\text{bpp})_2(\text{H}_2\text{O})_2] \cdot (\text{3-abs})_2 \cdot 2\text{H}_2\text{O}\}_n$ .

**Structural description of  $[\text{M}(\text{bpp})_2(\text{Mbs})_2]_n$  [ $\text{M} = \text{Zn}(\text{II})(\mathbf{19})$  or  $\text{Cd}(\text{II})(\mathbf{20})$ ]**

Single crystal X-ray diffraction analyses showed that complexes **(19)** and **(20)** crystallized in the orthorhombic space group  $Pnna$ . X-ray diffraction analysis revealed that the asymmetric unit of both complexes consisted of one metal ion ( $\text{Cd}(\text{II})$  and  $\text{Zn}(\text{II})$ ), two Mbs ligands, and two bpp ligands. Single-crystal X-ray analyses showed that the two complexes were isostructural. Two complexes existed in one-dimensional chains formed by 2 *trans* bridging bpp ligands through Zn atoms (**Figure 106**).

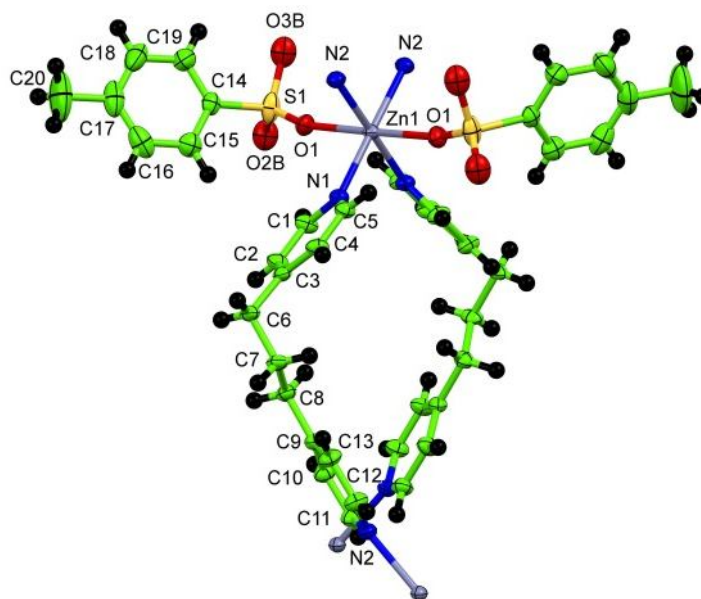


**Figure 106.** ORTEP representation of the asymmetric unit of  $[\text{Zn}(\text{bpp})_2(\text{Mbs})_2]_n$   
(Thermal ellipsoids are drawn at 50% probability).

In the structure, the metal atom exhibited slightly distorted octahedral coordination geometry by bonding to two O donors from two monodentate Mbs anion ligands in the axial positions ( $\text{Cd}-\text{O} = 2.320 \text{ \AA}$  and  $\text{Zn}-\text{O} = 2.1739 \text{ \AA}$ ) and four N atoms from four bpp ligand in the equatorial positions ( $\text{Cd}-\text{N} = 2.336 - 2.346 \text{ \AA}$  and  $\text{Zn}-\text{N} = 2.1697 - 2.1831 \text{ \AA}$ ). The angles subtended at the metal ions fit in the range  $178.55 - 179.56^\circ$  and  $88.00^\circ - 94.58^\circ$  (**Table 36**) for Cd complex and  $178.90^\circ$  and  $87.77^\circ - 91.42^\circ$  (**Table 37**) for Zn complex exhibiting slight departure from the corresponding value expected for a regular octahedron (theoretical values:  $180^\circ$  and  $90^\circ$ ), hence, a slight distortion of the octahedral coordination. The bpp ligand adopted a GG' (gauche – gauche) conformation with the N to N distance of  $8.977 \text{ \AA}$  and the bpp ligands in complexes acted as a typical bridging linker to join metal ion to form 1-D chain polymer.

**Table 36.** Selected bond distances and angles of  $[\text{Zn}(\text{bpp})_2(\text{Mbs})_2]_n$ .

Bond lengths (Å)		Bond angles (°)	
Zn1 — O1 <sup>1</sup>	2.1739(17)	O1 — Zn1 — O1 <sup>1</sup>	178.90(9)
Zn1 — O1	2.1739(17)	O1 <sup>1</sup> — Zn1 — N2 <sup>2</sup>	91.42(7)
Zn1 — N1 <sup>1</sup>	2.1697(18)	O1 <sup>1</sup> — Zn1 — N2 <sup>3</sup>	87.77(7)
Zn1 — N1	2.1697(18)	O1 — Zn1 — N2 <sup>2</sup>	87.78(7)
Zn1 — N2 <sup>2</sup>	2.1831(18)	O1 — Zn1 — N2 <sup>3</sup>	91.42(7)
Zn1 — N2 <sup>3</sup>	2.1831(18)	N1 — Zn1 — O1	91.05(7)
		N1 <sup>1</sup> — Zn1 — O1 <sup>1</sup>	91.05(7)
		N1 — Zn1 — O1 <sup>1</sup>	89.75(7)
		N1 <sup>1</sup> — Zn1 — O1	89.74(7)

Symmetry codes: <sup>1</sup>+x,3/2-y,3/2-z; <sup>2</sup>-1/2+x,3/2-y,1/2+z; <sup>3</sup>-1/2+x,+y,1-z

**Table 37.** Selected bond distances and angles of  $[\text{Cd}(\text{bpp})_2(\text{Mbs})_2]_n$ .

Bond lengths (Å)		Bond angles (°)	
Cd1 — O1 <sup>1</sup>	2.320(2)	O1 <sup>1</sup> — Cd1 — O1	179.56(12)
Cd1 — O1	2.320(2)	O1 — Cd1 — N1	90.76(9)
Cd1 — N1 <sup>1</sup>	2.336(2)	O1 <sup>1</sup> — Cd1 — N1	88.91(9)
Cd1 — N2 <sup>2</sup>	2.336(2)	O1 <sup>1</sup> — Cd1 — N2 <sup>2</sup>	88.00(9)
Cd1 — N2 <sup>3</sup>	2.346(2)	O1 — Cd1 — N2 <sup>2</sup>	92.32(9)
		N1 — Cd1 — N2 <sup>2</sup>	94.58(8)
		N1 <sup>1</sup> — Cd1 — N2 <sup>3</sup>	94.58(8)
		N1 — Cd1 — N2 <sup>3</sup>	178.55(8)
		N2 <sup>2</sup> — Cd1 — N2 <sup>3</sup>	84.70(11)

Symmetry codes: <sup>1</sup>+x,3/2-y,3/2-z; <sup>2</sup>-1/2+x,3/2-y,1/2+z; <sup>3</sup>-1/2+x,+y,1-z

Weak C—H···O interactions of complex **(19)** (**Table 38**) and complex **(20)** (**Table 39**) were generated via hydrogen atoms and oxygen atoms of Mbs ligands resulting in a 2-D layer (**Figure 107**).

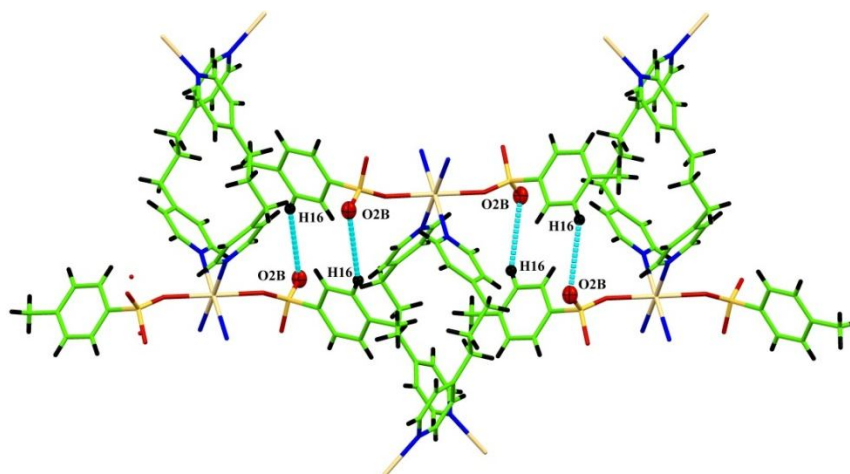
**Table 38.** Hydrogen-bond geometry (Å, °) of  $[\text{Zn}(\text{bpp})_2(\text{Mbs})_2]_n$ .

$D\text{—}H\cdots A$	$D\text{—}H$	$H\cdots A$	$D\cdots A$	$D\text{—}H\cdots A$
C16—H16···O2A <sup>1</sup>	0.93	2.41	3.185(8)	140.5

Symmetry codes: <sup>1</sup>1-x,1-y,1-z

**Table 39.** Hydrogen-bond geometry (Å, °) of [Cd(bpp)<sub>2</sub>(Mbs)<sub>2</sub>]<sub>n</sub>.

<i>D</i> —H··· <i>A</i>	<i>D</i> —H	H··· <i>A</i>	<i>D</i> ··· <i>A</i>	<i>D</i> —H··· <i>A</i>
C16—H16···O2A <sup>1</sup>	0.93	2.59	3.352(11)	139.8

Symmetry codes: <sup>1</sup>1-x,1-y,1-z**Figure 107.** Weak C—H···O hydrogen bond interactions of [M(bpp)<sub>2</sub>(Mbs)<sub>2</sub>]<sub>n</sub>.**Structural description of {[Cd(bpp)(sdz)<sub>2</sub>·2H<sub>2</sub>O]<sub>n</sub> (21)}**

Single crystal X-ray diffraction analyses showed that the complex crystallized in the monoclinic system, space group *P2*<sub>1</sub>/*c*. The Cd(II) ion located in an octahedral geometry with the CdN<sub>6</sub> chromophore originated from four nitrogen atoms from sdz ligands and two nitrogen atoms of the bpp ligands (**Figure 108**).

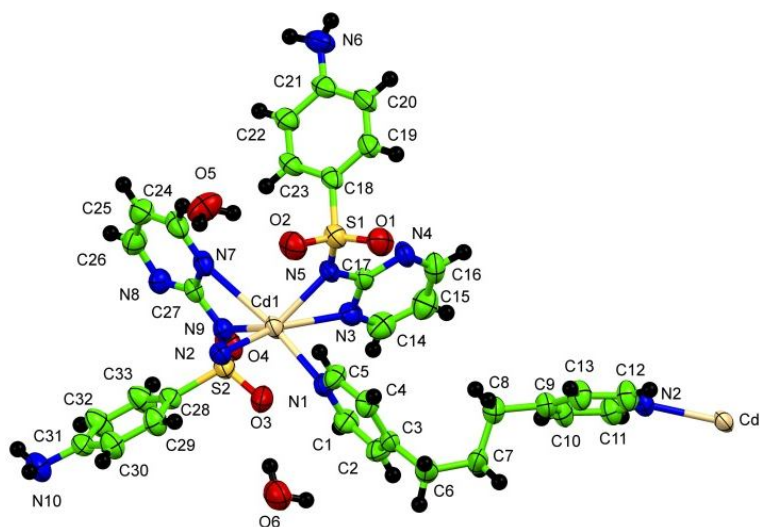


**Figure 108.** ORTEP representation of the asymmetric unit of  $\{[\text{Cd}(\text{bpp})(\text{sdz})_2] \cdot 2\text{H}_2\text{O}\}_n$  (Thermal ellipsoids are drawn at 50% probability).

**Table 40**, the Cd–N bond lengths were in the range 2.215(2) to 2.612(3) Å and N–Cd–N bond angles 83.72(8) to 96.26(8)° which were similar to those found in related complexes (Yan *et al.*, 2010). The bpp acted as the linkers leading to 1-D covalently bonded chains. The conformation of bpp ligand was GG (*trans–trans*) conformation with the N---N distance 9.016 Å. The molecular packing of complex plotted down *c* axis is shown in **Figure 109**.

**Table 40.** Selected bond distances and angles of  $\{[\text{Cd}(\text{bpp})(\text{sdz})_2] \cdot 2\text{H}_2\text{O}\}_n$ .

Bond lengths (Å)		Bond angles (°)	
Cd1—N1	2.317(2)	N1—Cd1—N2 <sup>1</sup>	83.72(8)
Cd1—N2 <sup>1</sup>	2.342(2)	N1—Cd1—N3	80.60(8)
Cd1—N3	2.612(3)	N2 <sup>1</sup> —Cd1—N3	164.23(8)
Cd1—N5	2.225(2)	N5—Cd1—N1	90.92(8)
Cd1—N9	2.215(2)	N5—Cd1—N2 <sup>1</sup>	124.64(8)
		N5—Cd1—N3	54.36(8)
		N9—Cd1—N1	132.56(8)
		N9—Cd1—N2 <sup>1</sup>	95.54(8)

Symmetry codes: <sup>1</sup>+*x*, 1/2-*y*, -1/2+*z*

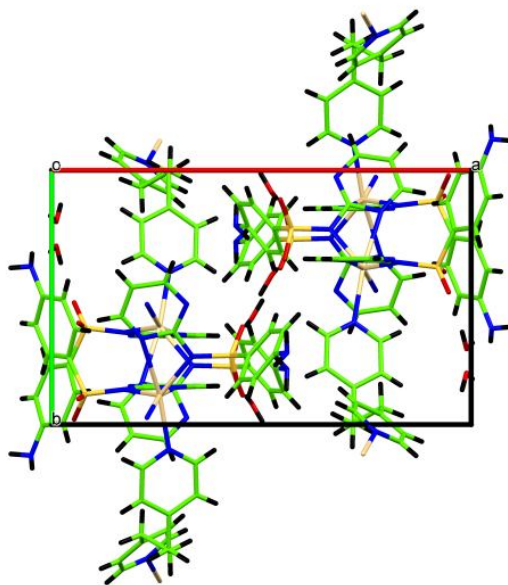


**Figure 109.** Packing diagram of  $\{[\text{Cd}(\text{bpp})(\text{sdz})_2] \cdot 2\text{H}_2\text{O}\}_n$  plotted down  $c$  axis.

In addition, each coordination polymer chain were linked by O—H $\cdots$ O [O6—H6F $\cdots$ O4<sup>1</sup>] (**Table 41**) intermolecular hydrogen bondings between oxygen atoms of sulfadiazine ligands and hydrogen of water molecules resulting in a 2-D supramolecular network (**Figure 110**).

**Table 41.** Hydrogen-bond geometry ( $\text{\AA}$ ,  $^\circ$ ) of  $\{[\text{Cd}(\text{bpp})(\text{sdz})_2] \cdot 2\text{H}_2\text{O}\}_n$ .

$D\text{---}H\cdots A$	$D\text{---}H$	$H\cdots A$	$D\cdots A$	$D\text{---}H\cdots A$
O5—H5B $\cdots$ O2	0.85	2.05	2.876(3)	163.1
O6—H6E $\cdots$ O3	0.85	1.97	2.811(3)	171.3
O6—H6F $\cdots$ O4 <sup>1</sup>	0.85	2.01	2.826(3)	160.8

Symmetry codes: <sup>1</sup>1-x,-1/2+y,3/2-z



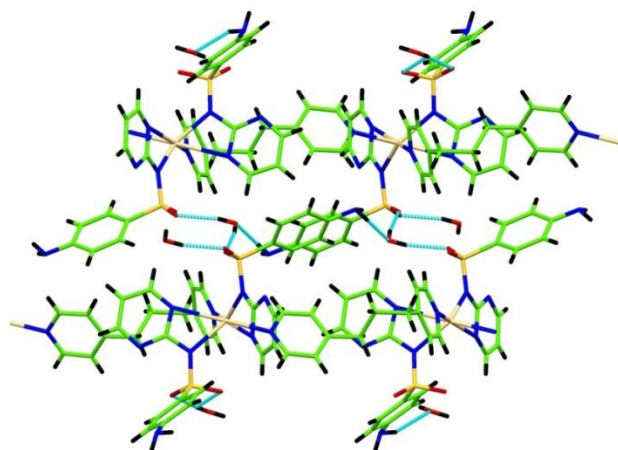


**Figure 110.** Coordination polymer chains are linked by O–H...O hydrogen bonding.

### Structural description of $\{[\text{Zn}(\text{bpe})(\text{sdz})(\text{ac})]\cdot 2\text{H}_2\text{O}\}_n$ (22)

Single crystal X-ray diffraction analyses showed that complex crystallized in the monoclinic system, space group  $P2_1/n$ . The 2-D coordination polymer was formed by the reaction between  $\text{Zn}(\text{ac})_2\cdot 2\text{H}_2\text{O}$ , bpe and sulfadiazine in a  $\text{H}_2\text{O}$ -MeOH solution by hydrothermal method. The complex contained one Zn atom, one bpe ligand, one acetate ligand, one sdz ligand, and one lattice water molecules in asymmetric unit. The Zn atom was four-coordinated in a tetrahedral geometry by coordinating to two nitrogen atoms from bpe ligands, one nitrogen atom from sdz ligand, and one oxygen atom from acetate ligand (**Figure 111**).

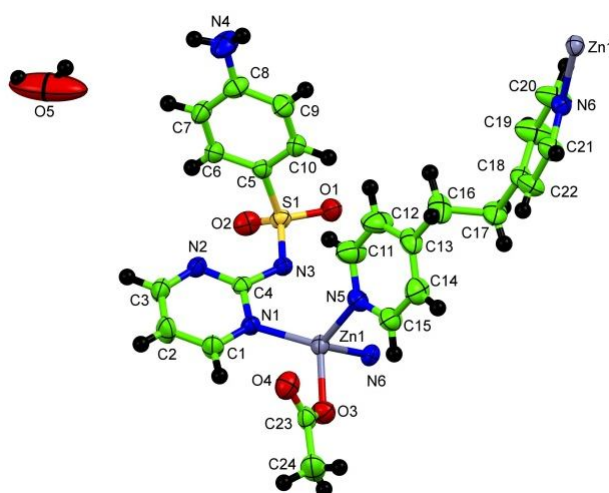


**Figure 111.** ORTEP representation of the asymmetric unit of  $\{[\text{Zn}(\text{bpe})(\text{sdz})(\text{ac})]\cdot 2\text{H}_2\text{O}\}_n$  (Thermal ellipsoids are drawn at 50% probability).

The Zn-O distances associated with the monodentate acetate ligand was 2.1287(18) Å, while Zn-N bond distances ranged from 2.071(2) Å to 2.0902(18) Å similar to those found in similar complex. The bond angles subtended at the Zn<sup>2+</sup> ions fit in the range 96.04(7)° - 126.29(7)° (**Table 42**) exhibiting slight departure from the corresponding value expected for a regular tetrahedron (theoretical values: 109.5), implying slight distortion of the tetrahedral coordination.

**Table 42.** Selected bond distances and angles of {[Zn(bpe)(sdz)(ac)]·2H<sub>2</sub>O}<sub>n</sub> (**22**).

Bond lengths (Å)		Bond angles (°)	
Zn1 — O3	2.1287(18)	O3 — Zn1 — N1	109.64(7)
Zn1 — N1	2.071(2)	O3 — Zn1 — N5	108.86(8)
Zn1 — N5	2.0785(18)	O3 — Zn1 — N6 <sup>1</sup>	96.04(7)
Zn1 — N6 <sup>1</sup>	2.0902(18)	N1 — Zn1 — N5	113.20(8)
		N1 — Zn1 — N6 <sup>1</sup>	126.29(7)
		N5 — Zn1 — N6 <sup>1</sup>	100.82(7)

Symmetry codes: <sup>1</sup>1/2-x, -1/2+y, 1/2-z

The crystal-packed molecular structure revealed the hydrogen bonds (**Table 43**) between the coordinated water molecules and the oxygen atoms of the sulfadiazine ligand [O5—H5A•••O1<sup>1</sup>] (**Figure 112**).

**Table 43.** Hydrogen-bond geometry (Å, °) of {[Zn(bpe)(sdz)(ac)]·2H<sub>2</sub>O}<sub>n</sub> (**22**).

<i>D</i> —H••• <i>A</i>	<i>D</i> —H	H••• <i>A</i>	<i>D</i> ••• <i>A</i>	<i>D</i> —H••• <i>A</i>
O5—H5A•••O1 <sup>1</sup>	0.85	2.21	2.859(4)	132.5

Symmetry codes: <sup>1</sup>1/2-x, 1/2+y, 3/2-z

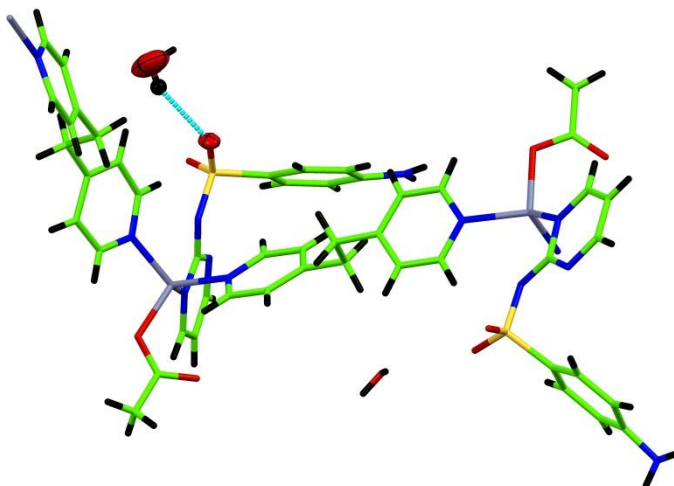


**Figure 112.** View of the O—H...O hydrogen bonds of  $\{[Zn(bpe)(sdz)(ac)] \cdot 2H_2O\}_n$ .

### 3.1.2 Elemental analysis

CHN analyzer is a scientific instrument which can determine the carbon (C), hydrogen (H), and nitrogen (N) elemental concentrations in a given sample. The CHN analysis of  $[Cd(Cin)_2(H_2O)_2]$  (**1**),  $[Zn(4,4'-bpy)_{0.5}(Cin)_2]_n$  (**2**),  $[Cd_3(4,4'-bpy)_2(cin)_6(H_2O)_2]_n$  (**3**),  $[Cd(4,4'-bpy)(3-Npt)(H_2O)]_n$  (**4**),  $[Mn_2(bpp)(3-Npt)_2(H_2O)_2]_n$  (**5**),  $[Ni(bpp)(3-Npt)(H_2O)]_n$  (**6**),  $\{[Ag_2(bpp)_2] \cdot (4H_2O) \cdot (3-Npt)\}_n$  (**7**),  $\{[Ag_2(bpe)_2(3-Npt)] \cdot 7H_2O\}_n$  (**8**),  $[Zn(bpp)_2(Sal)_2]_n$  (**9**),  $[Zn_2(bpe)_2(Sal)_4]$  (**10**),  $\{[Co(bpp)_2(H_2O)_2] \cdot (Abs)_2 \cdot H_2O\}_n$  (**11**),  $[Mn_{0.5}(bpp)(H_2O)_2] \cdot (4-abs)$  (**12**),  $\{[Cd_{0.5}(bpp)(4-abs)] \cdot (H_2O)\}_n$  (**13**),  $[Zn_{0.5}(bpp)(H_2O)_2] \cdot (4-abs)$  (**14**),  $\{[Zn(4,4'-bpy)(H_2O)_4] \cdot (4-abs)_2 \cdot 2H_2O\}_n$  (**15**),  $\{[Cd(4,4'-bpy)_{1.5}(H_2O)_3] \cdot (4-abs) \cdot (4,4'-bpy) \cdot (H_2O) \cdot NO_3\}_n$  (**16**),  $\{[Cd(bpe)_2(4-abs)_2] \cdot H_2O\}_n$  (**17**),  $[Zn(bpp)_2(Mbs)_2]_n$  (**19**),  $[Cd(bpp)_2(Mbs)_2]_n$  (**20**), and  $\{[Cd(bpp)(sdz)_2] \cdot 2H_2O\}_n$  (**21**) are reported in the **Table 44**.

**Table 44.** Analytical data (%) calcd (found) of complexes.

Code	Empirical formula	Formula weight	Cal. (Found)		
			C	H	N
1	C <sub>18</sub> H <sub>18</sub> CdO <sub>6</sub>	442.73	48.8 (48.88)	4.1 (4.06)	-
2	C <sub>23</sub> H <sub>18</sub> NO <sub>4</sub> Zn	437.77	63.1 (62.61)	4.1 (4.01)	3.2 (3.57)
3	C <sub>74</sub> H <sub>62</sub> Cd <sub>3</sub> N <sub>4</sub> O <sub>14</sub>	1568.51	56.7 (55.86)	4.0 (3.71)	3.6 (3.42)
4	C <sub>18</sub> H <sub>13</sub> CdN <sub>3</sub> O <sub>7</sub>	495.72	43.6 (42.23)	2.6 (2.38)	8.5 (8.39)
5	C <sub>29</sub> H <sub>28</sub> Mn <sub>2</sub> N <sub>4</sub> O <sub>16</sub>	798.43	43.6 (43.92)	3.5 (3.46)	7.0 (6.96)
6	C <sub>21</sub> H <sub>19</sub> N <sub>3</sub> NiO <sub>7</sub>	484.08	52.1 (51.76)	4.0 (3.87)	8.7 (8.53)
7	C <sub>34</sub> H <sub>39</sub> Ag <sub>2</sub> N <sub>5</sub> O <sub>10</sub>	893.38	45.7 (45.12)	4.4 (4.18)	7.8 (7.25)
8	C <sub>32</sub> H <sub>41</sub> Ag <sub>2</sub> N <sub>5</sub> O <sub>13</sub>	919.44	41.8 (42.02)	4.5 (4.21)	7.6 (7.59)
9	C <sub>27</sub> H <sub>24</sub> N <sub>2</sub> O <sub>6</sub> Zn	537.87	60.3 (59.24)	4.5 (4.02)	5.2 (5.14)
10	C <sub>52</sub> H <sub>44</sub> N <sub>4</sub> O <sub>12</sub> Zn <sub>2</sub>	1047.69	59.6 (59.21)	4.2 (4.10)	5.3 (5.35)
11	C <sub>38</sub> H <sub>48</sub> CoN <sub>6</sub> O <sub>10</sub> S <sub>2</sub>	871.87	52.3 (51.92)	5.5 (5.62)	9.6 (9.10)
12	C <sub>38</sub> H <sub>48</sub> MnN <sub>6</sub> O <sub>10</sub> S <sub>2</sub>	867.88	52.6 (52.31)	5.6 (5.24)	9.7 (9.29)
13	C <sub>38</sub> H <sub>44</sub> Cd N <sub>6</sub> O <sub>4</sub> S	889.32	51.2 (50.78)	4.9 (4.75)	9.4 (9.10)
14	C <sub>38</sub> H <sub>48</sub> N <sub>6</sub> O <sub>10</sub> S <sub>2</sub> Zn	878.32	52.0 (51.71)	5.5 (5.43)	9.6 (9.73)
15	C <sub>22</sub> H <sub>32</sub> N <sub>4</sub> O <sub>12</sub> S <sub>2</sub> Zn	674.01	39.2 (39.71)	4.7 (4.52)	8.3 (8.90)
16	C <sub>31</sub> H <sub>34</sub> Cd N <sub>7</sub> O <sub>10</sub> S	809.11	45.9 (46.12)	4.2 (4.45)	12.1 (11.43)
17	C <sub>36</sub> H <sub>40</sub> Cd N <sub>6</sub> O <sub>8</sub> S <sub>2</sub>	861.27	50.2 (50.16)	4.7 (4.18)	9.8 (9.02)
19	C <sub>40</sub> H <sub>42</sub> N <sub>4</sub> O <sub>6</sub> S <sub>2</sub> Zn	804.29	59.7 (60.15)	5.3 (5.27)	7.0 (6.23)
20	C <sub>40</sub> H <sub>42</sub> Cd N <sub>4</sub> O <sub>6</sub> S <sub>2</sub>	851.31	56.4 (55.96)	5.0 (4.55)	6.6 (6.22)
21	C <sub>33</sub> H <sub>36</sub> Cd N <sub>10</sub> O <sub>6</sub> S <sub>2</sub>	845.25	46.9 (46.78)	4.3 (4.25)	16.6 (16.14)

Results obtained from CHN analysis of complexes, % carbon, % nitrogen, and % hydrogen were comparable with the theoretical values of C, N, and H. From the data confirms that the compositions of the prepared complexes are in good agreement with theoretical values. The CHN information was consistent with the results from the X-ray single crystal analysis of the complexes. The disordered of lattice water molecules in complex (7) could not be located, and was thus removed by using the solvent mark in *Olex2*. So CHN analysis can confirm number of water molecules of complex (7) that has four water molecules in the molecular structure.

### 3.1.3 Infrared Spectroscopy

Infrared Spectroscopy is used to determine functional groups of organic and inorganic molecules. IR spectroscopy measures the vibrations of atoms, and based on this it is possible to determine the functional groups. Selected IR spectral data of the metal complexes (1) - (10) are displayed in **Table 45** and selected IR spectral data of the metal complexes (11) - (22) are displayed in **Table 46**.

**Table 45.** Characteristic IR vibration frequencies ( $\text{cm}^{-1}$ ) of the prepared complexes.

Code	$\nu(\text{-OH})$	$\nu \text{ CH sp}^2$	$\nu \text{ CH sp}^3$	$\nu_{\text{as}}(\text{C=O})$	$\nu_{\text{sym}}(\text{C=O})$	$\nu_s(\text{NO}_2)$	$\nu(\text{C-N})$	Pyridine ring
1	3368	3057	-	1581	1466	-	-	745,710, 631
2	-	3063	2948	1597, 1542	1389, 1359	-	1220	773,714, 688
3	3394	3024	2927	1594 1552 1573	1442 1394 1354	-	1220	809,715, 613
4	3368	3057	-	1581 1602	1466 1384	1390, 1358	1220	745,710, 631
5	3420	3063	2948	1597, 1542	1389, 1359	1390, 1386	1217	754,713, 619
6	3400	3066	2953	1604 1540	1380 1362	1351	1224	815,717, 690
7	3394	3024	2927	1590	1413	1386, 1345	1220	809,715, 613
8	3423	3055	2927	1598	1410	1353	1224	832,716
9	3420	3054	2945	1620	1396	-	1225	863,769, 621
10	3400	3057	2959	1619	1396	-	1229	864,759, 670

The FT-IR spectra of all complexes were recorded in the range 4000 – 400  $\text{cm}^{-1}$ .

The bands at about 3400  $\text{cm}^{-1}$  was assigned to the symmetric OH stretching of water molecules in the complexes **(1)** and **(3)** – **(8)** and OH stretching of hydroxyl group at benzene of salicylate ligand in the complexes **(9)** – **(10)**

The medium intensity absorption band of the unsaturated ( $\text{CH}$ ,  $sp^2$ ) and saturated ( $\text{CH}$ ,  $sp^3$ ) C-H stretching vibrations ( $\nu_{=\text{CH}}$  and  $\nu_{\text{CH}}$ ) appeared at about 3063  $\text{cm}^{-1}$  and 2948  $\text{cm}^{-1}$ , respectively.

From IR data of complexes with carboxylate ligands, the absence of bands in the area of  $\sim 1710 \text{ cm}^{-1}$  indicated full deprotonation of carboxylate groups in complexes **(1)** - **(10)**.

The C = O stretch vibrations of carboxylate ligand in complex compared with the same mode in free carboxylic acid molecule showed significant blue-shift due to the deprotonation of the carboxylic group and the coordination interactions between metal ions and ligand.

The strong band near  $\sim 1600 \text{ cm}^{-1}$  and  $\sim 1350 \text{ cm}^{-1}$  were assigned as asymmetric and symmetric stretching vibrations of the carboxylate groups respectively, which appeared from the presence of benzoate molecule in the complexes. The difference of  $[\nu_{\text{as}}(\text{COO}^-) - \nu_{\text{sym}}(\text{COO}^-)]$ ,  $\Delta\nu$ , value of carboxylate group can be used to discriminate between modes of coordination of carboxylate group, i.e. monodentate, chelating bidentate bridging mode, or ionic(non-coordinatate). In generally, the following order was proposed for metal carboxylates (Nara *et al.*, 2013).

$$\Delta\nu(\text{chelating}) (\approx 120 \text{ cm}^{-1}) < \Delta\nu \text{ of ionic} \sim \Delta\nu \text{ of bridging} (\approx 160-199 \text{ cm}^{-1}) < \Delta\nu \text{ of monodentate} (> 200 \text{ cm}^{-1})$$

As an example, the C = O stretch vibrations of cinnamate ligand in complex **(1)** had one value of  $\Delta\nu_{\text{COO}} = \nu_{\text{as}(\text{COO})}[1581] - \nu_{\text{sym}(\text{COO})}[1466] = 114 \text{ cm}^{-1}$  indicating bidentate chelate mode of carboxylate group.

For complex **(2)** and complex **(6)**, the positions of the stretching C = O vibrations (asym,sym) of carboxylate ligand occurred at (1597,1389) and (1542,1359)

for complex **(2)**, (1604,1380) and (1540,1362) for complex **(6)** indicating bidentate chelate mode and monodentate of carboxylate group.

Three C=O stretches of complex **(3)** appeared at (1594, 1442) , (1552, 1394), and (1574, 1354)  $\text{cm}^{-1}$  which were assigned to  $\nu_{\text{as}}(\text{COO})$  and  $\nu_{\text{s}}(\text{COO})$  vibrations of three types of cinnamate ligands. The  $\Delta\nu_{\text{COO}} = \nu_{\text{as}}(\text{COO}) - \nu_{\text{sym}}(\text{COO})$  were 152, 202 and 220  $\text{cm}^{-1}$  corresponding to the presence of bidentate, monodentate, and bridging carboxylate group, respectively, of cinnamic acid

The asymmetric and symmetric stretching vibrations of the carboxylate groups from complex **(4)** were observed at (1581, 1466) and (1602, 1384). The values of  $\Delta\nu_{\text{COO}}$  bands indicated the presence of chelating (155  $\text{cm}^{-1}$ ) and monodentate (208  $\text{cm}^{-1}$ ) coordination modes of the carboxyl groups.

For complex **(5)**, two values of  $\Delta\nu_{\text{COO}}$  were 183 and 208  $\text{cm}^{-1}$  which showed that bridging and monodentate carboxylate group of 3-nitrophthalate ligands were used, respectively.

Complexes **(7)** and **(8)** showed one value of  $\Delta\nu_{\text{COO}} = 187 \text{ cm}^{-1}$  for complex **(7)** and 198  $\text{cm}^{-1}$  for complex **(8)** indicating the carboxylate groups of both complexes were not coordinated to the Ag atoms.

Complexes **(9)** - **(10)** showed one value of  $\Delta\nu_{(\text{COO})} = 224 \text{ cm}^{-1}$  for complex **(9)** and 223  $\text{cm}^{-1}$  for complex **(10)** indicating monodentate mode of carboxylate group of the salicylate ligand.

The strong peaks of the symmetric stretching nitro group ligand ,  $\nu_{\text{s}}(\text{NO}_2)$ , at about 1390 and 1386  $\text{cm}^{-1}$  and asymmetric stretching ,  $\nu_{\text{as}}(\text{NO}_2)$ , at about 1530 and 1507  $\text{cm}^{-1}$  from 3-nitrophthalate were observed.



**Table 46.** Characteristic IR vibration frequencies ( $\text{cm}^{-1}$ ) of the prepared complexes.

Complexes	$\nu(\text{-OH})$	$\nu(\text{-NH}_2)$	$\nu \text{ CH } \text{sp}^2$	$\nu \text{ CH } \text{sp}^3$	$\nu(\text{C-N})$	$\nu_{\text{as}}(\text{SO}_3^-)$	Pyridine ring
11	3415	3340,3245	3024	2919	1217	1156-1029	819,784,696
12	3461	3357,3226	3057	2941	1246	1163-1033	819,783,693
13	3459	3357,3225	3068	2941	1221	1184-1034	834,819,692
14	3400	3381,3214	3077	2951	1222	1177-1041	822,707,690
15	3402	3320,3207	3036	2930	1224	1178-1037	821,791,689
16	3449	3351,3308	3015	2923	1240	1158-1034	829,781,690
17	3457	3367,3205	3064	2938	1228	1172-1096	820,705,695
18	3420	3320,3207	3036	2932	1224	1178-1037	826,703
19	-	-	3059	2945	1259	1175-1036	821,792,678
20	-	-	3065	2945	1257	1176-1137	824,798,679
21	3482	3320,3190	3033	2920	1247	-	832,741,680
22	-	3380,3307	3019	2923	1234	-	821,753,680

The bands at about  $3400 \text{ cm}^{-1}$  hinted the presence of water molecules in the complexes. The medium intensity bands about  $3320$  and  $3207 \text{ cm}^{-1}$  in complexes (11)-(18) were due to the stretching vibrations of primary amino group  $\nu(\text{N-H})$  of aminobenzenesulfonate ligand. The position of  $\nu(\text{N-H})$  was shifted to low wavenumber in complexes due to weak hydrogen bonding interaction.

The medium intensity band of the unsaturated ( $\text{CH}, \text{sp}^2$ ) and saturated ( $\text{CH}, \text{sp}^3$ ) C-H stretching vibrations ( $\nu_{=\text{CH}}$  and  $\nu_{\text{CH}}$ ) appeared at about  $3063 \text{ cm}^{-1}$  and  $2948 \text{ cm}^{-1}$ , respectively. Strong bands in the range  $1178\text{-}1037 \text{ cm}^{-1}$  was characteristic of the fundamental and splitting of  $\nu(\text{S-O})$  asymmetric and symmetric stretching modes. The C-N stretching vibration appeared at  $1224 \text{ cm}^{-1}$  indicating the pyridine group being included in the complexes.

The band at about 800 - 600  $\text{cm}^{-1}$  of all complexes was assigned to the out-of-plane C-H vibration of benzene ring of the organic ligand (Yu *et al.*, 2014). The analysis of IR spectra was consistent with the single crystal X-ray analysis.

The medium intensity bands in the low frequency regions 450-440  $\text{cm}^{-1}$  and 410–414  $\text{cm}^{-1}$  (**Figure A20-A41 in Appendix**) were due to metal oxygen [ $\nu(\text{M-O})$ ] and metal nitrogen [ $\nu(\text{M-N})$ ] stretching vibrations, which could be taken as evidences of coordination through oxygen and nitrogen atoms of the organic ligand.

### 3.1.4 Thermogravimetric analysis

Thermogravimetric analysis is commonly used to determine selected characteristics of materials that exhibit mass loss due to decomposition. Common applications of TGA are (1) materials characterization through analysis of characteristic decomposition patterns, (2) studies of degradation mechanisms and reaction kinetics, (3) determination of organic contents in a sample, and (4) determination of inorganic (e.g. ash) contents in a sample, which may be useful for corroborating predicted material structures or simply used as a chemical analysis (Nickolay *et al.*, 2009).

All complexes were measured by the thermogravimetric analyses under nitrogen atmosphere with a heating rate of 10°/minute in the temperature range 50–1000 °C. The results are shown in **Table 47** and **Appendix Figures A1-A19**.

**Table 47.** Thermal behavior of complexes.

Complexes	Thermogravimetry(TG)		Weight loss (%)	
	Stage	Temp. range()	Found	Calculated
[Cd(Cin) <sub>2</sub> (H <sub>2</sub> O) <sub>2</sub> ] ( <b>1</b> )	I	84-200	8.38	8.14
	II	200-610	62.44	66.96
[Zn(4,4'-bpy) <sub>0.5</sub> (Cin) <sub>2</sub> ] <sub>n</sub> ( <b>2</b> )	I	130-250	29.81	33.86
	II	250-370	52.12	51.73
[Cd <sub>3</sub> (4,4'-bpy) <sub>2</sub> (cin) <sub>6</sub> (H <sub>2</sub> O) <sub>2</sub> ] <sub>n</sub> ( <b>3</b> )	I	100-150	3.12	2.27
	II	160-360	56.88	54.41
	III	360-590	19.42	18.34
[Cd(4,4'-bpy)(3-Npt)(H <sub>2</sub> O)] <sub>n</sub> ( <b>4</b> )	I	70 -140	5.47	3.65
	II	140 – 850	71.43	74.14

**Table 47.** Thermal behavior of complexes (continued).

Complexes	Thermogravimetry(TG)		Weight loss (%)	
	Stage	Temp. range()	Found	Calculated
[Mn <sub>2</sub> (bpp)(3-Npt) <sub>2</sub> (H <sub>2</sub> O) <sub>2</sub> ] <sub>n</sub> ( <b>5</b> )	I	108-166	9.01	9.31
	II	166-352	26.44	26.92
	III	329-680	21.02	24.81
{[Ag <sub>2</sub> (bpp) <sub>2</sub> ](4H <sub>2</sub> O)(3-Npt)} <sub>n</sub> ( <b>7</b> )	I	120 - 160	7.47	8.24
	II	160 - 500	65.73	68.16
{[Ag <sub>2</sub> (bpe) <sub>2</sub> (3-Npt)]·7H <sub>2</sub> O} <sub>n</sub> ( <b>8</b> )	I	100-150	12.43	15.66
	II	150 - 350	59.92	62.97
[Zn(bpp) <sub>2</sub> (Sal) <sub>2</sub> ] <sub>n</sub> ( <b>9</b> )	I	250 – 720	87.98	87.84
[Zn <sub>2</sub> (bpe) <sub>2</sub> (Sal) <sub>4</sub> ] ( <b>10</b> )	I	250 - 850	88.08	87.94
{[Co(bpp) <sub>2</sub> (H <sub>2</sub> O) <sub>2</sub> ](4-abs) <sub>2</sub> ·H <sub>2</sub> O} <sub>n</sub> ( <b>11</b> )	I	100-180	6.43	6.19
	II	180-300	42.76	40.02
	III	300-500	20.21	17.32
[Mn <sub>0.5</sub> (bpp)(H <sub>2</sub> O) <sub>2</sub> ](4-abs) ( <b>12</b> )	I	80-200	3.95	4.12
	II	200-300	46.51	45.95
	III	300 - 850	35.43	39.95
{[Cd <sub>0.5</sub> (bpp)(4-abs)]·(H <sub>2</sub> O)} <sub>n</sub> ( <b>13</b> )	I	200-300	45.13	43.65
	II	300-850	45.71	44.75
[Zn <sub>0.5</sub> (bpp)(H <sub>2</sub> O) <sub>2</sub> ](4-abs) ( <b>14</b> )	I	100 – 200	8.52	8.20
	II	200 – 270	44.21	45.33
	III	270 - 700	37.21	39.40
{[Zn(4,4'-bpy)(H <sub>2</sub> O) <sub>4</sub> ](4-abs) <sub>2</sub> ·2H <sub>2</sub> O} <sub>n</sub> ( <b>15</b> )	I	70-160	14.27	16.02
	II	160-360	23.14	22.38
	III	360-560	52.01	51.33
{[Cd(4,4'-bpy) <sub>1.5</sub> (H <sub>2</sub> O) <sub>3</sub> ](4-abs)(4,4'-bpy)(H <sub>2</sub> O)·NO <sub>3</sub> } <sub>n</sub> ( <b>16</b> )	I	90-150	10.01	10.01
	II	150-270	24.72	25.95
	III	270-550	49.92	50.30
{[Cd(bpe) <sub>2</sub> (4-abs) <sub>2</sub> ](H <sub>2</sub> O)} <sub>n</sub> ( <b>17</b> )	I	240 - 280	46.21	44.35
	II	280 - 800	39.97	42.72
{[Cd(bpp) <sub>2</sub> (H <sub>2</sub> O) <sub>4</sub> ](3-abs) <sub>2</sub> ·2H <sub>2</sub> O} <sub>n</sub> ( <b>18</b> )	I	240-280	48.61	47.24
	II	275-800	40.19	41.41
[Zn(bpp) <sub>2</sub> (Mbs) <sub>2</sub> ] <sub>n</sub> ( <b>19</b> )	I	260 – 370	42.21	43.03
	II	370 - 560	48.12	49.50
[Cd(bpp) <sub>2</sub> (Mbs) <sub>2</sub> ] <sub>n</sub> ( <b>20</b> )	I	250-340	41.24	40.65
	II	340-560	48.15	46.53

The TGA curve for complex (**1**) showed the first weight loss (8.38 %) between 84 – 200 °C attributed to removal of two coordination water molecules (calculated 8.14%), and the second weight loss of 62.44% occurred in the range 200-610 °C

corresponded to loss of the two cinnamate ligands (cal. 66.96 %). The final residue was taken as a Cd oxide at 660 °C.

Complex **(2)** showed a two-step weight-loss process. The initial one (29.81%) between 130-250 °C was assigned to one cinnamate ligand (calculated 33.86%). The second weight loss (52.15%) between 250-370 °C was assigned to one cinnamate and 4,4'-bpy ligands (calculated 51.73%). On further heating the residue started to decompose completely to ZnO.

Complex **(3)** showed a three-step weight-loss process. The initial one (3.21%) between 100-150 °C was assigned to two water ligands (calculated 2.27%). The second weight loss (56.88%) between 160-360 °C was assigned to five cinnamate and 4,4'-bpy ligand (calculated 54.41%). The third weight loss was 19.42 % in the temperature range 400 – 590 °C corresponding to one cinnamate and 4,4'-bpy ligands (calculated 18.34%). On further heating the residue started to decompose completely to CdO.

Complex **(4)** showed a two-step weight-loss process. The initial one (5.47%) between 70-140 °C was assigned to one water ligand (calculated 3.65%). The second weight loss (71.43%) between 140 – 850 °C was assigned to two 3-Npt and 4,4'-bpy ligands (calculated 74.14%). On further heating the residue started to decompose completely to CdO.

Complex **(5)** showed a three-step weight-loss process. The initial one (9.01%) between 108-166°C was assigned to four water ligands (calculated 9.31%). The second weight loss (26.44%) between 166-352°C was assigned to two 3-Npt ligands (calculated 26.92%). The third weight loss was 21.02% in the temperature range 329-680 °C corresponding to one bpp ligand (calculated 24.81%). On further heating the residue started to decompose completely to MnO.

Complex **(7)** showed a two-step weight-loss process. The initial one (7.47%) between 120 – 160 °C was assigned to four water molecules (calculated 8.24%). The second weight loss (65.73%) between 160 – 500 °C was assigned to one bpp and 3-Npt ligands (calculated 68.16%). On further heating the residue started to decompose completely to Ag<sub>2</sub>O.

Complex **(8)** showed a two-step weight-loss process. The initial one (12.43%) between 100-150°C was assigned to seven water molecules (calculated 15.66%).

The second weight loss (59.92%) between 150 – 350 °C was assigned to two bpe and 3-Npt ligands (calculated 62.97%). On further heating the residue started to decompose completely to Ag<sub>2</sub>O.

Complex **(9)** and **(10)** showed a one-step weight-loss process. The initial one (87.98%) between 250 – 720 °C was assigned to one salicylate and one bpp ligands (calculated 87.84%) for complex **(9)**, and the initial step (88.08%) between 250 – 850 °C was assigned to one salicylate ligand and one bpe ligand (calculated 87.94%) for complex **(10)**. On further heating the residue started to decompose completely to ZnO. The TGA of complexes **(9)** – **(10)** showed no losses below ca. 250 °C which indicated that there were no crystallization water or coordinated water molecules.

Complex **(11)** showed a three-step weight-loss process. The initial one (6.43%) between 100-180 °C was assigned to three water ligands (calculated 6.19%). The second weight loss (44.76%) between 180-300 °C was assigned to two 4-Abs ligand (calculated 40.02 %). The third weight loss was 20.21% in the temperature range 300-500 °C corresponding to one bpp ligand (calculated 17.32%). On further heating the residue started to decompose completely to CoO.

Complex **(12)** showed a three-step weight-loss process. The initial one (5.24%) between 80-200 °C was assigned to water ligand (calculated 8.31%). The second weight loss (46.51%) between 200-350 °C was assigned to bpp ligand (calculated 45.32%). The third weight loss was 35.04% in the temperature range of 350-800 °C corresponding to 4-Abs ligand (calculated 39.95%). On further heating the residue started to decompose completely to MnO.

Complex **(13)** showed a two-step weight-loss process. The initial one (45.13%) between 200-300 °C was assigned to one 4-Abs ligand and one water molecule (calculated 43.65%). The second weight loss (45.71%) between 300-850 °C was assigned to bpp ligand (calculated 44.75 %). On further heating the residue started to decompose completely to CdO.

Complex **(14)** showed a three-step weight-loss process. The initial one (8.52%) between 100-200 °C was assigned to water ligand (calculated 8.20%). The second weight loss (44.21%) between 200-270 °C was assigned to bpp ligand (calculated 45.33%). The third weight loss was 37.21% in the temperature range

270 – 700 °C corresponding to 4-Abs ligand (calculated 39.40%). On further heating the residue started to decompose completely to ZnO.

Complex **(15)** showed a three-step weight-loss process. The initial one (14.27%) between 70 - 160 °C was assigned to six water ligands (calculated 16.02%). The second weight loss (23.14%) between 160-360 °C was assigned to 4,4'-bpy ligand (calculated 22.38%). The third weight loss was 52.01% in the temperature range 360 – 560 °C corresponding to two 4-Abs ligands (calculated 51.33%). On further heating the residue started to decompose completely to ZnO.

Complex **(16)** showed a three-step weight-loss process. The initial one (10.01%) between 90 - 150 °C was assigned to one water molecule and nitrate ion (calculated 10.01%). The second weight loss (24.72%) between 150-270 °C was assigned to 4,4'-bpy ligand and one water molecule (calculated 25.95%). The third weight loss was 49.92% in the temperature range 270 - 550 °C corresponding to 4-Abs and 4,4'-bpy (calculated 50.30%). On further heating the residue started to decompose completely to CdO.

Complex **(17)** showed a two-step weight-loss process. The initial one (46.21%) between 240 - 280 °C was assigned to one water molecule (calculated 44.35%). The second weight loss (39.97%) between 280 - 800 °C was assigned to one bpe ligand (calculated 4.72%). On further heating the residue started to decompose completely to CdO.

Complex **(18)** showed a two-step weight-loss process. The initial one (46.21%) between 240-280 °C was assigned to six water molecules and two 3-Abs ligands (calculated 47.24%). The second weight loss (40.19%) between 280-800 °C was assigned to bpp ligand (calculated 41.41 %). On further heating the residue started to decompose completely to CdO.

Complex **(19)** showed a two-step weight-loss process and there were no losses below ca. 250 °C which indicated that there were no crystallization water or coordinated water molecules. The initial step (42.21%) between 260 – 370 °C was assigned to two Mbs ligands (calculated 43.03%). The second weight loss (48.12%) between 370 – 560 °C was assigned to two bpp ligands (calculated 49.50%). On further heating the residue started to decompose completely to ZnO.

Complex **(20)** showed a two-step weight-loss process. The initial one (41.24%) between 250-340 °C was assigned to two Mbs ligands (calculated 40.65%). The second weight loss (48.15%) between 340-560 °C was assigned to two bpp ligands (calculated 46.53%). On further heating the residue started to decompose completely to CdO.

### 3.1.5 Electronic absorption studies

The UV and visible spectra of  $\{[\text{Co}(\text{bpp})_2(\text{H}_2\text{O})_2](4\text{-abs})_2\cdot\text{H}_2\text{O}\}_n$  (**11**) at room temperature in DMSO as the solvent are displayed in **Figure 113** and **Figure 114**.

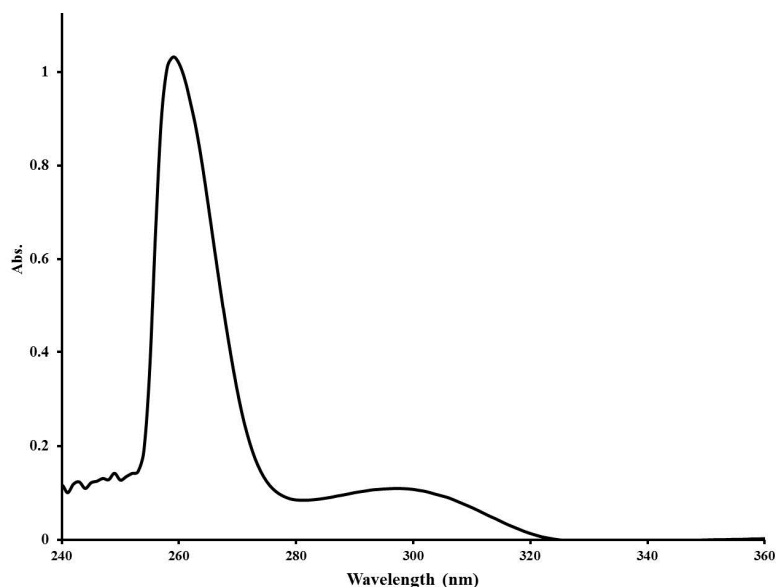


**Figure 113.** Ultraviolet absorption spectrum of  $\{[\text{Co}(\text{bpp})_2(\text{H}_2\text{O})_2](4\text{-abs})_2\cdot\text{H}_2\text{O}\}_n$  (**11**)

The strong absorption band in the ultraviolet region 250-280 nm was attributed to intraligand  $\pi \rightarrow \pi^*$  transition of benzene ring. The second band observed at 300 nm could be assigned to the intraligand charge transfer transitions.

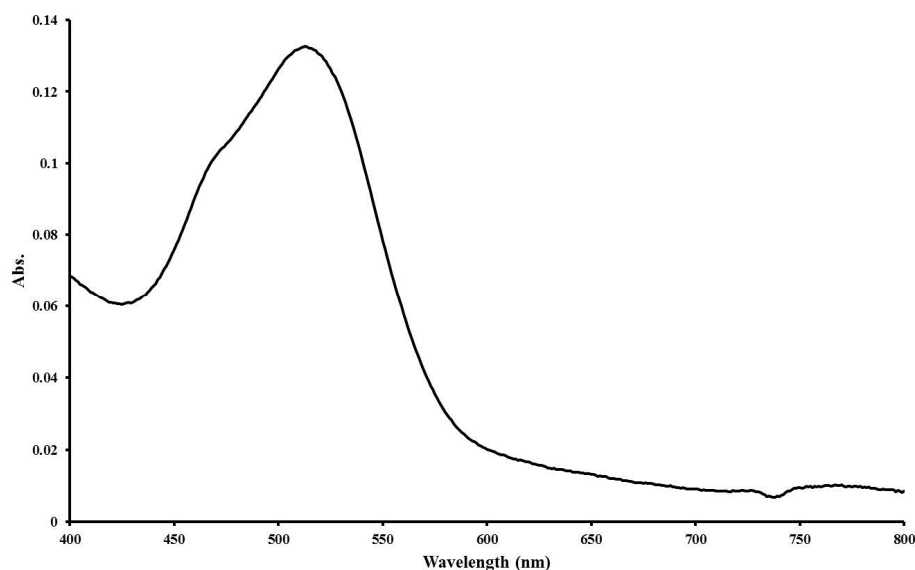


**Figure 114.** Visible absorption spectrum of  $\{[\text{Co}(\text{bpp})_2(\text{H}_2\text{O})_2] \cdot (4\text{-abs})_2 \cdot \text{H}_2\text{O}\}_n$  (**11**)

In the visible spectrum of  $\{[\text{Co}(\text{bpp})_2(\text{H}_2\text{O})_2] \cdot (4\text{-abs})_2 \cdot \text{H}_2\text{O}\}_n$  (**11**) one lower energy peak was observed at 515 nm which was assigned to d-d spin-allowed  ${}^4\text{T}_{1g} \rightarrow {}^4\text{A}_{2g}$  transition and a shoulder at around 470 nm assigned to  ${}^4\text{T}_{1g} \rightarrow {}^4\text{T}_{1g}(\text{P})$  transition. These absorption bands were consistent with high spin Co(II) in an octahedral coordination environment similar to those reported in the literatures (Timothy *et al.*, 2011 and Kai *et al.*, 2016).

### 3.1.6 Powder X-ray diffraction (PXRD)

Powder X-ray diffraction (PXRD) patterns of complexes were checked at room temperature, as shown in **Appendix (Figures A41-A59)**. From the data, one can see that PXRD pattern of the complexes agreed with the simulated pattern generated by the single-crystal X-ray data using the Mercury 3.8 program indicating pure phase purity of the as-synthesized product. The intensity difference between experimental and simulated PXRD patterns could be due to the preferred orientation of the crystalline powder sample.



### 3.1.7 Nuclear magnetic resonance spectroscopy

Nuclear Magnetic Resonance (NMR) spectroscopy has become the dominant method of analysis for organic and inorganic compounds, because in many cases it provides a way to determine an entire structure using one set of analytical tests. It is also increasingly used in inorganic chemistry and biochemistry, where it also provides a lot of valuable structural information (Ioannis *et al.*, 2002).

The  $^1\text{H}$  NMR spectra of the complex **(9)** and **(10)** were recorded in DMSO- $\text{d}_6$  as shown in **Appendix (Figures A64-A65)**. The resonance broad peak was observed at 13 ppm corresponding to the O–H $\cdots$ O proton involved in the relevant intramolecular hydrogen bond via hydroxyl group and carboxylic group of salicylate ligand.

The signal in the region of chemical shift ( $\delta$ ) 8.47 - 6.70 ppm were assigned to aromatic ring protons of bpp ligand (**Table 48**) for complex **(9)** or bpe ligand for complex **(10)** and salicylate ligand.

**Table 48.** Chemical shift of protons from aromatic ring (ppm).

Compound	Chemical shift of aromatic ring protons (ppm)
Bpp	8.52,7.14
Bpe	8.48,7.20
Salicylic acid	6.85 - 7.90
$[\text{Zn}(\text{bpp})_2(\text{Sal})_2]_n$ <b>(9)</b>	8.47, 7.76, 7.27, 6.76
$[\text{Zn}_2(\text{bpe})_2(\text{Sal})_4]$ <b>(10)</b>	8.55, 7.86, 7.30, 6.84

For complex **(9)**, two signals at  $\delta = 7.27$  and 8.47 ppm were assigned to the aromatic ring protons of bpp ligand and another set of signals at  $\delta = 7.76$  and 6.76 ppm for salicylate ligand. In addition, two other signals at  $\delta = 1.90$  and 2.62 ppm were assigned to the  $-\text{CH}_2\text{CH}_2\text{CH}_2-$  protons of the bpp ligand

In complex **(10)**, the signals at 7.30 and 8.55 were attributed to aromatic ring protons of bpe ligand and another two signals at  $\delta = 7.86$  and 6.84 ppm were due to protons from salicylate ligand. The signal at  $\delta = 2.93$  ppm was assigned to the  $-\text{CH}_2\text{CH}_2-$  protons of the bpe ligand. For the signal at  $\delta = 2.5$  ppm which showed up in both spectra of complexes **(9)** and **(10)** were due to DMSO- $\text{d}_6$ .

### 3.1.8 Photoluminescent property

Photoluminescence is light emission from any form of matter after a material absorbs light. It is one of many forms of luminescence (light emission) and is initiated by photoexcitation (excitation by photons), therefore the prefix photo-. Following excitation various relaxation processes typically occur in which other photons are re-radiated. Time periods between emission and absorption may vary: ranging from short femtosecond-regime for emission involving free-carrier plasma in inorganic semiconductors up to milliseconds for phosphorescent processes in molecular systems; and under circumstances delay of emission may even span to minutes or hours (Hayes *et al.*, 2002 and <https://en.wikipedia.org/Photoluminescence>).

#### **Photoluminescent property of metal complexes with O-donor ligand from benzoate ligand**

The solid-state luminescent properties of complex **(2)**, solution-state luminescent properties of complex **(9)** and **(10)** were investigated at room temperature. Complexes **(1)** and **(3) - (8)** did not show luminescent properties. The resulting emission spectra are given in **Figures 115- 118**.

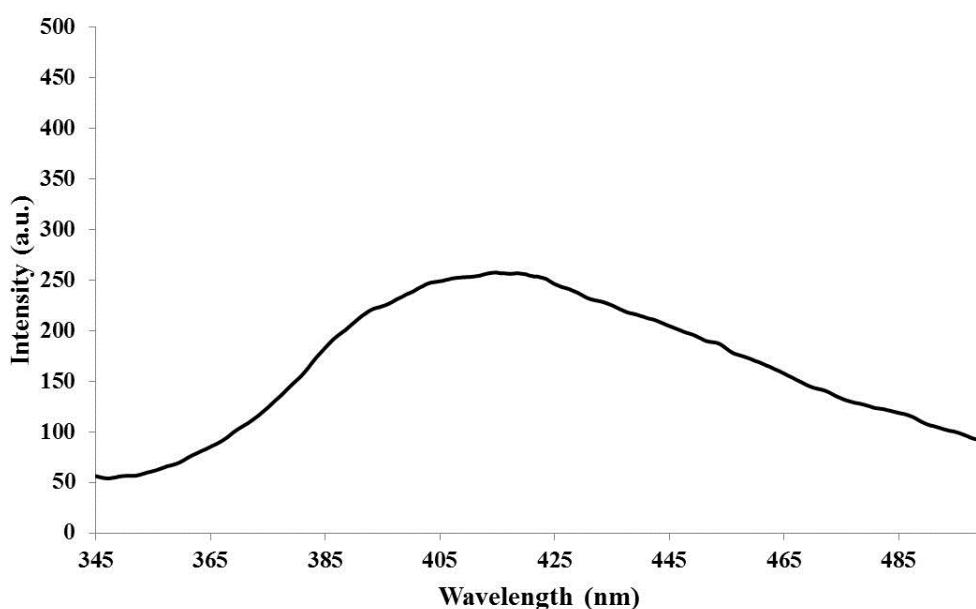


**Figure 115.** Solid-state emission spectrum of complex **(2)** at room temperature.

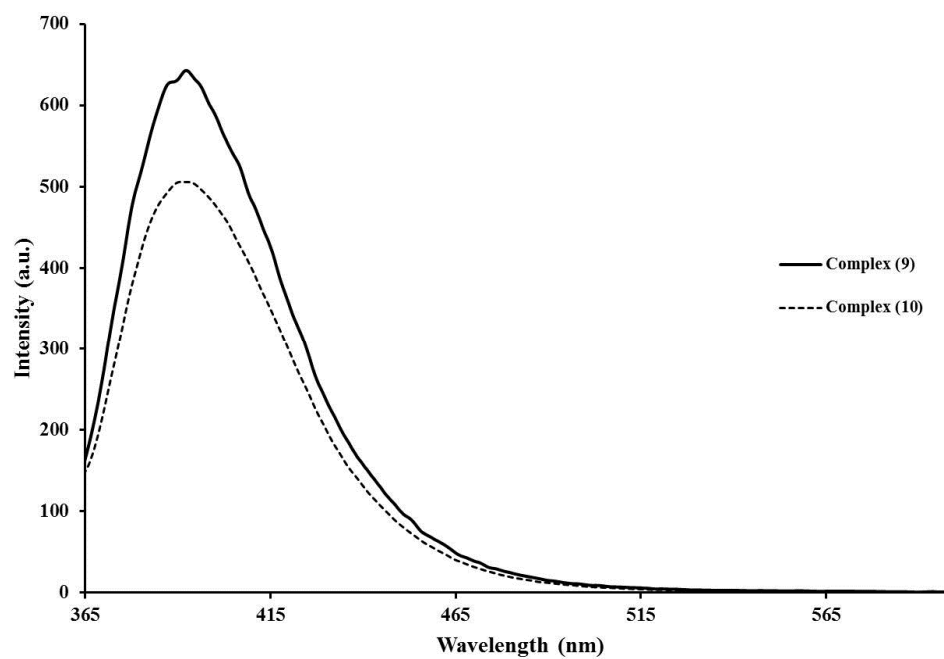


**Figure 116.** The emission spectra of complexes (9) - (10) at room temperature.



**Figure 117.** Fluorescent image of complex (9) in DMSO solution at room temperature.

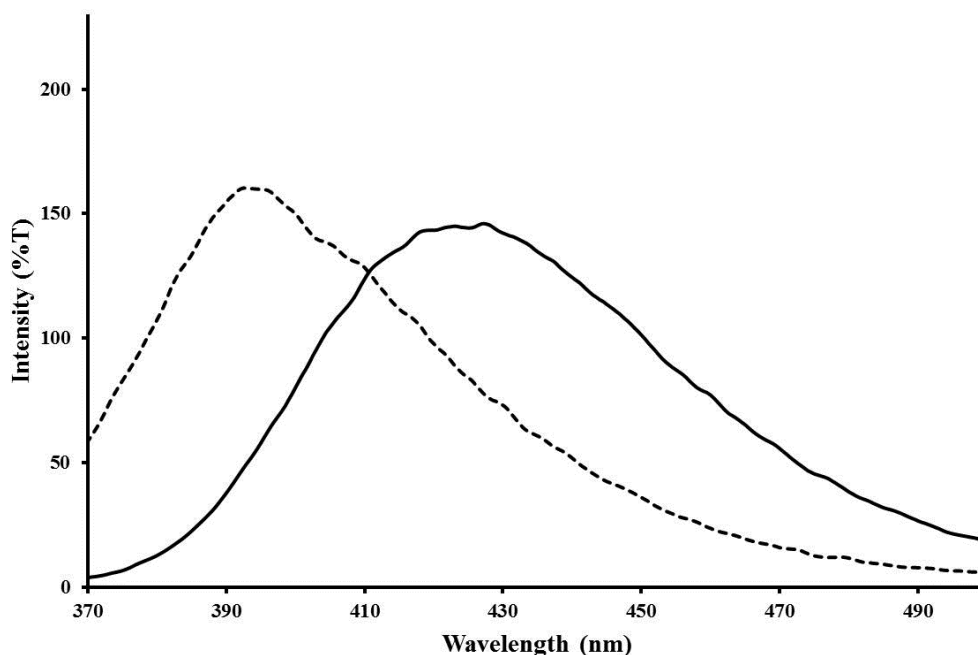


**Figure 118.** Luminescent spectra of complex **(9)** in the solid state (—) and dissolved state (- - -) in DMSO ( $\lambda_{\text{ex}}=320$  nm).

From **Figure 115**, complex **(2)** showed one emission band of medium intensity at 410 nm ( $\lambda_{\text{ex}}$  320 nm). In **Figure 116**, strong emission bands of complexes **(9) – (10)** in DMSO solution were observed at 393 nm ( $\lambda_{\text{ex}} = 350$  nm) for **(9)**, 390 nm ( $\lambda_{\text{ex}} = 320$  nm) for **(10)**, respectively, which correspond to the violet light.

In addition, in the solid-state, complex **(9)** showed one broad emission peak at 425 nm ( $\lambda_{\text{ex}} = 320$  nm) which could be attributed to mixed ligand-centered transition. This band was 32 nm red-shifted compared to the emission in DMSO solution. This could be due to the cooperative effect of diverse weak interactions controlled by hydrogen bonds and  $\pi$ - $\pi$  interaction playing an essential role to decrease the HOMO–LUMO energy gaps as discussed.

### **Photoluminescent property of metal complexes with O-donor ligand from sulfonate ligand**

The luminescent properties of complexes **(13) – (14)** and **(17) – (20)** were investigated in solid-state form at room temperature due to solubility in organic solvent not soluble at similar experimental conditions. Complexes **(11) – (12)**, **(15) –**

(16), and (21) - (22) did not show luminescent properties. The result emission spectra are given in Figures 119-121.

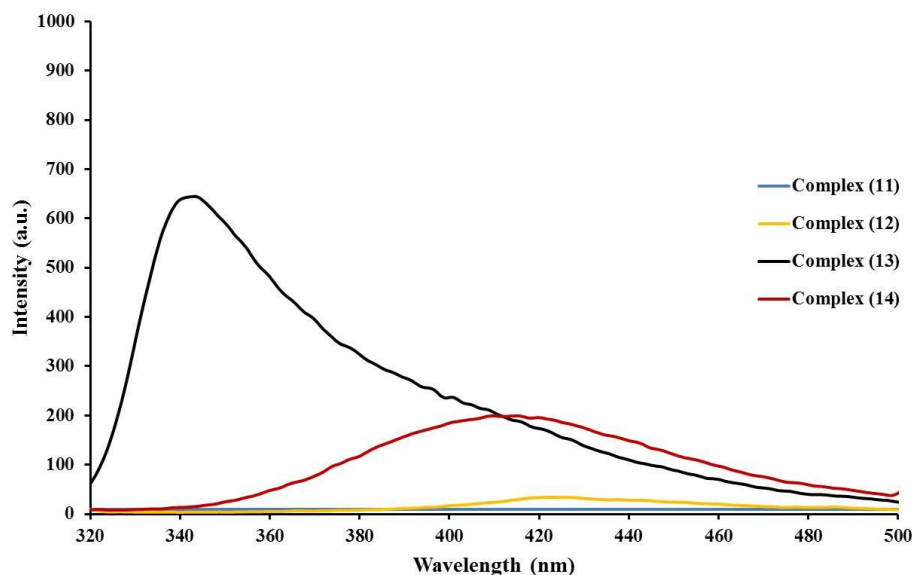


**Figure 119.** Solid-state emission spectra of complexes (11) - (14) at room temperature.

From **Figure 119**, complexes (11) and (12) displayed no emission ( $\lambda_{\text{ex}} = 320$  nm), which could be ascribed to the luminescence emission of complexes was quenched by coordination with Co(II) and Mn(II). The emission spectra of paramagnetic transition-metal complexes is usually not strong because ligand-field transitions (d-d transition) may lead to stronger absorption and/or quenching of fluorescence generated from the organic molecule, which can occur via electron or energy transfer through the partially filled d orbitals (Zhao *et al.*, 2015).

For complexes (13) and (14), one strong emission band was observed at 342 nm ( $\lambda_{\text{ex}} = 300$  nm) for (13), and 412 nm ( $\lambda_{\text{ex}} = 320$  nm) for (14). This band could originate from the complexation of the organic ligands with the zinc and cadmium metal centers. The Zn(II) and Cd(II) ions with its stable  $d^{10}$  configuration are difficult to oxidize or reduce, the enhancement of luminescence in  $d^{10}$  complexes may be attributed to the ligation of the ligand to the metal center. The coordination enhances the “rigidity” of the ligand and thus reduces the loss of energy through a radiationless pathway. And transition types of the electronic excited state, such as ligand-to-ligand charge transfer (LLCT) and ligand-to-metal charge transfer (LMCT), might be

possible for such Cd(II) and Zn(II) coordination complexes (He *et al.*, 2008, Wang *et al.*, 2014, and Jiang *et al.*, 2010) which indicates that the luminescence emission peaks of complex **(13)** and **(14)** may be due to the ligand-to-metal charge transfer (LMCT) or metal-to-ligand charge transfer (MLCT).

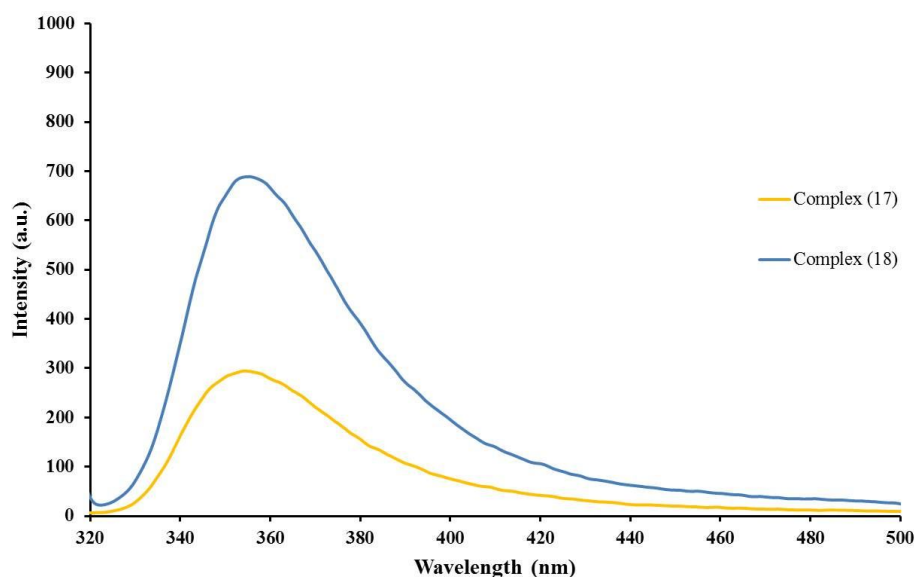


**Figure 120.** Solid-state emission spectra of complexes **(17)** - **(18)** at room temperature.

The emission spectra of complexes **(17)**-**(18)** were measured in the solid state (**Figure 120**) under similar experimental conditions. The strong emissions from both complexes **(17)** - **(18)** were observed at 358 nm ( $\lambda_{\text{ex}} = 300$  nm) for **17**, and 355 nm ( $\lambda_{\text{ex}} = 300$  nm) for **18**. Complex **(18)** showed stronger intensity than complex **(17)** at room temperature which might be attributed to effective increase of the rigidity of the complex and lower loss of energy by radiationless decay (Jang *et al.*, 2012). This is supported by X-ray structure data of complexes **(17)** - **(18)** which showed that the sulfonate ligand of complex **(17)** coordinated to Cd(II) but the sulfonate of complex **(18)** acted as counter anion.

The emission spectra of complexes **(19)** and **(20)** are shown in **Figure 121** from which the emission bands appeared at 409 nm for complex **(19)** and 412 nm for complex **(20)** ( $\lambda_{\text{ex}} = 320$  nm). These emission band of complexes **(19)** and **(20)**

showed a blue-shift at 36 and 33 nm compared with the free bpp ligand ( $\lambda_{em} = 445$  nm), respectively.

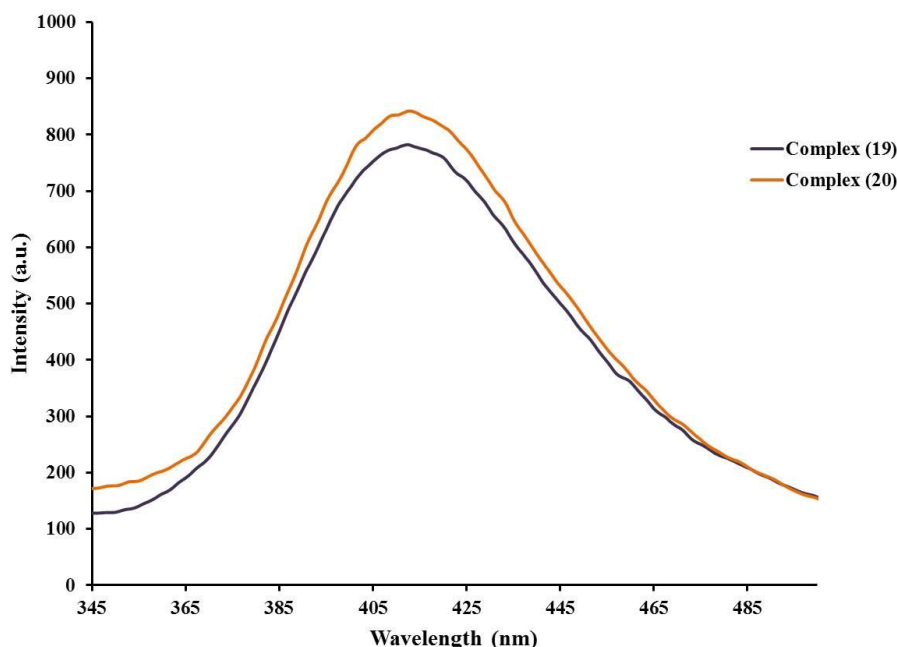


**Figure 121.** Solid-state emission spectra of complexes **(19)** - **(20)** at room temperature.

### 3.2 Luminescent sensing for metal ions

Complexes **(9)** and **(10)** were used as sensor for the detection of metal ions at room temperature due to their solubilities in organic solvents and their excellent luminescent property.

In the study of sensing metal ions, the metal chloride ( $M = Cd^{2+}$ ,  $Mn^{2+}$ ,  $Sr^{2+}$ ,  $K^+$ ,  $Na^+$ ,  $Ni^{2+}$ ,  $Co^{2+}$ ,  $Ca^{2+}$  and  $Cu^{2+}$ ) in aqueous solution (0.05 mM) was added to complexes **(9)** and **(10)** (0.005 mM, 4 mL) in DMSO solution for the fluorescence sensing as shown in **Figures 122-123**. From the data,  $Cd^{2+}$ ,  $Mn^{2+}$ ,  $Sr^{2+}$ ,  $K^+$ ,  $Na^+$ ,  $Ni^{2+}$ ,  $Co^{2+}$ , and  $Ca^{2+}$  had no effect on luminescence intensity of complexes but  $Cu^{2+}$  showed positive effect of fluorescence quenching by complexes. The fluorescence titration experiment of complexes **(9)** and **(10)** with  $Cu^{2+}$  was further carried out. The emission intensity of complexes at 398 nm was gradually quenched upon addition of different concentrations of  $Cu^{2+}$  (**Figures 125 and 127**). The limit of detection to  $Cu^{2+}$  of

complex **(9)** and **(10)** were about  $3.9 \times 10^{-7}$  mol/L and  $8.9 \times 10^{-7}$  mol/L, respectively (**Figures 126 and 128**).

. In addition, the effect of different counter anions such as  $\text{Cl}^-$ ,  $\text{Br}^-$ ,  $\text{NO}_3^-$ ,  $\text{SO}_4^{2-}$ , and  $(\text{OAC})^-$  on the sensing of  $\text{Cu}^{2+}$  were investigated and the results are shown in **Figures 129-130**. All counter anions had similar quenching efficiency to complexes **(9)** and **(10)**, hence, negligible effect of anions on the selectivity for  $\text{Cu}^{2+}$  detection. The photoluminescence quenched is likely to be caused by the interaction between  $\text{Cu}^{2+}$  ions with hydroxyl groups and oxygen atoms of uncoordinated carboxylate as has been described in literatures (Junwei Ye *et al.*, 2015, and Bei *et al.*, 2016)

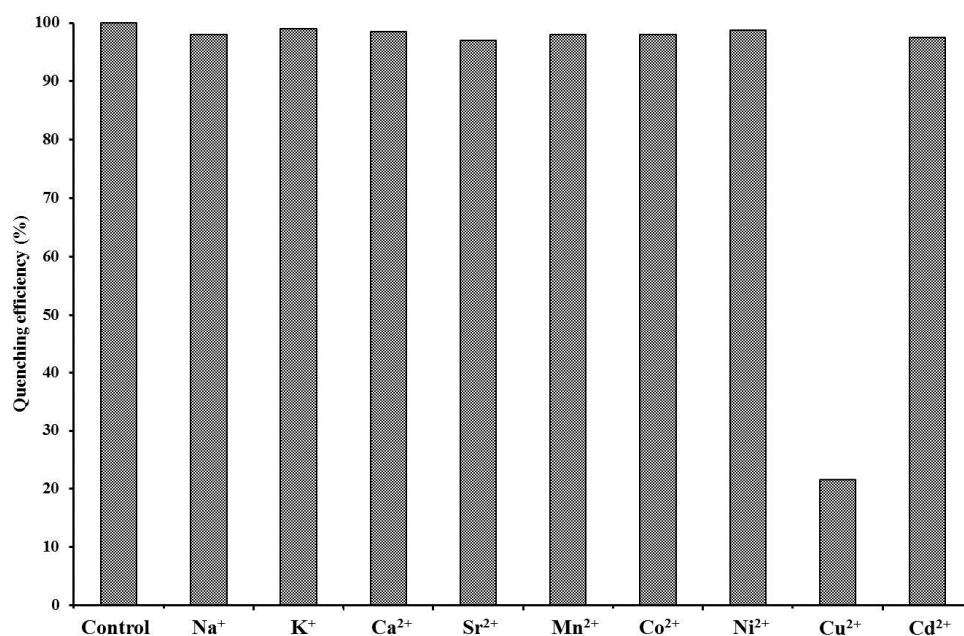


**Figure 122.** The quenching efficiency of complex **(9)** in the DMSO upon addition of metal ion aqueous solution.



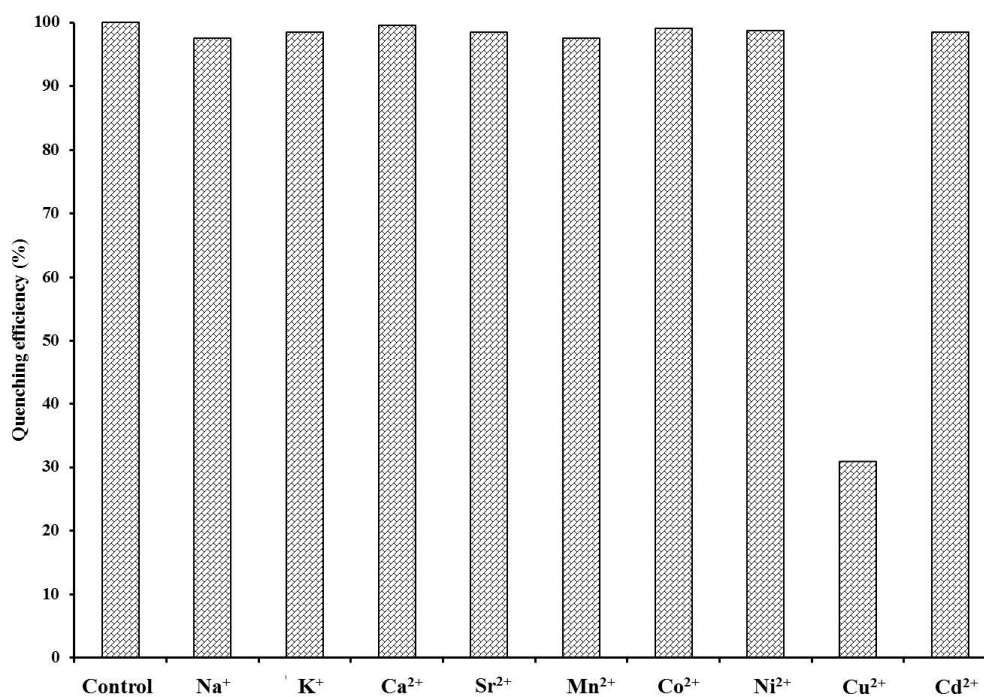


**Figure 123.** The quenching efficiency of complex (10) in the DMSO upon addition of metal ion aqueous solution.

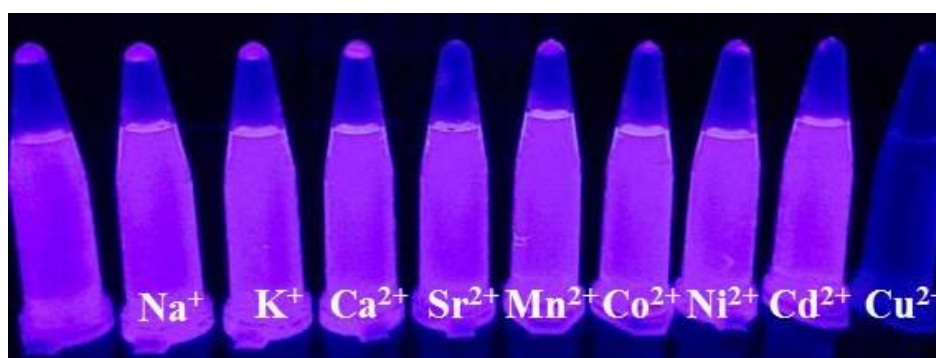


**Figure 124.** Fluorescent images of complex (10) in the DMSO upon addition of metal ion aqueous solution.

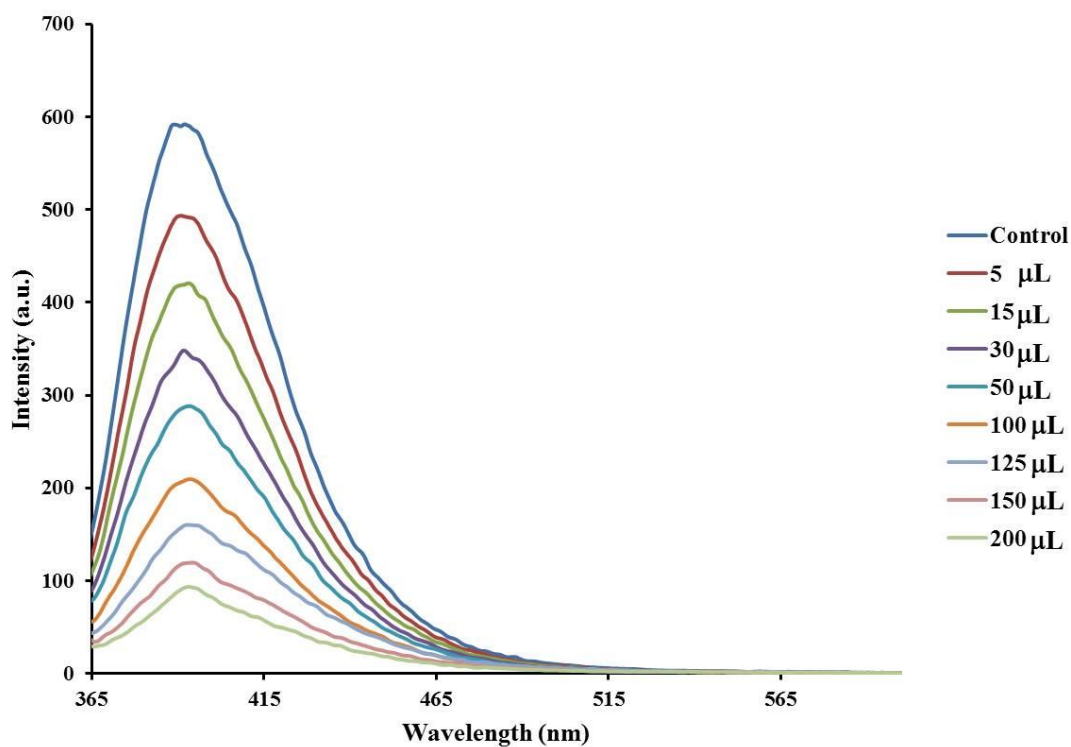


**Figure 125.** The fluorescence emission spectrum of complex (9) in the DMSO upon incremental addition of Cu<sup>2+</sup> aqueous solution.

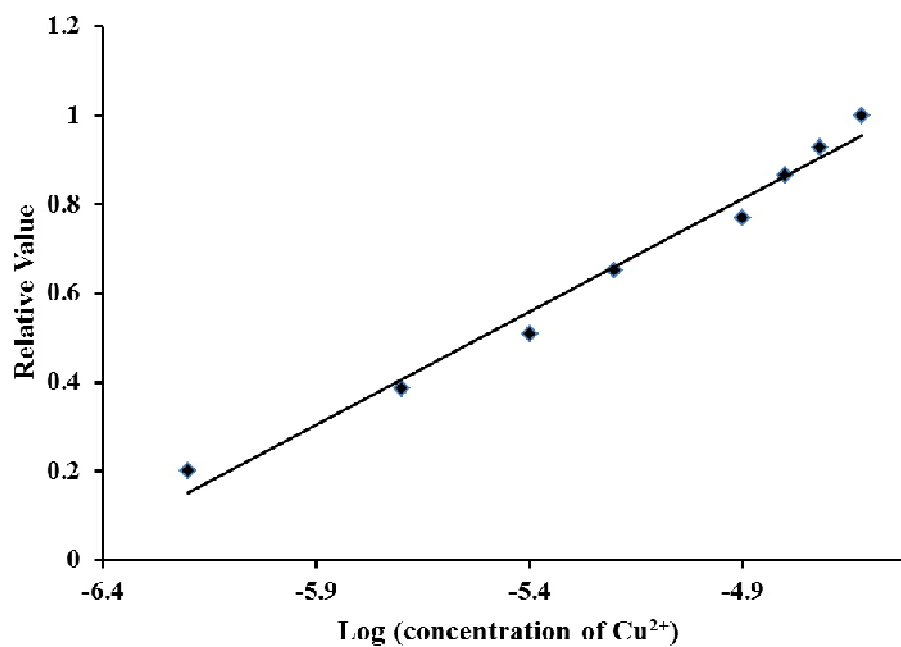


**Figure 126.** The relationship between the quenching efficiency and the logarithmic concentration of Cu<sup>2+</sup> of complex (9).

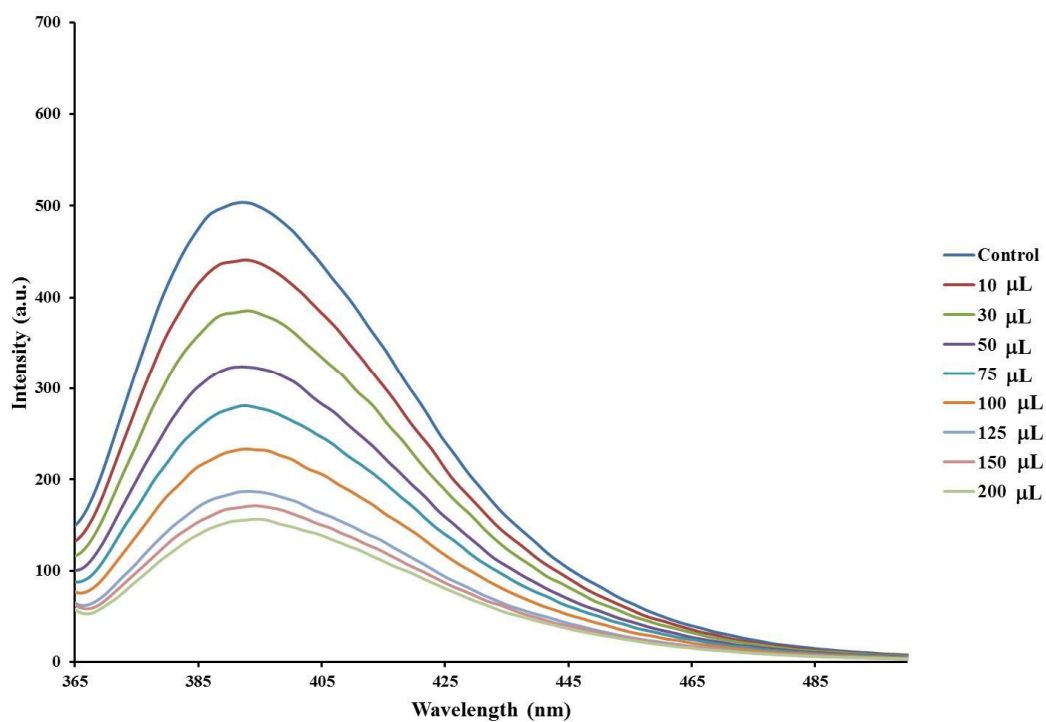


**Figure 127.** The fluorescence emission spectrum of complex (10) in the DMSO upon incremental addition of Cu<sup>2+</sup> aqueous solution.

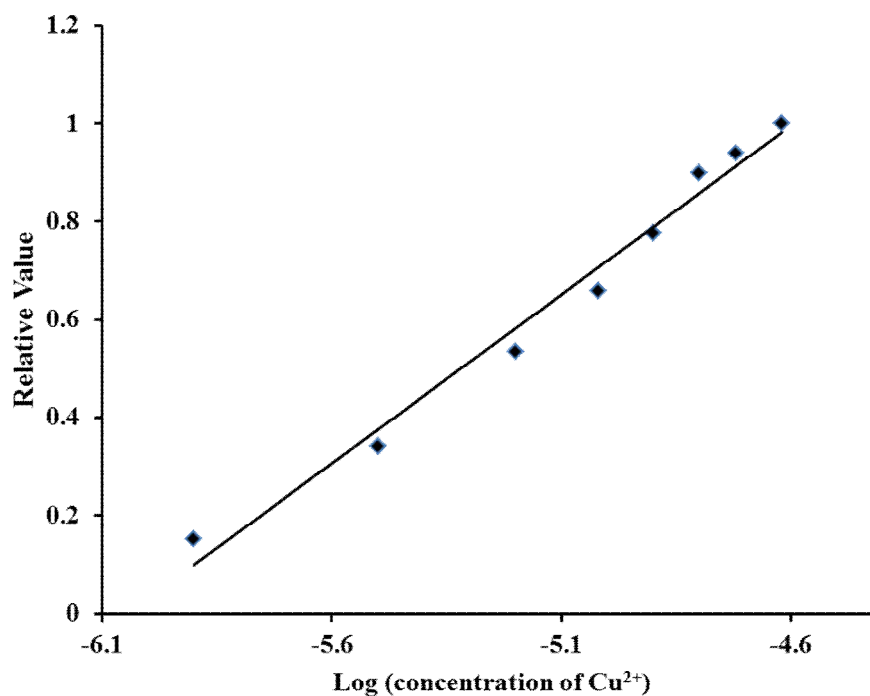


**Figure 128.** The relationship between the quenching efficiency and the logarithmic concentration of Cu<sup>2+</sup> of complex (10).

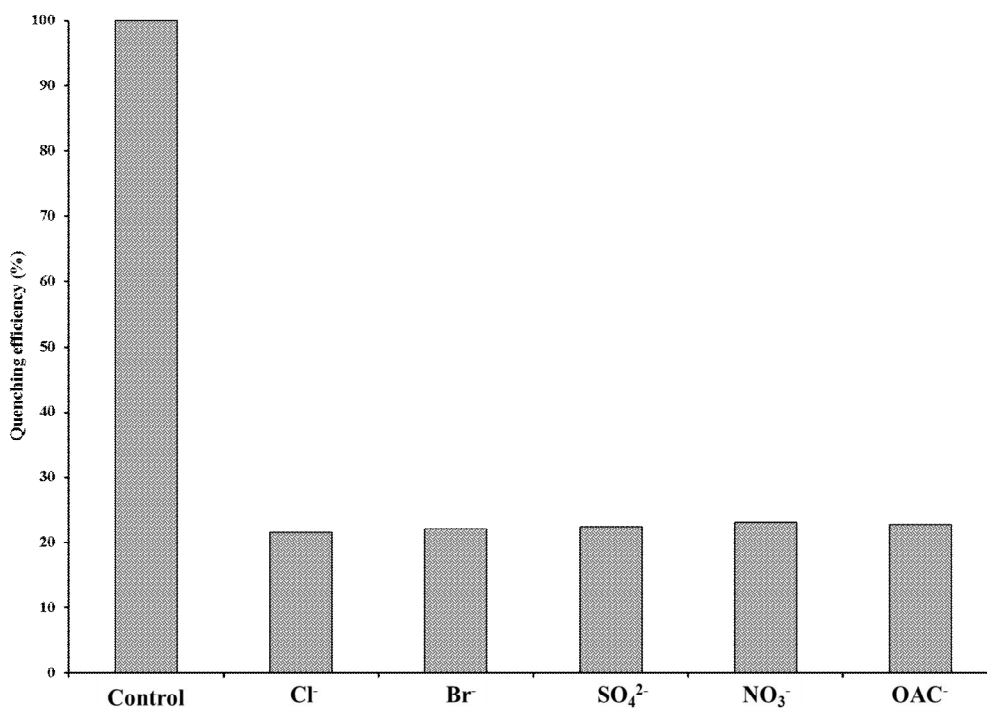


**Figure 129.** The quenching efficiency of complex (9) in the DMSO solutions upon addition of different counter anions to Cu<sup>2+</sup> aqueous solutions.

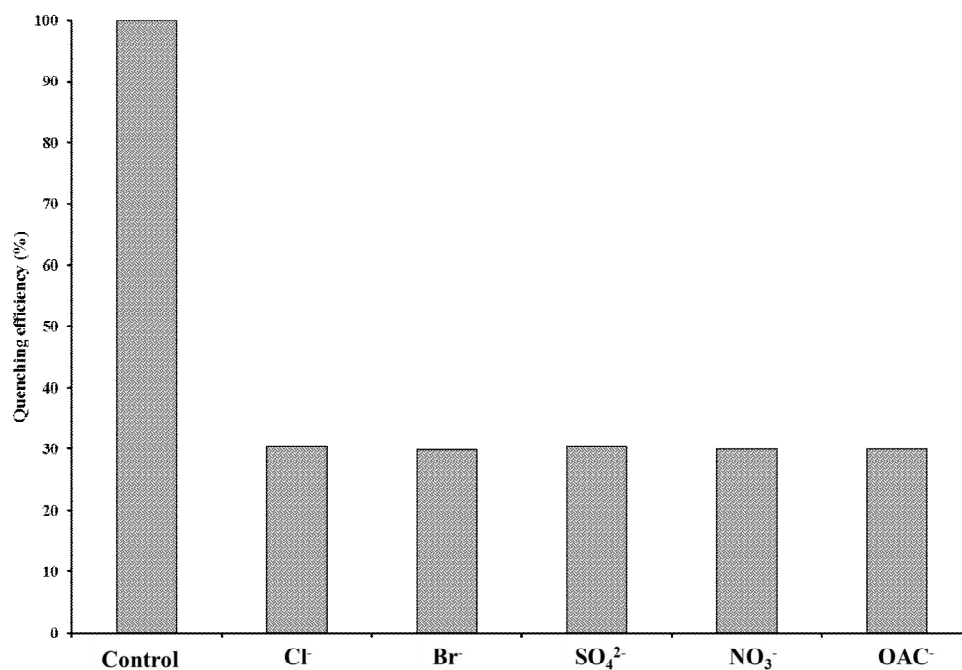


**Figure 130.** The quenching efficiency of complex (10) in the DMSO solutions upon addition of different counter anions to Cu<sup>2+</sup> aqueous solutions.

### 3.3 Test for photocatalytic activity

The photocatalytic activity studies of the complexes were investigated by using MB and RhB as a model of dye pollutants. Complexes (7) and (8) were used as photocatalyst due to the preliminary tests showed that complexes (7) and (8) could be used as photocatalyst for the degradation of MB and RhB dyes from wastewater.

#### 3.3.1 Photocatalytic activity under UV light

The results of the photodegradation of MB and RhB dye in aqueous solution under UV light of  $\{[Ag_2(bpp)] \cdot (4H_2O) \cdot (3-Npt)\}_n$  (7) and  $\{[Ag_2(bpe)_2(3-Npt)] \cdot 7H_2O\}_n$  (8) are displayed as a plot between decomposition rate of dye (%) versus reactions times (t) in Figures 131-132.

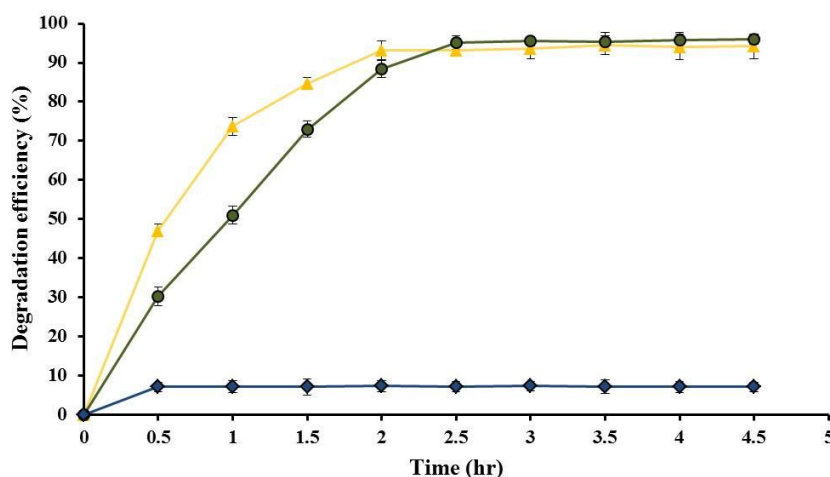


**Figure 131.** The efficiencies of photocatalytic degradation of MB dye on complex (7) and complex (8) under UV irradiation (n=3).

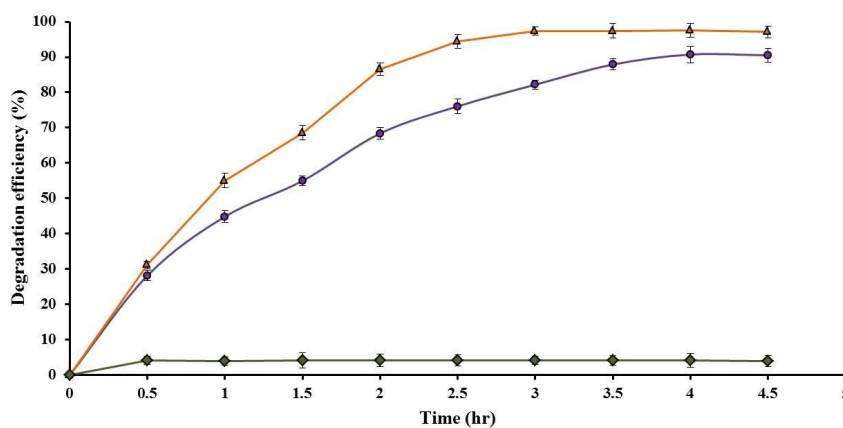


**Figure 132.** The efficiencies of photocatalytic degradation of RhB dye on complex (7) and complex (8) under UV irradiation (n=3).

The control experiments showed that the photocatalytic decomposition rate after 4.5 h of UV light irradiation of MB and RhB without catalyst were only 7.13 % and 4.25 %, respectively. The small change in the dye concentration with UV-light irradiation showed that the dye solution did not self-decompose. The results of degradation efficiency after 4.5 h were 94 % for complex (7), 96 % for complex (8) MB and 90 % for complex (7), 97 % for complex (8) for RhB.

### 3.3.2 Photocatalytic activity under Visible light

The results on the photodegradation of MB and RhB dye in aqueous solution under visible light of  $\{[\text{Ag}_2(\text{bpp})] \cdot (4\text{H}_2\text{O}) \cdot (3\text{-Npt})\}_n$  (7) and  $\{[\text{Ag}_2(\text{bpe})_2(3\text{-Npt})] \cdot 7\text{H}_2\text{O}\}_n$  (8) are displayed in **Figures 133-134**.

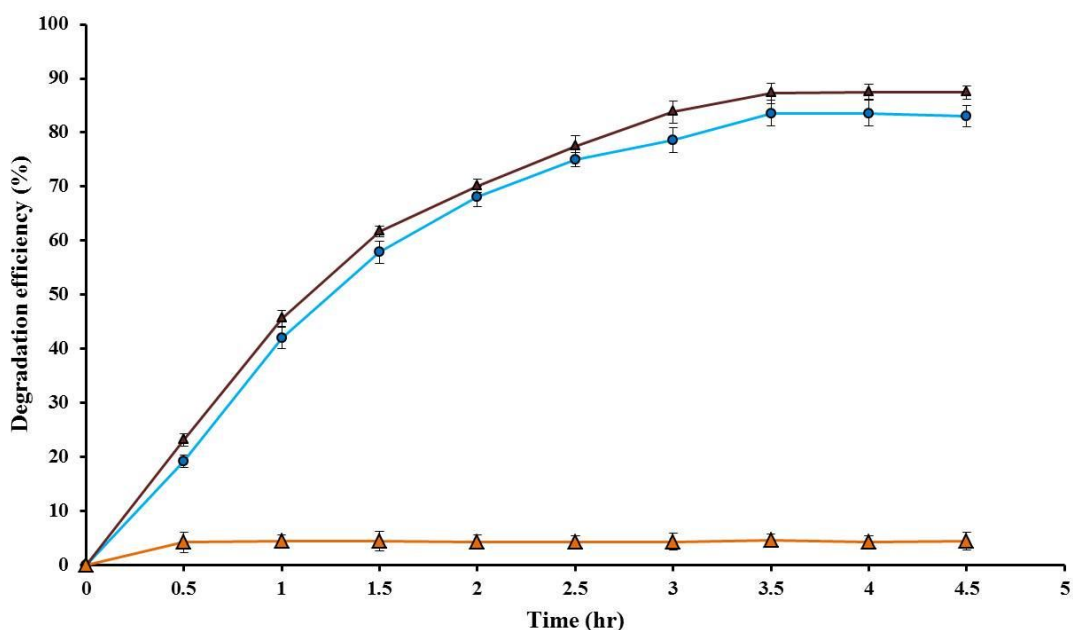


**Figure 133.** The efficiencies of photocatalytic degradation of MB dye on complex (7) and complex (8) under visible light irradiation (n=3).

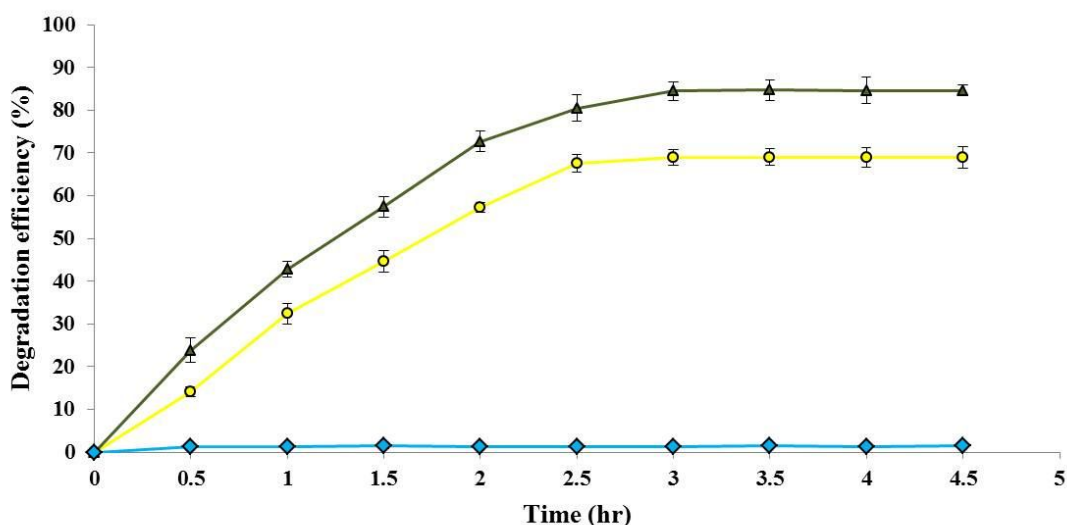


**Figure 134.** The efficiencies of photocatalytic degradation of RhB dye on complex (7) and complex (8) under visible light irradiation (n=3).

The control experiments showed that MB and RhB were not degraded after 4.5 h under visible light irradiation. The results of decomposition, in the presence of catalyst after 4.5 h were 83 % for complex (7), 87 % for complex (8) for MB and 68 % for complex (7), 84 % for complex (8) for RhB.

From data of photocatalytic test, the degradation curves of MB and RhB are shown in **Figures 131-134**. Under UV and visible light photocatalytic activity of complex (8) was higher than photocatalytic activity of complex (7), due to band gap energy of complex (8) was lower than band gap energy of complex (7). The optical band gap ( $E_g$ ) was factor influence to the speed of the photocatalytic degradation process of the organic dye (Liu *et al.*, 2015, Ming *et al.*, 2014, and Lu *et al.*, 2014).

### 3.3.3 Band gap energies of complexes (7) and complex (8)

UV-Vis diffused reflectance spectra of complexes (7) and (8) were measured by a UV-2401 Shimadzu spectrophotometer. The spectra were recorded by using  $\text{BaSO}_4$  as background reflectance at room temperature with a 2.0 nm slit range from 200 nm to 800 nm. The UV-Vis diffused reflectance spectra of complexes are shown in **Figures 135-136**. The band gap energy ( $E_g$ ) was calculated according to equation;

$$E_g = h \frac{c}{\lambda} = \frac{1240}{\lambda} \quad (1)$$

where  $E_g$  is the band gap energy (eV),  $h$  is the Planck's constant ( $6.63 \times 10^{-34}$  J.s),  $\lambda$  is the wavelength at onset of absorption (nm) and,  $c$  is the light velocity ( $3.0 \times 10^8$  m.s $^{-1}$ ). The  $E_g$  value was determined by the linear extrapolation of the steep part of the UV absorption toward the baseline.

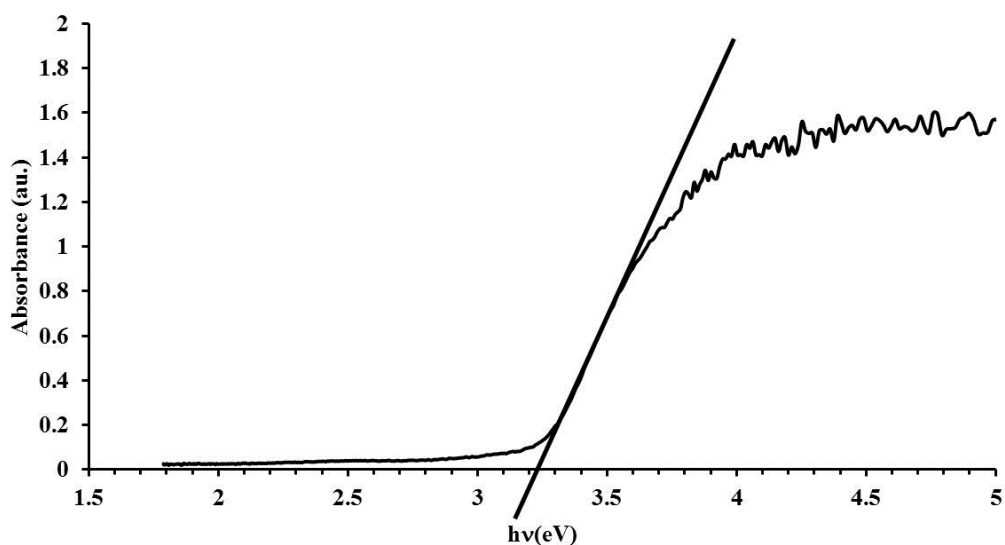


**Figure 135.** UV-visible diffused reflectance spectrum of complex (7).

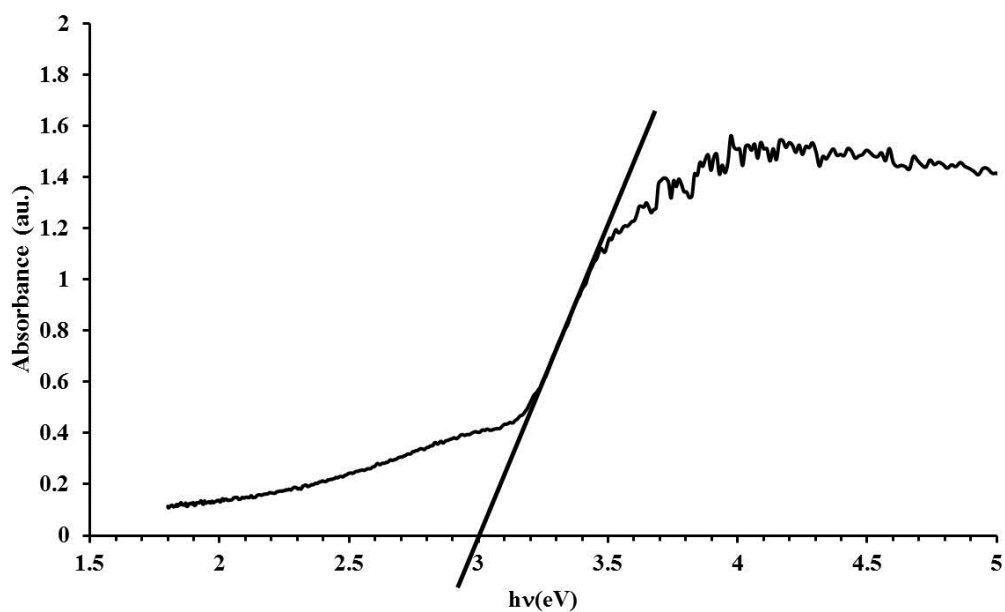


**Figure 136.** UV-visible diffused reflectance spectrum of complex (8).



From the DRS spectra, the band gap energies of complexes which calculated from the equation (1) were found to be at 3.22 eV for complex (7) and 3.00 eV for complex (8). These values were similar to that reported of  $[\text{Ag}_4(\text{dpe})_4]\cdot(\text{btec})\cdot(3.2\text{ eV})$  (Zhang *et al.*, 2016).

### 3.3.4 Mechanism of photocatalytic degradation

The mechanism of photocatalytic degradation had been proposed as follows: In the presence of UV or visible light irradiation of system, electrons ( $e^-$ ) charge transfer presumably takes place from the HOMO, involving N atoms, to the LUMO, involving the metal atom. The excited-state electron in the LUMO is usually very easily lost, while the HOMO of the excited species can accept one electron. Consequently, electrons are captured from water molecules to hydroxyl radicals ( $\cdot\text{OH}$ ). After that, it can annihilate the organic dye efficiently to complete the photocatalysis process (Mahata *et al.*, 2006 and Wen *et al.*, 2012).

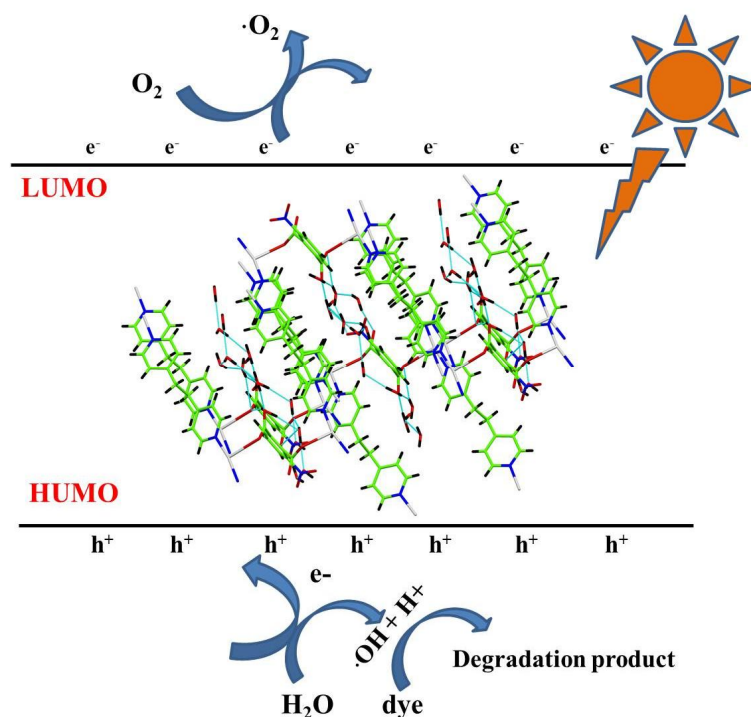


**Figure 137.** The proposed mechanism of photocatalytic reactions between of dyes and complex (8).

In addition, to confirm the proposed mechanism, radical trapping experiments were carried out to detect the  $\cdot\text{OH}$  species in the process of photocatalytic reactions by using complex **(8)** as an example. Isopropanol was used as a radical scavenger and 1 mL of it was added for this investigation. The data showed that photocatalytic degradation of RhB decreased from 97 % without isopropanol to 30.2 % with isopropanol, and for MB decreased from 96 % without isopropanol to 31.5 % with isopropanol, after 4.5 hours under UV light irradiation. These data indicated that  $\cdot\text{OH}$  radicals were the active species for photocatalytic process.

### 3.3.5 Recyclability of complex (7) and complex (8) in photodegradation

In this work, the recyclability of complexes **(7)** and **(8)** as a photocatalyst for photodegradation of MB and RhB were investigated and the results are shown in **Figures 138-141**. From the figures, one can see that the photocatalytic performance were practically unchanged during the three recycle runs. In addition, the PXRD patterns of the complexes **(7)** and **(8)** after photocatalytic experiments under UV irradiation (**Figures 142-143**) showed a good match with the simulated patterns from X-ray data of the freshly complexes **(7)** and **(8)** indicating no eminent change in the crystallographic structure of complexes **(7)** and **(8)** during photocatalytic reactions.

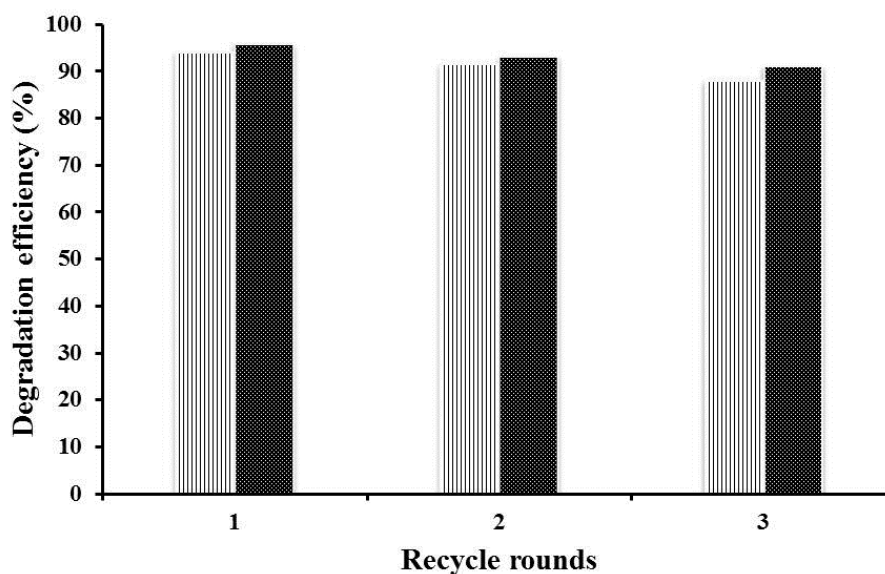


**Figure 138.** The photodegradation efficiencies of MB dye on complexes **(7)** and **(8)** from the recyclability test under UV-irradiation.

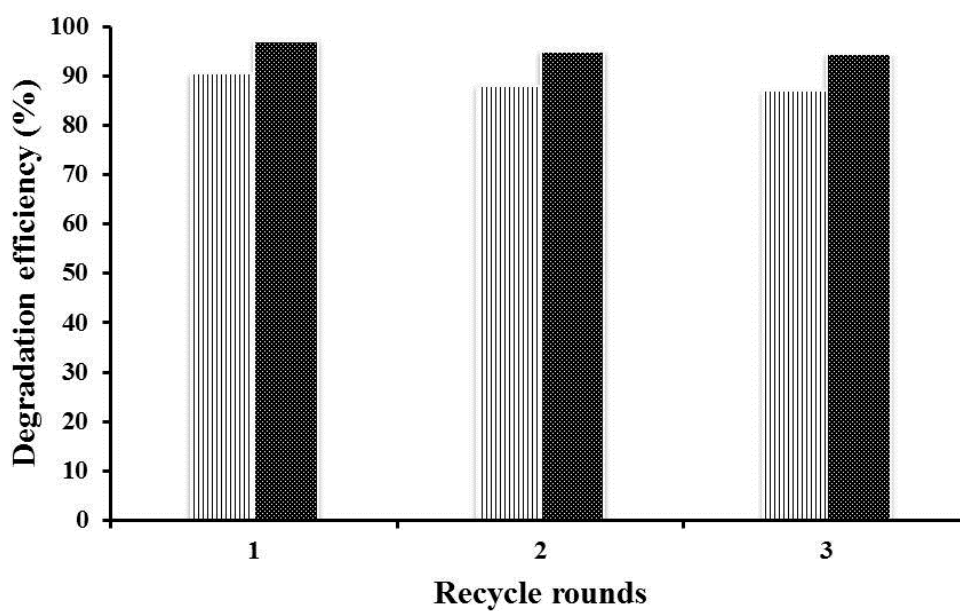


**Figure 139.** The photodegradation efficiencies of RhB dye on complexes (7) and (8) from the recyclability test under UV-irradiation.

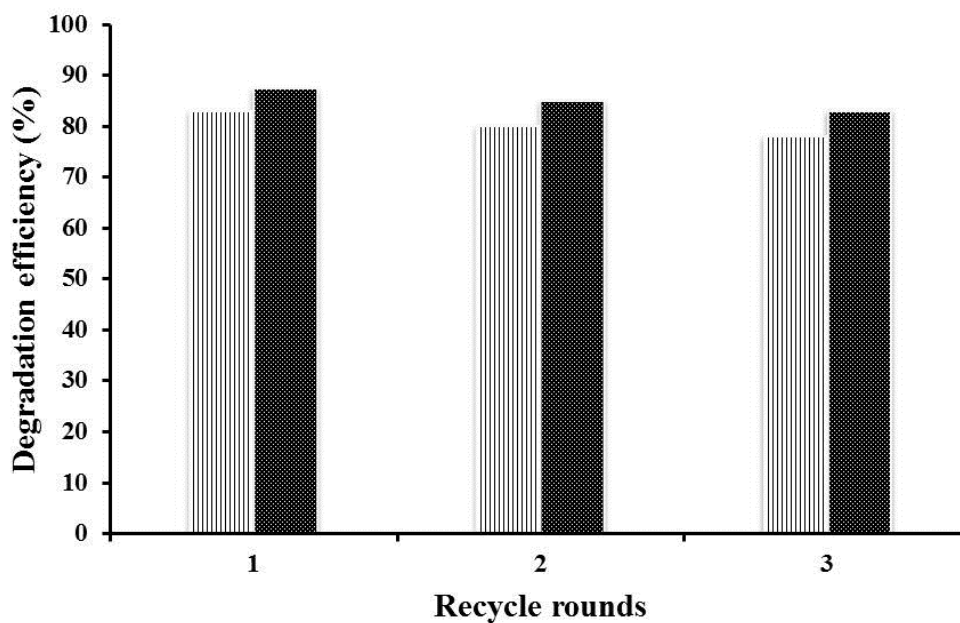


**Figure 140.** The photodegradation efficiencies of MB dye on complexes (7) and (8) from the recyclability test under visible irradiation.

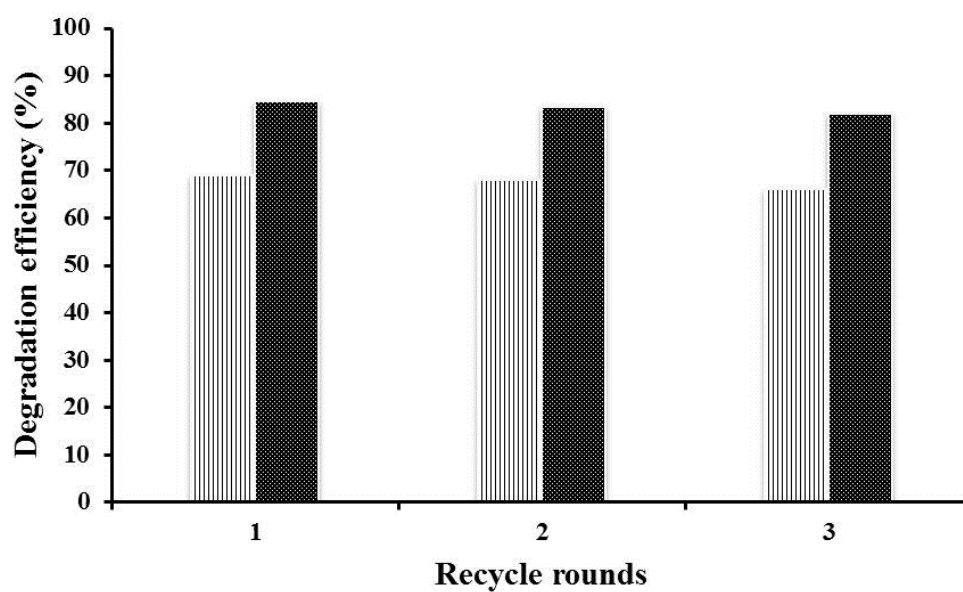


**Figure 141.** The photodegradation efficiencies of RhB dye on complexes (7) and (8) from the recyclability test under visible irradiation.

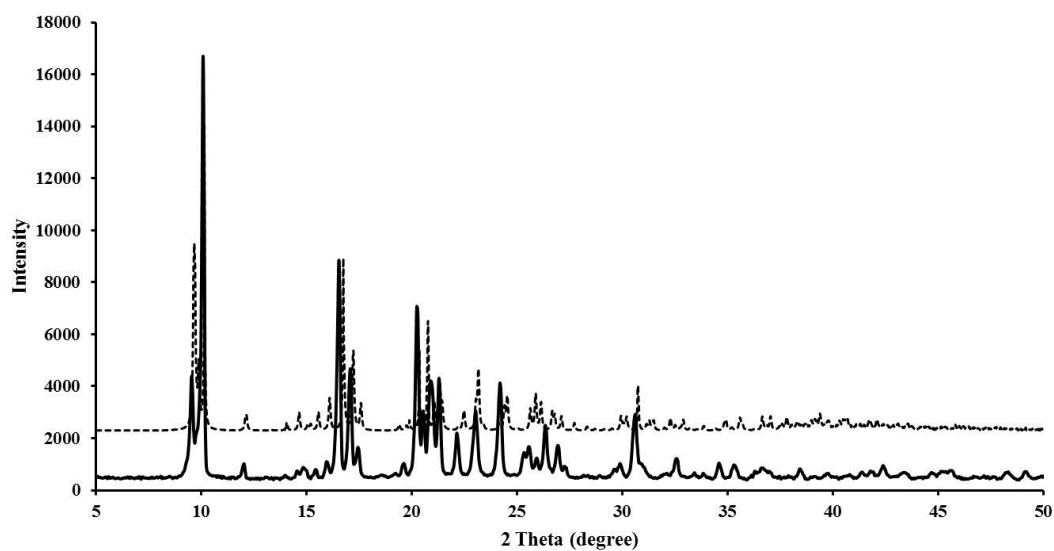


**Figure 142.** PXRD patterns of complex (7) before (—) and after (.....) photocatalytic process

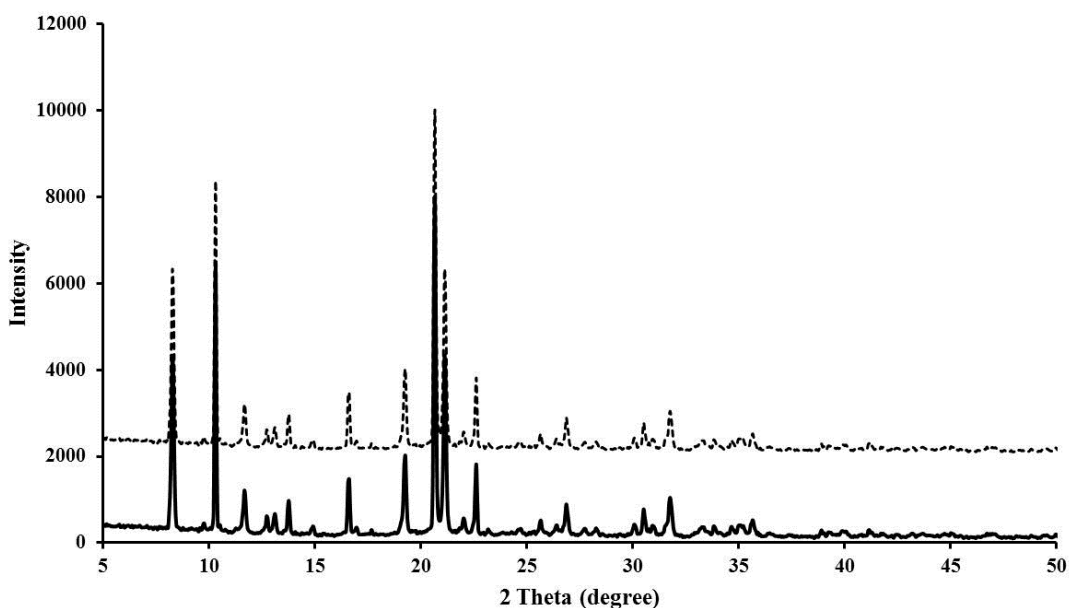


**Figure 143.** PXRD patterns of complex **(8)** before (—) and after (····) photocatalytic process.

### 3.4 Biological activity

The zone of inhibition values (*in vitro* study) of the complexes **(9)** and **(10)** against the bacteria are summarized in **Table 49**. The bacterial cultures used were *Staphylococcus aureus* ATCC 25923, *Escherichia coli* ATCC 25922, and *Pseudomonas aeruginosa* ATCC 27853). Test solutions were prepared by dissolving the complexes in DMSO at the concentration of 1 mg/mL and were deposited on paper discs which were subsequently placed on the inoculated petri dishes. Penicillin (10 µg/disc) and Gentamicin (10 µg/disc) were used as a standard.

**Table 49.** Diameter of zones of inhibition (mm) of complexes.

Complexes	Zones of inhibition of complexes		
	<i>E. coli</i>	<i>S. aureus</i>	<i>P. aeruginosa</i>
[Zn(bpp) <sub>2</sub> (Sal) <sub>2</sub> ] <sub>n</sub> <b>(9)</b>	11.5	6.3	10.0
[Zn <sub>2</sub> (bpe) <sub>2</sub> (Sal) <sub>4</sub> ] <b>(10)</b>	11	5.5	9.5
Penicillin	14	15	16
Gentamicin	15	17	17

The results of the antimicrobial screening revealed that the complexes were considerably active against *E. coli*, *S. aureus* and *P. aeruginosa*. Their activities were slightly lower than that of the standard drugs, Penicillin and Gentamicin. Complex (9) had diameter of inhibition 14 mm, while complex (10) was 10 mm for *E. coli*. Against *P. aeruginosa* complex (9) had diameter of inhibition 10 mm and complex (10) had diameter of inhibition 9.5 mm. For *S. aureus*, the diameters of inhibition were 6.3 mm and 5.5 mm for complexes (9) and (10), respectively. The negative control dimethyl sulfoxide produced no zone of inhibition in the test. This data suggested that the antibacterial activity of complexes (9) and (10) for Gram negative bacteria was higher than Gram positive bacteria due to their different cell structures. However, higher activities shown by complex (9) over complex (10) might indicate the influence of the molecular structure from coordination polymer in complex (9). Lastly, both complexes showed higher inhibition on the growth of *E.coli* in comparison with other bacterial.

### 3.5 Orange G dye adsorption studies

The adsorption studies of the complexes were investigated by using OG as a model of dye pollutant. The preliminary tests showed that complex (7) could be used as an adsorbent for the removal of OG dye from wastewater.

#### 3.5.1 Preparation of calibration graph of orange G (OG)

In this work, the calibration graph was used to find concentration of OG dye. The concentration of OG solutions were prepared in the range  $1 \times 10^{-5}$  to  $5 \times 10^{-5}$  M. The concentration of dye was analyzed by the spectrophotometric method. The maximum absorbance of OG dye found at 486 nm (Figure 144) and the calibration curve graph of OG solution is shown in Figure 145. The data showed a good linear relationship with  $R^2 = 0.9993$ .

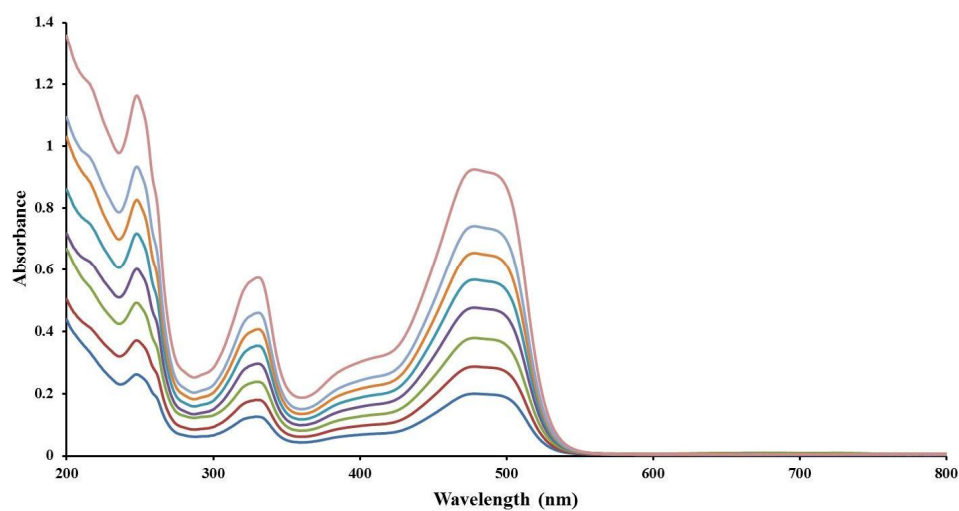


**Figure 144.** The UV-visible spectra of OG solution in the range  $1 \times 10^{-5}$  to  $5 \times 10^{-5}$  M.

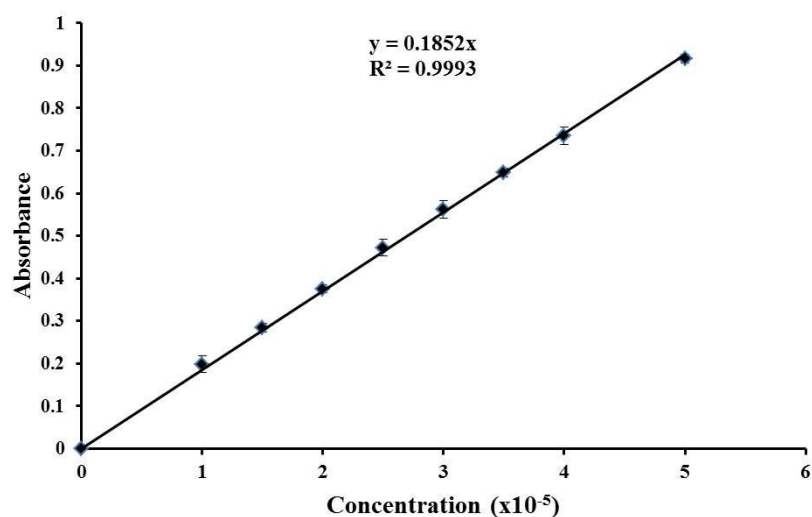


**Figure 145.** The standard calibration graph of OG solution in the range  $1 \times 10^{-5}$  to  $5 \times 10^{-5}$  M.

### 3.5.2 The optimum condition study

In this work, the adsorption studies were studied based on three main factors effect of contact time, adsorbent dosage, and initial dye concentration. All data obtained are reported as follows:

### 3.5.2.1 Effect of contact time

The result of the contact time is importance for adsorption study as it provides data regarding the time continuation taken for an adsorption system get to equilibrium adsorption.

The effect of contact time on the adsorption of OG dyes was studied by using complex (7) as adsorbent. The contact time was varied from 1-60 min with the following set up: 0.03 g of complex (7) in 100 mL of  $1 \times 10^{-4}$  mol/L of OG solution at pH 7 at room temperature. The adsorption efficiency of the complex is shown in **Figure 146**. From the figure, adsorption of OG by complex (7) reached 98% in about 40 min at room temperature.

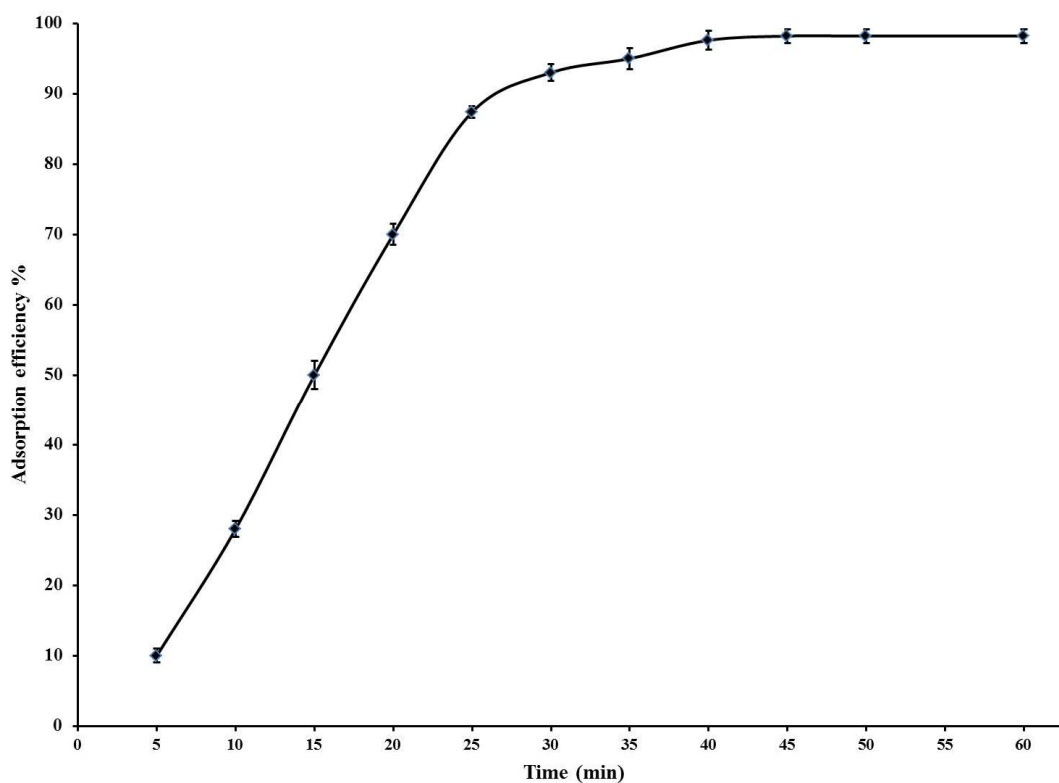


**Figure 146.** Effect of the contact time on OG dye adsorption by complex (7).

### 3.5.2.2 Effect of adsorbent dosage

The effect of adsorbent dosage on the adsorption OG dye was measured by varying the amount of complex (7) in the range 0.005 to 0.04 g. The concentration of dye was  $1 \times 10^{-4}$  mol/L (pH = 7). The dye solution was stirred for 30 min at room



temperature. The equilibrium data were plotted to the % adsorption efficiency of complex as shown in **Figure 147**.

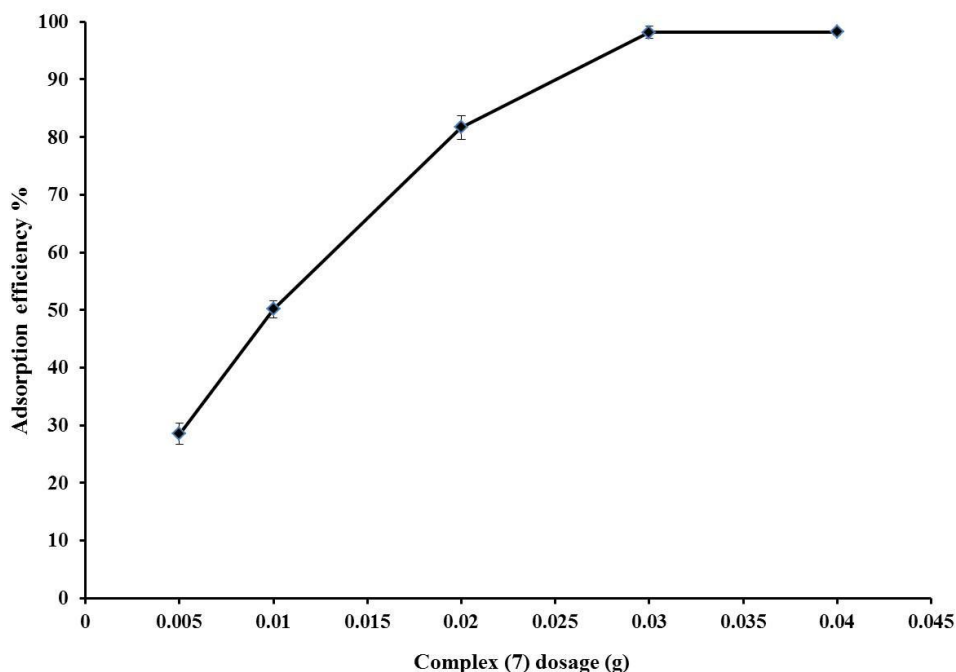


**Figure 147.** Effect of the dosage of adsorbent on OG dye removal by the complex (7).

The removal of OG rapidly increased as the adsorbent dosage was increased from 0.01 to 0.04 g. From the graph, the highest adsorption efficiency was 98% at adsorbent dosage of 0.03 g. Hence, 0.03g was chosen as the optimum dosage for the adsorption experiments.

### 3.5.2.3 Effect of initial dye concentration on dye adsorption

The initial dye concentration was varied from  $5 \times 10^{-5}$  mol/L to  $2.5 \times 10^{-4}$  mol/L of OG dye solution using 0.03 g of complex, contact time 60 min at room temperature. The graph demonstrating % adsorption efficiency was constructed as shown in **Figure 148**.

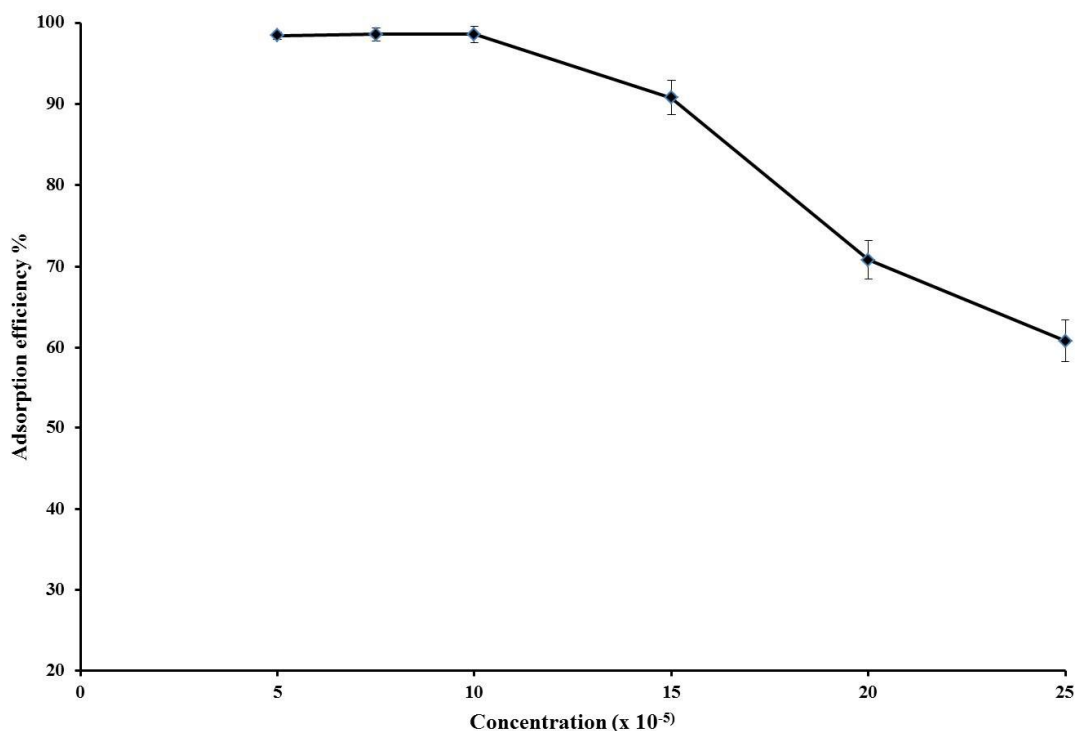


**Figure 148.** Effect of the initial concentration of OG dye on dye removal by the complex (7).

From **Figure 148**, the removal efficiency (%) of OG dye was as high as 98 % at concentration up to  $1 \times 10^{-4}$  mol/L, and the efficiency decreased down to 70% as the concentration was increased to  $1.5 \times 10^{-4}$  mol/L and up. The lower adsorption efficiency at higher concentrations of OG dye was due to the saturation of adsorption sites on complex.

### 3.5.3 Adsorption isotherms

The models of adsorption isotherm are basic for predictive of the interaction behavior between adsorbate and adsorbent and important for measurement mechanisms of adsorption systems (Elizabeth *et al.*, 2014). The isotherm data should correctly fit into different isotherm models to find the model that can be used for adsorption process pattern.

In this study, the evaluation of adsorption isotherms of OG dye were measured by adding 0.03 g of complex (7) in 100 mL of OG dye solution with a concentration

of  $5 \times 10^{-5}$  mol/L to  $4 \times 10^{-4}$  mol/L at room temperature and at pH 7. The dye solution was stirred for 60 min to equilibrium.

The models of adsorption isotherm by Langmuir (Eq.2) and Freundlich (Eq.3) equations were used to fit the adsorption data:

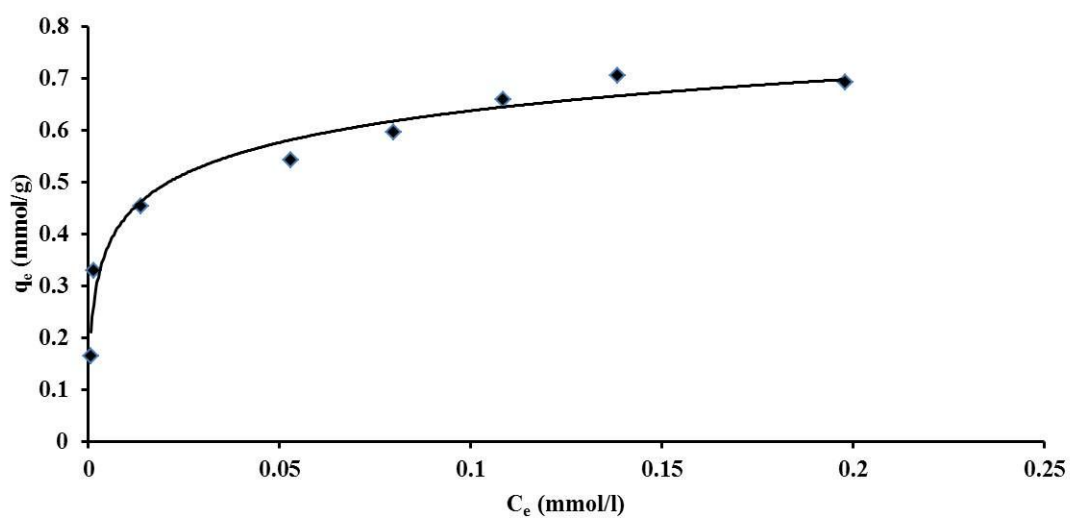
$$\frac{C_e}{q_e} = \frac{1}{bq_{\max}} + \frac{C_e}{q_{\max}} \quad (2)$$

$$\log q_e = \log K_F + \frac{1}{n} \log C_e \quad (3)$$

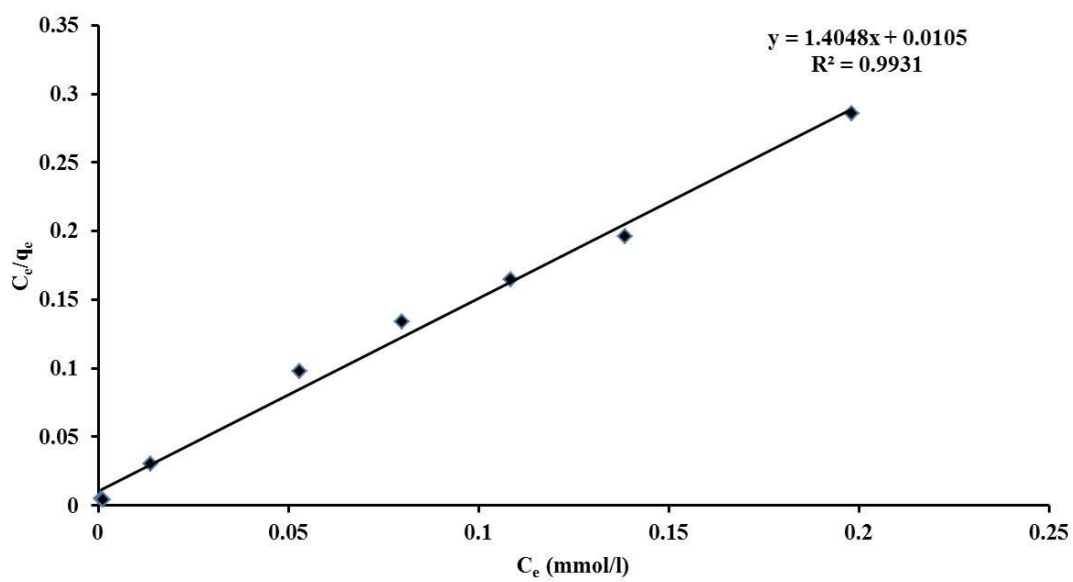
where  $q_e$  is the adsorption capacity (mmol/g),  $C_e$  is residual equilibrium dye concentration (mmol/L),  $q_{\max}$  is the maximum adsorption at monolayer coverage (mmol/g),  $b$  is the adsorption constant from Langmuir model (L/mmol),  $K_F$  and  $n$  are constants from the Freundlich equation.

The models of Langmuir and Freundlich isotherm were used to ascribe the adsorption equilibrium result obtained from the adsorption of OG dye over complex (7). Two models were applied to describe the relationship between the amount of dye per unit weight of adsorbent ( $q_e$ , mmol/g) and residual equilibrium concentration of dye ( $C_e$ , mmol/L). The Langmuir isotherm was plot between  $C_e/q_e$  and  $C_e$  (Eq.2), while the Freundlich isotherm was plot between  $\log C_e$  and  $\log q_e$  (Eq.3). The experimental equilibrium data for OG dye in Langmuir and Freundlich isotherms are presented in **Table 50**. The constants value of  $1/n$  and  $K_f$  can be obtained from the intercept and slope of the graph plot between  $\log q_e$  and  $\log C_e$ .

(a)



(b)



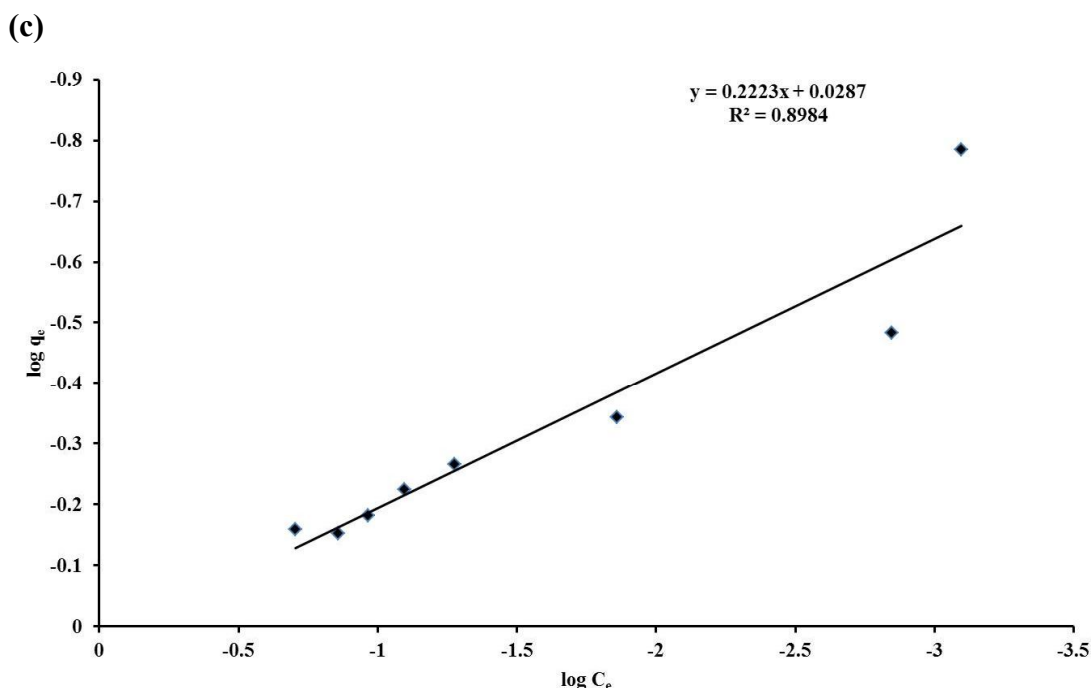


**Figure 149.** Non-linearized (a), linearized Langmuir (b) and Freundlich (c) adsorption isotherms of OG dye for complex (7).

**Table 50.** The constant values of Langmuir and Freundlich isotherms and linear correlation coefficient for adsorption of OG dye by complex (7).

Dye	Langmuir model			Freundlich model		
	$q_{\max}$	$b$	$R^2$	$K_F$	$n$	$R^2$
OG	0.7051	135.06	0.9931	1.06	4.498	0.8984

From data in the **Table 50**, the value of correlation coefficient ( $R^2$ ) for Langmuir model was 0.9931 and 0.8873 for Freundlich model. The value of  $R^2$  suggesting that Langmuir isotherm was the best fit of experimental data than Freundlich isotherm for the adsorption of OG dye on the as-synthesized complex (7). The adsorption in this experiment appeared as the monolayer dye adsorbed onto the adsorbent surface.

The constant values of  $q_{\max}$  and  $b$  from Langmuir equation are shown in **Table 50** of which the value of  $q_{\max}$  of OG is 0.7051 mmol dye/g for complex (7). The dye

adsorption process occurred by the physisorption when dye accumulated onto the surface of the complex might be mainly explained by  $\pi$ - $\pi$  stacking interaction and H-bonding due to its weak interaction in nature resulting in reversible adsorption (Avijit *et al.*, 2009 and Xiao *et al.*, 2013).

The favorability of the OG adsorption process onto complex (7) was evaluated using a dimensionless factor ( $R_L$ ) derived from the Langmuir equation, which is defined as

$$R_L = \frac{1}{1 + bC_i} \quad (4)$$

where  $b$  is the Langmuir constant (L/mmol) and  $C_i$  is the highest initial of OG dye concentration (mmol). The values of  $R_L$  indicates the shape of the isotherm is either unfavourable ( $R_L > 1$ ), linear ( $R_L = 1$ ), favourable ( $0 < R_L < 1$ ), or irreversible ( $R_L = 0$ ).

The values of  $R_L$  for adsorption of OG was 0.02 as calculated from Eq. 4, indicating that complex (7) was a favorable adsorbent ( $0 < R_L < 1$ ).

As shown in **Table 50**, the  $K_F$  values and  $n$  for the Freundlich equation for OG dye is 1.06 and 4.498, respectively. The constant value of ( $n$ ) is a characteristic coefficient related to the distribution of site bonding energies. Mainly, the value of  $1 < n < 10$  explains that adsorbate is favourably adsorbed on an adsorbent,  $n < 1$  indicates that adsorbate is unfavourably adsorbed on an adsorbent, and  $n > 10$  indicates that adsorbate is irreversible adsorption (Sriprang *et al.*, 2014 and García *et al.*, 2014). In this study, the high constant values of  $n$  and  $K_F$  values from Freundlich isotherm suggest that OG dye is favourably adsorbed on the complex (7). This means that use of complex (7) should provide the easy separation of the dye from the aqueous solution (or wastewater).

After the adsorption process, the removals of OG dye from the complex (7) by washing the used precipitate with ethanol. The color of complex (7) before and after being washed with ethanol and dried in air are shown in **Figure 150**.

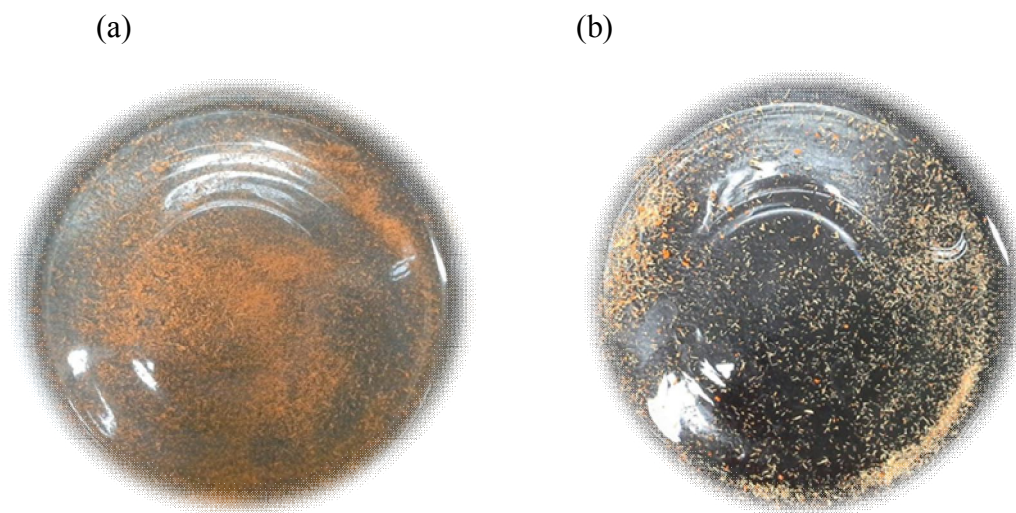


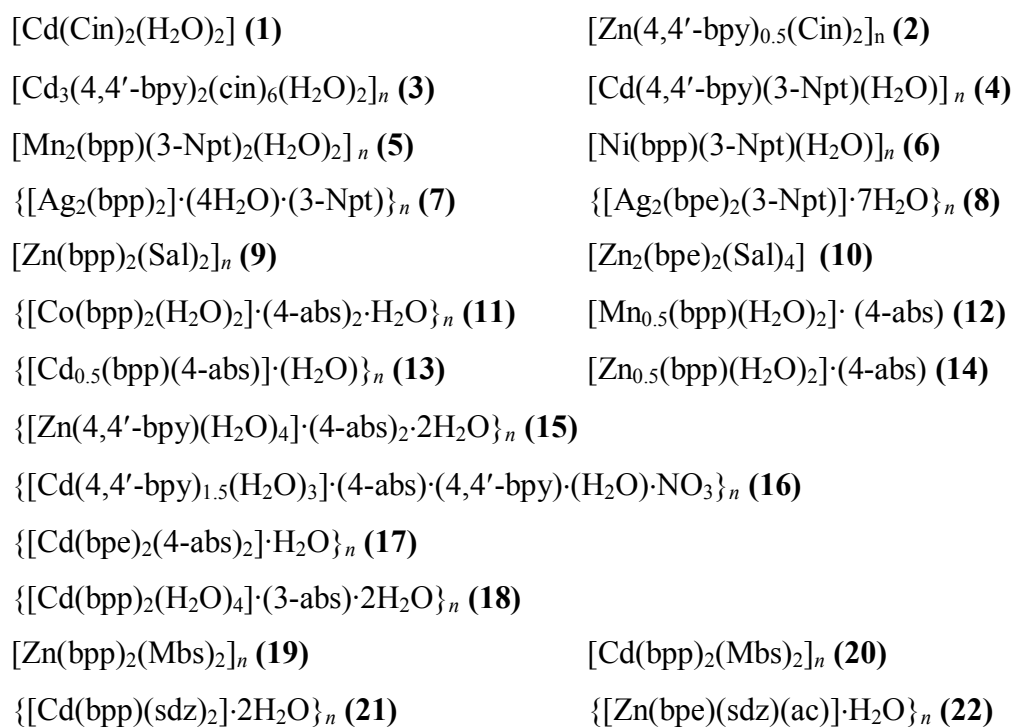
**Figure 150.** The photographs of complex (7) with OG dye: (a) used and (b) regenerated complex (7).

## CHAPTER 4

### CONCLUSIONS

In this thesis, the work can be divided into two parts; part 1 synthesis and characterization of all supramolecular complexes with N-donor and O-donor ligands; part 2, study of their possible applications of supramolecular complexes such as adsorption property, photocatalytic property, fluorescence sensing for metal ions property, and antibacterial activity.

The preparation of supramolecular complexes with N-donor and O-donor ligands by using metal salts [Ni(II), Co(II), Mn(II), Zn(II), Ag(I), and Cd(II)], N-donor ligand [4,4'-bipyridine (bpy), 1,3-bis(4-pyridyl)propane (bpp), 1,2-bis(4-pyridyl)ethane (bpe)]; O-donor ligand from carboxylate ligand [Cinnamic acid, 3-Nitroptalic acid and Aspirin] or O-donor ligand from sulfonate ligand [Sulfanilic acid, Sulfadiazine, 3-aminobenzinesulfonic acid, and *p*-Toluenesulfonic acid] as starting materials. The obtained complexes are as follows.



All complexes have been characterized by Fourier-transformed infrared spectroscopy, elemental analysis, thermogravimetric analyser, powder X-ray



diffraction, single crystal X-ray diffraction, nuclear magnetic resonance, and, UV-Visible spectrophotometer.

X-ray diffraction studies showed molecular structure of all complexes in details, viz., complexes (1), (10), (12), and (14) are 0-D structure; complexes (6), (7), (8), (9), (11), (13), (15), (17), (18), (19), (20), (21), and (22) are 1-D structure; complexes (3), (4), (5), and (16) are 2-D structure; and complex (2) is 3-D structure. The coordination geometry around metal atom is octahedral for complexes (1), (4) - (6), (11) - (21), tetrahedral for (9), (10), and (22), linear for (7), T-shaped for (8), and square pyramid for complex (2), while complex (3) shows coordination geometry around Cd atom as pentagonal bipyramidal geometry and octahedral geometry. In addition, supramolecular interactions; H-bonding (O-H...N, O-H...O and C-H...O) and  $\pi$ - $\pi$  interaction are seen to have been stabilizing the crystal structures.

All information obtained by spectroscopy and elemental analyses were consistent with the structures from the X-ray single crystal analyses of all complexes.

Powder X-ray diffraction patterns of the complexes agree with the simulated pattern obtained from the X-ray data generated by Mercury 3.8 program indicating good phase purity of the synthesized products.

The photodegradation activity of  $\{[Ag_2(bpp)] \cdot (4H_2O) \cdot (3-Npt)\}_n$  (7) and  $\{[Ag_2(bpe)_2(3-Npt)] \cdot 7H_2O\}_n$  (8) were studied in the degradation of MB and RhB dyes in aqueous solution under UV and visible light at room temperature. The results showed degradation efficiency about 94 % for complex (7), 96 % for complex (8) for the MB solution, and 90 % for complex (7), 97 % for complex (8) for the RhB solution after 4.5 h under UV light. In visible light irradiation, decomposition rate showed about 83 % for complex (7), 87 % for complex (8) for the MB solution, and 68 % for complex (7), 84 % for complex (8) for the RhB solution. In addition, PXRD patterns of the complexes before and after the photocatalytic study remained unchanged indicating the robustness of both complexes when used as a catalyst.

The solid-state photoluminescence property of complexes (2), (9), (10), (13), (14), (17), (18), (19), and (20) were measured at room temperature. The spectra showed strong emission spectra at 410 nm ( $\lambda_{ex}$  320 nm) for (2), 425 nm ( $\lambda_{ex}$  = 320 nm) for (9), 420 nm ( $\lambda_{ex}$  = 350 nm) for (10), 342 nm ( $\lambda_{ex}$  = 300 nm) for (13), 412 nm ( $\lambda_{ex}$  = 320 nm) for (14), 358 nm ( $\lambda_{ex}$  = 300 nm) for (17), 355 nm

( $\lambda_{\text{ex}} = 300$  nm) for **(18)**, 409 nm ( $\lambda_{\text{ex}} = 320$  nm) for **(19)**, 412 nm ( $\lambda_{\text{ex}} = 320$  nm) for **(20)**. These emissions are assigned to ligand-to-metal charge transfer (LMCT) or metal-to-ligand charge transfer (MLCT) due to the  $\text{Zn}^{2+}$  and  $\text{Cd}^{2+}$  ions are stable  $d^{10}$  configuration and are difficult to be reduced or oxidized. In addition, complexes **(9)** and **(10)** showed selectivity and sensitivity as metal ion sensor to  $\text{Cu}^{2+}$  ion compared with other metal ions such as  $\text{M} = \text{Cd}^{2+}$ ,  $\text{Mn}^{2+}$ ,  $\text{Sr}^{2+}$ ,  $\text{K}^+$ ,  $\text{Na}^+$ ,  $\text{Ni}^{2+}$ ,  $\text{Co}^{2+}$ , and  $\text{Ca}^{2+}$ . The limit of detection to  $\text{Cu}^{2+}$  of complexes **(9)** and **(10)** are  $3.9 \times 10^{-7}$  mol/L and  $8.9 \times 10^{-7}$  mol/L, respectively.

Antimicrobial teste of complexes **(9)** and **(10)** in DMSO solution were studied using the technique “measure zone of inhibition” with Penicillin and Gentamicin used as standards to compare the activity. Gram-positive (*S. aureus*) and gram-negative (*E. coli*, *P. aeruginosa*) bacteria were used in this study. The data showed that complexes had lower biological activity than Penicillin and Gentamicin. In addition, the antibacterial activity of complexes for Gam negative bacteria was higher than Gram positive bacteria.

In the adsorption study, the results showed the adsorption of OG onto complex **(7)** fit to the Langmuir model ( $R^2 = 0.9931$ ) better than the Freundlich model ( $R^2 = 0.8873$ ). The maximum adsorption capacities for OG dye was 0.7051 mmol dye/g for complex **(7)**.

## REFERENCES

- Adriana, M., and L. Wiklund. "Methylene blue, an old drug with new indications" J. Rom. Anest. Terap. Int. 2010, 17, 35-41.
- Avijit K. P., Giridhar M. and Srinivasan N. "Adsorption–desorption and photocatalytic properties of inorganic–organic hybrid cadmium thiosulfate compounds" Phys. Chem. Chem. Phys. 2009, 11, 11285–11296.
- Abbasia, A., Ghariba, M., Najafia, M., and Janczak, J. "Room temperature synthesis of a Zn(II) metal-organic coordination polymer for dye removal", J. Solid State Chem. 2016, 235, 12–17.
- Bao, H. Y., Ming, L. T., and Xiao, M. C. "Metal-organic molecular architectures with 2,2-bipyridyl-like and carboxylate ligands", Coordin. Chem. Rev. 2005, 249, 545–565.
- Bei, L., Xiaofang, W., Huai, -M. H., Yi, -F. Z., Meng, -L. Y., Ganglin, X. (2016). "Synthesis, structure and luminescent sensor of zinc coordination polymers based on a new functionalized bipyridyl carboxylate ligand", Inorg. Chim. Acta. 453, 771–778.
- Buragohain, A., Yousufuddin, M., Sarma, M., and Biswas, S. "3D Luminescent Amide-Functionalized Cadmium Tetrazolate Framework for Selective Detection of 2,4,6-Trinitrophenol" Cryst. Growth Des. 2016, 16, 842–851.
- Carlucci, L., Ciani, G., Proserpio D.M., and Silvia Rizzato, S. "New polymeric networks from the self-assembly of silver(I) salts and the flexible ligand 1,3-bis(4-pyridyl)propane (bpp). A systematic investigation of the effects of the counterions and a survey of the coordination polymers based on bpp", CrystEngComm. 2002, 4(22), 121–129.

- Cha, Y.E., Li, X., and Liang, H. "Two-dimensional open structures of transition metal(II) coordination polymers constructed from 3-fluorophthalic acid and 4,4'-bipyridine", Polyhedron. 2013, 50, 208–214.
- Chenini, H., Djebbar, K., Zendaoui, S.M., Sehili, T. Zouchoune, B. "Removal of an Azo Dye (Orange G) By Various Methods in Homogenous Phase. Comparative Study" Jordan J. Chem. 2011, 6(3), 307-319.
- Deng, Z.P., Huo, L.H. Li, M.S., Zhang L.W., Zhu, Z.B., Zhao, H., and Gao, S. "Syntheses, Structures, and Luminescent Properties of Silver(I) Complexes Constructed from ortho-Hydroxyl Arenesulfonic Acids" Cryst. Growth Des. 2011, 11, 3090–3100.
- Di, S., Na, Z., Rong, -B. H., and Lan, -S. Z. "Series of Ag(I) Coordination Complexes Derived from Aminopyrimidyl Ligands and Dicarboxylates: Syntheses, Crystal Structures, and Properties" Cryst. Growth Des. 2010, 10, 3699–3709.
- Faller, P. "Copper in Alzheimer disease: too much, too little, or misplaced?", Free Radic. Biol. Med. 2012, 52, 747–748.
- García, E.R., Medina, R.L., Lozano, M.M., Pérez, I.H., Valero, M.J., and Franco, A.M. "Adsorption of Azo-Dye Orange II from Aqueous Solutions Using a Metal-Organic Framework Material: Iron- Benzenetricarboxylate" Materials. 2014, 7, 8037-8057.
- Ge, J.Y., Cheng, J.Y. Wang, P., Liu Q.K., and Dong, Y.B. "Four M(II)-coordination polymers (M = Zn(II) and Cd(II)) based on a flexible 1,2-bis(pyridin-3-yloxy)ethane ligand: Syntheses, structures and photoluminescent properties", J. Mol. Struct. 2014, 1056–1057, 127–134.

- He, Y.H., Feng, Y.L. Lan, Y.Z., and Wen, Y.H. "Syntheses, Structures, and Photoluminescence of Four d10 Metal-Organic Frameworks Constructed from 3,5-Bis-oxyacetate-benzoic Acid" Cryst. Growth Des. 2008, 10, 3586–3594.
- Huan, D.H., Liu, Y.G., Dong, G.Y., and Wang, S.C. "Three cobalt(II) coordination polymers constructed from flexible bis(thiabendazole) and dicarboxylate linkers: crystal structures, fluorescence, and photocatalytic properties", Transit. Metal Chem. 2016, 41, 447–457.
- Ioannis P. G., Anastassios, T., Vassiliki, E., and Klimentini, B. "Nuclear magnetic resonance (NMR) spectroscopy: basic principles and phenomena, and their applications to chemistry, biology and medicine" Chemistry Education: Research and Practice in Europe. 2002, 3(2), 229-252.
- Irene, G., Eva, V., and Nikos, K. "A Study on the Degradation of Carbamazepine and Ibuprofen by TiO<sub>2</sub> & ZnO Photocatalysis upon UV/Visible-Light Irradiation" Am. J. Analyt. Chem. 2014, 5, 518-534.
- Jacqueline M. K., and Steven, W. K. "A Mixed-Ligand Coordination Polymer from the in Situ, Cu(I)-Mediated Isomerization of Bis(4-pyridyl)ethylene" Inorg. Chem. 2002, 41, 5650-5652.
- Jang, S.P., Poong, J.I., Kim, S.H., Lee, T.G., Noh, J.Y., Kim, C., Kim, Y., Kim, S.J. "Tuning structural topology of zinc(II)-benzoate coordination complexes with 1,2-bis(4-pyridyl)ethene by controlling metal-to-ligand ratios and solvent systems: Their photoluminescence and catalytic activities" Polyhedron. 2012, 33, 194–202.
- Jennifer, C. M., and Dennis, A. D., "The Cation- $\pi$  Interaction" Chem. Rev. 1997, 97, 1303-1324.

- Jia, Z., Chong, C. W., Peng, W., Xin, X. G., and Shi, J. G. "Silver-based coordination complexes of carboxylate ligands: crystal structures, luminescence and photocatalytic properties" Transit. Metal Chem. 2016, 41(6), 637–645.
- Jiang, H.L., Liu, B., and Xu, Q. "Rational Assembly of  $d^{10}$  Metal-Organic Frameworks with Helical Nanochannels Based on Flexible V-Shaped Ligand" Cryst. Growth Des. 2010, 10, 806–811.
- Junwei, Y., Limei, Z., Raji, F. B., Yuan, G., Xiaoxiao, W., Xiaomin, Q., Song, G., Jianzhang, Z., and Guiling, N. "Highly Selective Detection of 2,4,6-Trinitrophenol and  $Cu^{2+}$  Ions Based on a Fluorescent Cadmium–Pamoate Metal–Organic Framework" Chem. Eur. J. 2015, 21, 2029 – 2037.
- Kai, W., Xiao, -Y. Q., Qing, -L. W., Hong, -X. R., Yue, M., Peng, C., and Dai, -Z. L. "3D nickel(II) and cobalt(II) complexes based on 1,4-bis(1,2,4-triazol-1-yl)butane (btb) and  $PF_6^-$  synthons", Inorg. Chim. Acta. 2016, 441, 131–136
- Khan, T. A., Sharma, S., and Ali I. "Adsorption of Rhodamine B dye from aqueous solution onto acid activated mango (*Magnifera indica*) leaf powder: Equilibrium, kinetic and thermodynamic studies", J. Toxicol. Environ. Health Sci. 2011, 3(10), 286-297.
- Kuai, H.W., Cheng, X.C., and Zhu, X.H. "Zinc(II) and cadmium(II) coordination polymers with a tricarboxylate containing reduced Schiff base ligand: Structural characterization and luminescent property", Polyhedron. 2013, 50, 390–397.
- Lehn, J.-M. "Supramolecular Chemistry", VCH, Weinheim, 1995, Germany.

- Li, F.F., Ma, J.M. Song, S.Y., and Yang, J. “Syntheses, Structures, and Characterizations of Four New Silver(I) Sulfonate Coordination Polymers with Neutral Ligands”, Cryst. Growth Des. 2010, 6, 209-215.
- Li, S.H., Chen, S.J., and Zhang, M.Y. “Crystal structure of poly[bis(1,3-bi(4-pyridyl)propane)-bis(4-amino-3-methyl-benzenesulfonate)manganese(II)],  $C_{40}H_{44}MnN_6O_6S_2$ ”, Z. Kristallogr. NCS. 2015, 230, 119-120.
- Li, X.J., Cao, R., Bi, W.H., Wang, Y.Q., Wang, Y.L., and Li, X. “Three interpenetrated frameworks constructed by long flexible N,N'-bipyridyl and dicarboxylate ligands” Polyhedron. 2015, 24, 2955–2962.
- Liu, M., Liang, Y., Wang, H.C., Ma, J.C., and Niu, Y.Y. “Synthesis, Structures and Photocatalytic Properties of Two Novel Ag(I) Polymers Directed by 1,3-Bis(4-methylpyridine)alkane Cation”, J. Clust. Sci. 2015, 6, 1723–1733.
- Liu, P., Lian, Z.X., and Cai, J. “Crystal structures of two monoamine-coordinated zinc complexes obtained via solid-vapor reaction”, J. Chem. Crystallogr. 2006, 36(10), 673-678.
- Lu, L., Jie, D., Chao, H., Ming, L., Hongwei, H., and Yaoting, F. “Polynuclear  $Cd^{II}$  Polymers: Crystal Structures, Topologies, and the Photodegradation for Organic Dye Contaminants”, Cryst. Growth Des. 2014, 14, 3035–3043.
- Lucia, C., Gianfranco, C., Davide, M. P., and Silvia, R. “New polymeric networks from the self-assembly of silver(I) salts and the flexible ligand 1,3-bis(4-pyridyl)propane (bpp). A systematic investigation of the effects of the counterions and a survey of the coordination polymers based on bpp” CrystEngComm. 2002, 4(22), 121–129.

- Ma, J. F., Yang, J., Li, S., and Song, S.Y. “Two Coordination Polymers of Ag(I) with 5-Sulfosalicylic Acid”, Cryst. Growth Des. 2005, 5(2), 807–812.
- Ma, Z., and Moulton, B. “Recent advances of discrete coordination complexes and coordination polymers in drug delivery” Coordin. Chem. Rev. 2011, 255, 1623–1641.
- Mahasin, F. Al, K., Israa, F. A., and Ali, A. D. A. “Analysis of the Effect of the Concentration of Rhodamine B in Ethanol on the Fluorescence Spectrum Using the "Gauss Mod" Function” Phys. Sci. 2011, 22(2), 77–86.
- Mahata, P., Madras, G., and Natarajan, S. “Novel Photocatalysts for the Decomposition of Organic Dyes Based on Metal-Organic Framework Compounds”, J. Phys. Chem. B. 2006, 110, 13759-13768.
- Mao, L. H., Ali, M., Leila, A. “Lead(II) carboxylate supramolecular compounds: Coordination modes, structures and nano-structures aspects”, Coordin. Chem. Rev. 2011, 255, 2821– 2859.
- Mei, C.Z., Shan, W.W., and Liu, B.T. “Synthesis, crystal structure and luminescent properties of one 3D Cd(II) coordination polymer  $[Cd(H_3BPTC)_2(bpy)]_n$  ( $H_4BPTC = 1,1'$ -biphenyl-2,2',6,6'-tetracarboxylic acid,  $bpy = 4,4'$ -bipyridine)”, Spectrochim. Acta A. 2011, 81, 764-768.
- Min, H.X. Sheng, G.C., Li, J.L., Wei, H.W., Yong, L., and Dong, S.W. “Syntheses and Crystal Structures of Three Ag(I) Complexes with Chloro-phenylacetic Acid and Nitrogen Heterocyclic Ligand” Chinese J. Struct. Chem. 2015, 34(9), 1362–1370.



- Ming, L., Lu, L., Lin, Z., Xiaofeng, L., Jie, D., Hongwei, H., and Yaoting, F. “Novel coordination polymers of Zn(II) and Cd(II) tuned by different aromatic polycarboxylates: synthesis, structures and photocatalytic properties” CrystEngComm. 2014, 16, 6408-6416.
- Mondal, J., Dutta, A., Pal, P.K. Saha, R., Maji, P., and Patra, G.K. “Synthesis, structure, photo-physical properties and catalytic activities of Zn(II), Cd(II) and Hg(II) complexes of an azinopyridyl ligand”, Inorg. Chim. Acta. 2016, 448, 70–77.
- Mutasem, O. S., Edward, F. V., and C. D. Sherrill. “Estimates of the Ab Initio Limit for  $\pi$ - $\pi$  Interactions: The Benzene Dimer” J. Am. Chem. Soc. 2002, 124, 10887-10893.
- Nara, M., Morii, H., and Tanokura, M. “Coordination to divalent cations by calcium-binding proteins studied by FTIR spectroscopy”, Biochim. Biophys. Acta. 2013, 1828, 2319–2327.
- Sachin, M.K. and R.W.Gaikwad. “Removal of Methylene Blue from Effluent by Using Activated Carbon and Water Hyacinth as Adsorbent”, Int J Chem Eng Appl. 2011, 2(5), 317-319.
- Sanram, S., Boonmak, J., and Youngme, S. “Ni(II)-metal–organic frameworks based on 1,4-phenylenedipropionic acid: Solvothermal syntheses, structures, and photocatalytic properties” Polyhedron. 2016, 119, 151–159.
- Seidel, R. W., Richard, G., Zibrowius, B., and Oppel I. M. “A Molecular Antenna Coordination Polymer from Cadmium(II) and 4,4'-Bipyridine Featuring Three Distinct Polymer Strands in the Crystal”, Polymers. 2011, 3, 1458-1474.

- Shahryari, Z., Goharrizi, A. S., & Azadi, M. "Experimental study of methylene blue adsorption from aqueous solutions onto carbon nano tubes", Int. J. Water Res. Environ. Eng. 2010, 2(2), 016–028.
- Sivakami, M., Natarajan, B., and Vijayachandrasekar, M. "Synthesis, Characterisation and Biological Activity of a New Mannich Base and It's Metal Complexes" Chem. Sci. Trans. 2014, 3(3), 1110-1114.
- Sriprang, P., Wongnawa, S., and Sirichote, O. "Amorphous titanium dioxide as an adsorbent for dye polluted water and its recyclability" J. Sol-Gel Sci. Techn. 2014, 71(1), 86–95.
- Stuart, R. B., Neil R. C., Xiao, -M. C., Javier, G. M., Susumu, K., Lars, Ö, Michael, O.K., Myunghyun, P. S., and Jan, R. "Terminology of metal organic frameworks and coordination polymers (IUPAC Recommendations 2013)\*". Pure Appl. Chem. 2013, 85(8), 1715–1724.
- Steed, J. W., and Atwood, J. L. "Supramolecular Chemistry". Chichester: 2000, England.
- Steed, J. W., David, R. T., and Karl, J. W. "Core Concepts in Supramolecular Chemistry and Nanochemistry" 2007.
- Swiderski, G., Kalinowska, M., Swislockaa, R., Wojtulewski, S., Lewandowski, W. "Spectroscopic (FT-IR, FT-Raman and <sup>1</sup>H and <sup>13</sup>C NMR) and theoretical in MP2/6-311++G(d,p) and B3LYP/6-311++G(d,p) levels study of benzenesulfonic acid and alkali metal benzenesulfonates" Spectrochim. Acta A. 2013, 100, 41–50.

- Timothy, J. P., Bunlawee, Y., and Apinpus, R. “Microwave synthesis and crystal structures of two cobalt-4,4'-bipyridine-sulfate frameworks constructed from 1-D coordination polymers linked by hydrogen bonding”, Polyhedron. 2011, 30, 259–268.
- Wang, C. C., Li, J. R., Lv, X. L., Zhang, Y.Q., and Guo, G. “Photocatalytic organic pollutants degradation in metal–organic frameworks”, Energy Environ. Sci. 2014, 7, 2831–2867.
- Wang, J.H., Tang, G.M., Yan, S.C., Wang, Y.T., Zhan, S.J., Zhang, E., Sun, Y., Jiang, Y., and Cui, Y.Z. “Cobalt-based metal coordination polymers with 4,4'-bipyridinyl groups: highly efficient catalysis for one-pot synthesis of 3,4-dihydropyrimidin-2(1H)-ones under solvent-free conditions”, Appl. Organomet. Chem. 2016, 30, 1009–1021.
- Wang, X. X., Li, Z.X., Yu, B., Hecke, K. V., and Cui, G.H. “Synthesis and characterizations of a bis(triazole)-based 3D crystalline copper(II) MOF with high adsorption capacity for congo red dye” Inorg. Chem. Commun. 2015, 54, 9–11.
- Wang, Y., Feng, L., Li, Y., Hu, C., Wang, E., Hu, N., and Jia, H. “Novel Hydrogen-Bonded Three-Dimensional Networks Encapsulating One-Dimensional Covalent Chains:  $[M(4,4'\text{-bipy})(\text{H}_2\text{O})_4](4\text{-abs})_2 \cdot \text{H}_2\text{O}$  (4,4'-Bipyridine; 4-abs = 4-Aminobenzenesulfonate) (M =Co, n = 1; M = Mn, n = 2)”, Inorg. Chem. 2002, 41, 6351-6357.
- Wang, Y., Zhu, Y., Xu, J., Wei, C., Liu P., Wu, Y., and Xie, J. “Structures, photoluminescence and heterogeneous catalysis of five metal complexes constructed by a flexible tricarboxylate ligand”, Polyhedron. 2014, 81, 32–38.

- Wen, L., Zhao, J., Lv, K., Wu, Y., Deng, K., Leng, X., and Li, D. “Visible-Light-Driven Photocatalysts of Metal–Organic Frameworks Derived from Multi-Carboxylic Acid and Imidazole-Based Spacer”, Cryst. Growth Des. 2012, 12, 1603–1612.
- Xiao, L.S., Li, H.Y., Ma, P.J., and Cui, G.H. “Synthesis and characterizations of two bis(benzimidazole)-based cobaltous coordination polymers with high adsorption capacity for congo red dye” Inorg. Chem. Commun. 2013, 37, 54–58.
- Xiao, L., Xiong, Y., Tian, S., He, C., Su, Q., and Wen, Z. “One-dimensional coordination supramolecular polymer  $[\text{Cu}(\text{bipy})(\text{SO}_4)]_n$  as an adsorbent for adsorption and kinetic separation of anionic dyes”, Chem. Eng. J. 2015, 265, 157–163.
- Xiao, S.S., Li, X.X., Zheng, X.J., Jia, T.J. and Jin L.P. “4,4'-Bipyridine-aided synthesis and characterization of Zn(II) and Cd(II) 2-sulfoterephthalate complexes”, J. Solid State Chem. 2013, 205, 71–81.
- Xie, Y., Bai, F.Y., Li, J., Xing, Y.H., Wang, Z., Zhao, H.Y., Pu, Z.F., Ge, M.F., and Shi, Z. “Synthesis, crystal structure and photoelectric property of two new coordination polymers constructed by longer-spanning suberic acid and 4,4'-bipyridine ligands”, Spectrochim. Acta A Mol. Biomol. Spectrosc. 2010, 77, 749–754.
- Xu, Y.H., Ya, Q.L., Wang, X.L., Zang, H.Y., Shao, K.Z., Liao, Y., and Su, Z.M. “Self-assembly of zinc polymers based on a flexible linear ligand at different pH values: Syntheses, structures and fluorescent properties” Solid State Sci. 2009, 11, 635–642.

- Ye, J., Wang, X., Bogale, R. F., Zhao, L., Cheng, H., Gong, W., Zhao, J., and Ning, G. "A fluorescent zinc-pamoate coordination polymer for highly selective sensing of 2,4,6-trinitrophenol and Cu<sup>2+</sup> ion" Sensor Actuat. B-Chem. 2016, 210, 566–573.
- Yu, X., Ni, S., Zhang, D., Zheng, Y., and Zhu, H. "Crystal structure, magnetic properties and topological analysis of three Mn-nitro-dicarboxylate polymers", J. mol. Struct. 2014, 1076, 426–436.
- Zhang, J., Wang, C.C., Wang, P., Guo, X.X., and Gao, S.J. "Silver-based coordination complexes of carboxylate ligands: crystal structures, luminescence and photocatalytic properties", Transit Met Chem. 2016, 41, 637–645.
- Zhang, M., Zhang, L., Xiao, Z., Zhang, Q., Wang, R., Dai, F., and Su, D. "Pentipyrene-Based Luminescent Cu (II) MOF Exhibiting Selective Gas Adsorption and Unprecedentedly High-Sensitivity Detection of Nitroaromatic Compounds (NACs)", Sci. Rep. 2016, 6, 1-10.
- Zhao, J., Wang, X.L., Shi, X., Yang Q. H., and Li, C. "Synthesis, Structure, and Photoluminescent Properties of Metal Organic Coordination Polymers Assembled with Bithiophenedicarboxylic Acid", Inorg. Chem. 2011, 50, 3198–3205.

## Appendix A

**Table A1.** Crystallographic data and structure refinement for [Cd(Cin)<sub>2</sub>(H<sub>2</sub>O)<sub>2</sub>] (**1**), [Zn(4,4'-bpy)<sub>0.5</sub>(Cin)<sub>2</sub>]<sub>n</sub> (**2**), and [Cd<sub>3</sub>(4,4'-bpy)<sub>2</sub>(cin)<sub>6</sub>(H<sub>2</sub>O)<sub>2</sub>]<sub>n</sub> (**3**).

	<b>1</b>	<b>2</b>	<b>3</b>
Empirical formula	C <sub>18</sub> H <sub>18</sub> CdO <sub>6</sub>	C <sub>23</sub> H <sub>18</sub> NO <sub>4</sub> Zn	C <sub>74</sub> H <sub>62</sub> Cd <sub>3</sub> N <sub>4</sub> O <sub>14</sub>
Formula weight	442.72	437.75	1568.48
Temperature/K	99.65	99.65	296.15
Crystal system	monoclinic	trigonal	triclinic
Space group	<i>C2</i>	<i>R-3</i>	<i>P</i> $\bar{1}$
<i>a</i> /Å	11.7872(12)	31.5326(19)	10.8357(15)
<i>b</i> /Å	5.3498(5)	31.5326(19)	11.6010(16)
<i>c</i> /Å	13.8817(14)	12.6180(8)	13.9036(19)
$\alpha$ /°	90.00	90.00	74.388(2)
$\beta$ /°	99.9130(10)	90.00	80.131(2)
$\gamma$ /°	90.00	120.00	88.310(2)
Volume/Å <sup>3</sup>	862.30(15)	10865.3(12)	1658.1(4)
<i>Z</i>	2	18	1
$\rho_{\text{calc}}$ /cm <sup>3</sup>	1.705	1.204	1.571
$\mu$ /mm <sup>-1</sup>	1.297	1.041	1.023
<i>F</i> (000)	444.0	4050.0	790.0
Radiation	MoK $\alpha$ ( $\lambda$ = 0.71073)	MoK $\alpha$ ( $\lambda$ = 0.71073)	MoK $\alpha$ ( $\lambda$ = 0.71073)
2 $\Theta$ range for data collection/°	5.96 to 62.86	2.58 to 63.12	5.24 to 62.92
Index ranges	-17 $\leq$ <i>h</i> $\leq$ 16, -7 $\leq$ <i>k</i> $\leq$ 7, -20 $\leq$ <i>l</i> $\leq$ 19	-44 $\leq$ <i>h</i> $\leq$ 44, -45 $\leq$ <i>k</i> $\leq$ 45, -18 $\leq$ <i>l</i> $\leq$ 18	-15 $\leq$ <i>h</i> $\leq$ 15, -16 $\leq$ <i>k</i> $\leq$ 16, -20 $\leq$ <i>l</i> $\leq$ 20
Reflections collected	5087	42142	37273
Independent reflections	2531 [ <i>R</i> <sub>int</sub> = 0.0205, <i>R</i> <sub>sigma</sub> = 0.0343]	7710 [ <i>R</i> <sub>int</sub> = 0.0346, <i>R</i> <sub>sigma</sub> = 0.0300]	10019 [ <i>R</i> <sub>int</sub> = 0.0347, <i>R</i> <sub>sigma</sub> = 0.0343]
Data/restraints/parameters	2531/3/150	7710/0/262	10019/0/431
Goodness-of-fit on <i>F</i> <sup>2</sup>	1.044	1.092	1.044
Final <i>R</i> indexes [ <i>I</i> $\geq$ 2 $\sigma$ ( <i>I</i> )]	<i>R</i> <sub>1</sub> = 0.0197, <i>wR</i> <sub>2</sub> = 0.0458	<i>R</i> <sub>1</sub> = 0.0383, <i>wR</i> <sub>2</sub> = 0.1051	<i>R</i> <sub>1</sub> = 0.0429, <i>wR</i> <sub>2</sub> = 0.0991
Final <i>R</i> indexes [all data]	<i>R</i> <sub>1</sub> = 0.0198, <i>wR</i> <sub>2</sub> = 0.0458	<i>R</i> <sub>1</sub> = 0.0517, <i>wR</i> <sub>2</sub> = 0.1095	<i>R</i> <sub>1</sub> = 0.0546, <i>wR</i> <sub>2</sub> = 0.1063
Largest diff. peak/hole / e Å <sup>-3</sup>	1.09/-0.42	0.54/-0.34	1.86/-1.93
Flack parameter	0.01(2)		

**Table A2.** Crystallographic data and structure refinement for [Cd(4,4'-bpy)(3-Npt)(H<sub>2</sub>O)]<sub>n</sub> (**4**), [Mn<sub>2</sub>(bpp)(3-Npt)<sub>2</sub>(H<sub>2</sub>O)<sub>2</sub>]<sub>n</sub> (**5**), and [Ni(bpp)(3-Npt)(H<sub>2</sub>O)]<sub>n</sub> (**6**).

	<b>4</b>	<b>5</b>	<b>6</b>
Empirical formula	C <sub>18</sub> H <sub>13</sub> CdN <sub>3</sub> O <sub>7</sub>	C <sub>29</sub> H <sub>28</sub> Mn <sub>2</sub> N <sub>4</sub> O <sub>16</sub>	C <sub>21</sub> H <sub>19</sub> N <sub>3</sub> NiO <sub>7</sub>
Formula weight	495.71	798.43	484.10
Temperature/K	100(2)	100(2)	100(2)
Crystal system	monoclinic	orthorhombic	monoclinic
Space group	<i>P2<sub>1</sub>/c</i>	<i>Aba2</i>	<i>P2<sub>1</sub>/n</i>
a/Å	7.6726(6)	30.1451(10)	12.0924(5)
b/Å	23.2722(18)	9.8718(3)	13.3043(6)
c/Å	9.9942(8)	11.3258(4)	12.5950(5)
α/°	90	90	90
β/°	97.786(2)	90	90.092(2)
γ/°	90	90	90
Volume/Å <sup>3</sup>	1768.1(2)	3370.40(19)	2026.29(15)
Z	4	4	4
ρ <sub>calc</sub> /g/cm <sup>3</sup>	1.862	1.573	1.587
μ/mm <sup>-1</sup>	10.355	0.829	1.837
F(000)	984.0	1632.0	1000.0
Radiation	CuKα (λ = 1.54178)	MoKα (λ = 0.71073)	CuKα (λ = 1.54178)
2θ range for data collection/°	7.598 to 133.996	5.406 to 61.044	9.67 to 133.382
Index ranges	-9 ≤ h ≤ 9, -27 ≤ k ≤ 27, -11 ≤ l ≤ 11	-42 ≤ h ≤ 31, -10 ≤ k ≤ 14, -14 ≤ l ≤ 16	-14 ≤ h ≤ 14, 0 ≤ k ≤ 15, 0 ≤ l ≤ 14
Reflections collected	22510	13624	3616
Independent reflections	3072 [R <sub>int</sub> = 0.0310, R <sub>sigma</sub> = 0.0173]	4737 [R <sub>int</sub> = 0.0239, R <sub>sigma</sub> = 0.0321]	3616 [R <sub>sigma</sub> = 0.1726]
Data/restraints/parameters	3072/0/272	4737/106/241	3616/2/296
Goodness-of-fit on F <sup>2</sup>	1.145	1.117	0.999
Final R indexes [I ≥ 2σ (I)]	R <sub>1</sub> = 0.0194, wR <sub>2</sub> = 0.0477	R <sub>1</sub> = 0.0273, wR <sub>2</sub> = 0.0642	R <sub>1</sub> = 0.0506, wR <sub>2</sub> = 0.1534
Final R indexes [all data]	R <sub>1</sub> = 0.0194, wR <sub>2</sub> = 0.0477	R <sub>1</sub> = 0.0283, wR <sub>2</sub> = 0.0646	R <sub>1</sub> = 0.0581, wR <sub>2</sub> = 0.1666
Largest diff. peak/hole / e Å <sup>-3</sup>	0.32/-0.50	0.45/-0.39	0.55/-0.45
Flack parameter			

**Table A3.** Crystallographic data and structure refinement for {[Ag<sub>2</sub>(bpp)<sub>2</sub>]}·3-Npt}<sub>n</sub> (**7**), {[Ag<sub>2</sub>(bpe)<sub>2</sub>(3-Npt)]·7H<sub>2</sub>O}<sub>n</sub> (**8**), and [Zn(bpp)<sub>2</sub>(Sal)<sub>2</sub>]<sub>n</sub> (**9**).

	<b>7</b>	<b>8</b>	<b>9</b>
Empirical formula	C <sub>34</sub> H <sub>31</sub> Ag <sub>2</sub> N <sub>5</sub> O <sub>6</sub>	C <sub>32</sub> H <sub>41</sub> Ag <sub>2</sub> N <sub>5</sub> O <sub>13</sub>	C <sub>27</sub> H <sub>24</sub> N <sub>2</sub> O <sub>6</sub> Zn
Formula weight	821.38	919.44	537.85
Temperature/K	273.15	273.15	296.0
Crystal system	orthorhombic	triclinic	monoclinic
Space group	<i>Pnma</i>	<i>P</i> $\bar{1}$	<i>P2</i> <sub>1</sub> / <i>n</i>
<i>a</i> /Å	8.6468(3)	10.012(5)	13.1199(4)
<i>b</i> /Å	17.5743(7)	10.882(6)	11.2017(4)
<i>c</i> /Å	25.7781(10)	17.883(10)	16.9977(6)
$\alpha$ /°	90.00	74.95(2)	90.00
$\beta$ /°	90.00	80.420(18)	94.0160(10)
$\gamma$ /°	90.00	79.906(17)	90.00
Volume/Å <sup>3</sup>	3917.3(3)	1837.4(18)	2491.94(15)
<i>Z</i>	4	2	4
$\rho_{\text{calc}}$ /cm <sup>3</sup>	1.393	1.662	1.434
$\mu$ /mm <sup>-1</sup>	1.044	1.136	1.030
<i>F</i> (000)	1648.0	932.0	1112.0
Radiation	MoK $\alpha$ ( $\lambda$ = 0.71073)	MoK $\alpha$ ( $\lambda$ = 0.71073)	MoK $\alpha$ ( $\lambda$ = 0.71073)
2 $\Theta$ range for data collection/°	6.12 to 52.84	5.92 to 50.7	6.02 to 54
Index ranges	-10 ≤ <i>h</i> ≤ 10, -21 ≤ <i>k</i> ≤ 21, -32 ≤ <i>l</i> ≤ 32	-12 ≤ <i>h</i> ≤ 12, -13 ≤ <i>k</i> ≤ 13, -21 ≤ <i>l</i> ≤ 21	-16 ≤ <i>h</i> ≤ 16, -13 ≤ <i>k</i> ≤ 14, -21 ≤ <i>l</i> ≤ 21
Reflections collected	105633	47647	47678
Independent reflections	4150 [ <i>R</i> <sub>int</sub> = 0.0643, <i>R</i> <sub>sigma</sub> = 0.0160]	6711 [ <i>R</i> <sub>int</sub> = 0.0681, <i>R</i> <sub>sigma</sub> = 0.0434]	5418 [ <i>R</i> <sub>int</sub> = 0.0657, <i>R</i> <sub>sigma</sub> = 0.0352]
Data/restraints/parameters	4150/1/236	6711/0/490	5418/0/327
Goodness-of-fit on <i>F</i> <sup>2</sup>	1.040	1.022	1.018
Final <i>R</i> indexes [ <i>I</i> ≥ 2 $\sigma$ ( <i>I</i> )]	<i>R</i> <sub>1</sub> = 0.0352, <i>wR</i> <sub>2</sub> = 0.0883	<i>R</i> <sub>1</sub> = 0.0469, <i>wR</i> <sub>2</sub> = 0.0893	<i>R</i> <sub>1</sub> = 0.0379, <i>wR</i> <sub>2</sub> = 0.0761
Final <i>R</i> indexes [all data]	<i>R</i> <sub>1</sub> = 0.0539, <i>wR</i> <sub>2</sub> = 0.0940	<i>R</i> <sub>1</sub> = 0.0873, <i>wR</i> <sub>2</sub> = 0.1030	<i>R</i> <sub>1</sub> = 0.0703, <i>wR</i> <sub>2</sub> = 0.0878
Largest diff. peak/hole / e Å <sup>-3</sup>	0.48/-0.39	1.90/-1.35	0.28/-0.20
Flack parameter			



**Table A4.** Crystallographic data and structure refinement for  $[\text{Zn}_2(\text{bpe})_2(\text{Sal})_4]$  (**10**),  $\{[\text{Co}(\text{bpp})_2(\text{H}_2\text{O})_2](4\text{-abs})_2 \cdot \text{H}_2\text{O}\}_n$  (**11**), and  $[\text{Mn}_{0.5}(\text{bpp})(4\text{-abs})(\text{H}_2\text{O})_2]$  (**12**).

	<b>10</b>	<b>11</b>	<b>12</b>
Empirical formula	$\text{C}_{52}\text{H}_{44}\text{N}_4\text{O}_{12}\text{Zn}_2$	$\text{C}_{38}\text{H}_{48}\text{CoN}_6\text{O}_{10}\text{S}_2$	$\text{C}_{19}\text{H}_{24}\text{Mn}_{0.5}\text{N}_3\text{O}_5\text{S}$
Formula weight	1047.65	871.87	433.94
Temperature/K	296.15	296.0	273.15
Crystal system	triclinic	triclinic	monoclinic
Space group	$P\bar{1}$	$P\bar{1}$	$P2_1/n$
a/Å	11.2840(6)	9.550(4)	6.5178(2)
b/Å	11.4948(6)	9.784(3)	14.6593(5)
c/Å	12.0972(7)	11.839(4)	21.9010(8)
$\alpha/^\circ$	66.129(2)	94.673(11)	90.00
$\beta/^\circ$	63.384(2)	112.045(11)	95.1420(10)
$\gamma/^\circ$	63.697(2)	98.586(11)	90.00
Volume/Å <sup>3</sup>	1215.26(11)	1002.4(6)	2084.14(12)
Z	1	1	4
$\rho_{\text{calc}}/\text{g}/\text{cm}^3$	1.432	1.444	1.383
$\mu/\text{mm}^{-1}$	1.054	0.597	0.479
F(000)	540.0	457.0	910.0
Radiation	MoK $\alpha$ ( $\lambda =$ 0.71073)	MoK $\alpha$ ( $\lambda =$ 0.71073)	MoK $\alpha$ ( $\lambda =$ 0.71073)
2 $\Theta$ range for data collection/ $^\circ$	6.34 to 53.32	6.08 to 56.58	6.38 to 53.48
Index ranges	$-14 \leq h \leq 14,$ $14 \leq k \leq 14,$ $-15 \leq l \leq 15$	$-12 \leq h \leq 12,$ $k \leq 13,$ $-15 \leq l \leq 15$	$-12 \leq h \leq 8,$ $-18 \leq k \leq 18,$ $-27 \leq l \leq 26$
Reflections collected	21587	40223	36640
Independent reflections	5062 [ $R_{\text{int}} =$ 0.0539, $R_{\text{sigma}} =$ 0.0450]	4948 [ $R_{\text{int}} =$ 0.0322, $R_{\text{sigma}} =$ 0.0182]	4424 [ $R_{\text{int}} =$ 0.0465, $R_{\text{sigma}} =$ 0.0294]
Data/restraints/parameters	5062/0/318	4948/0/264	4424/41/263
Goodness-of-fit on F <sup>2</sup>	1.040	1.023	1.033
Final R indexes [ $I \geq 2\sigma(I)$ ]	$R_1 = 0.0451,$ $wR_2 = 0.0936$	$R_1 = 0.0317,$ $wR_2 = 0.0782$	$R_1 = 0.0435,$ $wR_2 = 0.0982$
Final R indexes [all data]	$R_1 = 0.0716,$ $wR_2 = 0.1031$	$R_1 = 0.0410,$ $wR_2 = 0.0830$	$R_1 = 0.0668,$ $wR_2 = 0.1088$
Largest diff. peak/hole / e Å <sup>-3</sup>	0.62/-0.35	0.41/-0.36	0.41/-0.38
Flack parameter			

**Table A5.** Crystallographic data and structure refinement for  $\{[\text{Cd}_{0.5}(\text{bpp})(4\text{-abs})]\cdot(\text{H}_2\text{O})\}_n$ (**13**),  $[\text{Zn}(\text{bpp})_2(\text{H}_2\text{O})_4](4\text{-abs})_2$ (**14**), and  $\{[\text{Zn}(4,4'\text{-bpy})(\text{H}_2\text{O})_4](4\text{-abs})_2\cdot 2\text{H}_2\text{O}\}_n$ (**15**).

	<b>13</b>	<b>14</b>	<b>15</b>
Empirical formula	$\text{C}_{19}\text{H}_{22}\text{Cd}_{0.5}\text{N}_3\text{O}_4\text{S}$	$\text{C}_{19}\text{H}_{24}\text{N}_3\text{O}_5\text{SZn}_{0.5}$	$\text{C}_{22}\text{H}_{32}\text{N}_4\text{O}_{12}\text{S}_2\text{Zn}$
Formula weight	444.66	439.16	674.01
Temperature/K	273.15	273.15	296.0
Crystal system	monoclinic	monoclinic	monoclinic
Space group	$P2_1/n$	$P2_1/n$	$P2_1$
a/Å	10.8343(3)	6.5000(3)	11.3601(4)
b/Å	17.2350(5)	14.3988(6)	8.0430(3)
c/Å	11.2060(3)	22.0563(10)	15.7168(6)
$\alpha/^\circ$	90.00	90.00	90.00
$\beta/^\circ$	112.2910(10)	93.967(2)	92.8090(10)
$\gamma/^\circ$	90.00	90.00	90.00
Volume/Å <sup>3</sup>	1936.11(9)	2059.35(16)	1434.31(9)
Z	4	4	2
$\rho_{\text{calc}}/\text{g}/\text{cm}^3$	1.525	1.416	1.561
$\mu/\text{mm}^{-1}$	0.732	0.761	1.069
F(000)	916.0	920.0	700.0
Radiation	MoK $\alpha$ ( $\lambda = 0.71073$ )	MoK $\alpha$ ( $\lambda = 0.71073$ )	MoK $\alpha$ ( $\lambda = 0.71073$ )
2 $\Theta$ range for data collection/ $^\circ$	6.14 to 56.66	5.96 to 55.08	6.16 to 54.32
Index ranges	$-13 \leq h \leq 14, -22 \leq k \leq 22, -14 \leq l \leq 14$	$-8 \leq h \leq 8, -18 \leq k \leq 18, -28 \leq l \leq 28$	$-14 \leq h \leq 14, -10 \leq k \leq 10, -20 \leq l \leq 20$
Reflections collected	24636	23019	60021
Independent reflections	4783 [ $R_{\text{int}} = 0.0367, R_{\text{sigma}} = 0.0306$ ]	4756 [ $R_{\text{int}} = 0.0448, R_{\text{sigma}} = 0.0402$ ]	6323 [ $R_{\text{int}} = 0.0286, R_{\text{sigma}} = 0.0157$ ]
Data/restraints/parameters	4783/41/273	4756/0/262	6323/7/389
Goodness-of-fit on F <sup>2</sup>	1.061	1.017	1.040
Final R indexes [ $I \geq 2\sigma(I)$ ]	$R_1 = 0.0371, wR_2 = 0.0845$	$R_1 = 0.0454, wR_2 = 0.1036$	$R_1 = 0.0381, wR_2 = 0.0977$
Final R indexes [all data]	$R_1 = 0.0551, wR_2 = 0.0920$	$R_1 = 0.0750, wR_2 = 0.1160$	$R_1 = 0.0427, wR_2 = 0.1007$
Largest diff. peak/hole / e Å <sup>-3</sup>	0.68/-0.82	0.71/-0.30	0.44/-0.27
Flack parameter			0.489(11)

**Table A6.** Crystallographic data and structure refinement for  $\{[\text{Cd}(4,4'\text{-bpy})_{1.5}(\text{H}_2\text{O})_3](4\text{-abs})\cdot(4,4'\text{-bpy})\cdot(\text{H}_2\text{O})\cdot\text{NO}_3\}_n$  (**16**),  $\{[\text{Cd}_{0.5}(\text{bpe})(4\text{-abs})]\cdot\text{H}_2\text{O}\}_n$  (**17**), and  $\{[\text{Cd}(\text{bpp})_2(\text{H}_2\text{O})_4](3\text{-abs})_2\cdot 2\text{H}_2\text{O}\}_n$  (**18**).

	<b>16</b>	<b>17</b>	<b>18</b>
Empirical formula	$\text{C}_{31}\text{H}_{34}\text{CdN}_7\text{O}_{10}\text{S}$	$\text{C}_{18}\text{H}_{20}\text{Cd}_{0.5}\text{N}_3\text{O}_4\text{S}$	$\text{C}_{38}\text{H}_{52}\text{CdN}_6\text{O}_{12}\text{S}_2$
Formula weight	809.11	430.63	961.38
Temperature/K	273.15	296.0	273.15
Crystal system	monoclinic	monoclinic	monoclinic
Space group	$P2_1/c$	$C2/c$	$C2/c$
a/Å	7.4659(2)	18.7843(6)	23.1360(7)
b/Å	23.3966(8)	11.0010(4)	12.7756(5)
c/Å	19.3429(7)	18.7773(7)	14.9772(5)
$\alpha/^\circ$	90.00	90.00	90.00
$\beta/^\circ$	94.6780(10)	95.6510(10)	103.4610(10)
$\gamma/^\circ$	90.00	90.00	90.00
Volume/Å <sup>3</sup>	3367.50(19)	3861.4(2)	4305.3(3)
Z	4	8	4
$\rho_{\text{calc}}/\text{g}/\text{cm}^3$	1.596	1.481	1.483
$\mu/\text{mm}^{-1}$	0.778	0.731	0.671
F(000)	1652.0	1768.0	1992.0
Radiation	MoK $\alpha$ ( $\lambda =$ 0.71073)	MoK $\alpha$ ( $\lambda =$ 0.71073)	MoK $\alpha$ ( $\lambda =$ 0.71073)
2 $\theta$ range for data collection/ $^\circ$	5.96 to 56.56	5.86 to 52.86	5.92 to 56.66
Index ranges	$-9 \leq h \leq 9, -31 \leq k \leq 30, -19 \leq l \leq 25$	$-21 \leq h \leq 23, -13 \leq k \leq 13, -23 \leq l \leq 23$	$-30 \leq h \leq 30, -17 \leq k \leq 17, -19 \leq l \leq 19$
Reflections collected	20513	62015	52583
Independent reflections	8318 [ $R_{\text{int}} =$ 0.0345, $R_{\text{sigma}} =$ 0.0557]	3968 [ $R_{\text{int}} =$ 0.0895, $R_{\text{sigma}} =$ 0.0313]	5354 [ $R_{\text{int}} =$ 0.0458, $R_{\text{sigma}} =$ 0.0256]
Data/restraints/parameters	8318/0/462	3968/0/244	5354/0/276
Goodness-of-fit on F <sup>2</sup>	1.030	1.062	1.039
Final R indexes [ $I \geq 2\sigma(I)$ ]	$R_1 = 0.0430,$ $wR_2 = 0.0810$	$R_1 = 0.0360,$ $wR_2 = 0.0695$	$R_1 = 0.0350,$ $wR_2 = 0.0806$
Final R indexes [all data]	$R_1 = 0.0726,$ $wR_2 = 0.0908$	$R_1 = 0.0575,$ $wR_2 = 0.0762$	$R_1 = 0.0543,$ $wR_2 = 0.0897$
Largest diff. peak/hole / e Å <sup>-3</sup>	0.61/-0.56	0.55/-0.42	0.71/-0.52
Flack parameter			

**Table A7.** Crystallographic data and structure refinement for  $[\text{Zn}(\text{bpp})_2(\text{Mbs})_2]_n$  (**19**),  $[\text{Cd}(\text{bpp})_2(\text{Mbs})_2]_n$  (**20**), and  $\{[\text{Cd}(\text{bpp})(\text{sdz})_2] \cdot 2\text{H}_2\text{O}\}_n$  (**21**).

	<b>19</b>	<b>20</b>	<b>21</b>
Empirical formula	$\text{C}_{40}\text{H}_{42}\text{N}_4\text{O}_6\text{S}_2\text{Zn}$	$\text{C}_{40}\text{H}_{42}\text{CdN}_4\text{O}_6\text{S}_2$	$\text{C}_{33}\text{H}_{36}\text{CdN}_{10}\text{O}_6\text{S}_2$
Formula weight	804.27	851.30	845.24
Temperature/K	296.0	296.0	273.15
Crystal system	orthorhombic	orthorhombic	monoclinic
Space group	<i>Pnna</i>	<i>Pnna</i>	<i>P2<sub>1</sub>/c</i>
<i>a</i> /Å	23.6349(9)	24.0751(7)	18.449(3)
<i>b</i> /Å	17.0958(5)	17.2717(5)	10.3730(16)
<i>c</i> /Å	9.2145(3)	9.2489(3)	20.939(3)
$\alpha$ /°	90.00	90.00	90.00
$\beta$ /°	90.00	90.00	111.811(5)
$\gamma$ /°	90.00	90.00	90.00
Volume/Å <sup>3</sup>	3723.2(2)	3845.9(2)	3720.3(9)
<i>Z</i>	4	4	4
$\rho_{\text{calc}}/\text{g}/\text{cm}^3$	1.435	1.470	1.509
$\mu/\text{mm}^{-1}$	0.825	0.728	0.757
<i>F</i> (000)	1680.0	1752.0	1728.0
Radiation	MoK $\alpha$ ( $\lambda =$ 0.71073)	MoK $\alpha$ ( $\lambda =$ 0.71073)	MoK $\alpha$ ( $\lambda =$ 0.71073)
2 $\theta$ range for data collection/°	5.88 to 60.14	5.8 to 56.66	5.74 to 52.88
Index ranges	$-33 \leq h \leq 32,$ $k \leq 22, -12 \leq l \leq$ 12	$-30 \leq h \leq 32, -23$ $\leq k \leq 22, -12 \leq l \leq$ 12	$-23 \leq h \leq 23, -12$ $\leq k \leq 12, -26 \leq l \leq$ 25
Reflections collected	98353	50218	57980
Independent reflections	5442 [ <i>R</i> <sub>int</sub> = 0.0598, <i>R</i> <sub>sigma</sub> = 0.0277]	4793 [ <i>R</i> <sub>int</sub> = 0.0504, <i>R</i> <sub>sigma</sub> = 0.0276]	7624 [ <i>R</i> <sub>int</sub> = 0.0701, <i>R</i> <sub>sigma</sub> = 0.0370]
Data/restraints/parameters	5442/63/242	4793/63/242	7624/0/477
Goodness-of-fit on <i>F</i> <sup>2</sup>	1.035	1.024	1.021
Final <i>R</i> indexes [ <i>I</i> ≥ 2σ ( <i>I</i> )]	<i>R</i> <sub>1</sub> = 0.0474, <i>wR</i> <sub>2</sub> = 0.1072	<i>R</i> <sub>1</sub> = 0.0383, <i>wR</i> <sub>2</sub> = 0.0890	<i>R</i> <sub>1</sub> = 0.0347, <i>wR</i> <sub>2</sub> = 0.0685
Final <i>R</i> indexes [all data]	<i>R</i> <sub>1</sub> = 0.0749, <i>wR</i> <sub>2</sub> = 0.1188	<i>R</i> <sub>1</sub> = 0.0599, <i>wR</i> <sub>2</sub> = 0.0983	<i>R</i> <sub>1</sub> = 0.0655, <i>wR</i> <sub>2</sub> = 0.0782
Largest diff. peak/hole / e Å <sup>-3</sup>	0.89/-0.94	1.06/-0.92	0.33/-0.34
Flack parameter			

**Table A8.** Crystallographic data and structure refinement for {[Zn(bpe)(sdz)(ac)]  
·2H<sub>2</sub>O}<sub>n</sub> (**22**).

<b>22</b>	
Empirical formula	C <sub>24</sub> H <sub>26</sub> N <sub>6</sub> O <sub>5</sub> SZn
Formula weight	575.94
Temperature/K	273.15
Crystal system	monoclinic
Space group	<i>P2<sub>1</sub>/n</i>
a/Å	8.9648(3)
b/Å	16.7001(6)
c/Å	17.7255(6)
α/°	90.00
β/°	98.8230(10)
γ/°	90.00
Volume/Å <sup>3</sup>	2622.34(16)
Z	4
ρ <sub>calc</sub> /cm <sup>3</sup>	1.459
μ/mm <sup>-1</sup>	1.062
F(000)	1192.0
Radiation	MoKα (λ = 0.71073)
2Θ range for data collection/°	5.98 to 52.78
Index ranges	-11 ≤ h ≤ 11, -20 ≤ k ≤ 20, -22 ≤ l ≤ 22
Reflections collected	34803
Independent reflections	5354 [R <sub>int</sub> = 0.0351, R <sub>sigma</sub> = 0.0208]
Data/restraints/parameters	5354/0/433
Goodness-of-fit on F <sup>2</sup>	1.034
Final R indexes [I >= 2σ (I)]	R <sub>1</sub> = 0.0333, wR <sub>2</sub> = 0.0818
Final R indexes [all data]	R <sub>1</sub> = 0.0425, wR <sub>2</sub> = 0.0870
Largest diff. peak/hole / e Å <sup>-3</sup>	0.73/-0.57

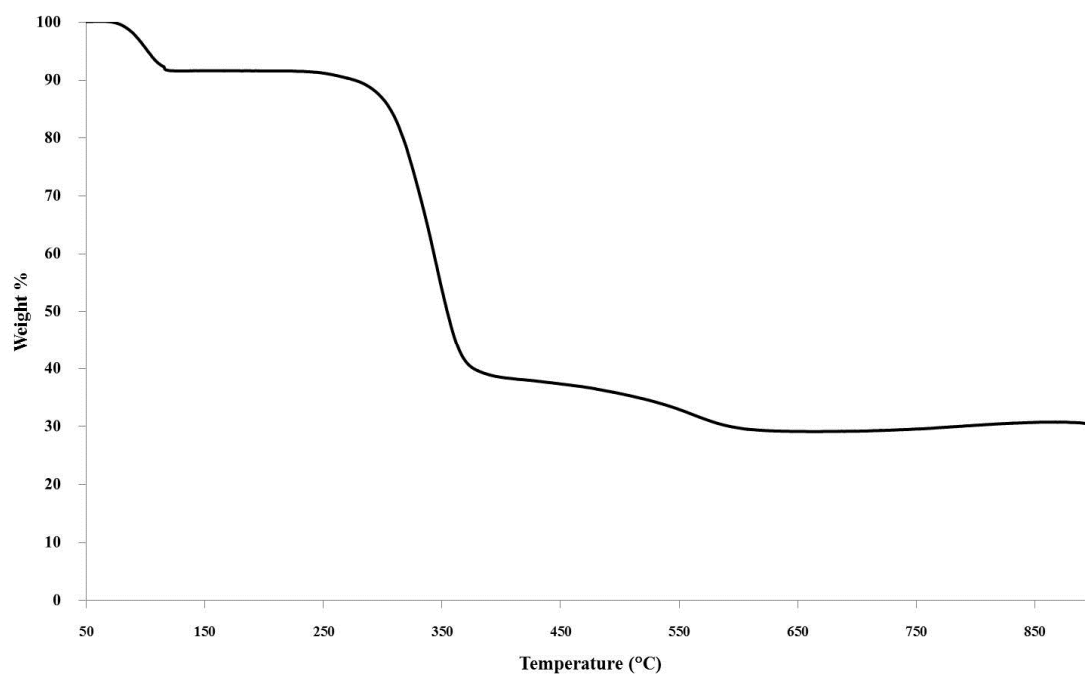


**Figure A1.** The TGA curve of [Cd(Cin)<sub>2</sub>(H<sub>2</sub>O)<sub>2</sub>] (1).

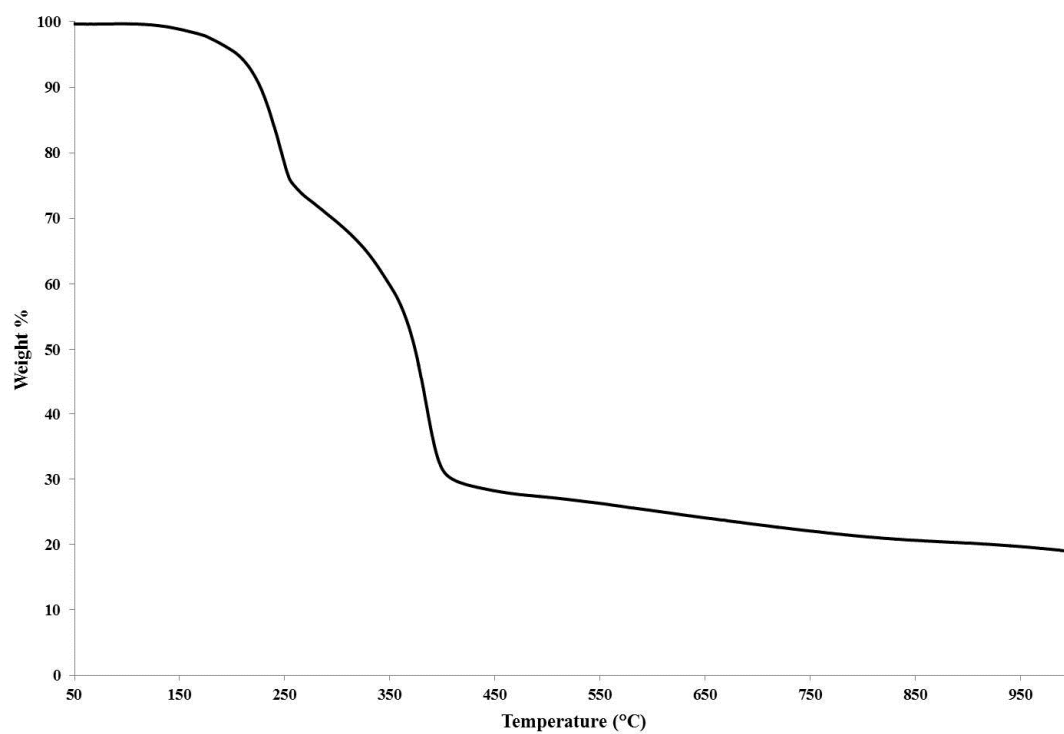


**Figure A2.** The TGA curve of [Zn(4,4'-bpy)<sub>0.5</sub>(Cin)<sub>2</sub>]<sub>n</sub> (2).

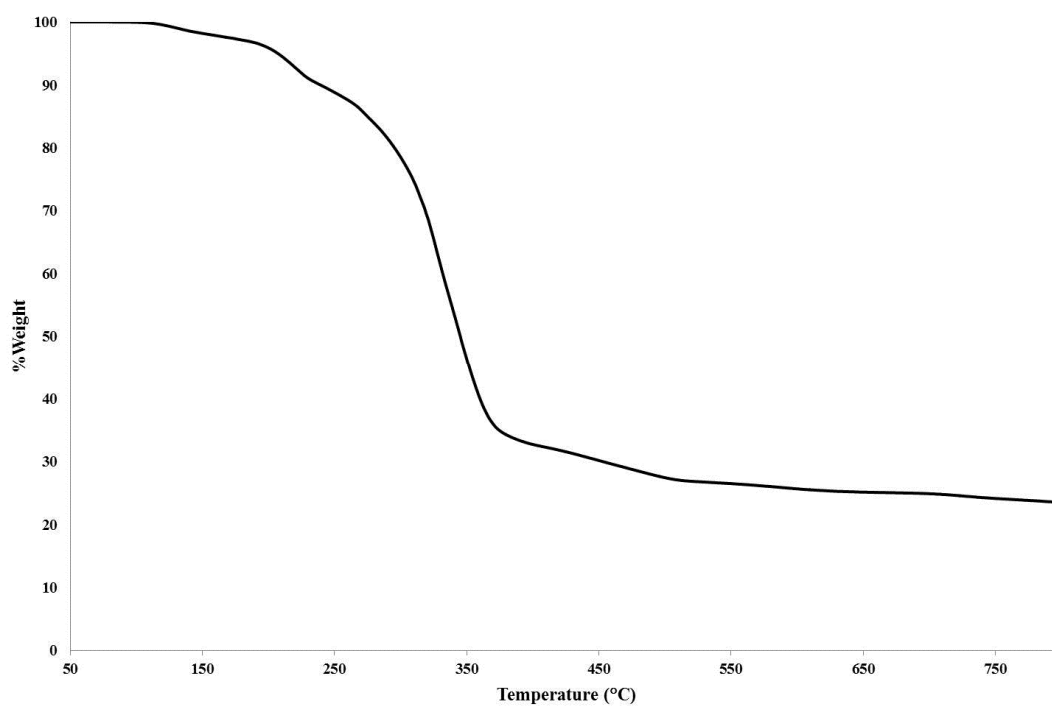


**Figure A3.** The TGA curve of  $[\text{Cd}_3(4,4'\text{-bpy})_2(\text{cin})_6(\text{H}_2\text{O})_2]_n$  (**3**).

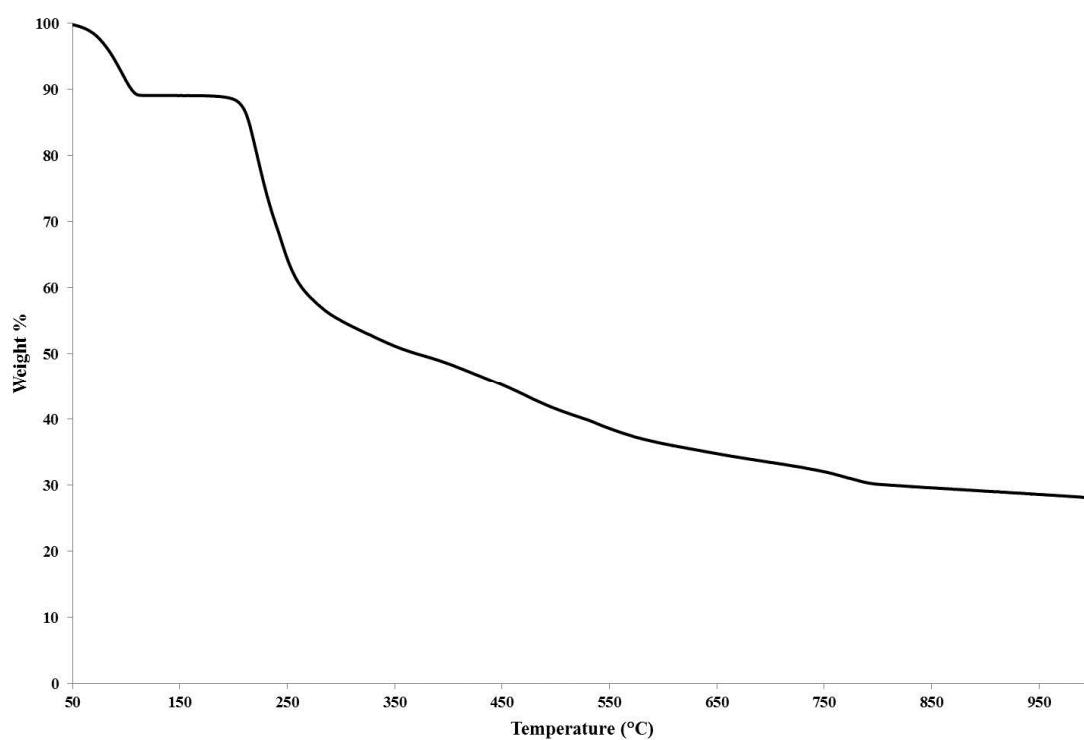


**Figure A4.** The TGA curve of  $[\text{Cd}(4,4'\text{-bpy})(3\text{-Npt})_2(\text{H}_2\text{O})]_n$  (**4**).

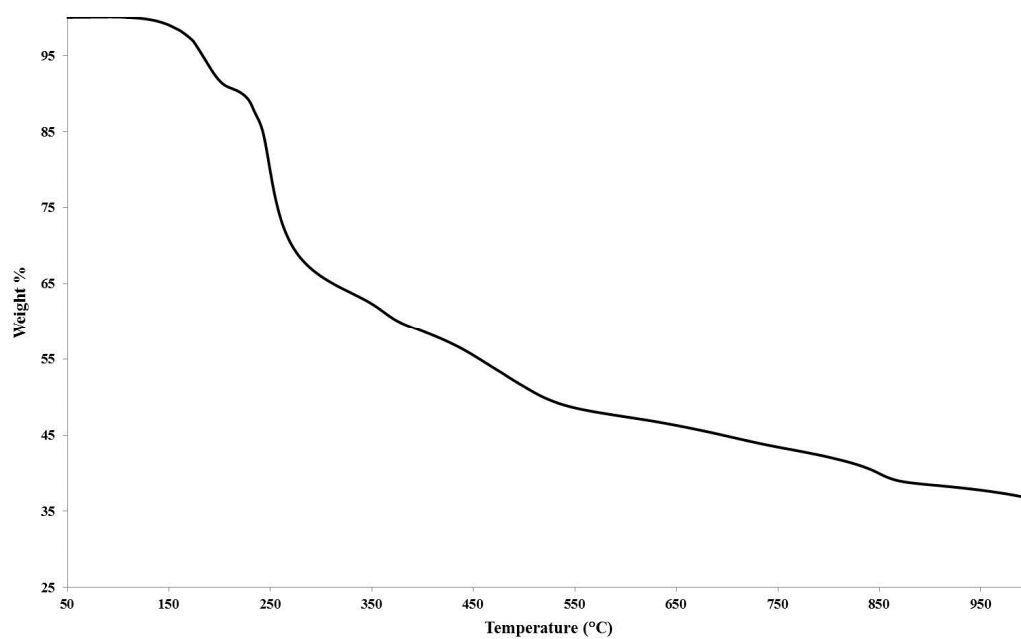


**Figure A5.** The TGA curve of  $[\text{Mn}_2(\text{bpp})(3\text{-Npt})_2(\text{H}_2\text{O})_2]_n$  (**5**).

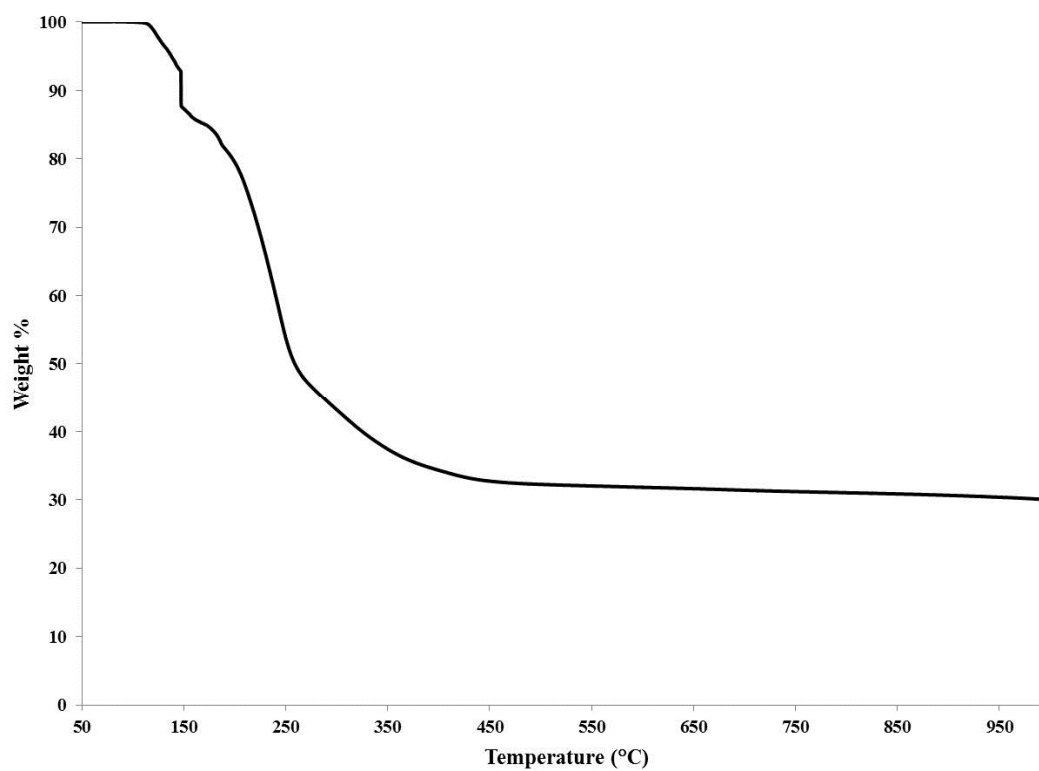


**Figure A6.** The TGA curve of  $\{[\text{Ag}_2(\text{bpp})_2](4\text{H}_2\text{O})(3\text{-Npt})\}_n$  (**7**).



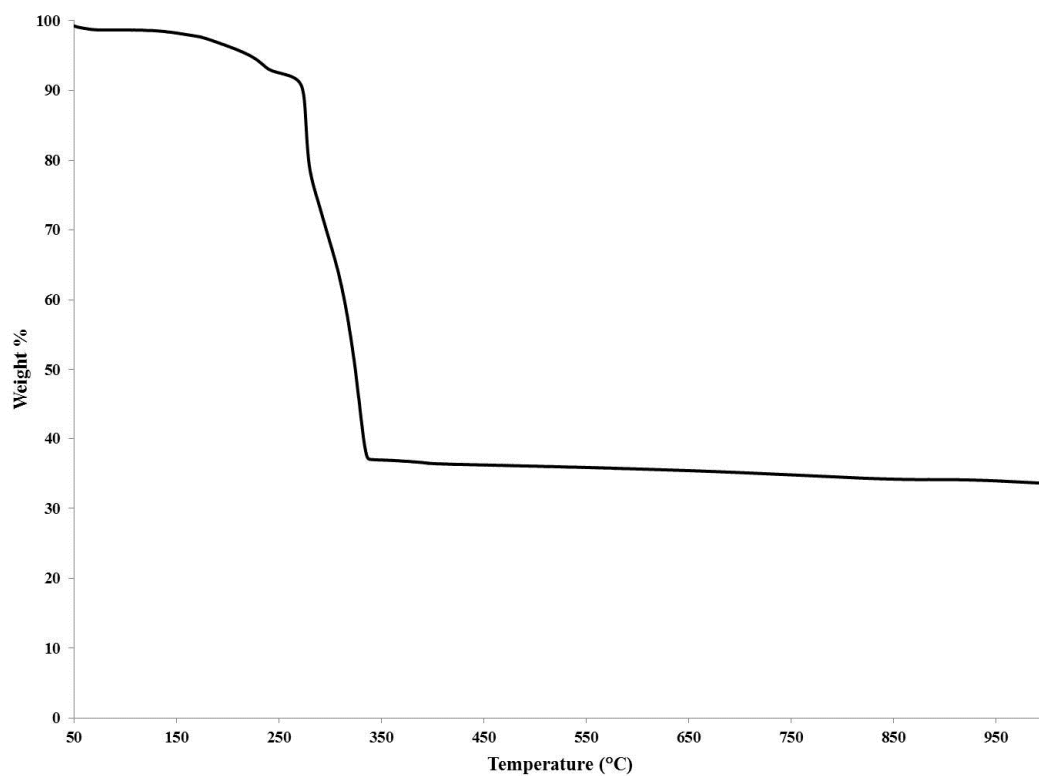


**Figure A7.** The TGA curve of  $\{[\text{Ag}_2(\text{bpe})_2(3\text{-Npt})]\cdot 7\text{H}_2\text{O}\}_n$  (**8**).

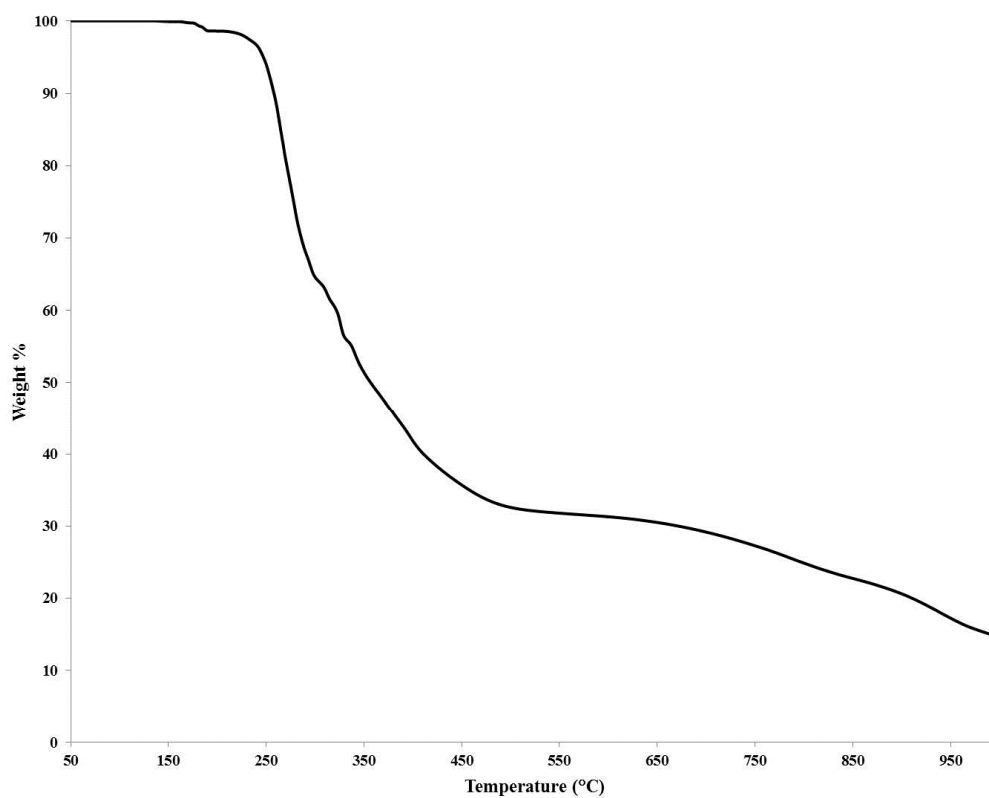


**Figure A8.** The TGA curve of  $[\text{Zn}(\text{bpp})_2(\text{Sal})_2]_n$  (**9**).

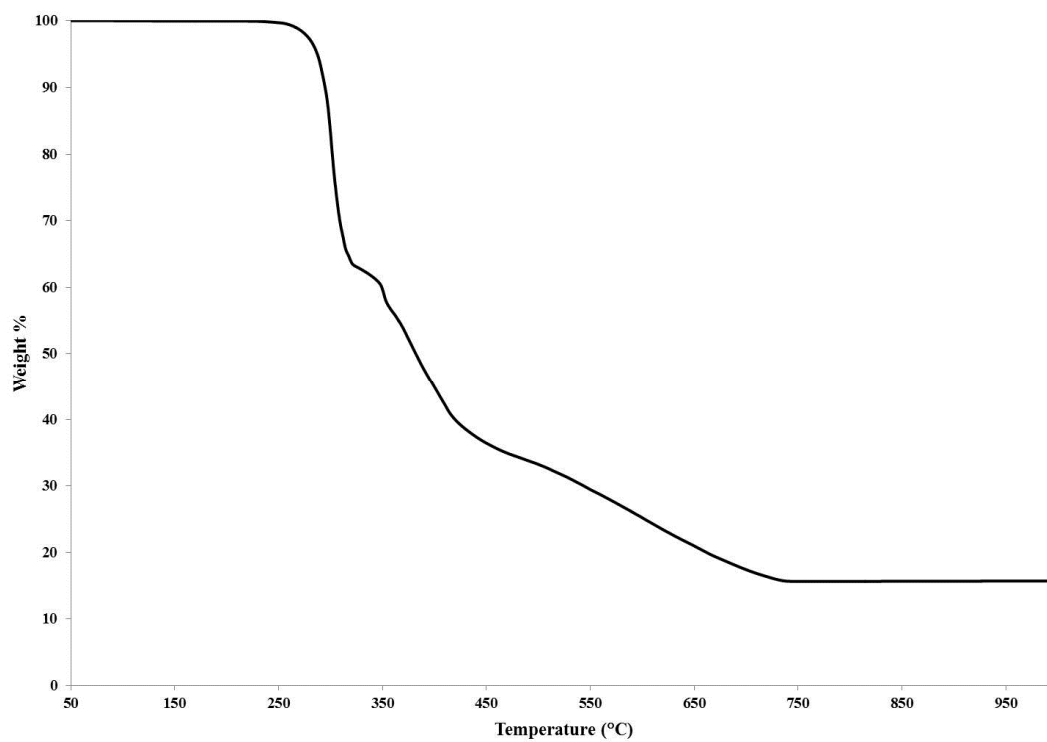


**Figure A9.** The TGA curve of  $[\text{Zn}_2(\text{bpe})_2(\text{Sal})_4]$  (10).

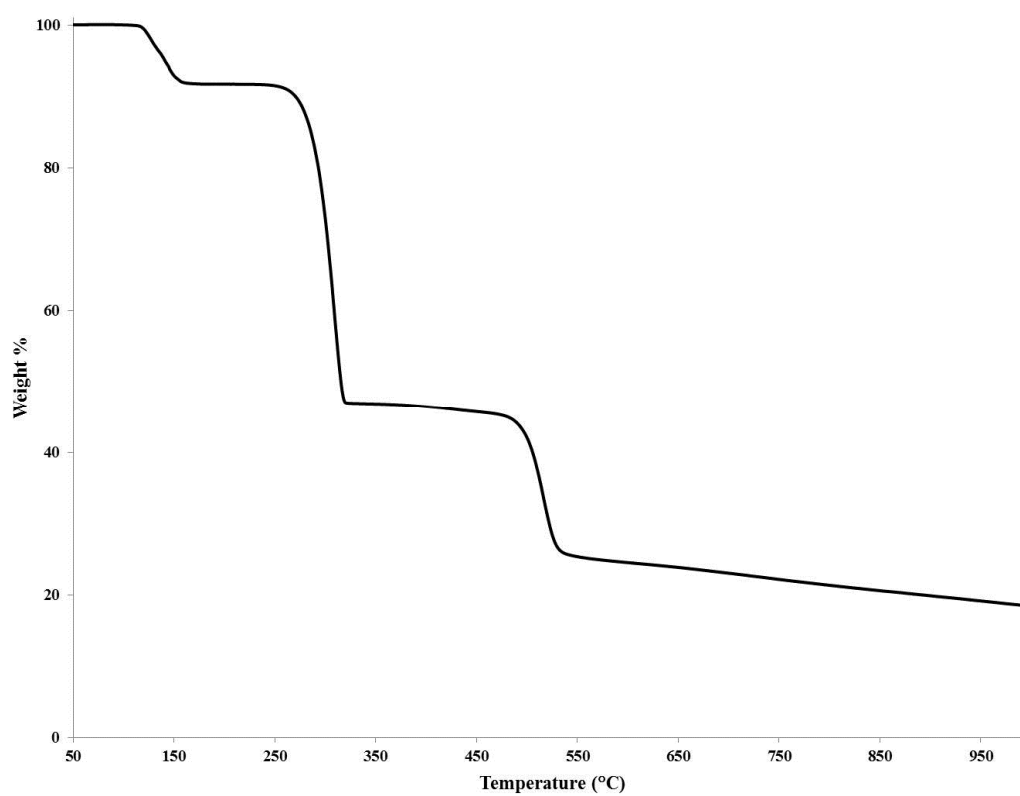


**Figure A10.** The TGA curve of  $\{[\text{Co}(\text{bpp})_2(\text{H}_2\text{O})_2](4\text{-abs})_2 \cdot \text{H}_2\text{O}\}_n$  (11).

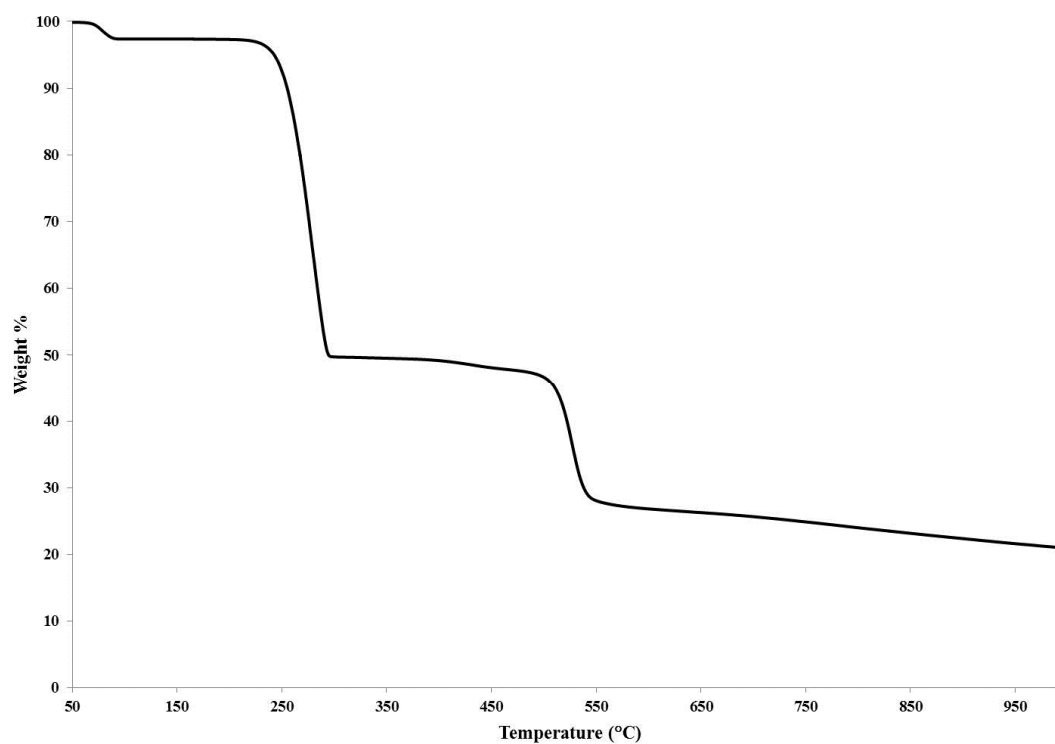


**Figure A11.** The TGA curve of  $[\text{Mn}_{0.5}(\text{bpp})(\text{H}_2\text{O})_2] \cdot (4\text{-abs})$  (12).

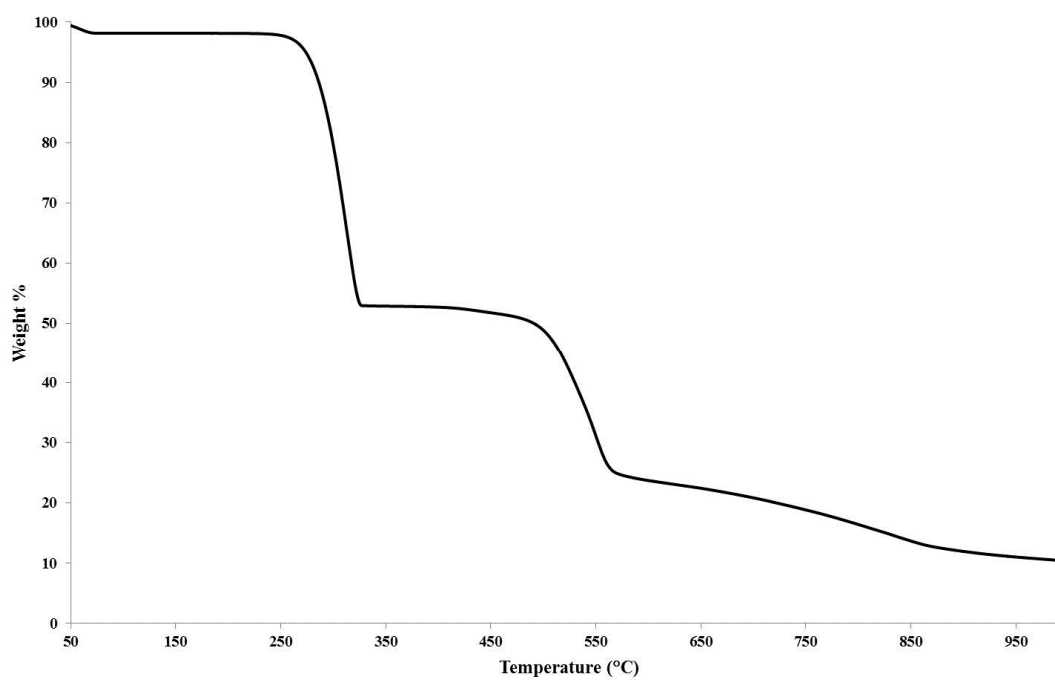


**Figure A12.** The TGA curve of  $\{[\text{Cd}_{0.5}(\text{bpp})(4\text{-abs})] \cdot (\text{H}_2\text{O})\}_n$  (13).

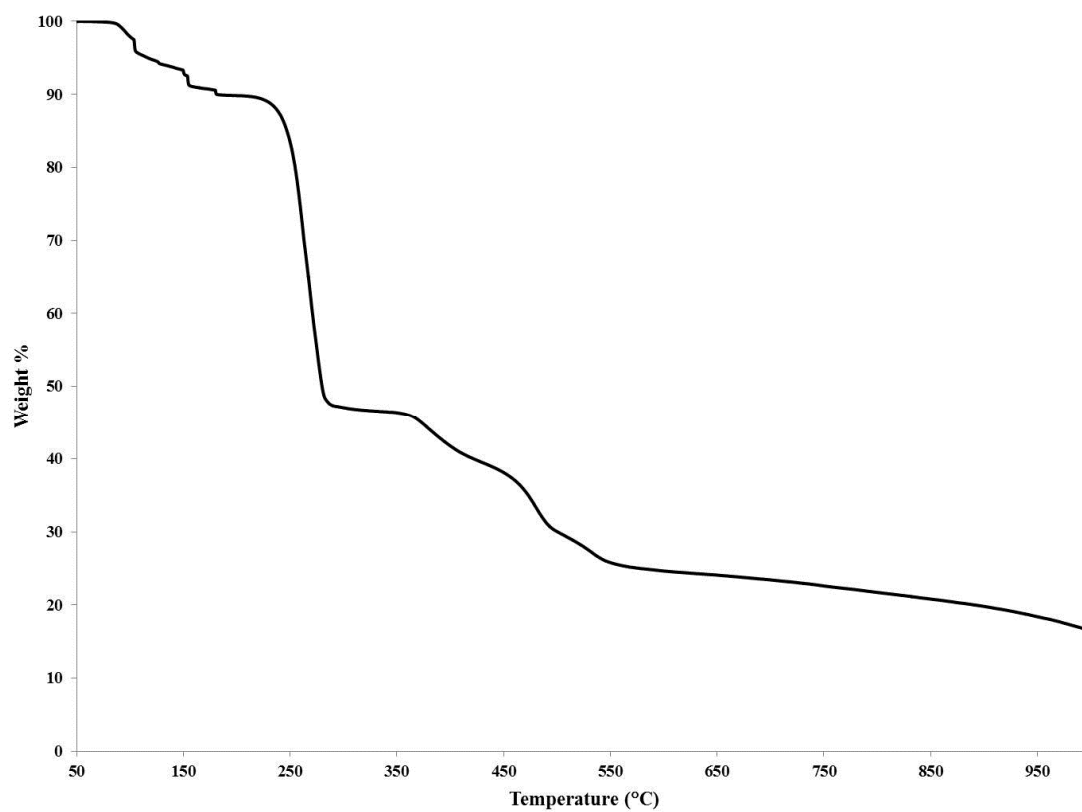


**Figure A13.** The TGA curve of  $[\text{Zn}_{0.5}(\text{bpp})(\text{H}_2\text{O})_2] \cdot (4\text{-abs})$  (14).

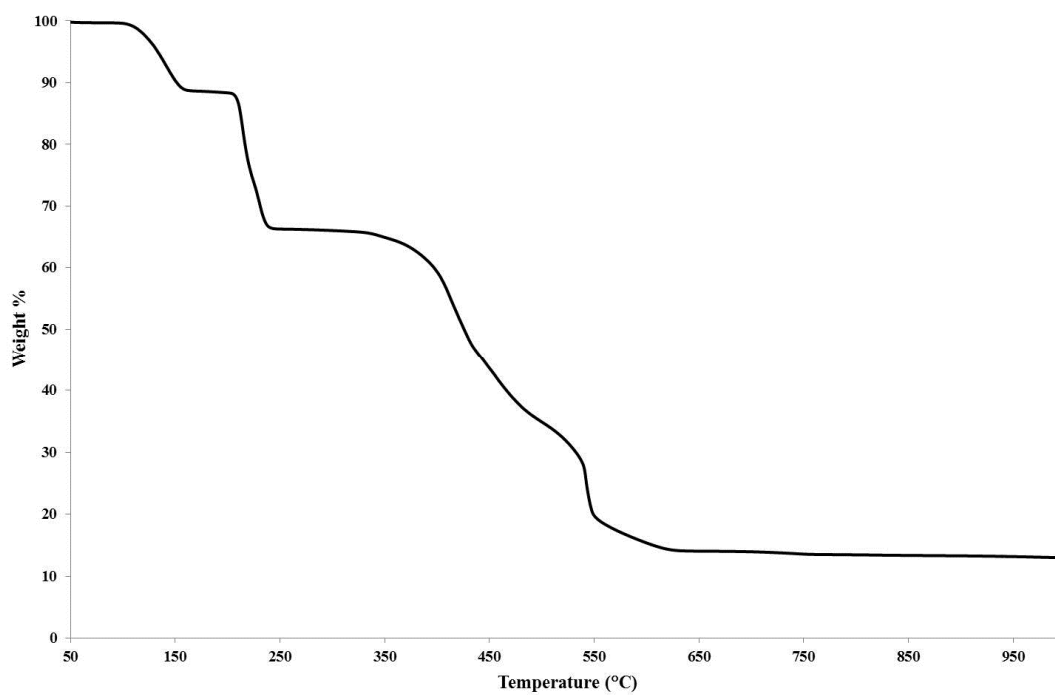


**Figure A14.** The TGA curve of  $\{[\text{Zn}(4,4'\text{-bpy})(\text{H}_2\text{O})_4] \cdot (4\text{-abs})_2 \cdot 2\text{H}_2\text{O}\}_n$  (15).

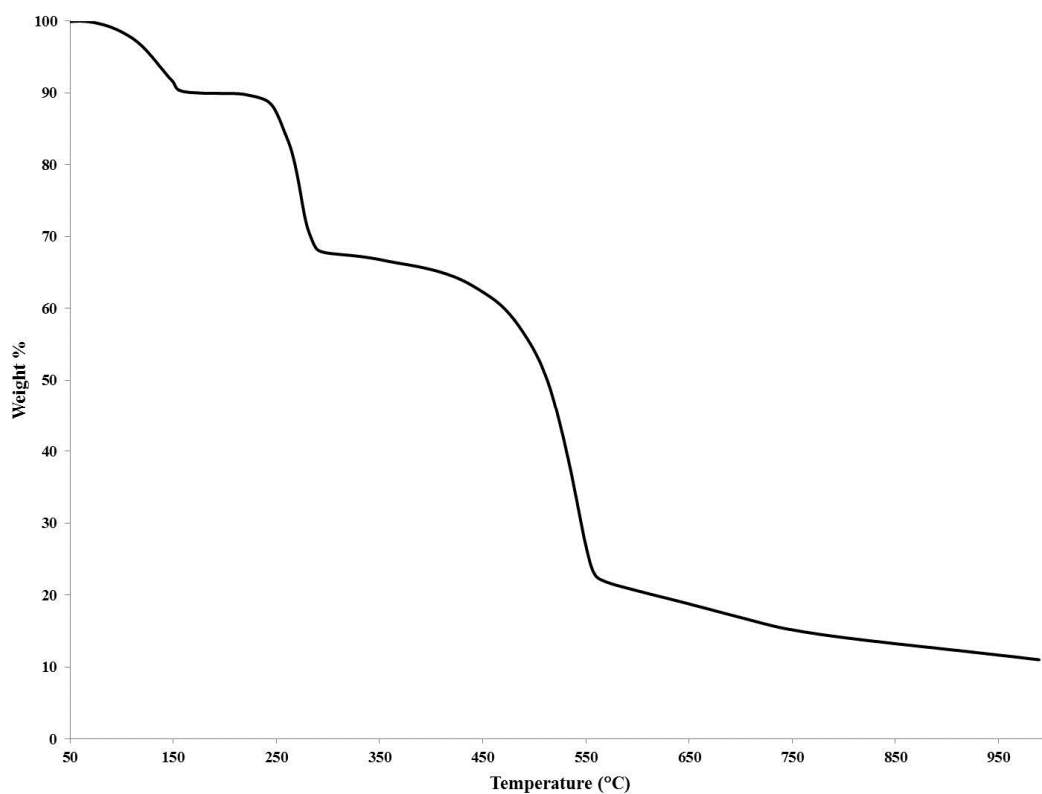


**Figure A15.** The TGA curve of  $\{[\text{Cd}(4,4'\text{-bpy})_{1.5}(\text{H}_2\text{O})_3]\cdot(4\text{-abs})\cdot(4,4'\text{-bpy})\cdot(\text{H}_2\text{O})\cdot\text{NO}_3\}_n$  (**16**).

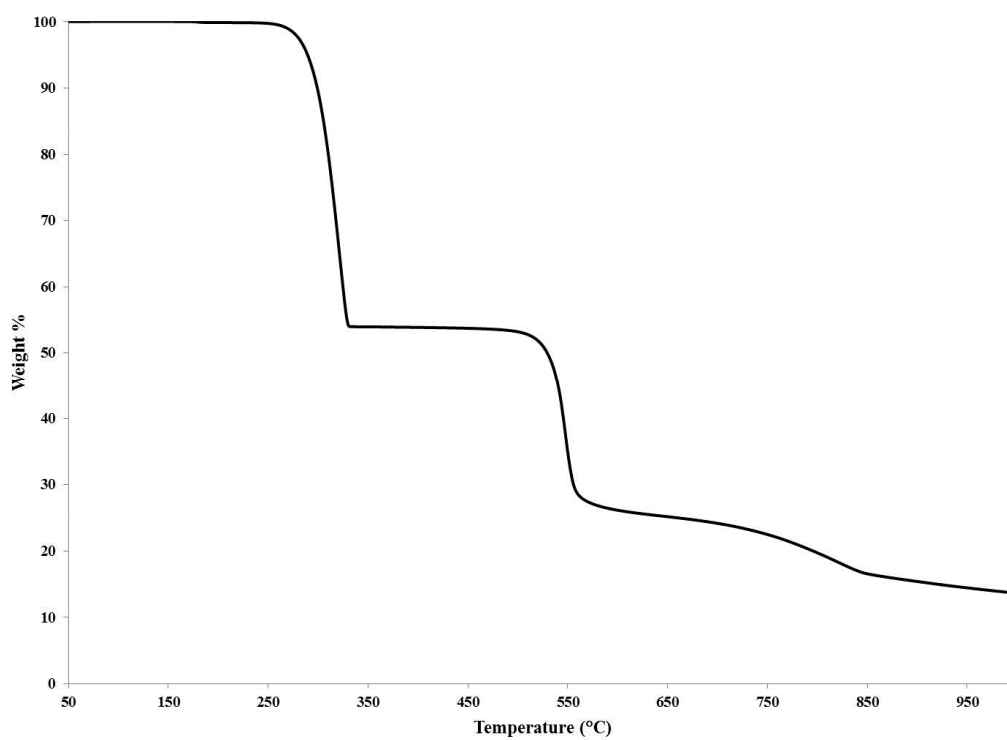


**Figure A16.** The TGA curve of  $\{[\text{Cd}_{0.5}(\text{bpe})(4\text{-abs})]\cdot\text{H}_2\text{O}\}_n$  (**17**).

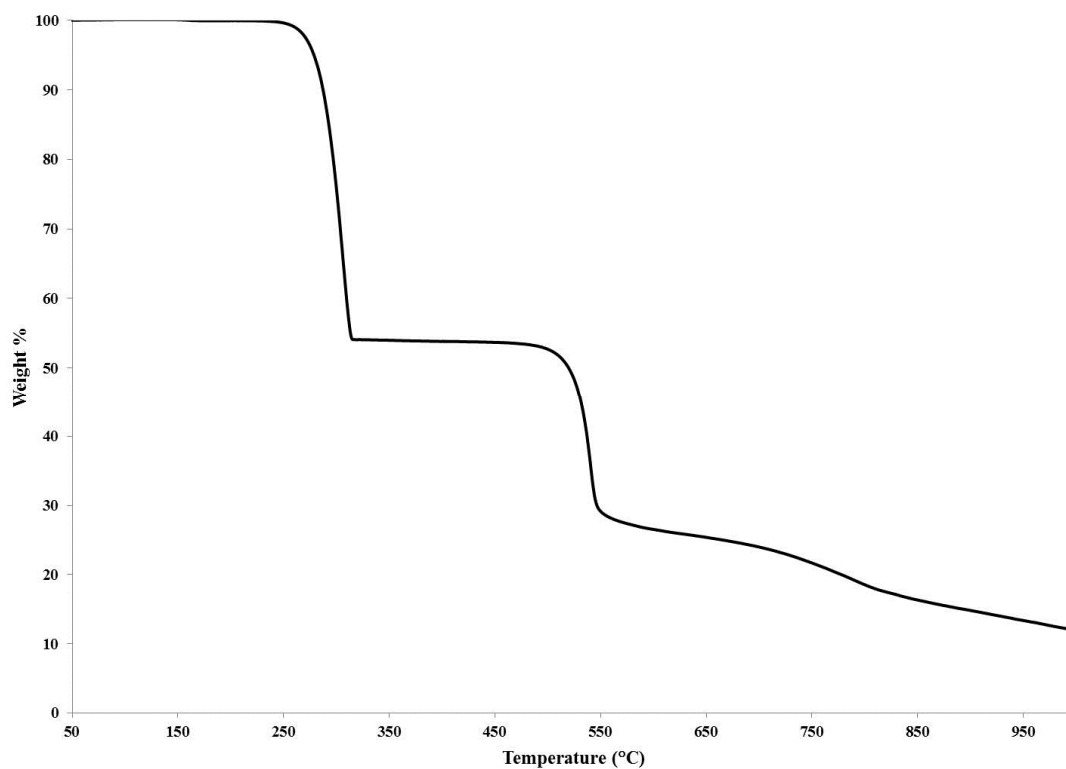


**Figure A17.** The TGA curve of  $\{[\text{Cd}(\text{bpp})_2(\text{H}_2\text{O})_4] \cdot (3\text{-abs})_2 \cdot 2\text{H}_2\text{O}\}_n$  (**18**).

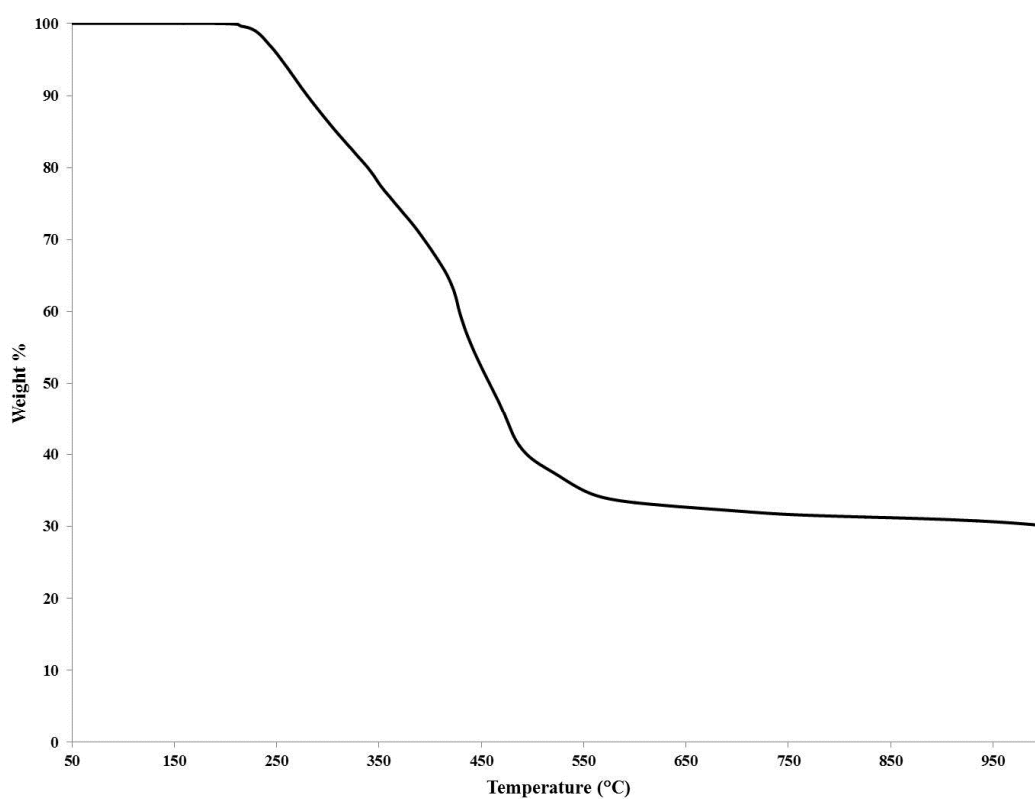


**Figure A18.** The TGA curve of  $[\text{Zn}(\text{bpp})_2(\text{Mbs})_2]_n$  (**19**).

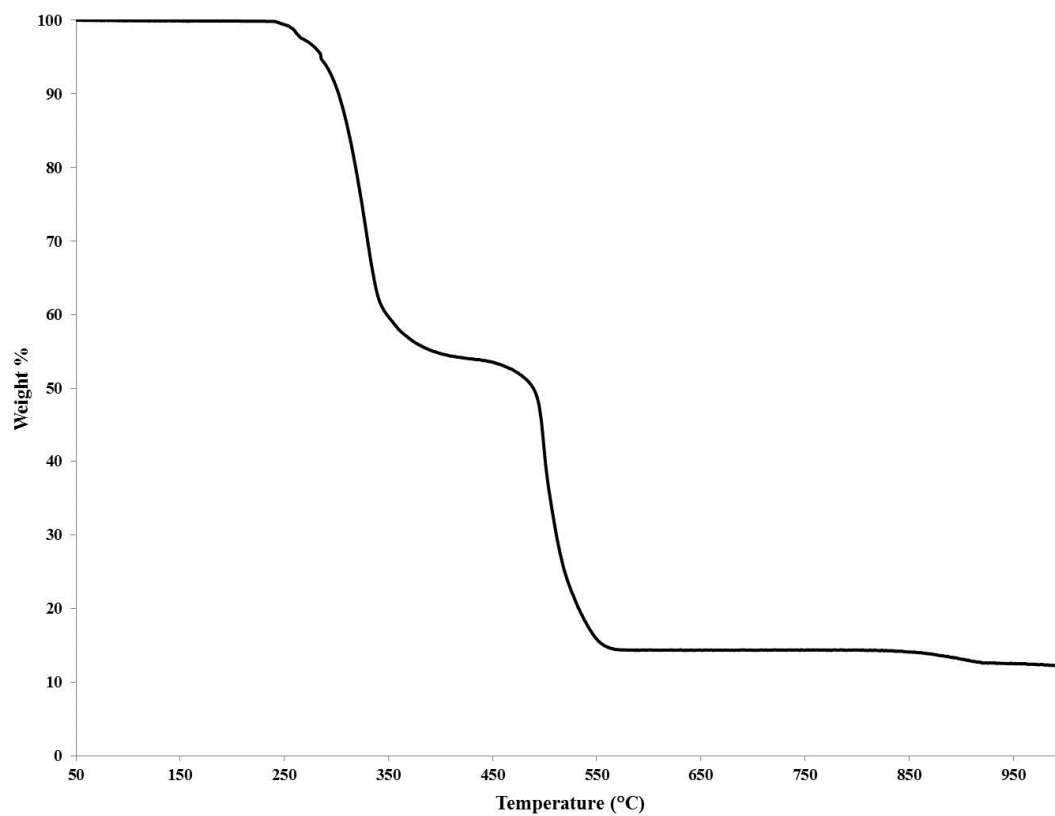


**Figure A19.** The TGA curve of  $[\text{Cd}(\text{bpp})_2(\text{Mbs})_2]_n$  (20).

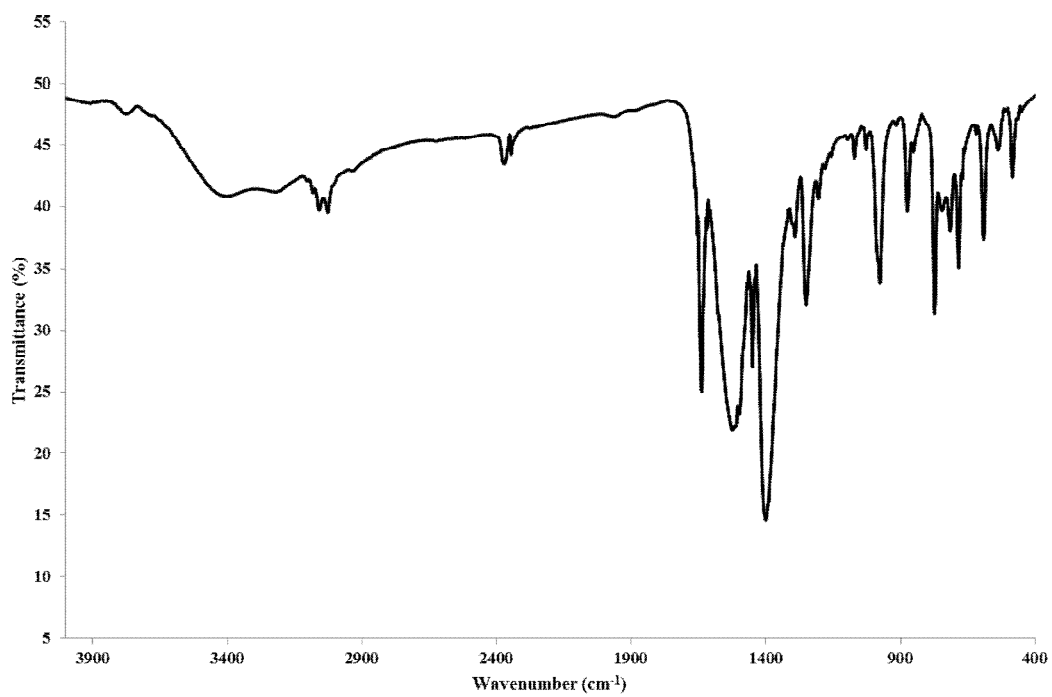


**Figure A20.** The infrared spectrum of  $[\text{Cd}(\text{Cin})_2(\text{H}_2\text{O})_2]$  (1).

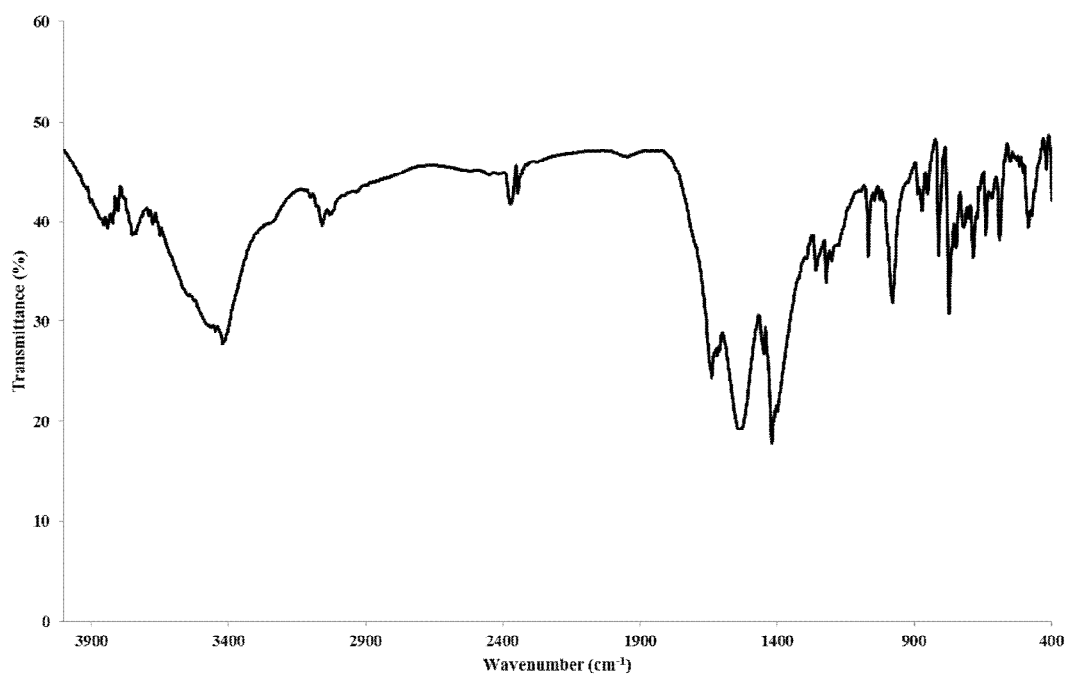


**Figure A21.** The infrared spectrum of  $[\text{Zn}(4,4'\text{-bpy})_{0.5}(\text{Cin})_2]$  (**2**).

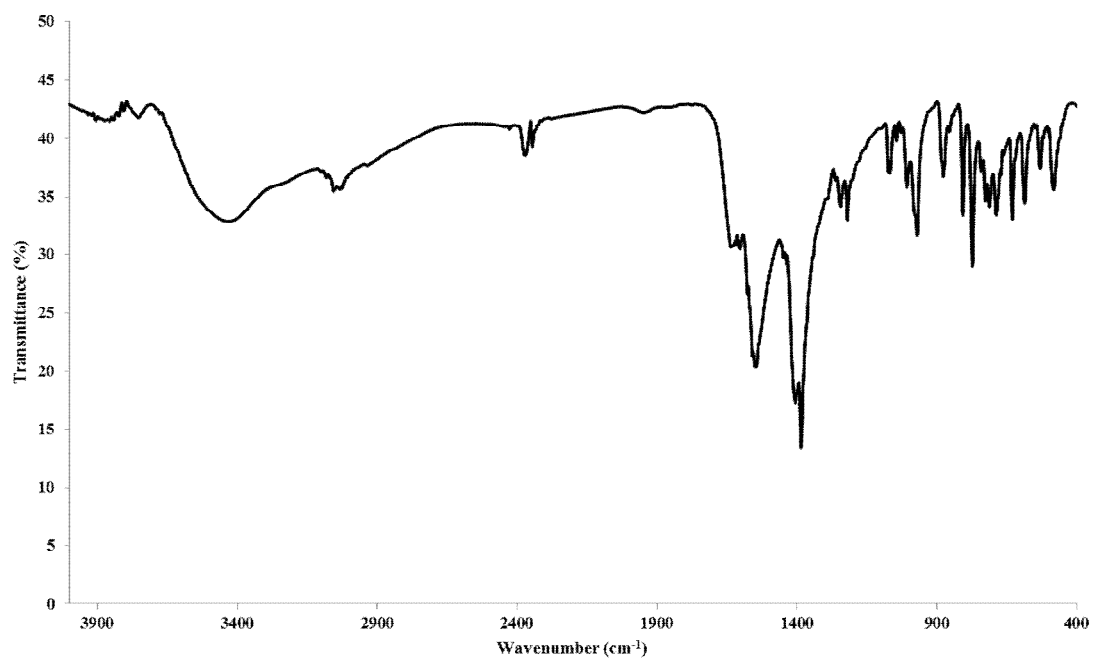


**Figure A22.** The infrared spectrum of  $[\text{Cd}_3(4,4'\text{-bpy})_2(\text{cin})_6(\text{H}_2\text{O})_2]_n$  (**3**).



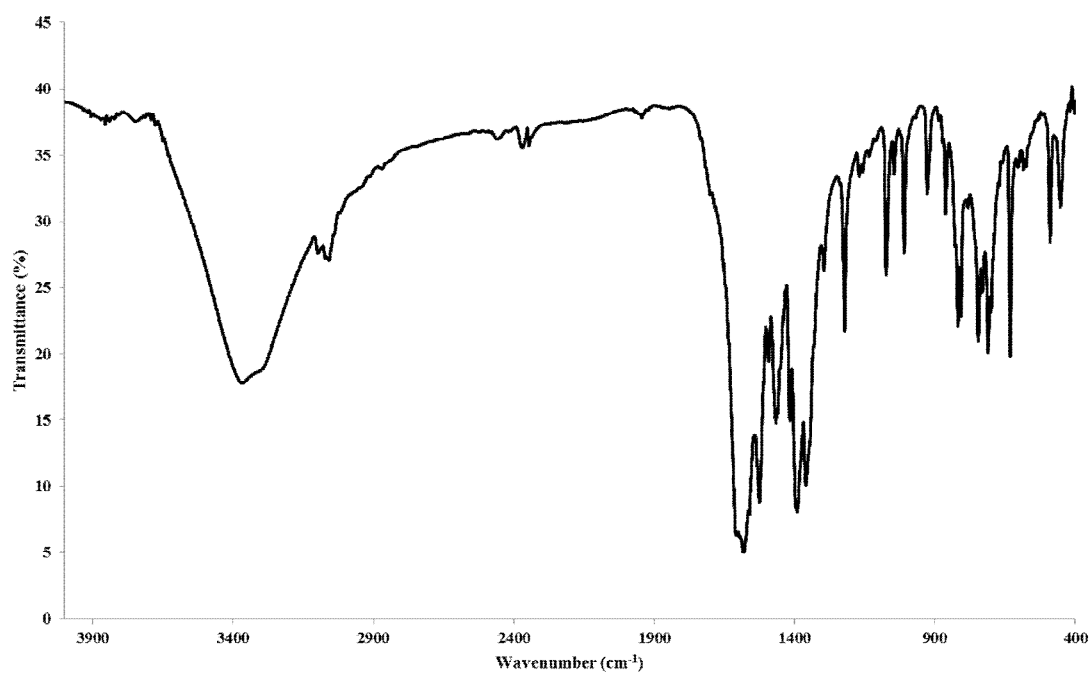


**Figure A23.** The infrared spectrum of  $[\text{Cd}(4,4'\text{-bpy})(3\text{-Npt})_2(\text{H}_2\text{O})]_n$  (**4**).

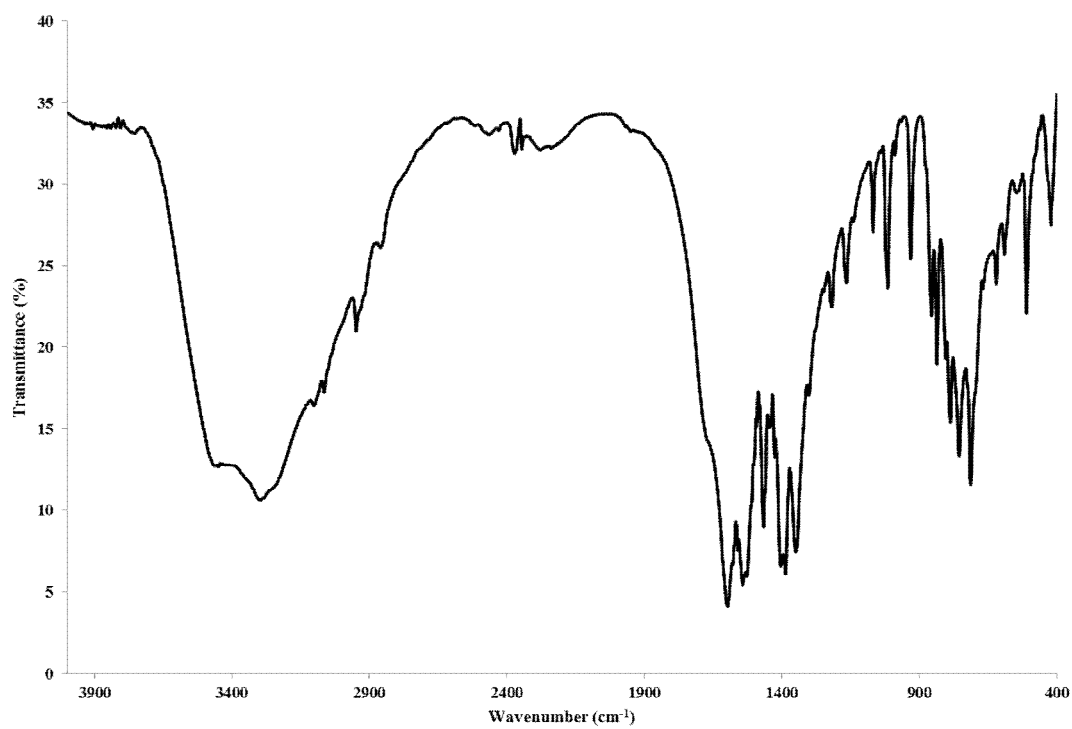


**Figure A24.** The infrared spectrum of  $[\text{Mn}_2(\text{bpp})(3\text{-Npt})_2(\text{H}_2\text{O})_2]_n$  (**5**).

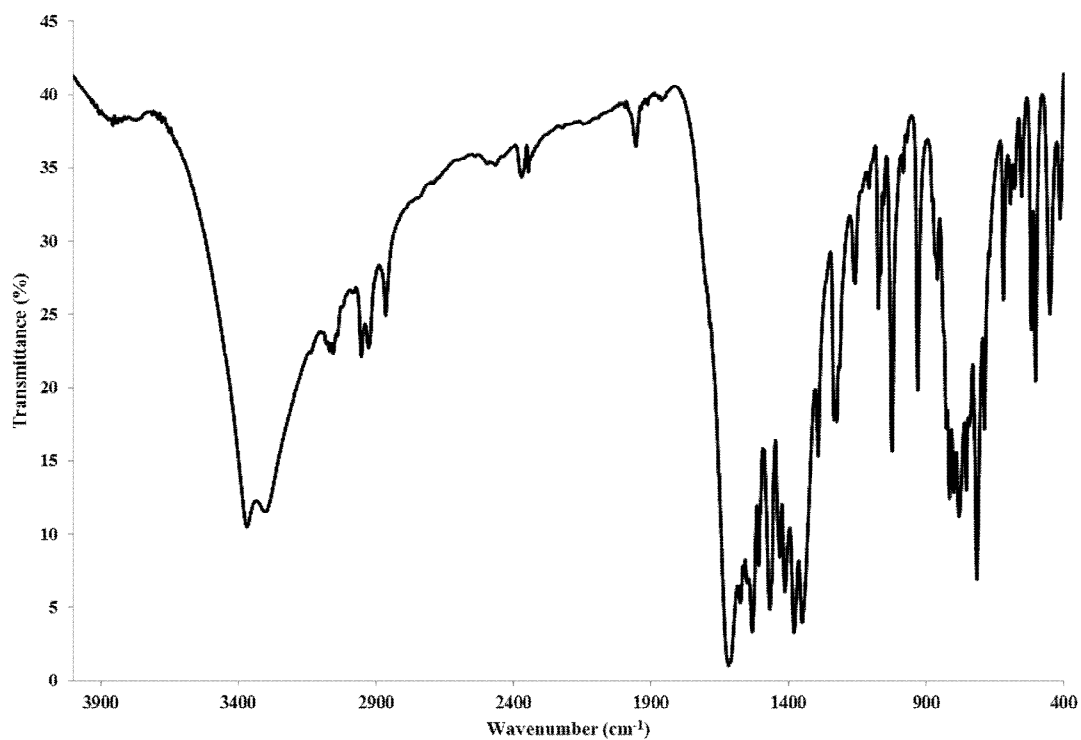


**Figure A25.** The infrared spectrum of  $[\text{Ni}(\text{bpp})(3\text{-Npt})(\text{H}_2\text{O})]_n$  (**6**).

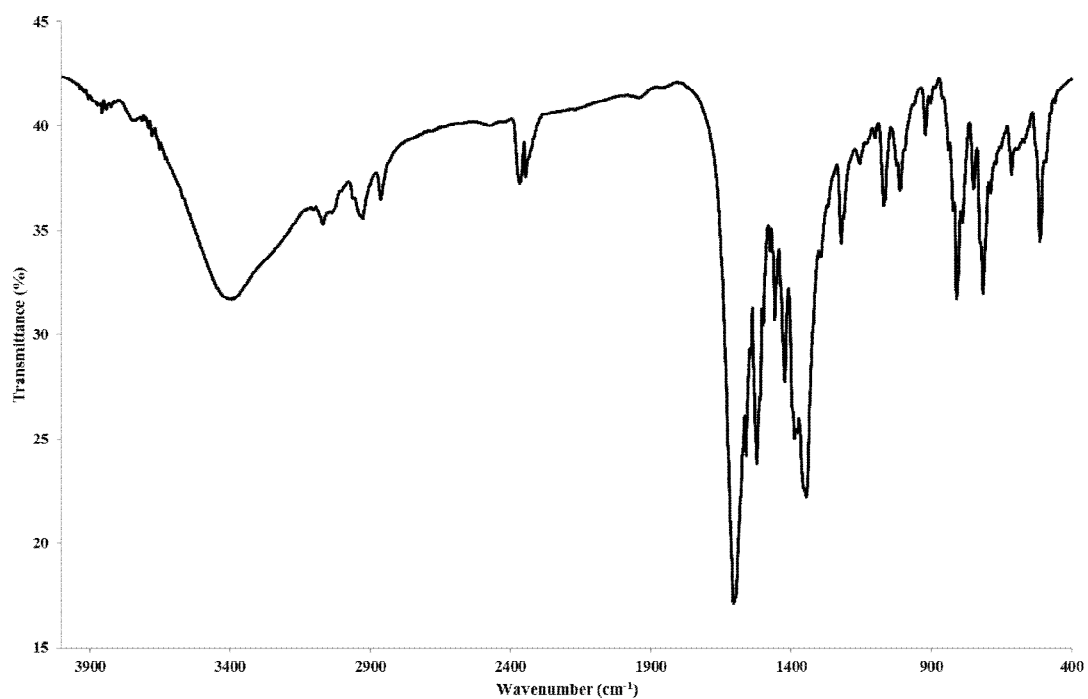


**Figure A26.** The infrared spectrum of  $\{[\text{Ag}_2(\text{bpp})_2] \cdot (4\text{H}_2\text{O}) \cdot (3\text{-Npt})\}_n$  (**7**).

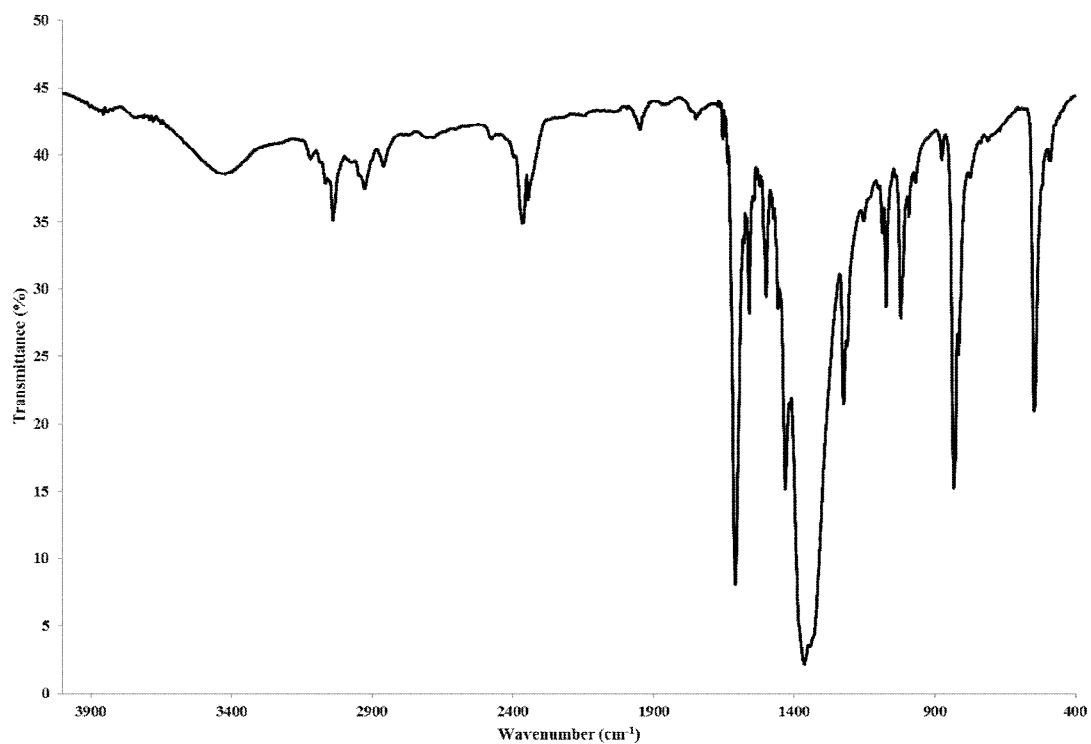


**Figure A27.** The infrared spectrum of  $\{[Ag_2(bpe)_2(3-Npt)] \cdot 7H_2O\}_n$  (**8**).

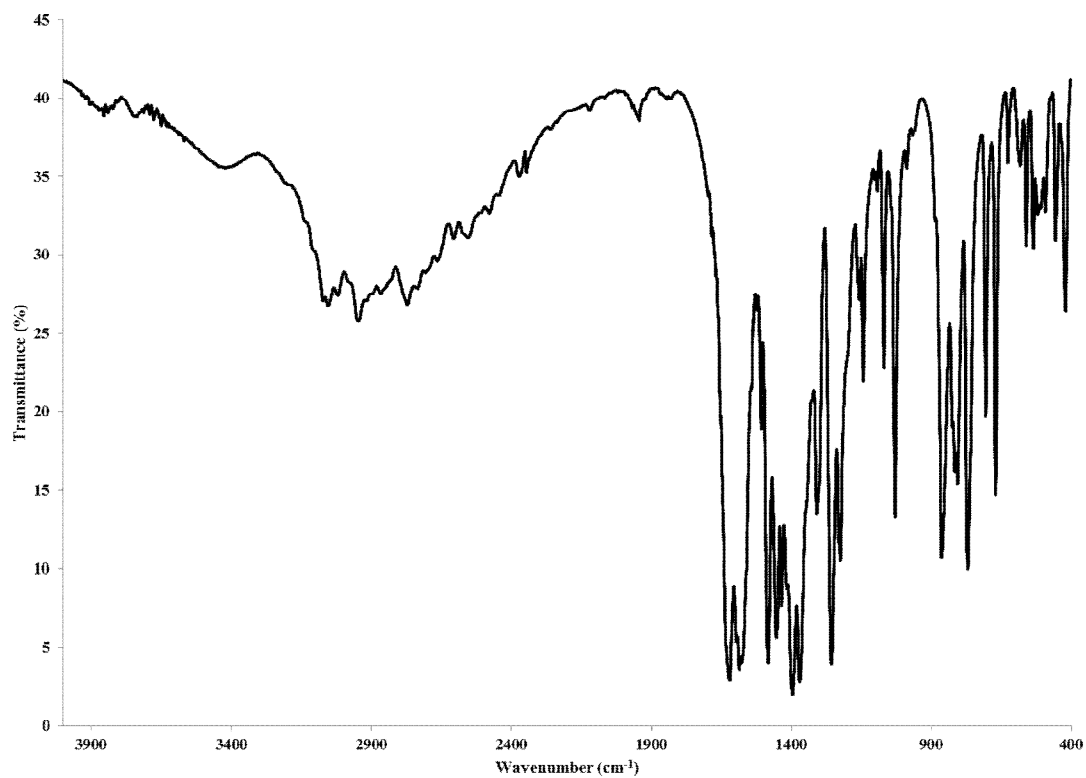


**Figure A28.** The infrared spectrum of  $[Zn(bpp)_2(Sal)_2]_n$  (**9**).

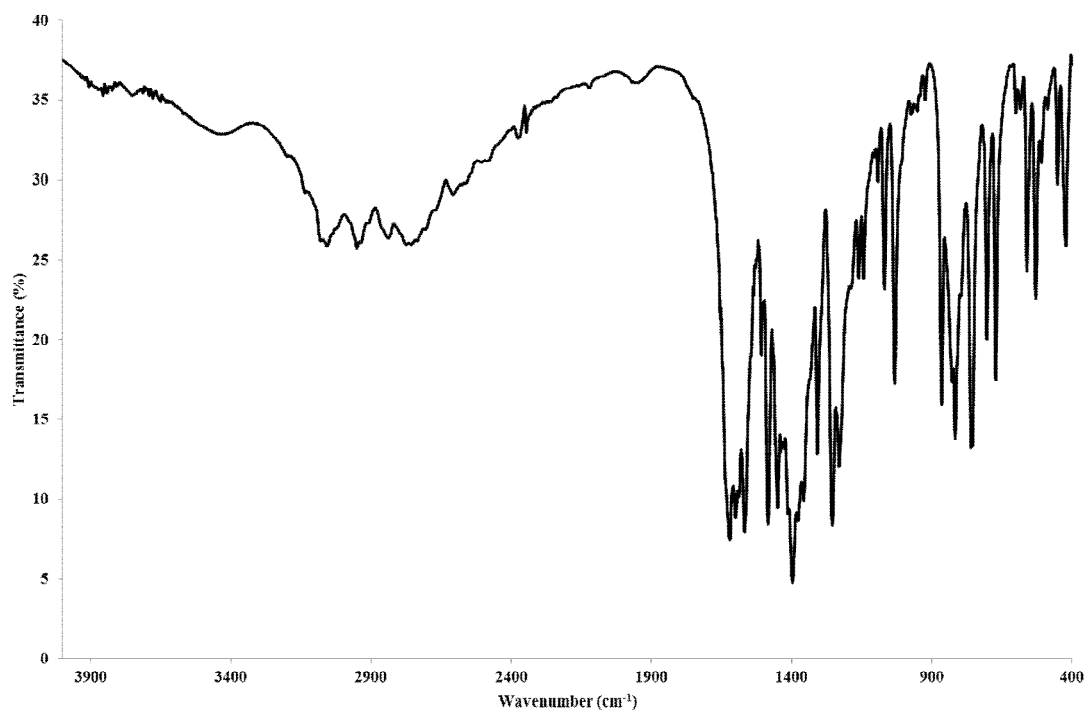


**Figure A29.** The infrared spectrum of  $[\text{Zn}_2(\text{bpe})_2(\text{Sal})_4]$  (**10**).

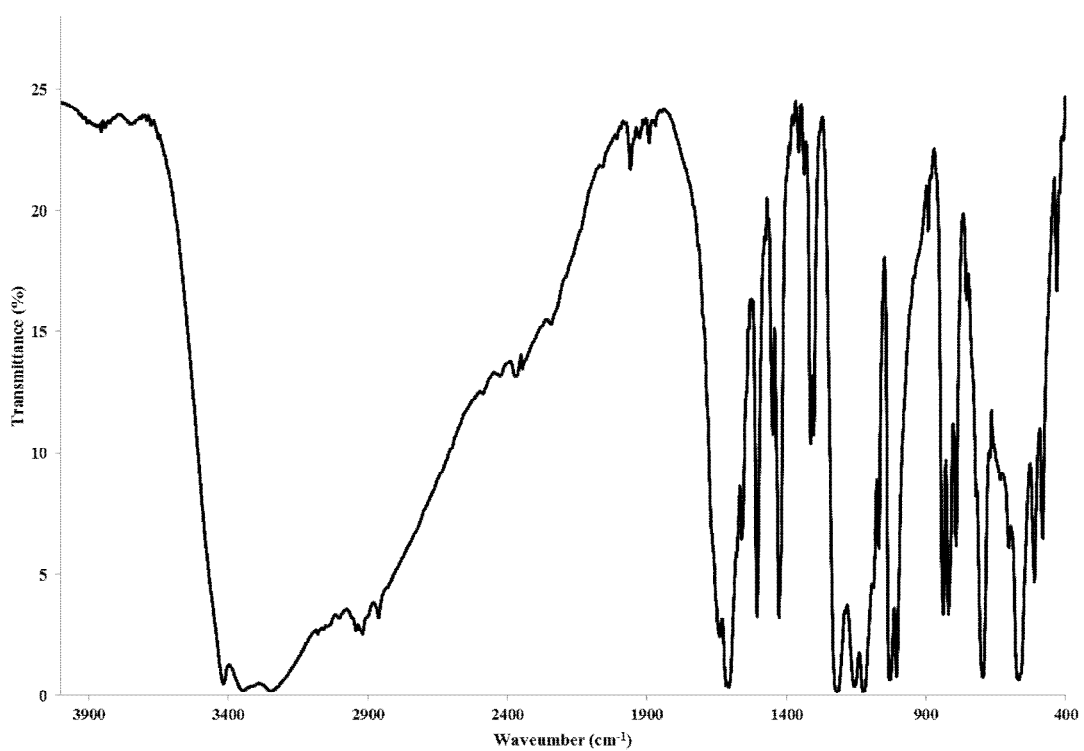


**Figure A30.** The infrared spectrum of  $\{[\text{Co}(\text{bpp})_2(\text{H}_2\text{O})_2] \cdot (4\text{-abs})_2 \cdot \text{H}_2\text{O}\}_n$  (**11**).

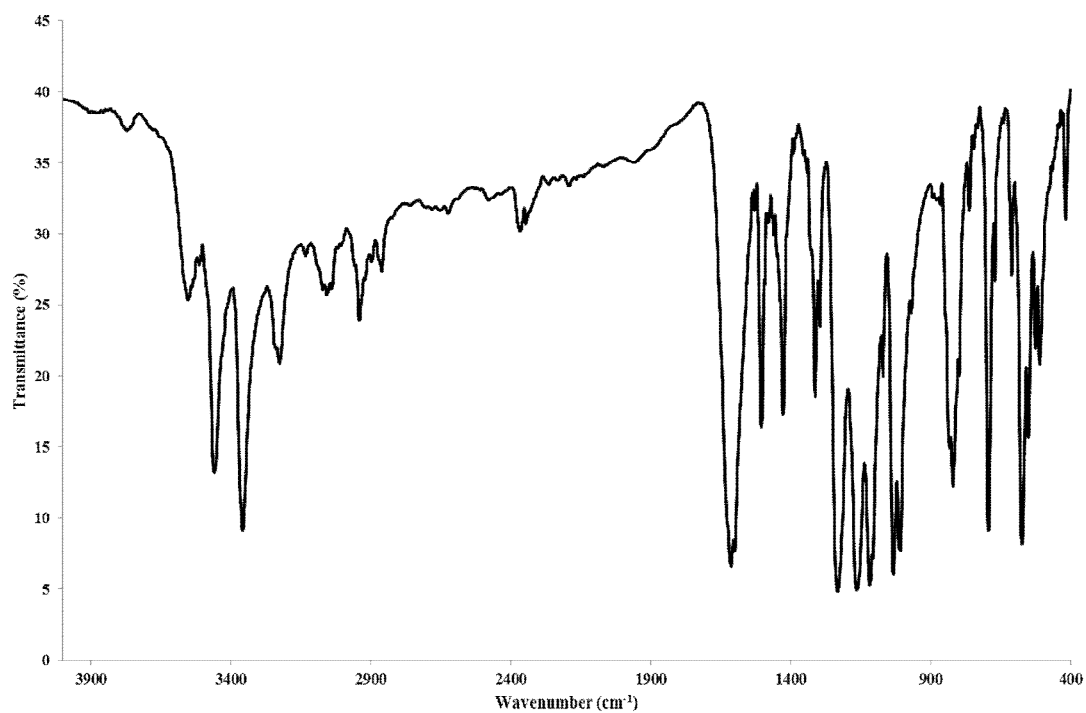


**Figure A31.** The infrared spectrum of  $[\text{Mn}_{0.5}(\text{bpp})(\text{H}_2\text{O})_2] \cdot (4\text{-abs})$  (**12**).

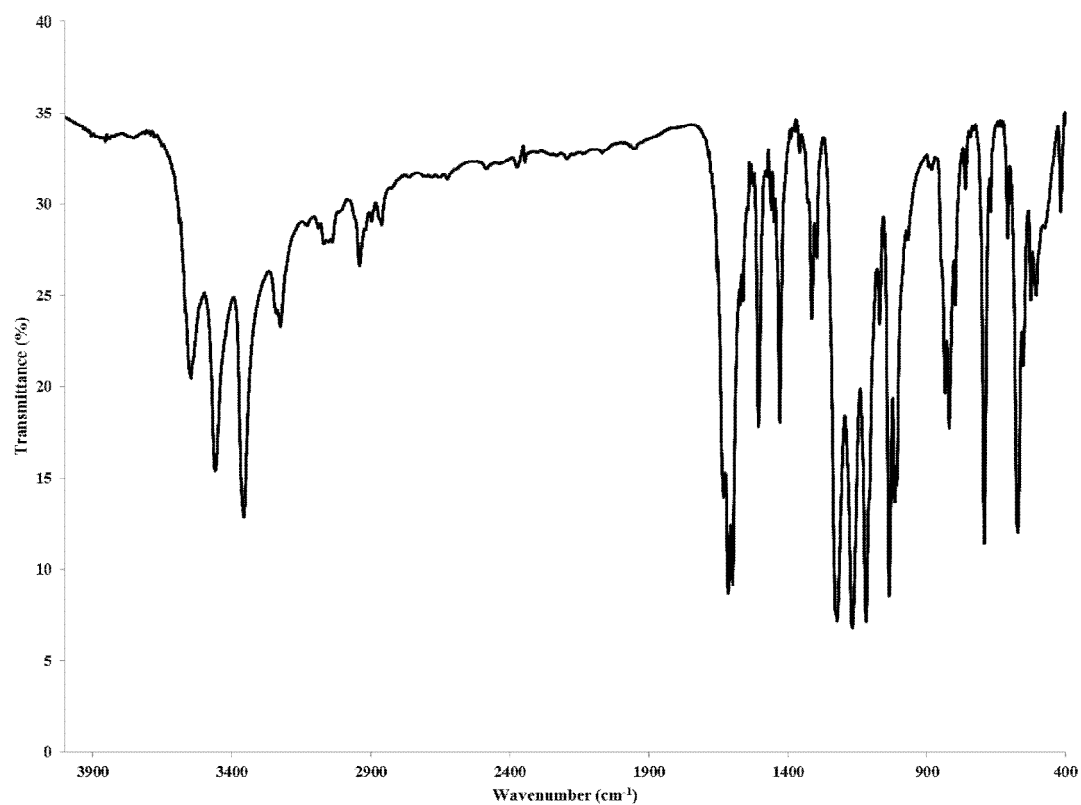


**Figure A32.** The infrared spectrum of  $\{[\text{Cd}_{0.5}(\text{bpp})(4\text{-abs})] \cdot (\text{H}_2\text{O})\}_n$  (**13**).

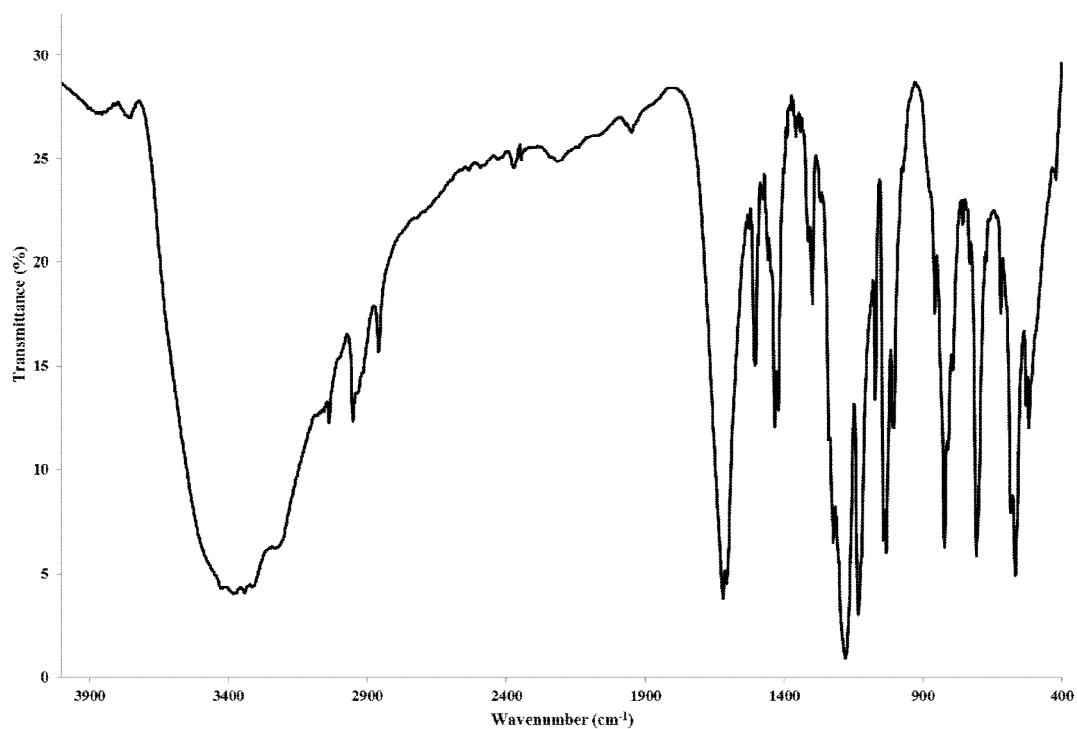


**Figure A33.** The infrared spectrum of  $[\text{Zn}_{0.5}(\text{bpp})(\text{H}_2\text{O})_2] \cdot (4\text{-abs})$  (**14**).

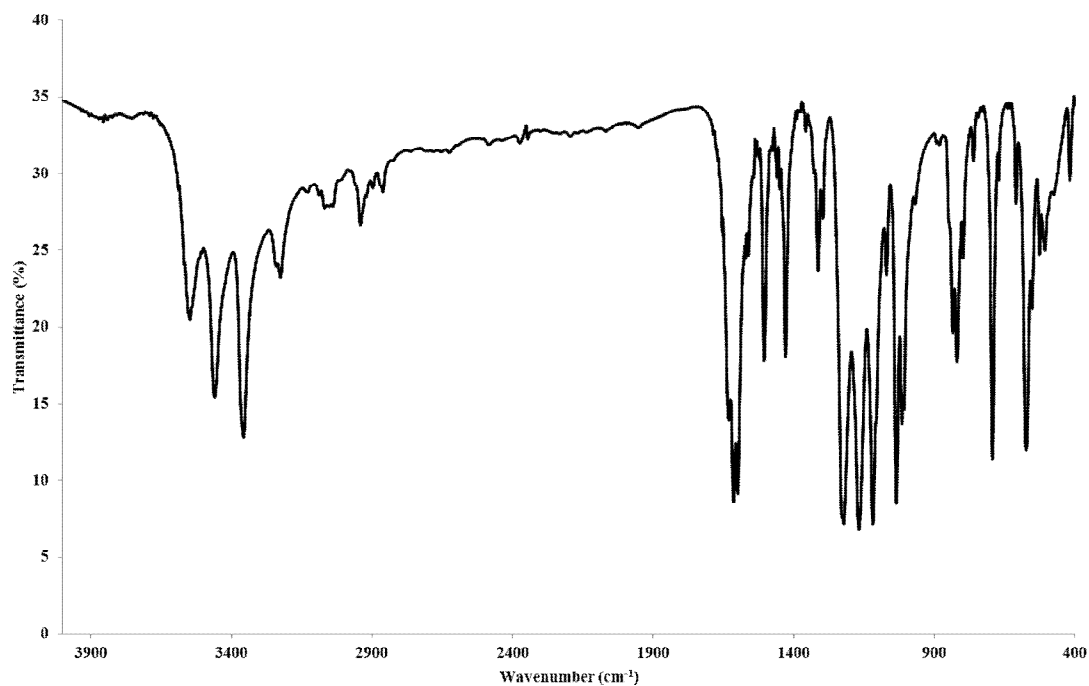


**Figure A34.** The infrared spectrum of  $\{[\text{Zn}(4,4'\text{-bpy})(\text{H}_2\text{O})_4] \cdot (4\text{-abs})_2 \cdot 2\text{H}_2\text{O}\}_n$  (**15**).

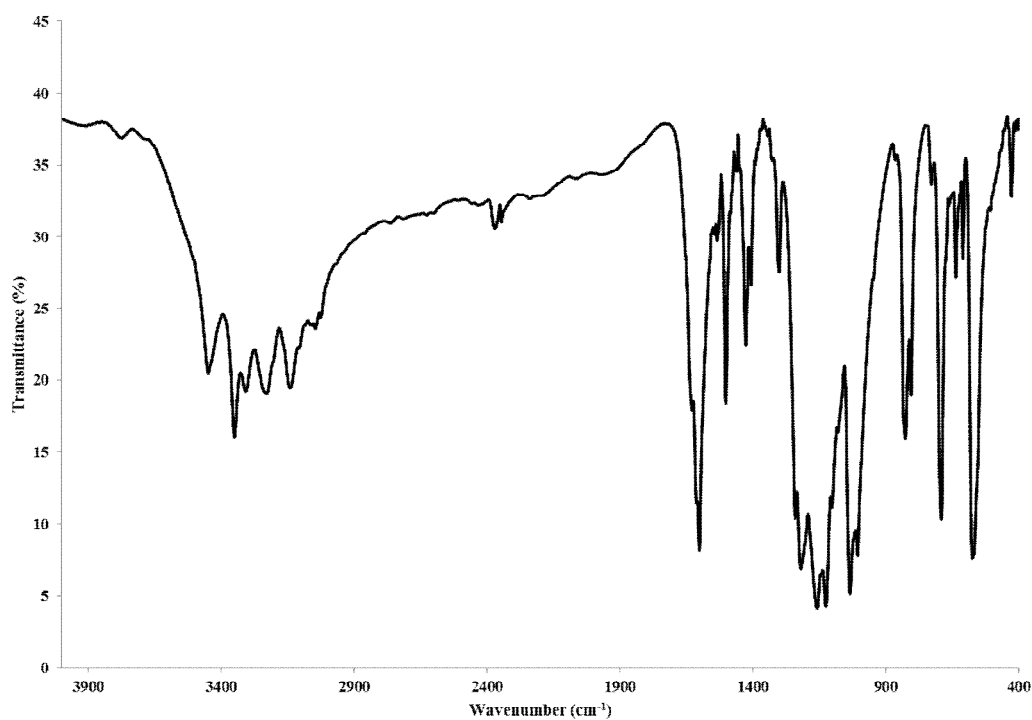


**Figure A35.** The infrared spectrum of  $\{[\text{Cd}(4,4'\text{-bpy})_{1.5}(\text{H}_2\text{O})_3]\cdot(4\text{-abs})\cdot(4,4'\text{-bpy})\cdot(\text{H}_2\text{O})\cdot\text{NO}_3\}_n$  (**16**).

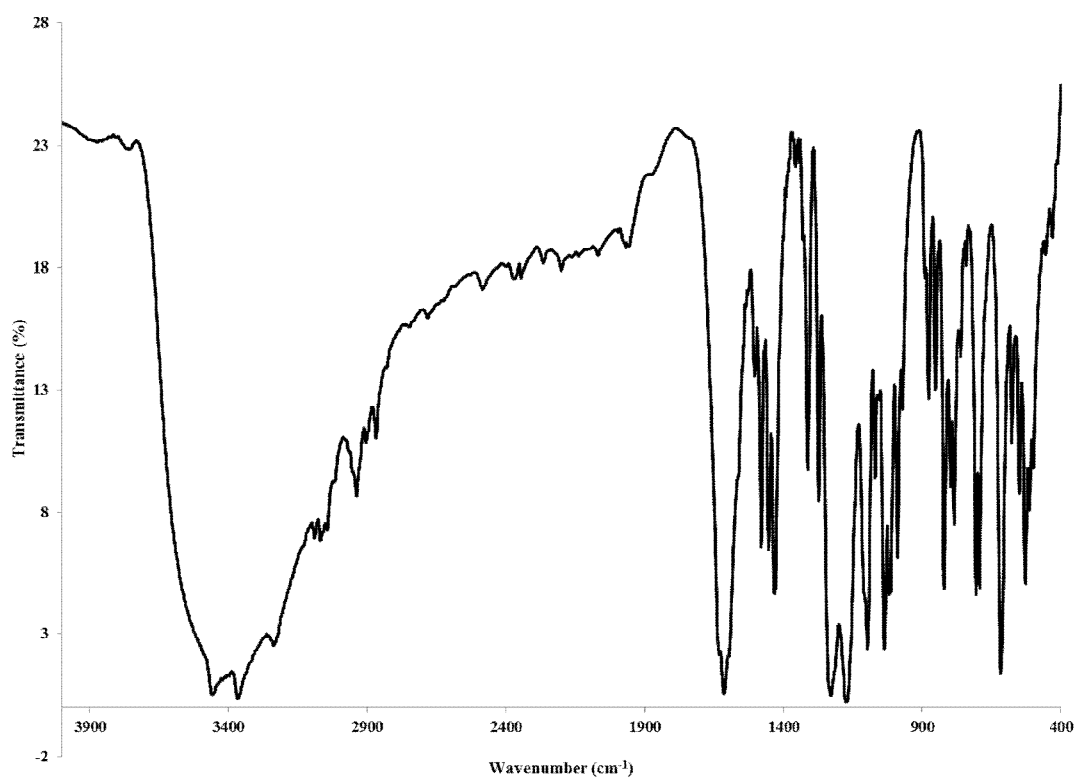


**Figure A36.** The infrared spectrum of  $\{[\text{Cd}_{0.5}(\text{bpe})(4\text{-abs})]\cdot\text{H}_2\text{O}\}_n$  (**17**).

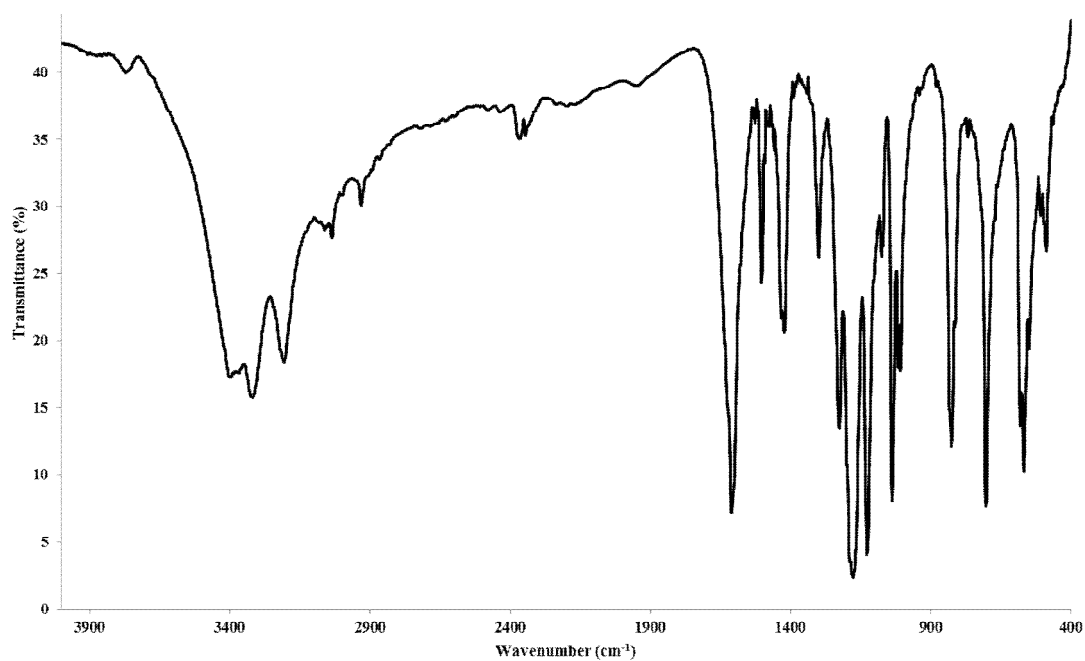


**Figure A37.** The infrared spectrum of  $\{[\text{Cd}(\text{bpp})_2(\text{H}_2\text{O})_4] \cdot (\text{3-abs})_2 \cdot 2\text{H}_2\text{O}\}_n$  (**18**).

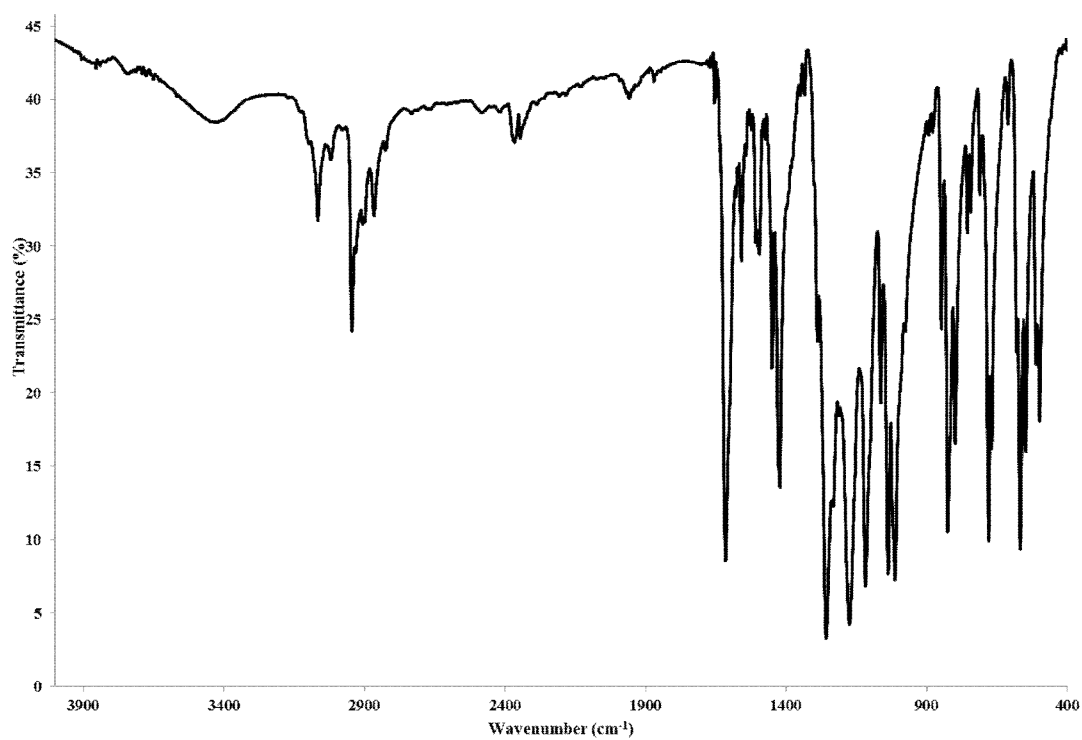


**Figure A38.** The infrared spectrum of  $[\text{Zn}(\text{bpp})_2(\text{Mbs})_2]_n$  (**19**).



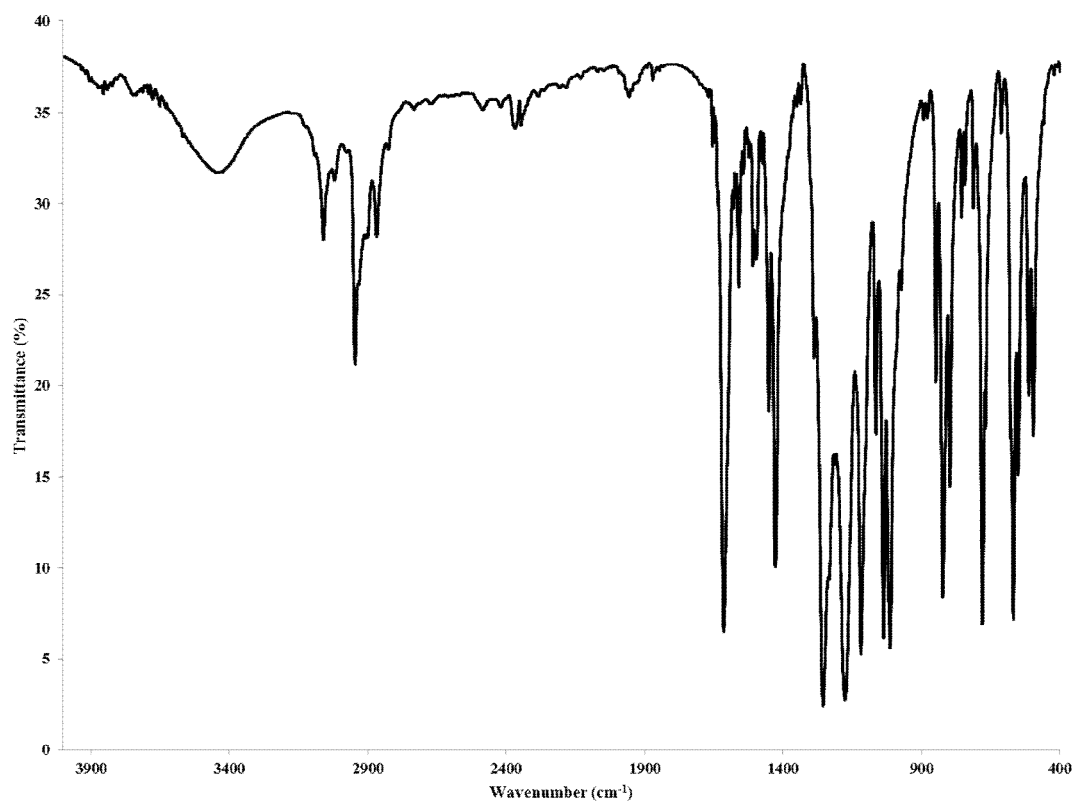


**Figure A39.** The infrared spectrum of  $[\text{Cd}(\text{bpp})_2(\text{Mbs})_2]_n$  (**20**).

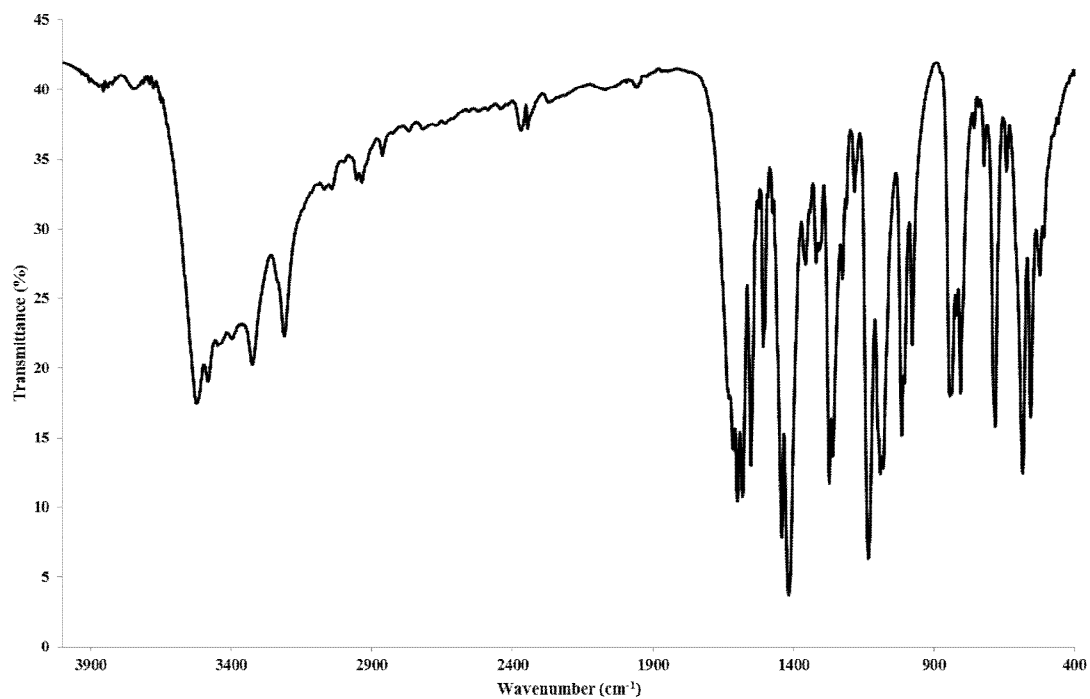


**Figure A40.** The infrared spectrum of  $\{[\text{Cd}(\text{bpp})(\text{sdz})_2] \cdot 2\text{H}_2\text{O}\}_n$  (**21**).

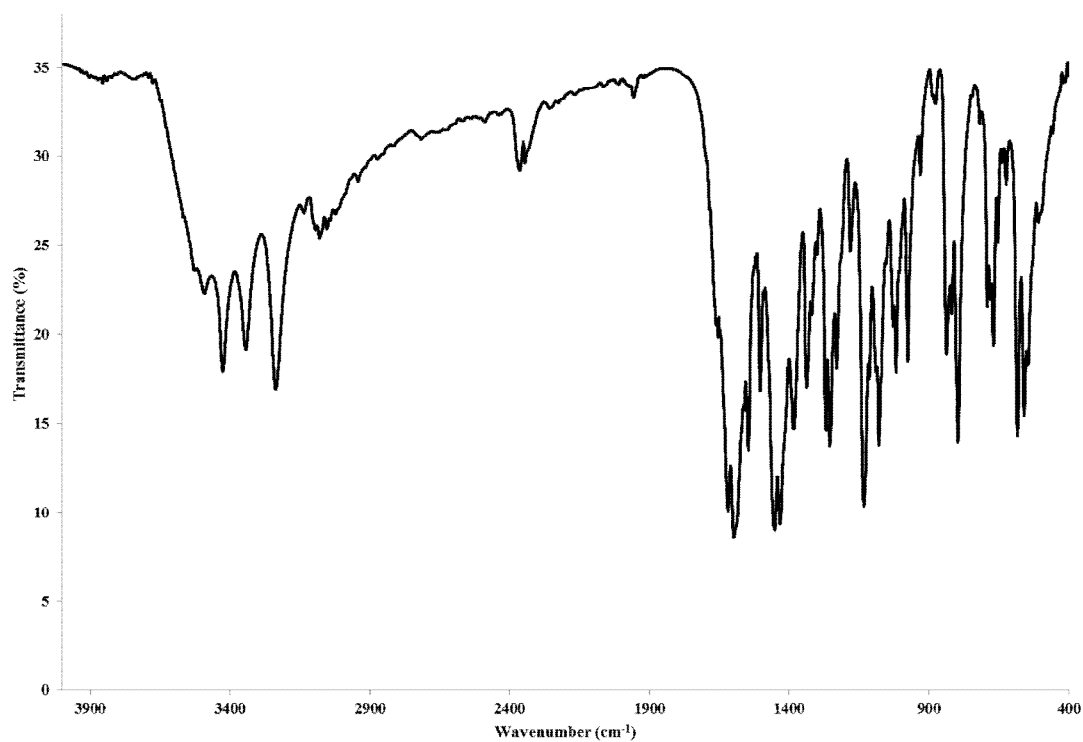


**Figure A41.** The infrared spectrum of  $\{[\text{Zn}(\text{bpe})(\text{sdz})(\text{ac})]\cdot\text{H}_2\text{O}\}_n$  (**22**).

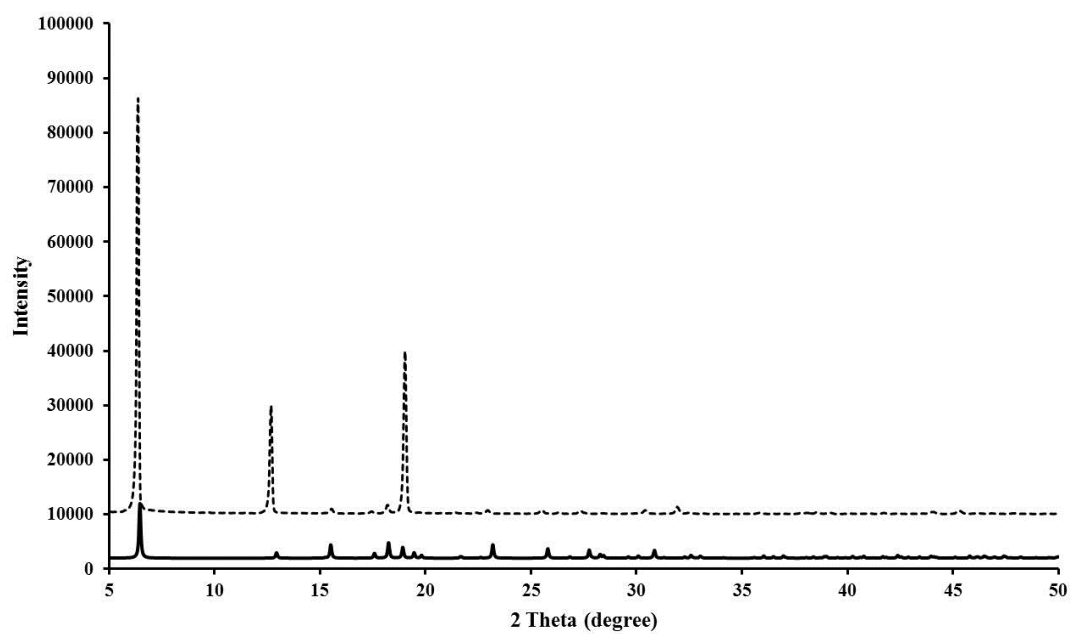


**Figure A42.** The simulated (—) and measured (····) PXRD patterns for  $[\text{Cd}(\text{Cin})_2\text{H}_2\text{O}]$  (**1**).

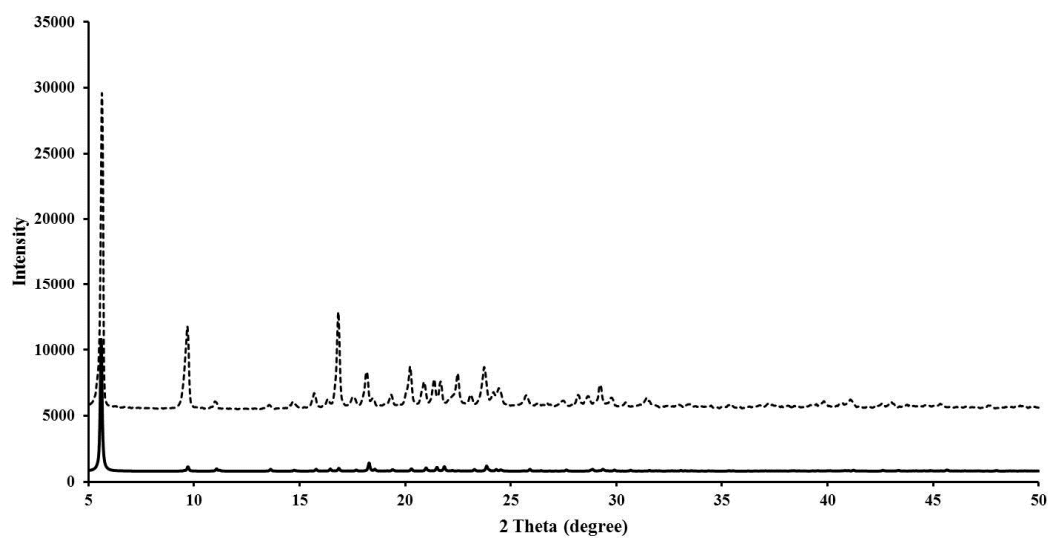


**Figure A43.** The simulated (—) and measured (·····) PXRD patterns for  $[\text{Zn}(4,4'\text{-bpy})_{0.5}(\text{Cin})_2]$  (**2**).

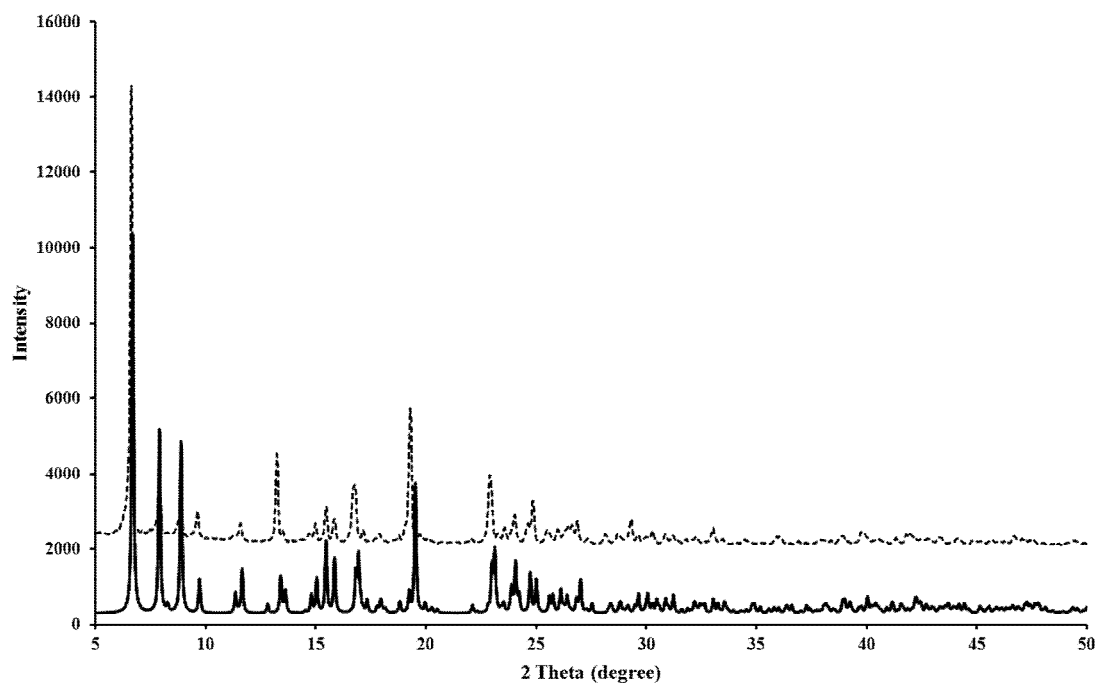


**Figure A44.** The simulated (—) and measured (·····) PXRD patterns for  $[\text{Cd}_3(4,4'\text{-bpy})_2(\text{cin})_6(\text{H}_2\text{O})_2]_n$  (**3**).

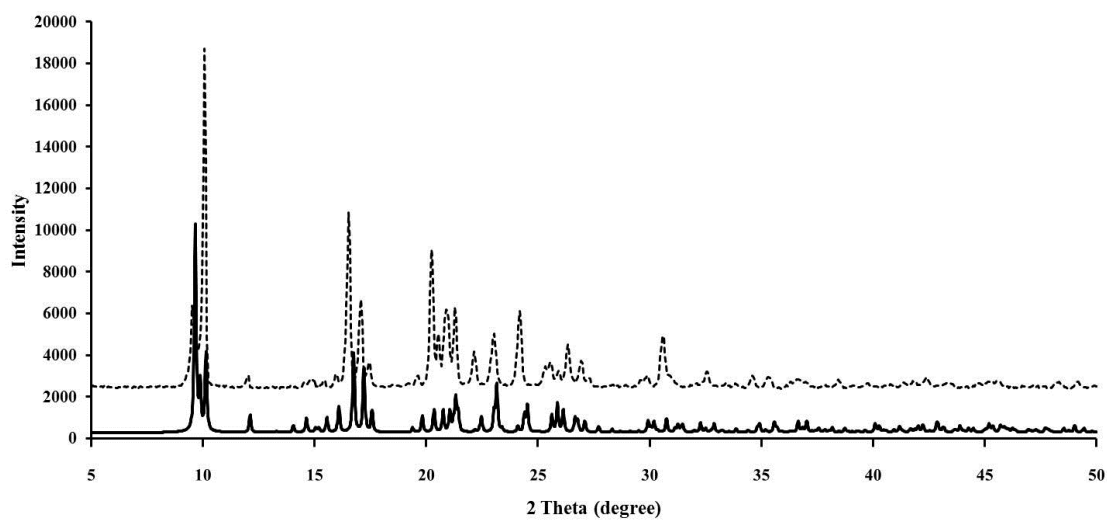


**Figure A45.** The simulated (—) and measured (.....) PXRD patterns for  $[\text{Mn}_2(\text{bpp})(3\text{-Npt})_2(\text{H}_2\text{O})_2]_n$  (5).

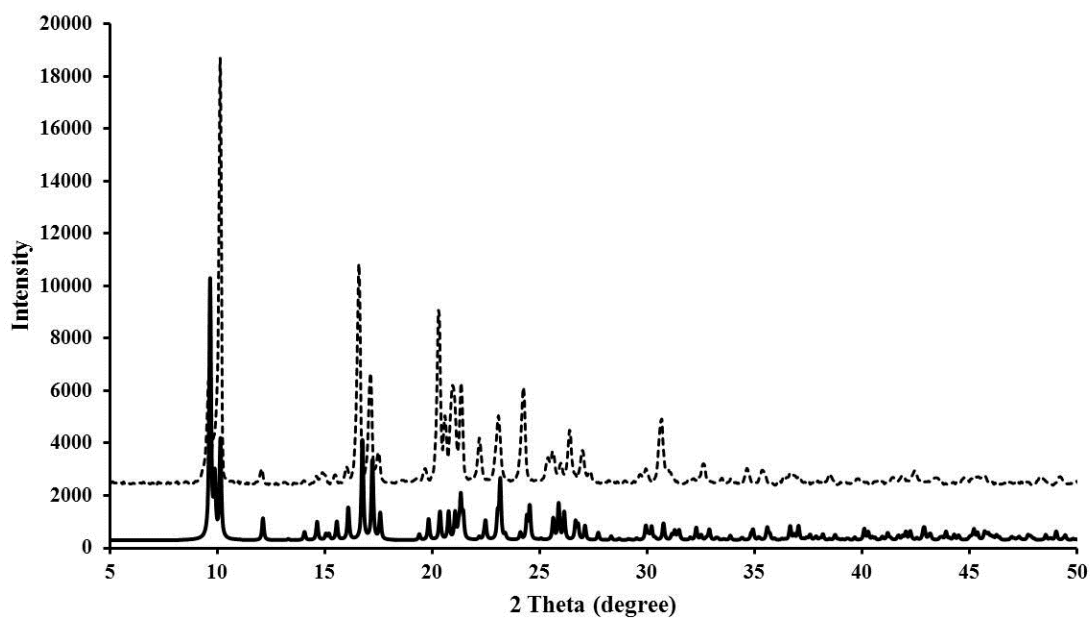


**Figure A46.** The simulated (—) and measured (.....) PXRD patterns for  $[\text{Ni}(\text{bpp})(3\text{-Npt})(\text{H}_2\text{O})]_n$  (6).

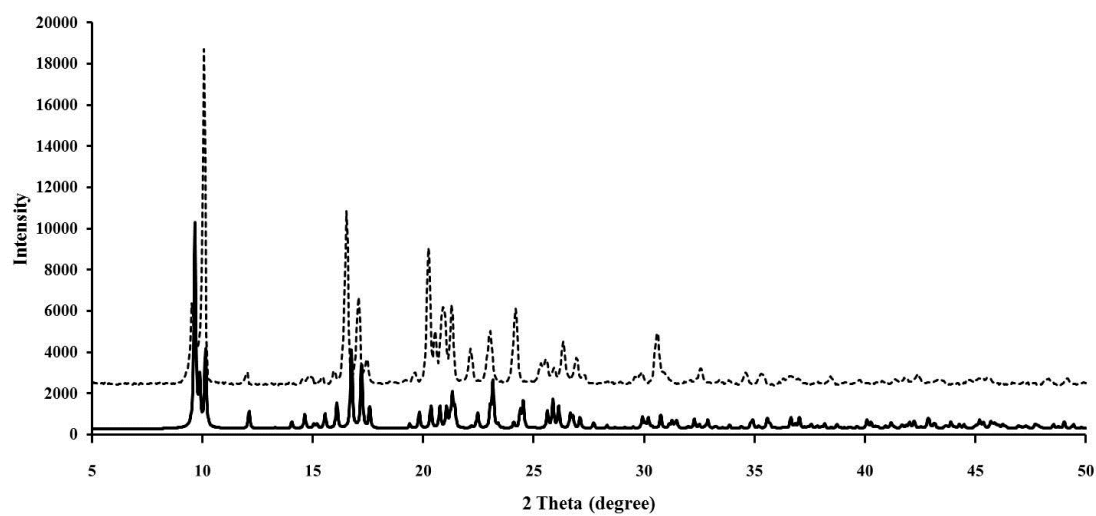


**Figure A47.** The simulated (—) and measured (····) PXRD patterns for  $\{[\text{Ag}_2(\text{bpp})_2] \cdot (4\text{H}_2\text{O}) \cdot (3\text{-Npt})\}_n$  (**7**).

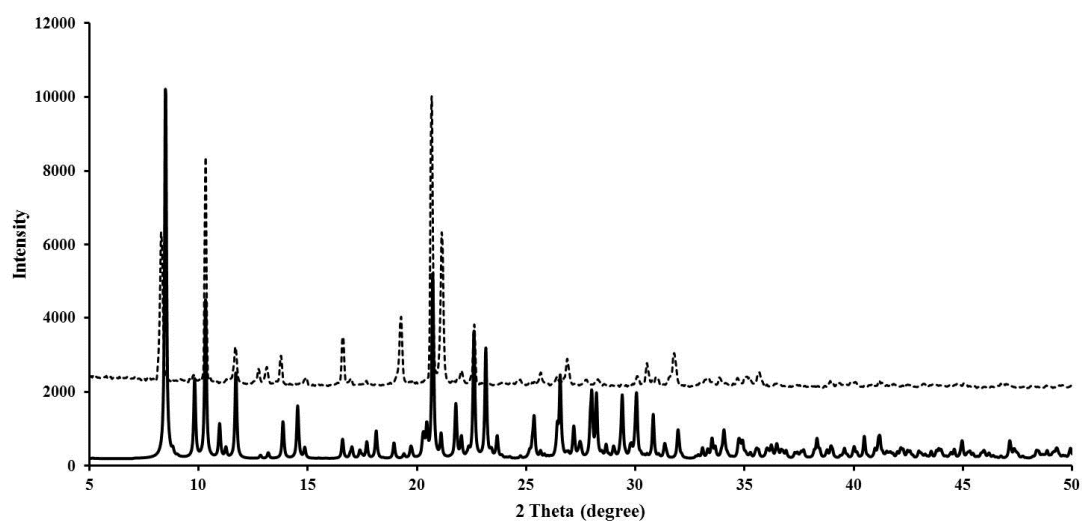


**Figure A48.** The simulated (—) and measured (····) PXRD patterns for  $\{[\text{Ag}_2(\text{bpe})_2(3\text{-Npt})] \cdot 7\text{H}_2\text{O}\}_n$  (**8**).

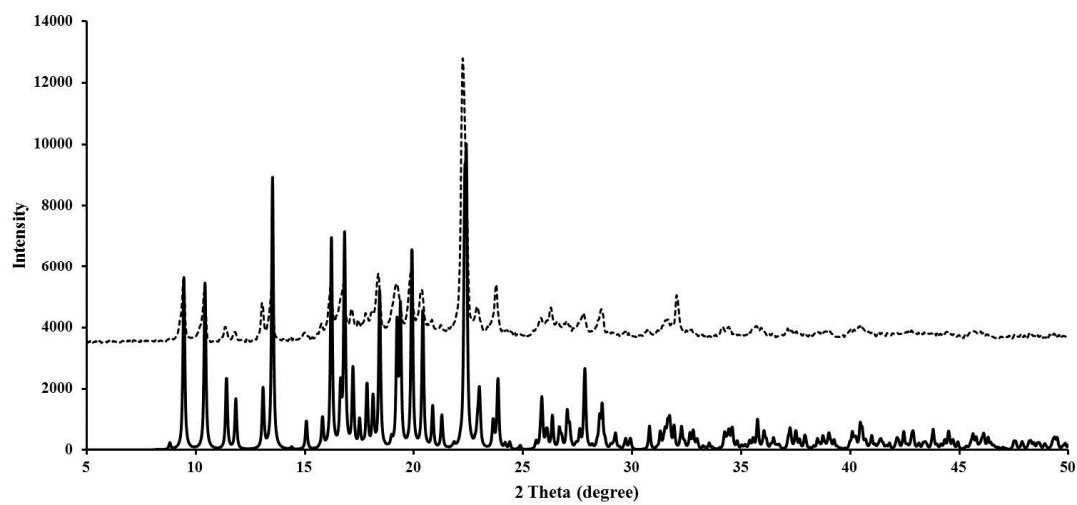


**Figure A49.** The simulated (—) and measured (····) PXRD patterns for  $[\text{Zn}(\text{bpp})_2(\text{Sal})_2]_n$  (**9**).

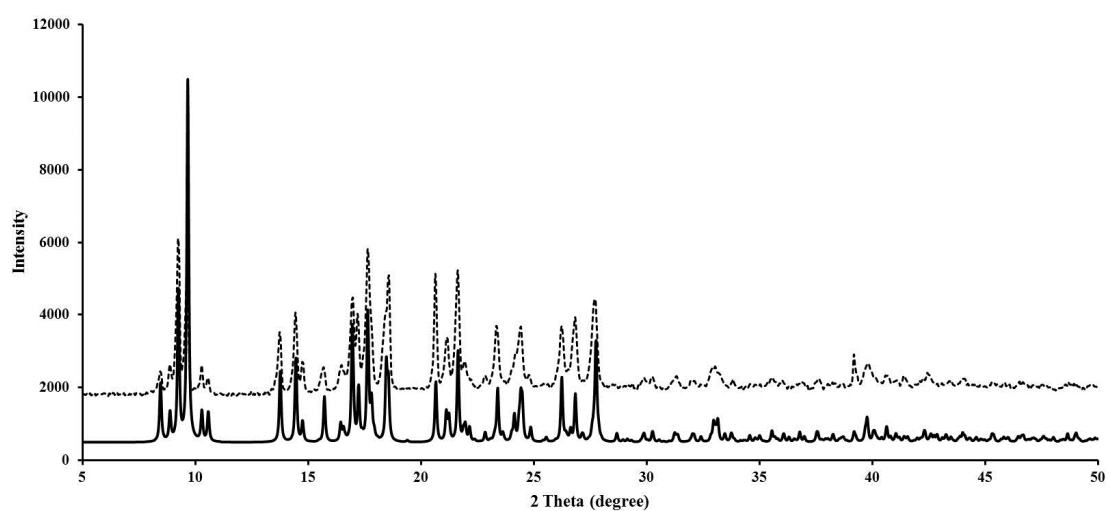


**Figure A50.** The simulated (—) and measured (····) PXRD patterns for  $[\text{Zn}_2(\text{bpe})_2(\text{Sal})_4]$  (**10**).

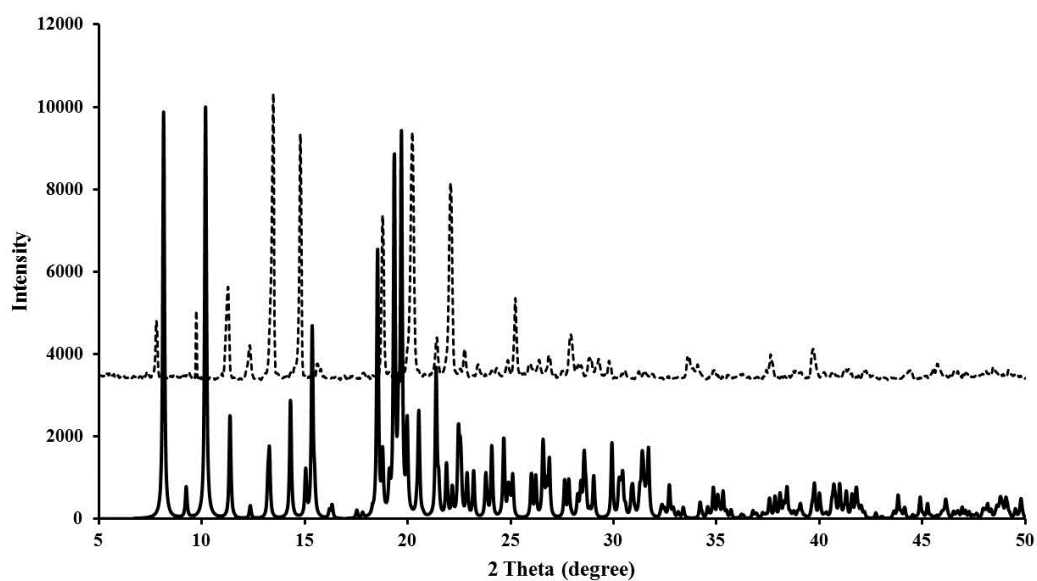


**Figure A51.** The simulated (—) and measured (····) PXRD patterns for  $\{[\text{Co}(\text{bpp})_2(\text{H}_2\text{O})_2] \cdot (4\text{-abs})_2 \cdot \text{H}_2\text{O}\}_n$  (**11**).

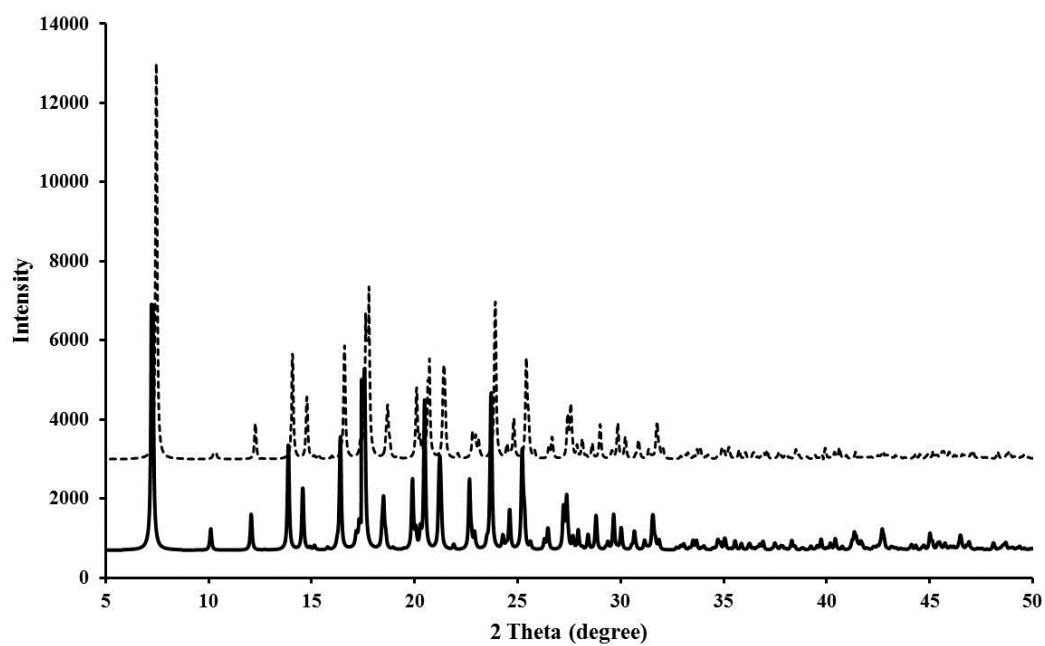


**Figure A52.** The simulated (—) and measured (····) PXRD patterns for  $[\text{Mn}_{0.5}(\text{bpp})(\text{H}_2\text{O})_2] \cdot (4\text{-abs})$  (**12**).

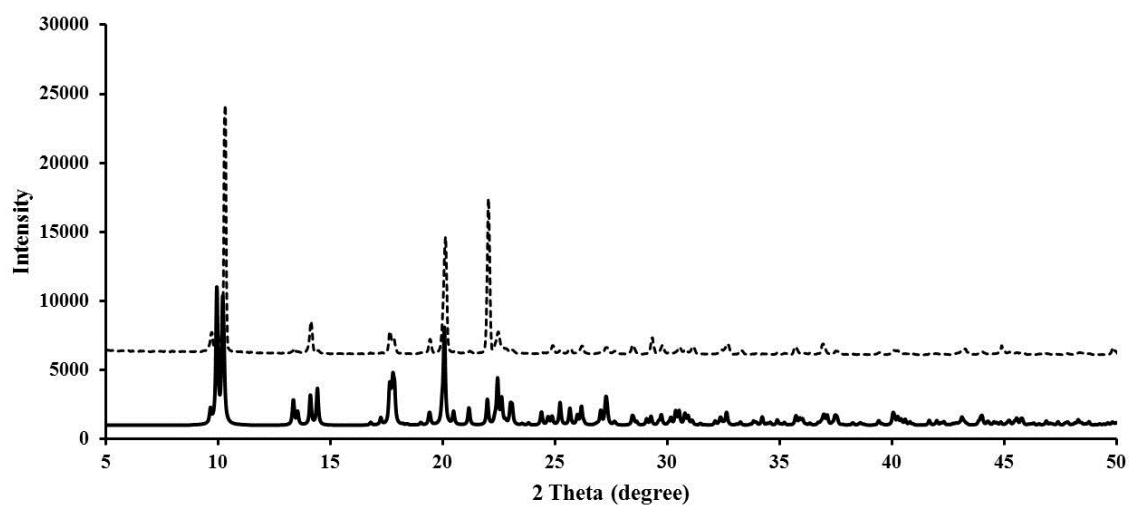


**Figure A53.** The simulated (—) and measured (.....) PXR D patterns for  $\{[\text{Cd}_{0.5}(\text{bpp})(4\text{-abs})]\cdot(\text{H}_2\text{O})\}_n$  (**13**).

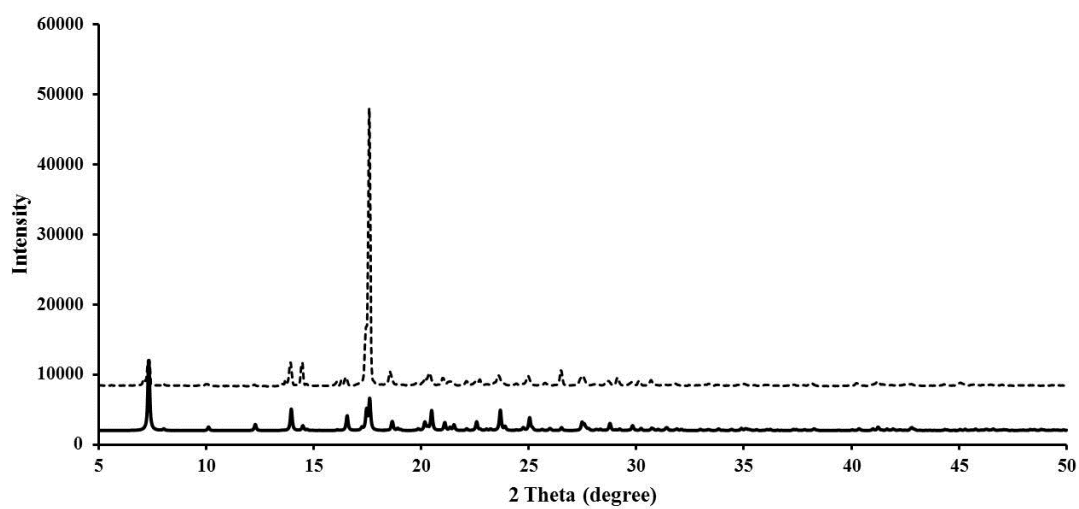


**Figure A54.** The simulated (—) and measured (.....) PXR D patterns for  $[\text{Zn}_{0.5}(\text{bpp})(\text{H}_2\text{O})_2]\cdot(4\text{-abs})$  (**14**).



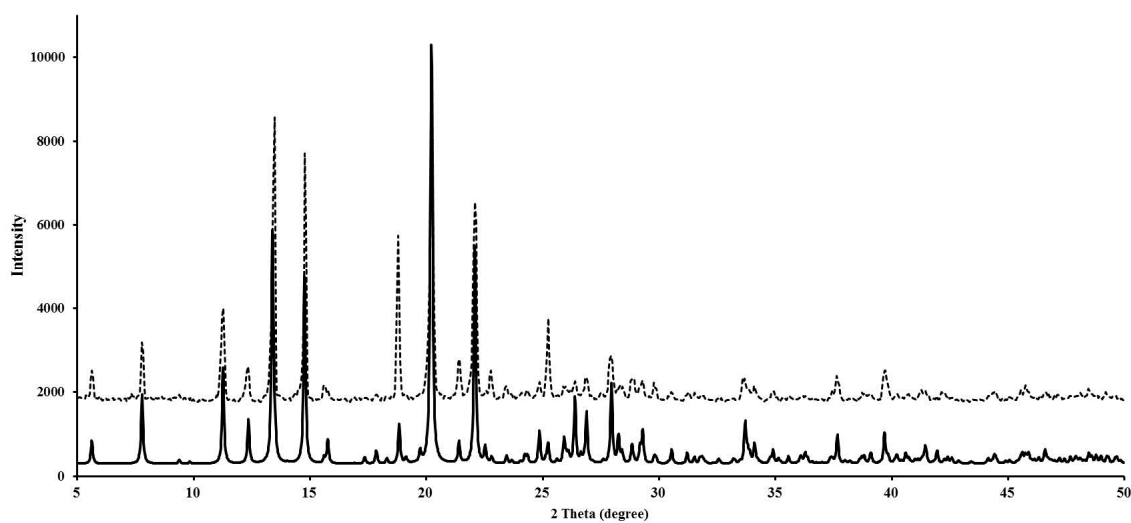


**Figure A55.** The simulated (—) and measured (····) PXRD patterns for  $\{[\text{Zn}(4,4'\text{-bpy})(\text{H}_2\text{O})_4]\cdot(4\text{-abs})_2\cdot 2\text{H}_2\text{O}\}_n$  (**15**).

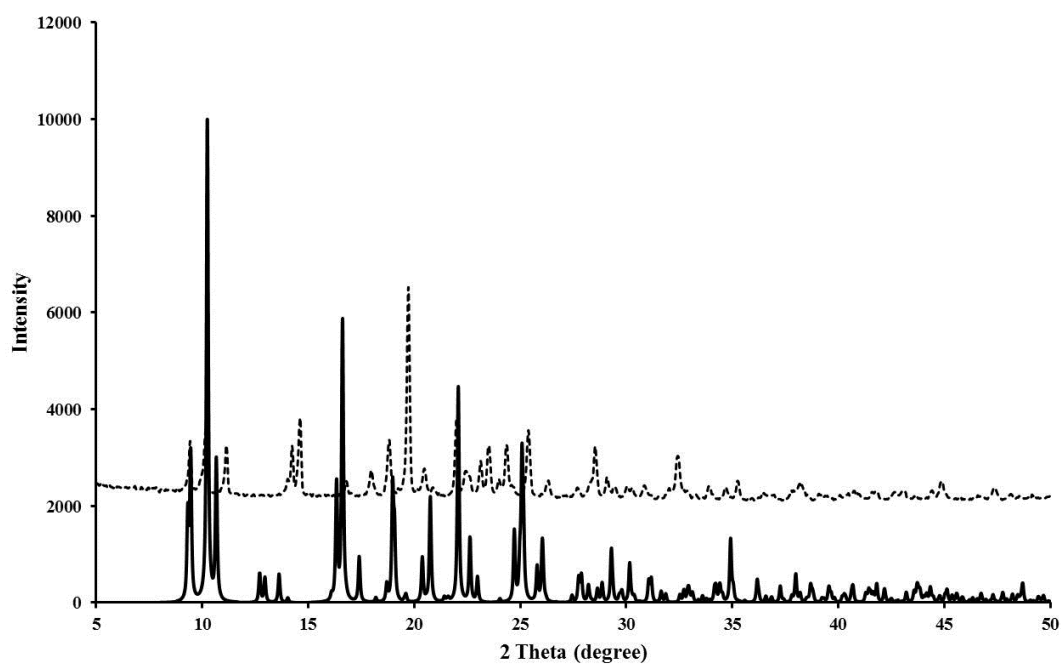


**Figure A56.** The simulated (—) and measured (····) PXRD patterns for  $\{[\text{Cd}_{0.5}(\text{bpe})(4\text{-abs})]\cdot\text{H}_2\text{O}\}_n$  (**17**).

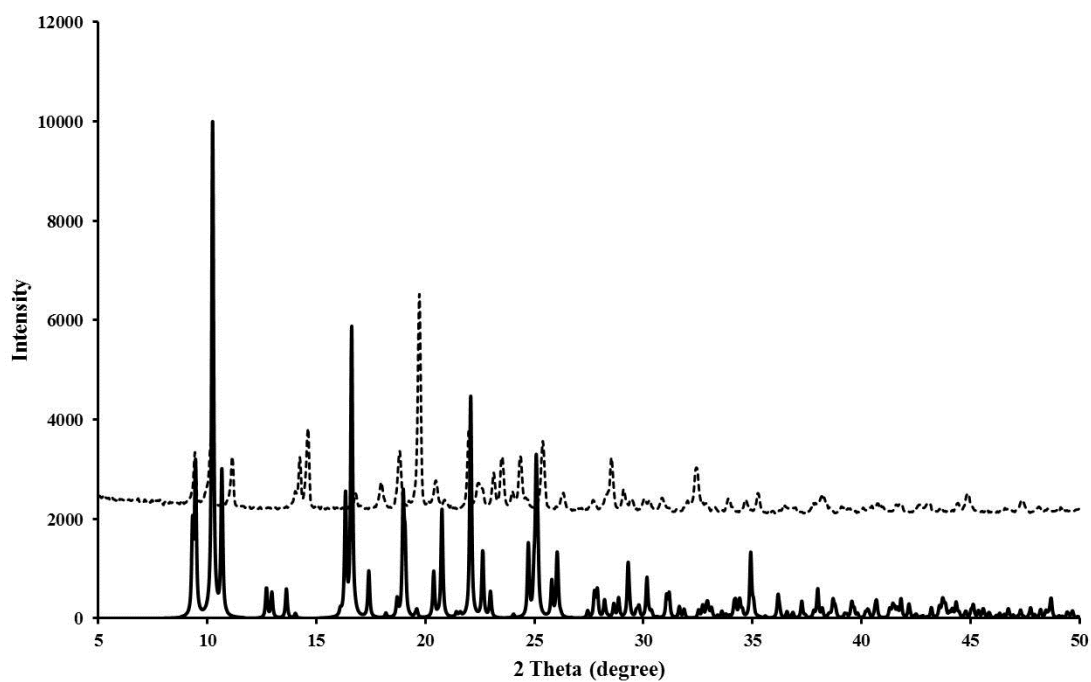


**Figure A57.** The simulated (—) and measured (.....) PXRD patterns for  $\{[\text{Cd}(\text{bpp})_2(\text{H}_2\text{O})_4] \cdot (\text{3-abs})_2 \cdot 2\text{H}_2\text{O}\}_n$  (**18**).

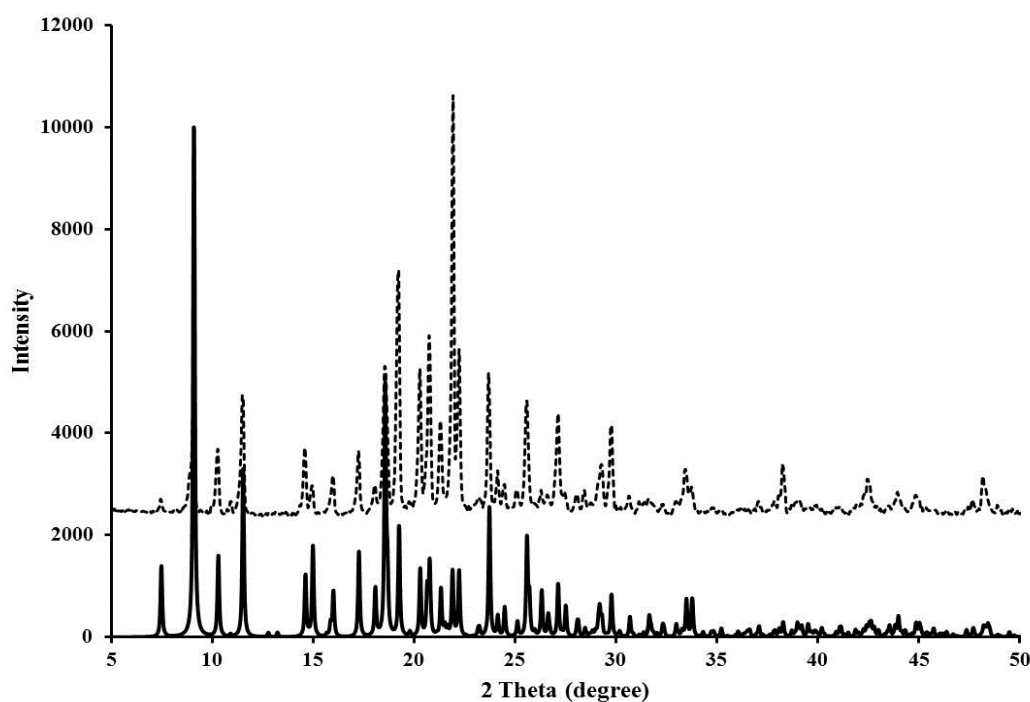


**Figure A58.** The simulated (—) and measured (.....) PXRD patterns for  $[\text{Zn}(\text{bpp})_2(\text{Mbs})_2]_n$  (**19**).

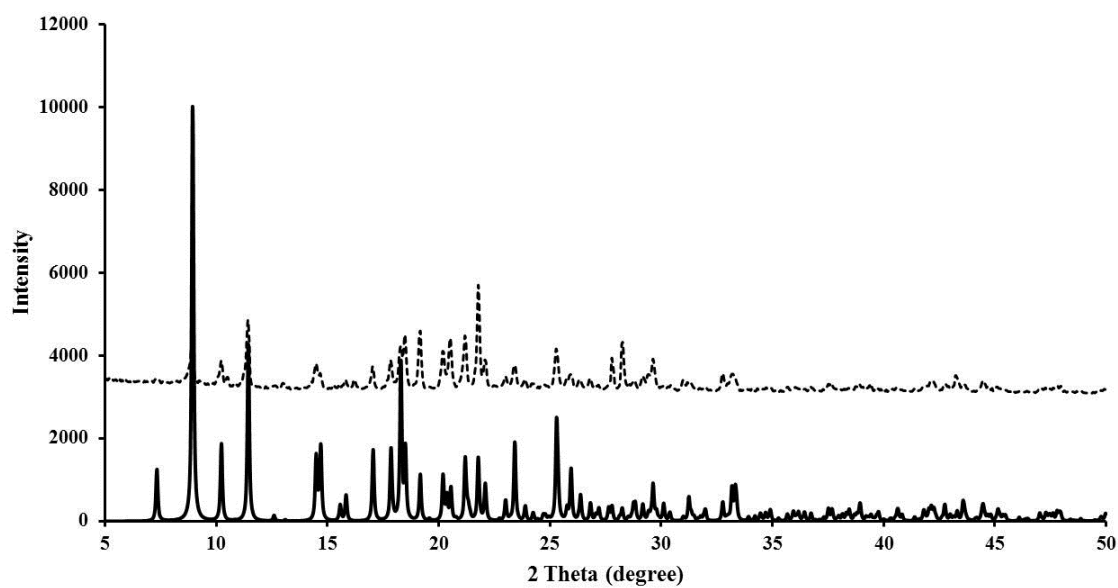
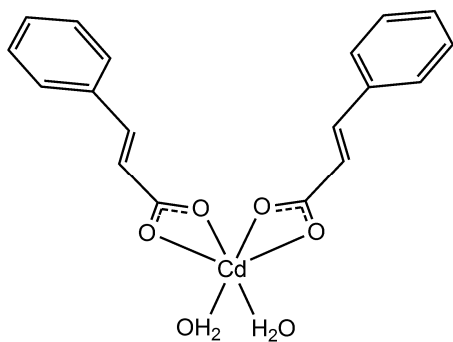
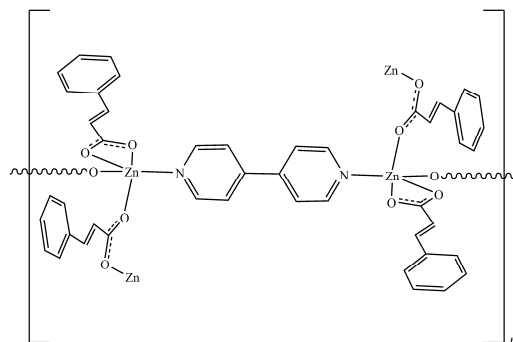


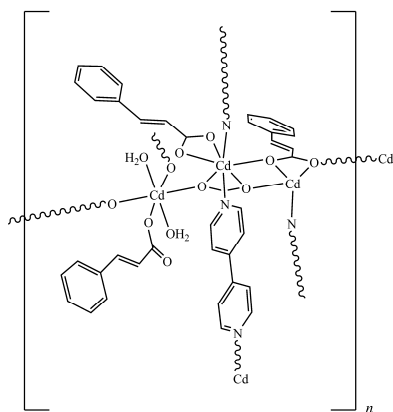
**Figure A59.** The simulated (—) and measured (·····) PXRD patterns for  $[\text{Cd}(\text{bpp})_2(\text{Mbs})_2]_n$  (**20**).



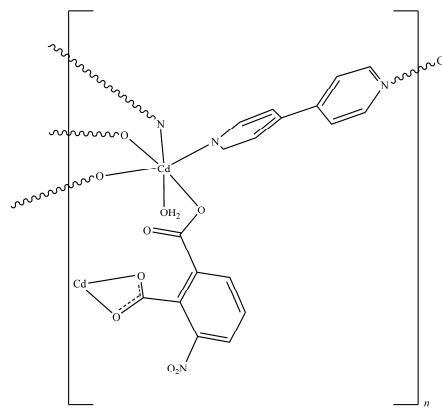
(1)



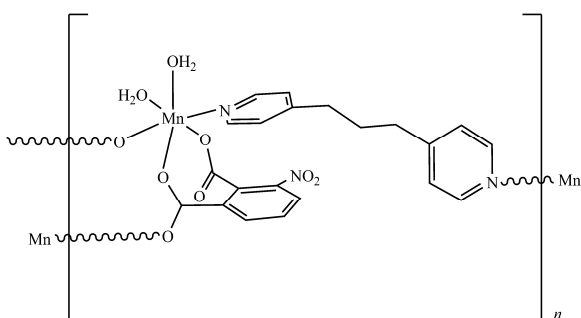
(2)



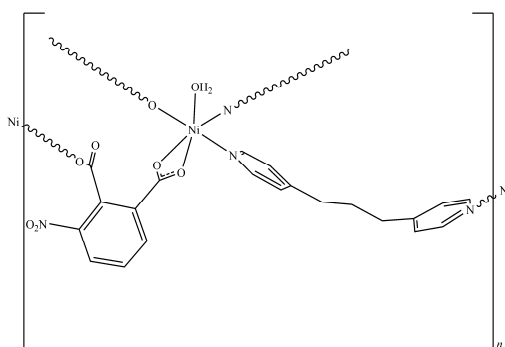
(3)



(4)

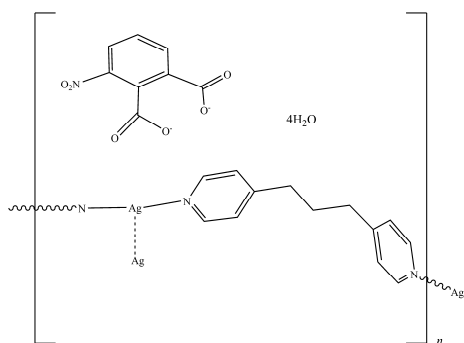


(5)

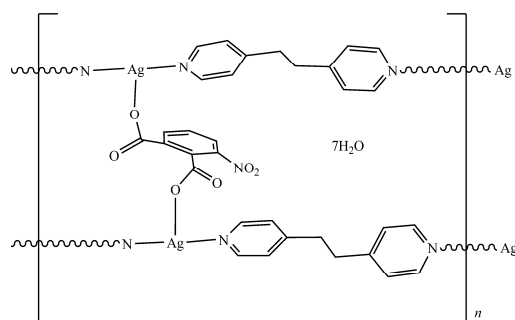


(6)

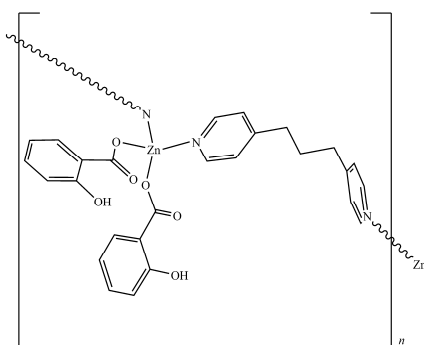
**Figure A60.** Molecular structure of complexes (1) – (6).



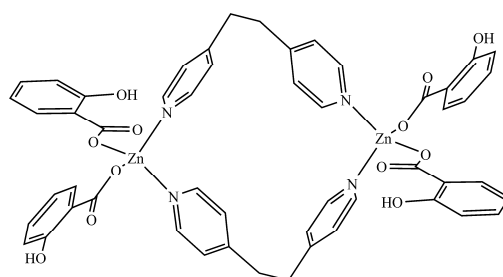
(7)



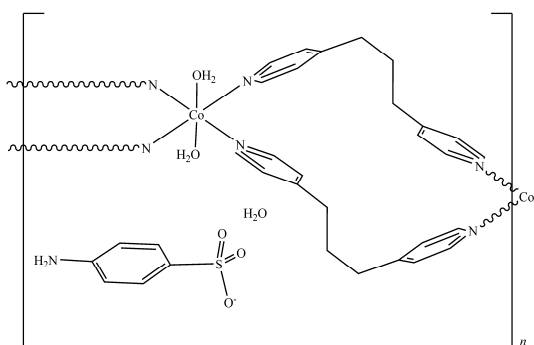
(8)



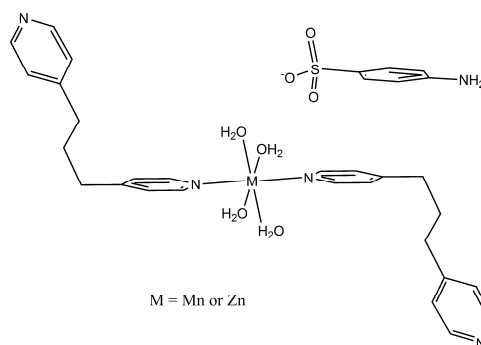
(9)



(10)

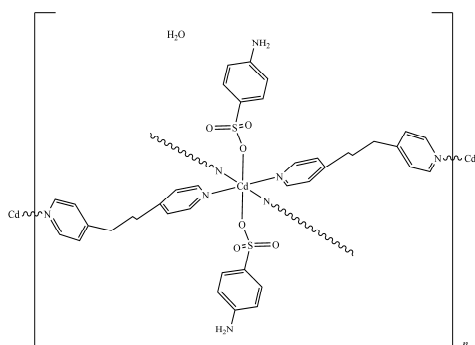


(11)

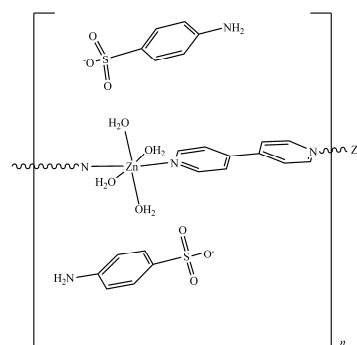


(12) and (14)

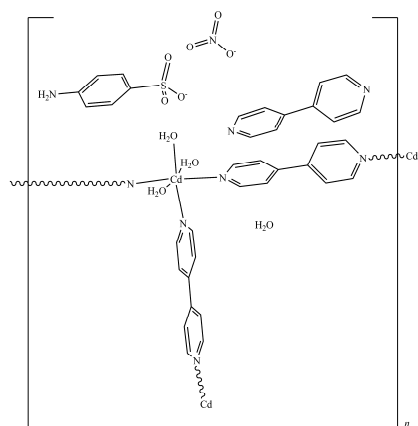
**Figure A61.** Molecular structures of complexes (7) – (12) and (14).



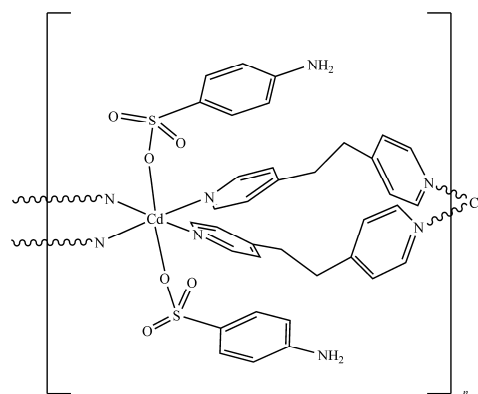
(13)



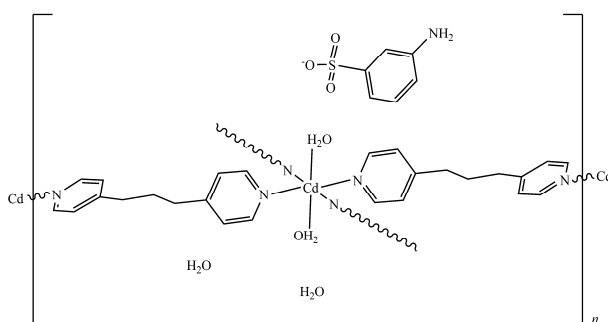
(15)



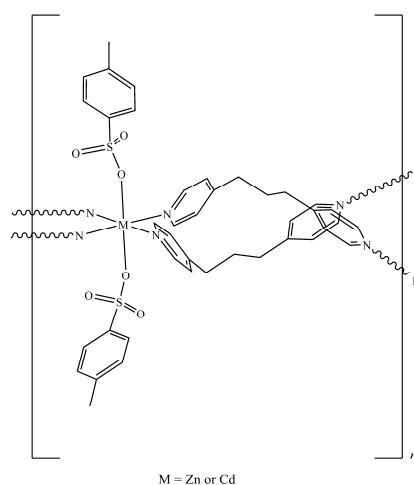
(16)



(17)



(18)



(19) and (20)

Figure A62 Molecular structures of complexes (13) and (15) - (20).

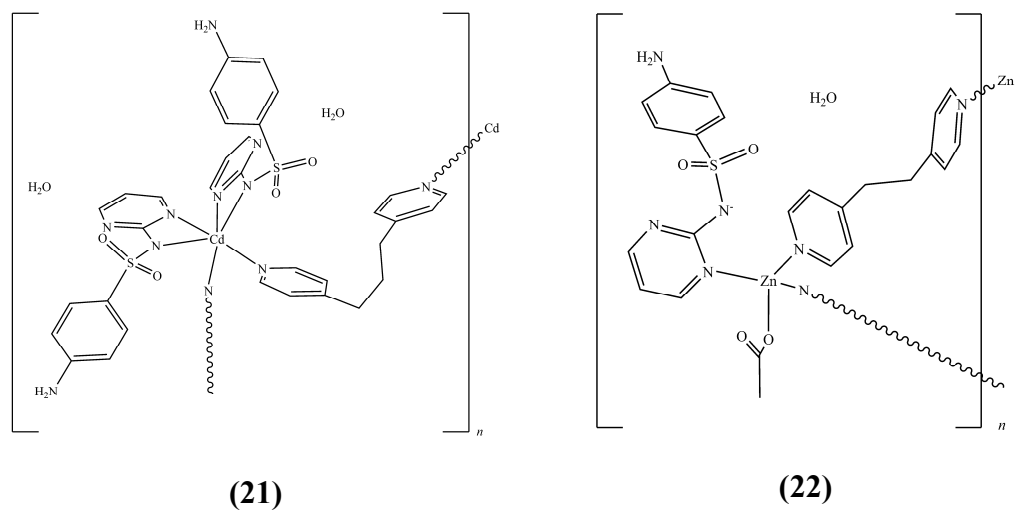


Figure A63. Molecular structures of complexes (21) - (22).

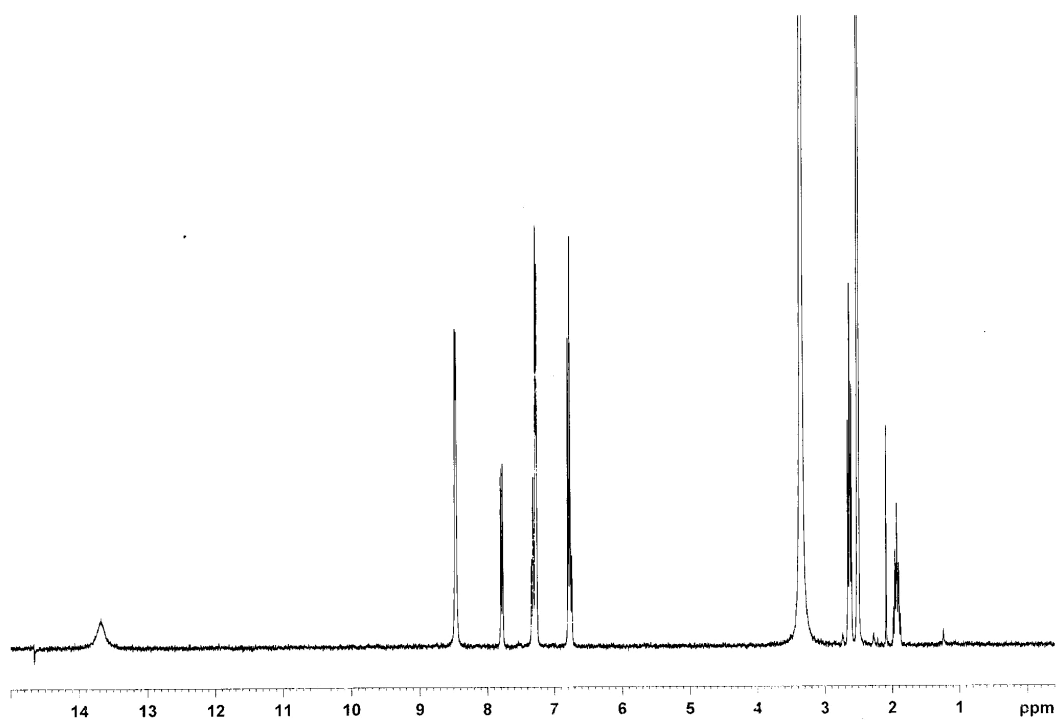
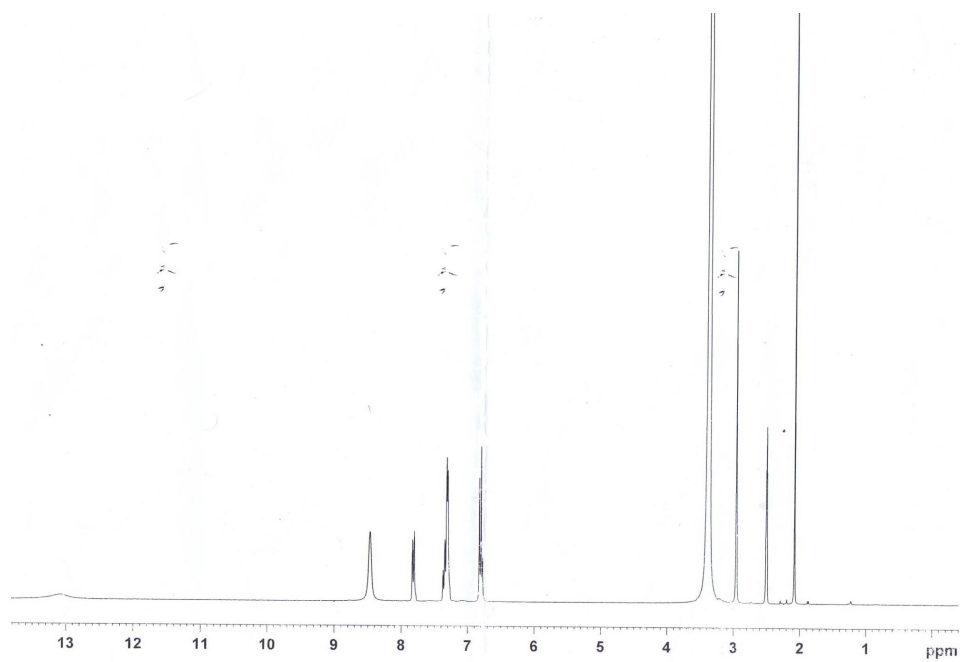


Figure A64.  $^1\text{H-NMR}$  of complex (9) in  $\text{DMSO-d}_6$



**Figure A65.**  $^1\text{H-NMR}$  of complex (10) in  $\text{DMSO-d}_6$



## Appendix B

## metal-organic compounds



Acta Crystallographica Section E

## Structure Reports

Online

ISSN 1600-5368

Diaquabis(cinnamato- $\kappa^2O,O'$ )cadmiumSirinart Chooset,<sup>a</sup> Bryan Cunningham,<sup>b</sup> Anob Kantacha,<sup>c</sup> Matthias Zeller<sup>b</sup> and Sumpun Wongnawa<sup>a\*</sup>

<sup>a</sup>Department of Chemistry, Faculty of Science, Prince of Songkla University, Hat Yai, Songkhla 90112, Thailand, <sup>b</sup>Department of Chemistry, Youngstown State University, One University Plaza, Youngstown, OH 44555, USA, and <sup>c</sup>Department of Chemistry, Faculty of Science, Thaksin University, (Paththalung Campus), Paththalung 93110, Thailand

Correspondence e-mail: sumpun.w@psu.ac.th

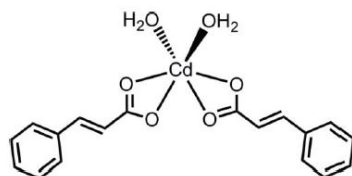
Received 23 January 2014; accepted 18 February 2014

Key indicators: single-crystal X-ray study;  $T = 100$  K; mean  $\sigma(C-C) = 0.005$  Å;  $R$  factor = 0.020;  $wR$  factor = 0.046; data-to-parameter ratio = 16.9.

The title complex,  $[Cd(C_9H_7O_2)_2(H_2O)_2]$ , was obtained as an unintended product of the reaction of cadmium nitrate with hexamethylenetetramine and cinnamic acid. The  $Cd^{II}$  ion lies on a twofold rotation axis and is coordinated in a slightly distorted trigonal-prismatic environment. In the crystal, the V-shaped molecules are arranged in an interlocking fashion along [010] and O—H...O hydrogen bonds link the molecules, forming a two-dimensional network parallel to (001).

## Related literature

For a previous conference report of the title compound, see: Amma *et al.* (1983). For related structures, see: Hosomi *et al.* (2000); Mak *et al.* (1985); Smith *et al.* (1981); O'Reilly *et al.* (1984). For a description of the Cambridge Structural Database, see: Allen (2002).



## Experimental

## Crystal data

$[Cd(C_9H_7O_2)_2(H_2O)_2]$   $V = 862.30$  (15) Å<sup>3</sup>  
 $M_r = 442.72$   $Z = 2$   
 Monoclinic,  $C_2$   $Mo K\alpha$  radiation  
 $a = 11.7872$  (12) Å  $\mu = 1.30$  mm<sup>-1</sup>  
 $b = 5.3498$  (5) Å  $T = 100$  K  
 $c = 13.8817$  (14) Å  $0.28 \times 0.09 \times 0.02$  mm  
 $\beta = 99.913$  (1)°

## Data collection

Bruker SMART APEX CCD diffractometer  
 Absorption correction: multi-scan (SADABS; Bruker, 2012)  
 $T_{min} = 0.617$ ,  $T_{max} = 0.746$   
 5087 measured reflections  
 2531 independent reflections  
 2529 reflections with  $I > 2\sigma(I)$   
 $R_{int} = 0.021$

## Refinement

$R[F^2 > 2\sigma(F^2)] = 0.020$   
 $wR(F^2) = 0.046$   
 $S = 1.05$   
 2531 reflections  
 150 parameters  
 3 restraints  
 All H-atom parameters refined  
 $\Delta\rho_{max} = 1.09$  e Å<sup>-3</sup>  
 $\Delta\rho_{min} = -0.42$  e Å<sup>-3</sup>  
 Absolute structure: Flack parameter determined using 1059 quotients  $[(I^+) - (I^-)] / [(I^+) + (I^-)]$  (Parsons *et al.*, 2013)  
 Absolute structure parameter: 0.018 (14)

Table 1

Hydrogen-bond geometry (Å, °).

$D-H\cdots A$	$D-H$	$H\cdots A$	$D\cdots A$	$D-H\cdots A$
$O3-H3A\cdots O1^i$	0.82 (2)	1.86 (2)	2.679 (3)	174 (4)
$O3-H3B\cdots O2^{ii}$	0.80 (2)	1.86 (3)	2.658 (3)	171 (5)

Symmetry codes: (i)  $-x + 2, y - 1, -z + 2$ ; (ii)  $-x + \frac{3}{2}, y - \frac{1}{2}, -z + 2$ .

Data collection: APEX2 (Bruker, 2012); cell refinement: SAINTE (Bruker, 2012); data reduction: SAINTE and SHELXTL (Sheldrick, 2008); program(s) used to solve structure: SHELXS97 (Sheldrick, 2008); program(s) used to refine structure: SHELXL2013 (Sheldrick, 2008) and SHELXLE (Hübschle *et al.*, 2011); molecular graphics: Mercury (Macrae *et al.*, 2008) and PLATON (Spek, 2009); software used to prepare material for publication: publCIF (Westrip, 2010).

This work was supported by the Songklanagarind Scholarship for Graduate Studies from Prince of Songkla University. SC would like to thank Ruthairat Nimthong for assistance in the manuscript preparation. The X-ray diffractometer at Youngstown State University was funded by NSF grant 0087210, Ohio Board of Regents grant CAP-491, and by Youngstown State University.

Supporting information for this paper is available from the IUCr electronic archives (Reference: LH5688).

## References

- Allen, F. H. (2002). *Acta Cryst.* **B58**, 380–388.  
 Amma, E. L., Griffith, E. A. H., Charles, N. G. & Rodesier, P. F. (1983). *ACS Abstr. Papers*, p. 39.  
 Bruker (2012). APEX2, SAINTE and SADABS. Bruker AXS Inc., Madison, Wisconsin, USA.  
 Hosomi, H., Ohba, S. & Ito, Y. (2000). *Acta Cryst.* **C56**, e123.  
 Hübschle, C. B., Sheldrick, G. M. & Ditttrich, B. (2011). *J. Appl. Cryst.* **44**, 1281–1284.  
 Macrae, C. F., Bruno, I. J., Chisholm, J. A., Edgington, P. R., McCabe, P., Pidcock, E., Rodriguez-Monge, L., Taylor, R., van de Streek, J. & Wood, P. A. (2008). *J. Appl. Cryst.* **41**, 466–470.  
 Mak, T. C. W., Yip, W. H., O'Reilly, E. J., Smith, G. & Kennard, C. H. L. (1985). *Inorg. Chim. Acta*, **100**, 267–273.  
 O'Reilly, E. J., Smith, G. & Kennard, C. H. L. (1984). *Inorg. Chim. Acta*, **90**, 63–71.

---

**metal-organic compounds**

---

- Parsons, S., Flack, H. D. & Wagner, T. (2013). *Acta Cryst.* **B69**, 249–259.  
Sheldrick, G. M. (2008). *Acta Cryst.* **A64**, 112–122.  
Smith, G., O'Reilly, E. J., Kennard, C. H. L., Stadnicka, K. & Oleksyn, B. (1981). *Inorg. Chim. Acta*, **47**, 111–120.  
Spek, A. L. (2009). *Acta Cryst.* **D65**, 148–155.  
Westrip, S. P. (2010). *J. Appl. Cryst.* **43**, 920–925.

## supplementary materials

*Acta Cryst.* (2014). E70, m106–m107 [doi:10.1107/S160053681400364X]

**Diaquabis(cinnamato- $\kappa^2O,O'$ )cadmium**

**Sirinart Chooset, Bryan Cunningham, Anob Kantacha, Matthias Zeller and Sumpun Wongnawa**

**1. Comment**

The title compound was obtained as an accidental product of the reaction of cadmium nitrate with hexamethylenetetramine and cinnamic acid in ethanol in an attempt to synthesize a potentially interesting framework compound of the metal with both tetraamine and carboxylic acid groups. The potentially bridging hexamethylenetetramine ligand may have acted as a linker between cadmium ions; however, it was not incorporated into the material. A mononuclear cadmium complex with water and cinnamate ligands was the product formed in 75% yield, from an ethanolic solution.

The structure of diaqua-bis(cinnamato)-cadmium(II) had been previously recorded and was presented at the 1983 meeting of the American Chemical Society, but complete structural details are not available (Amma *et al.*, 1983). In the Cambridge Structural Database (Version 5.35, with updates up to May 2013; Allen, 2002) [REFCODE: BUYTUK] only the data collection temperature (room temperature), unit cell parameters and space group, and the *R* value (10.4%) are reported but no atomic coordinates are available. Given the relatively poor precision of the previously reported structure and the lack of three-dimensional coordinates, we herein report the crystal structure of the title compound at 100 K.

The Cd<sup>II</sup> lies on a two-fold rotation axis and is coordinated by two cinnamate ligands and two water molecules (Fig. 1). The carboxylate groups are bidentate-chelating, the water molecules monodentate and non bridging. The two oxygen atoms of each carboxylate group take coordination sites, the overall coordination environment of the metal center is best described as distorted trigonal prism, with angles varying between 92.86 (11)° (between the O atoms of the two water molecules), and 116.30 (8)° (for the angle between a water molecule O atom and a neighboring carboxylate group, using the carboxylate carbon atom as a substitute for the average of the two oxygen atoms).

The Cd—O bond distances are in the expected ranges. The bonds involving the water O atoms are 2.208 (2) Å, which compares well with those in similar Cd(II) complexes (O'Reilly *et al.*, 1984, Mak *et al.*, 1985). The Cd—O bond distances involving the two carboxylate O atoms are longer than those involving the water molecules, as would be expected due to the chelating coordination mode of the cinnamate ligand. The actual bond distances are 2.330 (2) and 2.375 (2) Å for Cd—O1 and Cd—O2, respectively. The similarity of the two Cd—O distances indicates an essentially symmetric coordination and a delocalization of the negative charge of the cinnamate carboxylate group. This is confirmed by the C—O bond distances within the carboxylate groups, which are also the same within experimental error, with values of 1.276 (3) and 1.269 (3) Å for O1—C9 and O2—C9, respectively.

In the crystal, the V-shape of the molecule results in a linear arrangement along [010] with the Cd(OH<sub>2</sub>)<sub>2</sub> part of one molecule oriented towards the V-shaped part of a symmetry related molecule (Fig. 2). In addition, intermolecular O—H...O hydrogen bonds connect molecules forming a two-dimensional network parallel to (001) (Fig. 3).

A search against the Cambridge Structural Database provided several similar reported structures that are related to the title compound: the zinc derivative diaqua-bis(cinnamato)-zinc(II) (Hosomi *et al.*, 2000; CSD refcode KIYSEQ), and several of the zinc and cadmium phenoxycetato derivatives: diaqua-bis(phenoxycetato)-cadmium(II) (Mak *et al.*, 1985, csd refcode DEBGAS) and diaqua-bis(phenoxycetato)-zinc(II) (Smith *et al.*, 1981, CSD refcode PHXCUB), diaqua-bis-



## supplementary materials

(4-fluorophenoxyacetato)-cadmium(II) (O'Reilly *et al.*, 1984; CSD refcode CUPMUV). Figures 4 and 5 show representative overlays of the title compound diaqua-bis(cinnamic)-cadmium(II) with diaqua-bis(phenoxyacetato)-zinc(II) (Smith *et al.*, 1981), indicating the isomorphous nature of the two compounds.

## 2. Experimental

To a stirred colorless solution of  $\text{Cd}(\text{NO}_3)_2 \cdot 4\text{H}_2\text{O}$  (0.3084 g, 1 mmol) in 10 mL of water was added hexamethylenetetramine (0.2802 g, 2 mmol) in 5 mL of water to give a colorless solution. Then, cinnamic acid (0.2962 g, 2 mmol) in 20 mL of ethanol was added to give a colorless solution. The solution was stirred at room temperature for 6 h, was filtered and then left to evaporate at room temperature. After several days, colorless needle shaped crystals suitable for X-ray analysis were obtained in 75% yield. A single-crystal was isolated while suspended in mineral oil, was mounted with the help of a trace of mineral oil on a Mitegen micromesh mount and flash frozen to 100 K on the diffractometer.

## 3. Refinement

Reflection 0 0 1 was affected by the beam stop and was omitted from the refinement. All H atoms positions were refined. Positions of carbon bound H atoms were freely refined, O bound H atoms were refined with an O—H distances restrained of 0.84 (2) Å. All  $U_{\text{iso}}(\text{H})$  values were refined.

## Computing details

Data collection: *APEX2* (Bruker, 2012); cell refinement: *SAINTE* (Bruker, 2012); data reduction: *SAINTE* (Bruker, 2012) and *SHELXTL* (Sheldrick, 2008); program(s) used to solve structure: *SHELXS97* (Sheldrick, 2008); program(s) used to refine structure: *SHELXL2013* (Sheldrick, 2008) and *SHELXL* (Hübschle *et al.*, 2011); molecular graphics: *Mercury* (Macrae *et al.*, 2008) and *PLATON* (Spek, 2009); software used to prepare material for publication: *pubCIF* (Westrip, 2010).

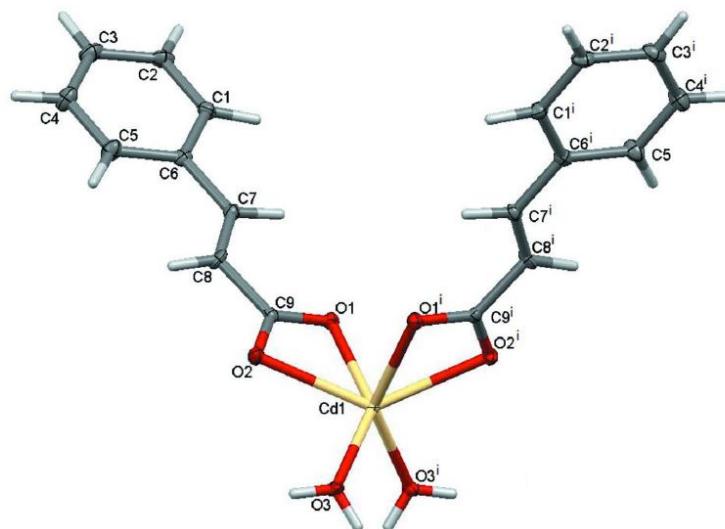


**Figure 1**

The molecular structure of the title compound, shown with ellipsoids at the 50% probability level. Symmetry operator (i):  $-x + 2, y, -z + 2$ .

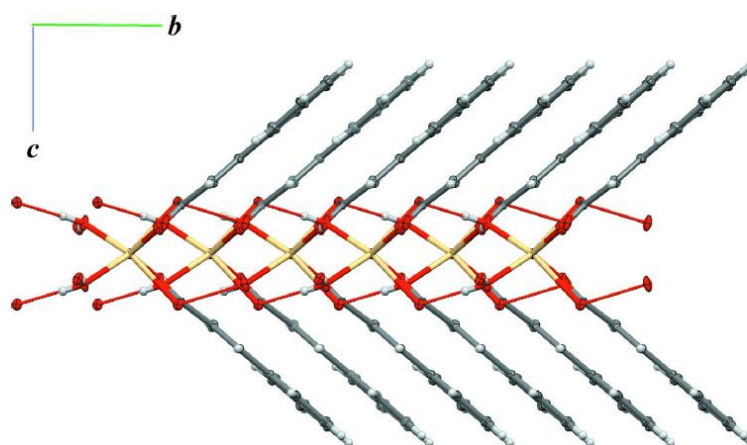


**Figure 2**

Part of the crystal structure showing molecules arranged along [010]. Hydrogen bonds are shown as blue dotted lines.

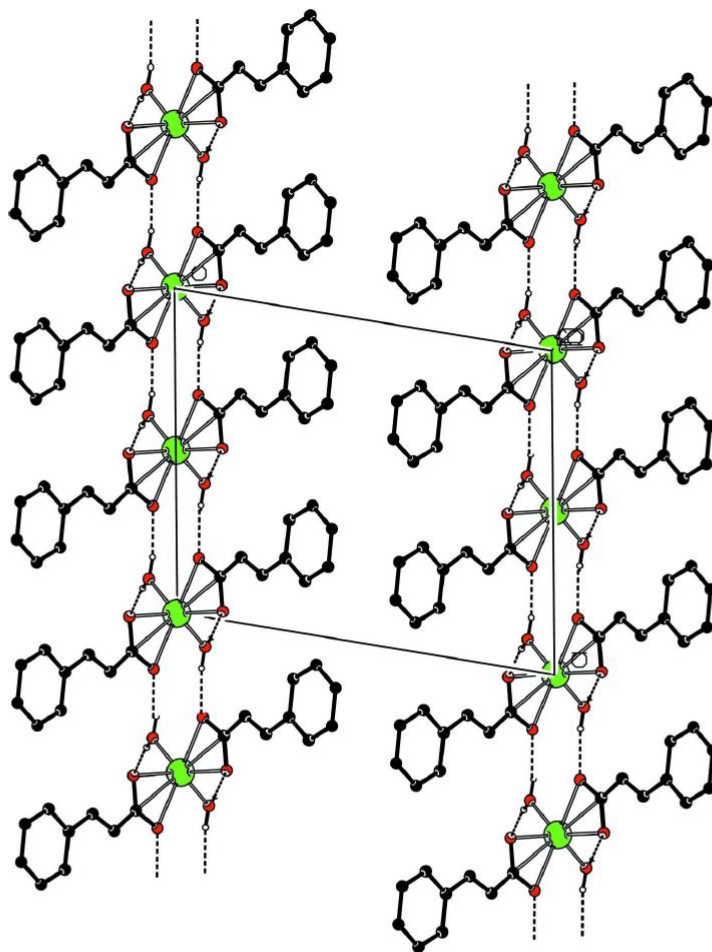
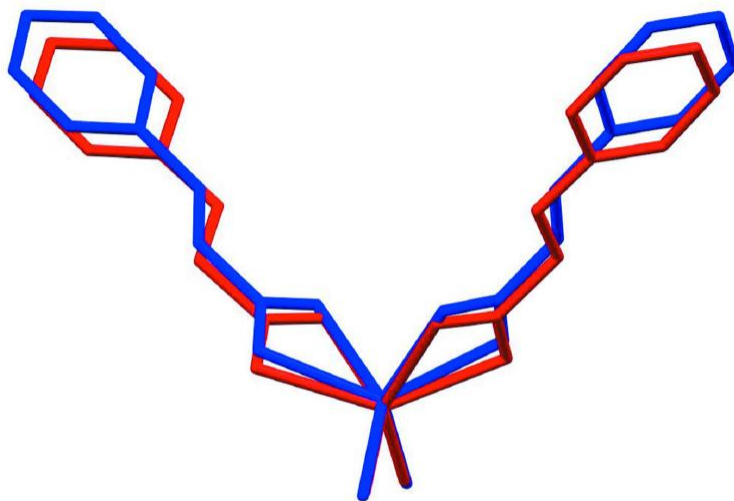


Figure 3

Part of the crystal structure showing layers perpendicular to the *c*-axis direction of the structure. Hydrogen bonds are illustrated by blue dotted lines.



**Figure 4**  
Overlaid stick presentation of diaqua-bis(cinnamate)-cadmium(II) (blue) and diaqua-bis(phenoxyacetato)-zinc(II) (red) (Smith *et al.*, 1981).

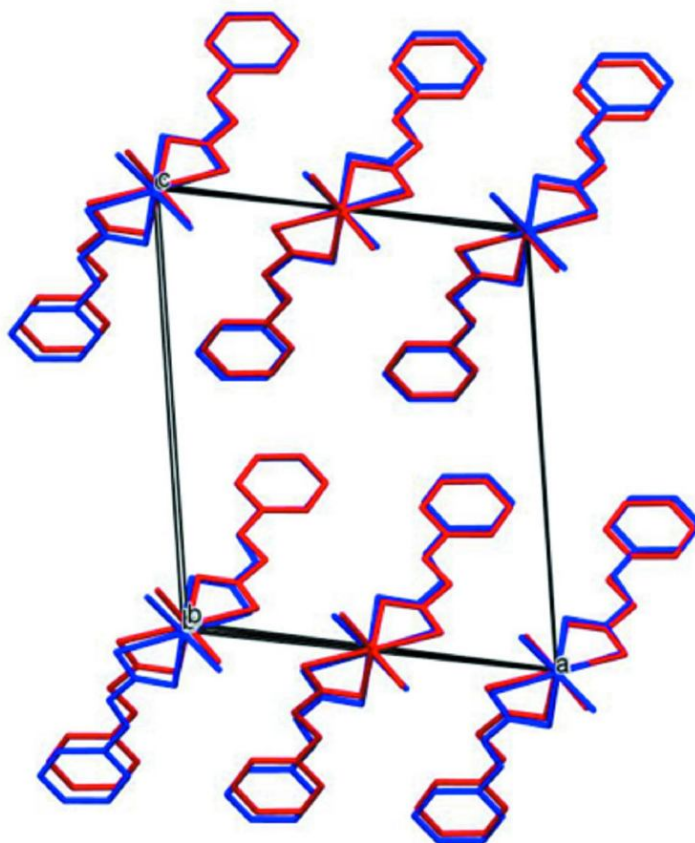


Figure 5

Overlaid stick presentation of diaqua-bis(cinnamic)-cadmium(ii) (blue) and diaqua-bis(phenoxyacetato)-zinc(II) (red) (Smith *et al.*, 1981).

#### Diaquabis(cinnamato- $\kappa^2O,O'$ )cadmium

##### Crystal data

[Cd(C<sub>9</sub>H<sub>7</sub>O<sub>2</sub>)<sub>2</sub>(H<sub>2</sub>O)<sub>2</sub>]

$M_r = 442.72$

Monoclinic, C2

$a = 11.7872$  (12) Å

$b = 5.3498$  (5) Å

$c = 13.8817$  (14) Å

$\beta = 99.913$  (1)°

$V = 862.30$  (15) Å<sup>3</sup>

$Z = 2$

$F(000) = 444$

$D_x = 1.705$  Mg m<sup>-3</sup>

Mo  $K\alpha$  radiation,  $\lambda = 0.71073$  Å

Cell parameters from 4501 reflections

$\theta = 3.0$ – $31.4$ °

$\mu = 1.30$  mm<sup>-1</sup>

$T = 100$  K

Plate, colourless

$0.28 \times 0.09 \times 0.02$  mm



## supplementary materials

### Data collection

Bruker SMART APEX CCD diffractometer	5087 measured reflections
Radiation source: fine focus sealed tube	2531 independent reflections
Graphite monochromator	2529 reflections with $I > 2\sigma(I)$
$\omega$ and $\varphi$ scans	$R_{\text{int}} = 0.021$
Absorption correction: multi-scan (SADABS; Bruker, 2012)	$\theta_{\text{max}} = 31.4^\circ$ , $\theta_{\text{min}} = 3.0^\circ$
$T_{\text{min}} = 0.617$ , $T_{\text{max}} = 0.746$	$h = -17 \rightarrow 16$
	$k = -7 \rightarrow 7$
	$l = -20 \rightarrow 19$

### Refinement

Refinement on $F^2$	Hydrogen site location: difference Fourier map
Least-squares matrix: full	All H-atom parameters refined
$R[F^2 > 2\sigma(F^2)] = 0.020$	$w = 1/[\sigma^2(F_o^2) + (0.0239P)^2]$
$wR(F^2) = 0.046$	where $P = (F_o^2 + 2F_c^2)/3$
$S = 1.05$	$(\Delta/\sigma)_{\text{max}} = 0.002$
2531 reflections	$\Delta\rho_{\text{max}} = 1.09 \text{ e } \text{\AA}^{-3}$
150 parameters	$\Delta\rho_{\text{min}} = -0.42 \text{ e } \text{\AA}^{-3}$
3 restraints	Absolute structure: Flack parameter determined
Primary atom site location: structure-invariant direct methods	using 1059 quotients $[(I^-)-(I)]/[I^+(I^-)]$
Secondary atom site location: difference Fourier map	(Parsons <i>et al.</i> , 2013)
	Absolute structure parameter: 0.018 (14)

### Special details

**Geometry.** All e.s.d.'s (except the e.s.d. in the dihedral angle between two l.s. planes) are estimated using the full covariance matrix. The cell e.s.d.'s are taken into account individually in the estimation of e.s.d.'s in distances, angles and torsion angles; correlations between e.s.d.'s in cell parameters are only used when they are defined by crystal symmetry. An approximate (isotropic) treatment of cell e.s.d.'s is used for estimating e.s.d.'s involving l.s. planes.

### Fractional atomic coordinates and isotropic or equivalent isotropic displacement parameters ( $\text{\AA}^2$ )

	$x$	$y$	$z$	$U_{\text{iso}}^*/U_{\text{eq}}$
Cd1	1.0000	0.42839 (2)	1.0000	0.00869 (6)
O3	0.90970 (17)	0.1439 (4)	1.07385 (17)	0.0152 (4)
H3A	0.943 (3)	0.013 (5)	1.091 (3)	0.020 (10)*
H3B	0.841 (2)	0.127 (10)	1.064 (4)	0.044 (14)*
O1	0.96843 (16)	0.7270 (4)	0.87606 (14)	0.0116 (4)
C1	0.8274 (2)	1.4604 (9)	0.65368 (19)	0.0130 (8)
H1	0.910 (3)	1.43 (2)	0.661 (2)	0.027 (8)*
O2	0.81721 (16)	0.6060 (4)	0.93838 (15)	0.0129 (4)
C2	0.7702 (3)	1.6408 (5)	0.5914 (2)	0.0160 (5)
H2	0.810 (3)	1.741 (8)	0.558 (3)	0.013 (9)*
C3	0.6509 (3)	1.6611 (6)	0.5806 (2)	0.0170 (5)
H3	0.615 (3)	1.787 (8)	0.540 (3)	0.020 (10)*
C4	0.5903 (3)	1.5009 (6)	0.6322 (2)	0.0180 (6)
H4	0.505 (3)	1.511 (7)	0.623 (3)	0.021 (10)*
C5	0.6473 (3)	1.3212 (6)	0.6945 (2)	0.0163 (5)
H5	0.605 (3)	1.209 (8)	0.726 (3)	0.020 (10)*
C6	0.7674 (2)	1.2971 (5)	0.70604 (19)	0.0116 (5)
C7	0.8322 (2)	1.1060 (5)	0.76880 (19)	0.0113 (5)
H7	0.915 (3)	1.100 (7)	0.769 (3)	0.019 (10)*

## supplementary materials

C8	0.7895 (2)	0.9423 (16)	0.82500 (18)	0.0134 (6)
H8	0.708 (3)	0.92 (2)	0.831 (3)	0.031 (9)*
C9	0.8621 (2)	0.7486 (5)	0.88228 (19)	0.0097 (4)

Atomic displacement parameters ( $\text{\AA}^2$ )

	$U^{11}$	$U^{22}$	$U^{33}$	$U^{12}$	$U^{13}$	$U^{23}$
Cd1	0.00734 (9)	0.00637 (10)	0.01212 (10)	0.000	0.00096 (6)	0.000
O3	0.0085 (9)	0.0093 (9)	0.0282 (11)	0.0011 (7)	0.0046 (8)	0.0044 (8)
O1	0.0089 (8)	0.0106 (9)	0.0152 (9)	0.0004 (7)	0.0022 (7)	0.0007 (7)
C1	0.0150 (10)	0.011 (2)	0.0127 (10)	-0.0026 (11)	0.0010 (8)	0.0008 (10)
O2	0.0082 (8)	0.0122 (9)	0.0179 (9)	-0.0003 (7)	0.0013 (7)	0.0047 (7)
C2	0.0233 (14)	0.0117 (12)	0.0128 (12)	-0.0010 (10)	0.0027 (10)	0.0027 (10)
C3	0.0237 (14)	0.0140 (13)	0.0122 (12)	0.0054 (11)	0.0001 (10)	0.0019 (10)
C4	0.0170 (12)	0.0210 (15)	0.0158 (13)	0.0058 (9)	0.0024 (11)	0.0034 (9)
C5	0.0158 (12)	0.0182 (13)	0.0152 (13)	0.0025 (10)	0.0038 (11)	0.0040 (10)
C6	0.0142 (12)	0.0113 (13)	0.0091 (11)	0.0020 (9)	0.0013 (9)	-0.0010 (9)
C7	0.0118 (11)	0.0110 (12)	0.0104 (11)	0.0014 (9)	-0.0002 (9)	0.0001 (9)
C8	0.0109 (9)	0.0130 (15)	0.0158 (9)	0.0069 (19)	0.0015 (7)	0.0020 (19)
C9	0.0100 (11)	0.0082 (11)	0.0103 (11)	-0.0015 (9)	-0.0003 (9)	-0.0012 (9)

Geometric parameters ( $\text{\AA}$ ,  $^\circ$ )

Cd1—O3 <sup>i</sup>	2.208 (2)	O2—C9	1.269 (3)
Cd1—O3	2.208 (2)	C2—C3	1.392 (4)
Cd1—O1 <sup>i</sup>	2.330 (2)	C2—H2	0.89 (4)
Cd1—O1	2.330 (2)	C3—C4	1.391 (4)
Cd1—O2	2.3753 (19)	C3—H3	0.94 (4)
Cd1—O2 <sup>i</sup>	2.375 (2)	C4—C5	1.386 (4)
Cd1—C9	2.708 (3)	C4—H4	0.99 (4)
Cd1—C9 <sup>i</sup>	2.708 (3)	C5—C6	1.403 (4)
O3—H3A	0.82 (2)	C5—H5	0.93 (4)
O3—H3B	0.80 (2)	C6—C7	1.469 (4)
O1—C9	1.276 (3)	C7—C8	1.328 (7)
C1—C2	1.390 (5)	C7—H7	0.98 (4)
C1—C6	1.403 (5)	C8—C9	1.485 (7)
C1—H1	0.98 (4)	C8—H8	0.99 (4)
O3 <sup>i</sup> —Cd1—O3	92.86 (11)	C2—C1—C6	121.4 (3)
O3 <sup>i</sup> —Cd1—O1 <sup>i</sup>	141.89 (7)	C2—C1—H1	124 (5)
O3—Cd1—O1 <sup>i</sup>	99.10 (8)	C6—C1—H1	114 (5)
O3 <sup>i</sup> —Cd1—O1	99.10 (8)	C9—O2—Cd1	90.74 (15)
O3—Cd1—O1	141.89 (7)	C1—C2—C3	119.6 (3)
O1 <sup>i</sup> —Cd1—O1	93.45 (10)	C1—C2—H2	120 (3)
O3 <sup>i</sup> —Cd1—O2	126.04 (8)	C3—C2—H2	121 (2)
O3—Cd1—O2	87.88 (7)	C4—C3—C2	119.7 (3)
O1 <sup>i</sup> —Cd1—O2	90.65 (7)	C4—C3—H3	122 (2)
O1—Cd1—O2	55.96 (7)	C2—C3—H3	118 (2)
O3 <sup>i</sup> —Cd1—O2 <sup>i</sup>	87.88 (7)	C5—C4—C3	120.8 (3)
O3—Cd1—O2 <sup>i</sup>	126.04 (8)	C5—C4—H4	120 (2)

## supplementary materials

O1 <sup>i</sup> —Cd1—O2 <sup>i</sup>	55.96 (7)	C3—C4—H4	120 (2)
O1—Cd1—O2 <sup>i</sup>	90.65 (7)	C4—C5—C6	120.4 (3)
O2—Cd1—O2 <sup>i</sup>	132.85 (10)	C4—C5—H5	119 (3)
O3 <sup>i</sup> —Cd1—C9	116.30 (8)	C6—C5—H5	120 (3)
O3—Cd1—C9	115.41 (8)	C5—C6—C1	118.2 (3)
O1 <sup>i</sup> —Cd1—C9	90.85 (7)	C5—C6—C7	122.9 (3)
O1—Cd1—C9	28.08 (7)	C1—C6—C7	118.9 (3)
O2—Cd1—C9	27.95 (7)	C8—C7—C6	126.6 (3)
O2 <sup>i</sup> —Cd1—C9	112.16 (8)	C8—C7—H7	117 (2)
O3 <sup>i</sup> —Cd1—C9 <sup>i</sup>	115.41 (8)	C6—C7—H7	116 (2)
O3—Cd1—C9 <sup>i</sup>	116.30 (8)	C7—C8—C9	122.2 (2)
O1 <sup>i</sup> —Cd1—C9 <sup>i</sup>	28.08 (7)	C7—C8—H8	127 (5)
O1—Cd1—C9 <sup>i</sup>	90.85 (8)	C9—C8—H8	111 (5)
O2—Cd1—C9 <sup>i</sup>	112.16 (8)	O2—C9—O1	120.3 (2)
O2 <sup>i</sup> —Cd1—C9 <sup>i</sup>	27.96 (7)	O2—C9—C8	119.0 (3)
C9—Cd1—C9 <sup>i</sup>	101.50 (11)	O1—C9—C8	120.6 (2)
Cd1—O3—H3A	119 (3)	O2—C9—Cd1	61.30 (13)
Cd1—O3—H3B	123 (4)	O1—C9—Cd1	59.28 (13)
H3A—O3—H3B	112 (5)	C8—C9—Cd1	174.6 (3)
C9—O1—Cd1	92.64 (15)		

Symmetry code: (i)  $-x+2, y, -z+2$ .Hydrogen-bond geometry ( $\text{\AA}, ^\circ$ )

$D-H\cdots A$	$D-H$	$H\cdots A$	$D\cdots A$	$D-H\cdots A$
O3—H3A $\cdots$ O1 <sup>ii</sup>	0.82 (2)	1.86 (2)	2.679 (3)	174 (4)
O3—H3B $\cdots$ O2 <sup>iii</sup>	0.80 (2)	1.86 (3)	2.658 (3)	171 (5)

Symmetry codes: (ii)  $-x+2, y-1, -z+2$ ; (iii)  $-x+3/2, y-1/2, -z+2$ .

## Synthesis and X-ray crystal structure of novel 2D-Mn(II) coordination polymer with 4,4'-trimethylene dipyridine and 3-nitrophthalate as ligands

Sirinart Chooset<sup>1</sup>, Anob Kantacha<sup>2</sup>, Arunpatcha Nimthong<sup>3</sup>, Matthias Zeller<sup>3</sup>, and Sumpun Wongnawa<sup>1\*</sup>

<sup>1</sup>Department of Chemistry, Faculty of Science, Prince of Songkla University, Hat Yai, Songkhla, 90112, Thailand

<sup>2</sup>Department of Chemistry, Faculty of Science, Thaksin University, Papayom, Phatthalung, 93110, Thailand

<sup>3</sup>Department of Chemistry, Youngstown State University, One University Plaza, Youngstown, OH 44555, USA

\*E-mail: sumpun.w@psu.ac.th

$[\text{Mn}_2(\mu\text{-}4,4'\text{-trimethylenedipyridine})(\mu\text{-}3\text{-nitrophthalate})_2(\text{H}_2\text{O})_4]_n$  was synthesized using  $\text{MnCl}_2 \cdot 4\text{H}_2\text{O}$ , 4, 4'-trimethylenedipyridine, and 3-nitrophthalic acid as starting materials. The complex was investigated by Fourier-transformed infrared spectroscopy (FT-IR), single crystal X-ray diffraction (SCXRD), elemental analysis, powder X-ray diffraction (PXRD), diffused reflectance spectroscopy (DRS), photoluminescent spectroscopy (PL), and thermogravimetric analysis (TGA). The complex crystallized in orthorhombic system in the space group  $\text{Aba}2$  with cell parameters  $a = 30.1451(10) \text{ \AA}$ ,  $b = 9.8718(3) \text{ \AA}$ ,  $c = 11.3258(4) \text{ \AA}$ ,  $V = 3370.40(19) \text{ \AA}^3$ , and  $Z=4$ . The complex exhibited a 2D structure with each Mn(II) octahedrally coordinated to three oxygen atoms from two 3-nitrophthalate units, two oxygen atoms from two water molecules, and one nitrogen atom from 4,4'-trimethylenedipyridine.

**Keywords** Manganese(II) complexes, Supramolecular chemistry, Coordination polymer, 2-dimensional polymer, Dicarboxylate complexes



## Introduction

Large proportion of current interest is focused on metal-organic coordination polymers due to their potential applications as functional materials in many fields such as catalysis [1-2], gas storage [3-4], ion-exchange [5-6], magnetism [7], and molecular sensing [8] etc. Synthesis of these compounds is highly affected by several factors such as coordination geometry of metal ions, structure of organic ligands, solvent system, pH value, temperature, counter anions, and ligand-to-metal ratio [9].

Dicarboxylic acids form an important class of ligands in the chemistry of coordination polymers, often dicarboxylic acids such as 1,2-phthalic, 1,3-phthalic, and 1,4-phthalic acids are extensively used. Carboxylate group can coordinate with one, two or more metal centers leading to the formation of polynuclear complexes ranging from discrete entities to 1-, 2-, and 3-dimensional systems [11, 27]. 3-nitrophthalic acid, as a derivative of 1,2-phthalic acid, contains four potential coordination sites which can act in a monodentate, bidentate, or bridging fashion through two carboxylic groups coordinating to metals (see Chart 1). The nitro group ( $-\text{NO}_2$ ), as an electron-withdrawing group, not only acts as a hydrogen bond acceptor, but also creates spatial effects in the formation of polymeric networks.

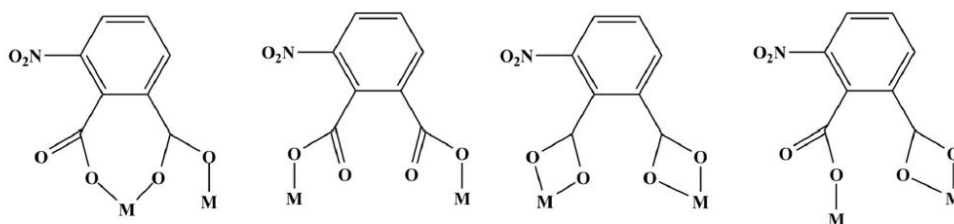


**Chart 1** Possible coordinating modes of 3-nitrophthalate ligand

The 4,4'-bipyridine (4,4'-bipy) derivatives such as 4,4'-trimethylenedipyridine show good coordinating ability and flexibility, so that the resulting coordination polymers can adapt to different conformations of the polymethylene chain. By twisting the trimethylene group ( $-\text{CH}_2-\text{CH}_2-\text{CH}_2-$ ), 4,4'-trimethylenedipyridineligand can assume TT, TG, GG, and GG' conformations (where T = trans, G = gauche, see Chart 2).

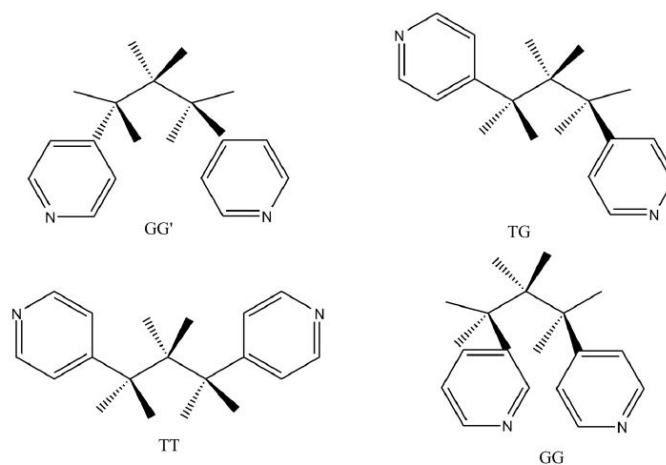


**Chart 2** TT, TG, GG, and GG' conformations (T = trans, G=gauche) of 4, 4'-trimethylenedipyridine

Manganese complexes play important role in bioinorganic chemistry. A great number of manganese carboxylate complexes have been studied with the intention of understanding basic exchange mechanisms in the context of dimensionality, coordination, valency, nearest neighbor distance, hydration, phase, frequency response, temperature, and applied magnetic field [10].

In this work, we report the synthesis and structural characterization of a new Mn(II) complex with 4, 4'-trimethylenedipyridine and 3-nitrophthalic acid as ligands. Several techniques were used to characterize the product and its molecular structure, and the results are presented below.

## Experimental

MnCl<sub>2</sub>·4H<sub>2</sub>O, 4,4'-trimethylenedipyridine, 3-nitrophthalic acid, and all the solvents were purchased from commercial sources and used without further purification. FT-IR spectra were obtained in a KBr pellet on a Perkin-Elmer Spectrum One Fourier-transformed infrared spectrophotometer between 4000-400 cm<sup>-1</sup>. Thermogravimetric analysis (TGA) was carried out on a Perkin Elmer TGA 7 equipment in the range 50-1000 °C with a heating rate of 10 °C/min under N<sub>2</sub> atmosphere. Elemental analysis for carbon, hydrogen, and nitrogen was performed on a Perkin-Elmer 240 elemental analyzer. Powder X-ray diffraction measurements were carried out using an X'Pert MPD PHILIPS X-ray diffractometer with Cu Kα radiation in the 2θ range of 5-50° to check phase purity. Solid state UV-Vis diffused reflectance spectra were recorded with a Shimadzu 2450 PC UV-Vis recording spectrophotometer. Fluorescence spectra were recorded with a PerkinElmer LS55 Luminescence spectrometer at room temperature.

### Synthesis of $[\text{Mn}_2(\mu\text{-4,4'-trimethylenedipyridine})(\mu\text{-3-nitrophthalate})_2(\text{H}_2\text{O})_4]_n$

To a stirred solution of  $\text{MnCl}_2 \cdot 4\text{H}_2\text{O}$  (0.1979 g, 1 mmol) in 7 mL of water was added 4,4'-trimethylenedipyridine (0.20 g, 1.0 mmol) in 5 mL of ethanol to give a colorless solution. Then, 3-nitrophthalic acid (0.21 g, 1.0 mmol) in 15 mL of water was added to give a yellow solution, and the pH was adjusted to 7 with 1 M NaOH. The solution was stirred at room temperature for 24 h, filtered, and left to evaporate at room temperature. After several days, colorless block crystals suitable for X-ray analysis were obtained in 52 % yield based on manganese. Anal.Calc. for  $\text{C}_{29}\text{H}_{28}\text{Mn}_2\text{N}_4\text{O}_{16}$  (798.43); C, 43.62; H, 3.50; N, 7.01 %. Found: C, 43.92; H, 3.46; N, 6.96 %. FT-IR spectrum (KBr disc,  $\text{cm}^{-1}$ ) 3420s, 3063m, 2948m, 1597s, 1542s, 1466m, 1425m, 1386s, 1349s, 1217m, 1164w, 1067w, 1014m, 931m, 855m, 835m, 803m, 786m, 754s, 713s, 619w, 590w, 509m, 420m.

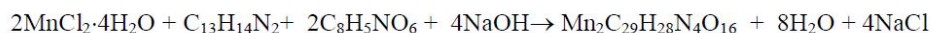
### X-ray crystallography

A crystal of the title complex with suitable size was picked up and mounted on a Bruker Smart APEX II CCD diffractometer. Absorption corrections were based on symmetry equivalent reflections using the SADABS program [12]. A total of 13624 reflections for complex were collected, of which 4737 were unique ( $R_{\text{int}} = 0.024$ ) and 4613 were observed with  $I > 2\sigma(I)$  for the former. The molecular structure was solved by direct method and refined by full-matrix least squares on  $F^2$  using SHELXS-97 and SHELXL-2013 [13]. All H atoms positions were refined. Positions of carbon bound H atoms were freely refined, O bound H atoms were refined with an O—H distances restrained at 0.84 (2) Å. All  $U_{\text{iso}}(\text{H})$  values were refined. All packing diagrams and wireframe plots were produced using the Mercury 3.5 software program.

## Results and Discussion

### Structural investigation

The formation of new Mn(II) complex may be described by the following equation :



The product was air stable and insoluble in water and several organic solvents such as ethanol, methanol, acetone, chloroform, N,N-dimethylformamide, and dimethylsulfoxide. Crystal data as well as refinement details of the complex are given below while the selected bond lengths and bond angles are given in Table 1.

Empirical formula =  $\text{C}_{29}\text{H}_{28}\text{Mn}_2\text{N}_4\text{O}_{16}$ , FW=798.43, T=100(2) K, orthorhombic,  $\text{Aba2}$ ,  $a = 30.1451(10)$ ,  $b = 9.8718(3)$ ,  $c = 11.3258(4)$  Å,  $\alpha = \beta = \gamma = 90^\circ$ ,  $V = 3370.40(19)$  Å<sup>3</sup>,  $Z = 4$ ,  $\rho_{\text{calc}} = 1.573$  g/cm<sup>3</sup>,  $\mu = 0.829$  mm<sup>-1</sup>,  $F(000) = 1632.0$ , Crystal size =  $0.450 \times 0.310 \times 0.280$  mm, Radiation Mo  $K\alpha$  ( $\lambda = 0.71073$ ),  $2\theta$  range for data collection  $5.406$  to  $61.044^\circ$ , Index ranges  $-42 \leq h \leq 31$ ,  $-10 \leq k \leq$



14,  $-14 \leq l \leq 16$ , Reflections collected 13624, Independent reflections 4737 [ $R_{\text{int}} = 0.0239$ ,  $R_{\text{sigma}} = 0.0321$ ], Data/restraints/parameters 4737/106/241, Goodness-of-fit on  $F^2 = 1.117$ , Final R indexes [ $I \geq 2\sigma(I)$ ]  $R_1 = 0.0273$ ,  $wR_2 = 0.0642$ , Final R indexes [all data]  $R_1 = 0.0283$ ,  $wR_2 = 0.0646$ , Largest diff. peak/hole =  $0.45/-0.39 \text{ e } \text{\AA}^{-3}$ .

**Table 1** Selected bond lengths and angles of  $[\text{Mn}_2(\mu\text{-}4,4'\text{-trimethylenedipyridine})(\mu\text{-}3\text{-nitrophthalate})_2(\text{H}_2\text{O})_4]_n$

Bond lengths		Bond angles	
Mn1—O3	2.1397 (17)	O3—Mn1—O7	82.61 (7)
Mn1—O7	2.1640 (14)	O3—Mn1—O8	177.99 (7)
Mn1—O8	2.1703 (18)	O7—Mn1—O8	96.73 (7)
Mn1—O1 <sup>i</sup>	2.2068 (15)	O3—Mn1—O1 <sup>i</sup>	95.02 (7)
Mn1—O2	2.2248 (15)	O7—Mn1—O1 <sup>i</sup>	86.26 (6)
Mn1—N1	2.2539 (19)	O8—Mn1—O1 <sup>i</sup>	86.82 (7)
O1—Mn1 <sup>ii</sup>	2.2069 (15)	O3—Mn1—O2	85.36 (6)
		O7—Mn1—O2	164.81 (7)
		O8—Mn1—O2	95.59 (6)
		O1 <sup>i</sup> —Mn1—O2	85.59 (6)
		O3—Mn1—N1	90.51 (7)

Symmetry codes: (i)  $-x+1/2, y+1/2, z$ ; (ii)  $-x+1/2, y-1/2, z$ .

According to the X-ray crystallographic data, the complex crystallizes in a non-centrosymmetric space group *Aba2* in the orthorhombic system as shown in Fig. 1. The structure of complex can be described as a two-dimensional coordination polymer (symmetry operations  $-x+1/2, y+1/2, z$ ,  $-x+1/2, y-1/2, z$  and  $-x+1, -y+1, z$ ) with the dinuclear manganese(II) as nodes while 4, 4'-trimethylenedipyridine and 3-nitrophthalate act as the linkers. Both  $\text{Mn}^{2+}$  ions are coordinated by three oxygen atoms from two 3-nitrophthalate units and two oxygen atoms from two water molecules. Coordination of the nitrogen atom from a pyridine ring completes octahedral geometry (Fig. 1). The Mn-O distances associated with the chelating/bridging 3-nitrophthalate ligands range from 2.1397 (17) to 2.2248 (15) Å similar to those found in  $[\text{Mn}(\text{H}_2\text{O})_2(3\text{-nitrophthalate})]$  [14]. The Mn-N distance of 2.2539 (19) Å is in good agreement with the literature reports [15-17, 25]. The transoid and cisoid angles subtended at the  $\text{Mn}^{2+}$  ions fit in the range of  $164.81 (7)^\circ$ -  $177.99 (7)^\circ$  and  $82.61 (7)^\circ$ -  $96.73 (7)^\circ$  (Table 2), respectively, exhibiting slight departure from the corresponding value expected for a regular octahedron (theoretical values:  $180^\circ$  and  $90^\circ$ ), implying slight distortion of the octahedral coordination. One of the two carboxylate groups of 3-nitrophthalate (Fig. 1) adopts terminal monodentate bonding mode while the other bridges to neighboring Mn to form 2D polymer propagating along the *c* axis (Fig.2). Two Mn...Mn distances linked by 3-nitrophthalate and 4, 4'-trimethylenedipyridine were found at 5.558(6) and 13.2737(9) Å, respectively. In this structure, 4,4'-trimethylenedipyridine molecule adopted a TT



(*trans-trans*) conformation with the N---N distance of 10.768 Å, similar to those reported in the literatures [18,24,26].

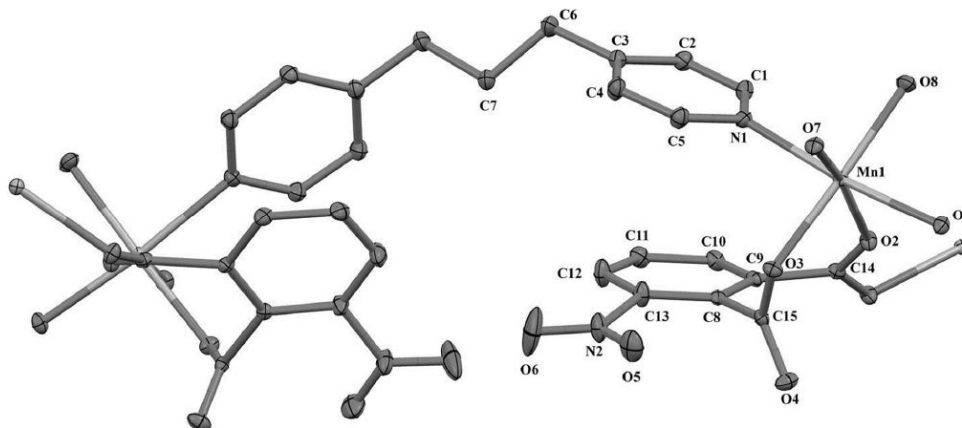


**Fig.1** Molecular structure of  $[\text{Mn}_2(\mu\text{-}4,4'\text{-trimethylenedipyridine})(\mu\text{-}3\text{-nitrophthalate})_2(\text{H}_2\text{O})_4]_n$  (ellipsoid probability at 40%). Only the minor component of the disorder is shown.

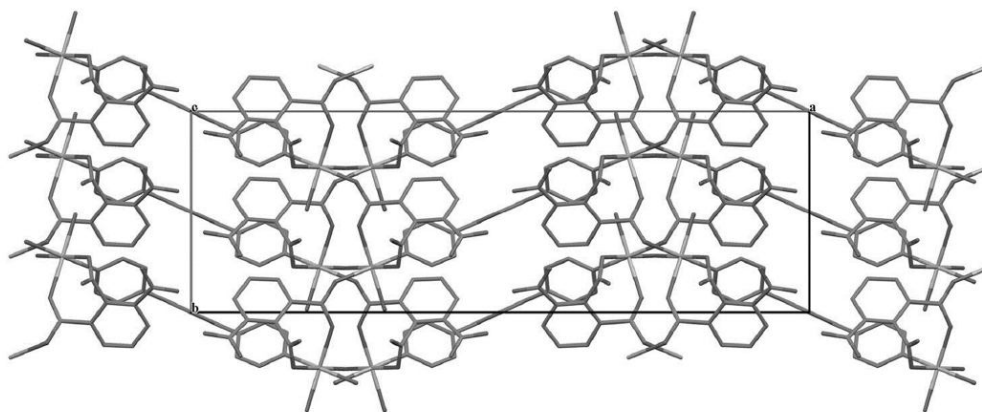


**Fig. 2** Packing diagram of two-dimensional framework of  $[\text{Mn}_2(\mu\text{-}4,4'\text{-trimethylenedipyridine})(\mu\text{-}3\text{-nitrophthalate})_2(\text{H}_2\text{O})_4]_n$  (H atoms omitted for clarity; plotted down *c* axis)

The nitro group on 3-nitrophthalate ligand (N2, O5, O6) was modeled as a disordered group over two orientations and was refined to give an occupancy ratio of 0.344(5) : 0.656(5).

Each  $\text{Mn}^{2+}$  ion is linked to two adjacent ions through single syn-anti carboxylates from 3-nitrophthalate ligands. The crystal-packed structure shows a 3D supramolecular network formed by the hydrogen bonds between the coordinated water molecules and the oxygen atoms of the carboxylates. The supramolecular unit is linked by the weak intermolecular H-bonding using  $\text{O7}\cdots\text{O2}^i$ ,  $\text{O7}\cdots\text{H7B}\cdots\text{O4}^{iv}$ ,  $\text{O8}\cdots\text{H8A}\cdots\text{O1}^{iv}$ , and  $\text{O8}\cdots\text{H8B}\cdots\text{O4}^v$  to generate a 3D supramolecular network as shown in Fig. 3. Hence, the crystal packing is stabilized by intermolecular hydrogen bonds. The details of the intermolecular H-bonding are listed in Table 2.

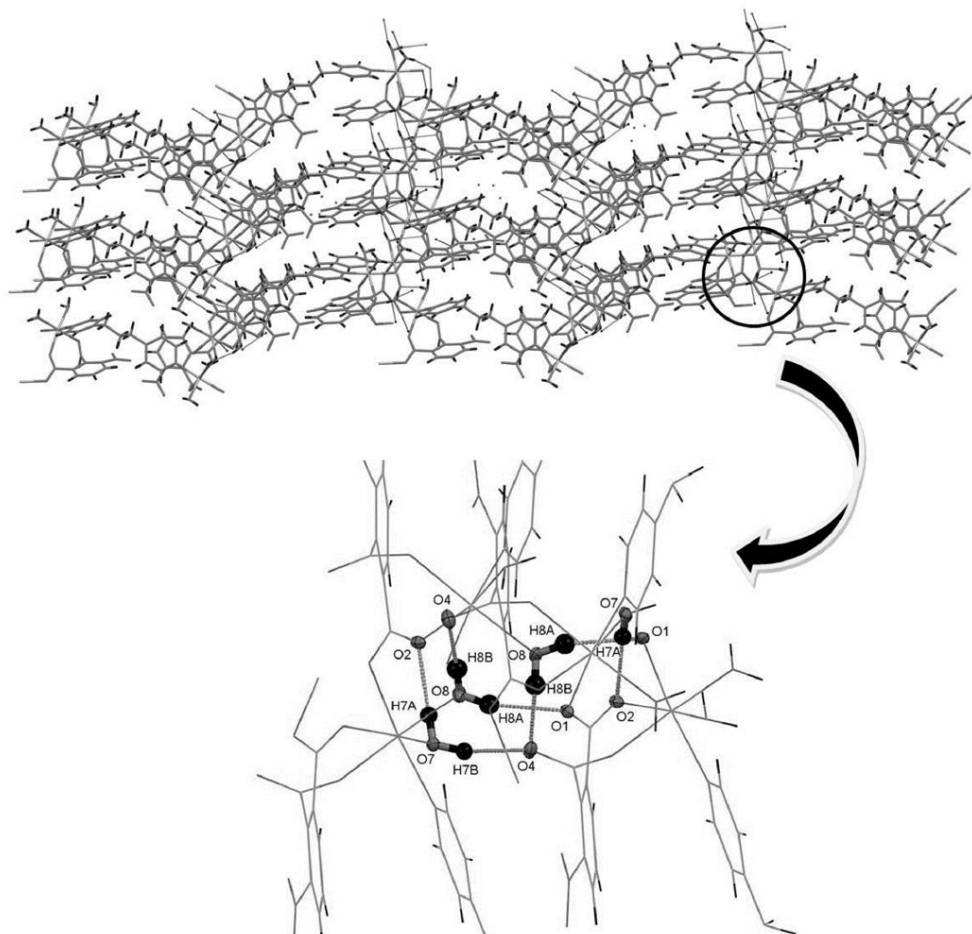


**Fig. 3** View of the 3D supramolecular network via weak O—H...O interactions

**Table 2** Hydrogen-bond geometry ( $\text{\AA}$ ,  $^\circ$ ) of  $[\text{Mn}_2(\mu\text{-}4,4'\text{-trimethylenedipyridine})(\mu\text{-}3\text{-nitrophenalate})_2(\text{H}_2\text{O})_4]_n$

D—H...A	D—H	H...A	D...A	D—H...A
O7—H7A...O2 <sup>i</sup>	0.84	1.95	2.769 (2)	163
O7—H7B...O4 <sup>iv</sup>	0.84	1.81	2.623 (2)	162
O8—H8A...O1 <sup>iv</sup>	0.83	2.09	2.898 (2)	165
O8—H8B...O4 <sup>v</sup>	0.82	1.88	2.693 (2)	169

Symmetry codes: (i)  $-x+1/2, y+1/2, z$ ; (iv)  $x, y+1/2, z+1/2$ ; (v)  $-x+1/2, y, z+1/2$ .

### Infrared spectroscopy

The IR spectrum of  $[\text{Mn}_2(\mu\text{-}4,4'\text{-trimethylenedipyridine})(\mu\text{-}3\text{-nitrophthalate})_2(\text{H}_2\text{O})_4]_n$  complex is displayed in Fig. 4. The bands at  $3420\text{ cm}^{-1}$  was assigned to the symmetric OH stretching of water molecules. The unsaturated and saturated C-H stretching vibrations ( $\nu_{\text{=CH}}$  and  $\nu_{\text{CH}}$ ) appeared at  $3063\text{ cm}^{-1}$  and  $2948\text{ cm}^{-1}$ , respectively. The absence of the characteristic band of C=O at  $1715\text{-}1600\text{ cm}^{-1}$  (in free ligand) indicated the complete deprotonation of the carboxylic group of 3-nitrophthalic acid by NaOH upon coordination to  $\text{Mn}^{2+}$ . Two sets of C=O stretching vibrations at  $1542 / 1359$  and  $1597 / 1389\text{ cm}^{-1}$  which can be assigned to  $\nu_{\text{as(COO)}}$  and  $\nu_{\text{s(COO)}}$  vibrations of three types of 3-nitrophthalate ligands. The C=O stretching vibration of 3-nitrophthalate ligand in complex as compared with the same mode in free 3-nitrophthalic acid molecule shows significant hypsochromic shift due to the coordination interactions. The two values of  $\Delta\nu_{\text{COO}}$ , i.e.  $\nu_{\text{as(COO)}} - \nu_{\text{sym(COO)}}$ , were found to be  $183$  and  $208\text{ cm}^{-1}$  indicating monodentate and bridging carboxylate group of 3-nitrophthalate ligand, respectively [19-21]. The  $\text{-N=C-}$  stretching vibration mode of the 4, 4'-trimethylenedipyridine ligand appears at  $1565\text{ cm}^{-1}$ . For the  $\text{-NO}_2$  moieties, both the symmetric stretching,  $\nu_{\text{s(NO}_2\text{)}}$ , at  $1390$  and  $1386\text{ cm}^{-1}$  and asymmetric stretching,  $\nu_{\text{as(NO}_2\text{)}}$ , at  $1530$  and  $1507\text{ cm}^{-1}$ , were observed. The band at  $754\text{ cm}^{-1}$  was assigned to the out-of-plane C-H vibration of the benzene ring of the organic ligand [14]. The FT-IR information, therefore, was consistent with the results from the X-ray single crystal analysis of the complex.

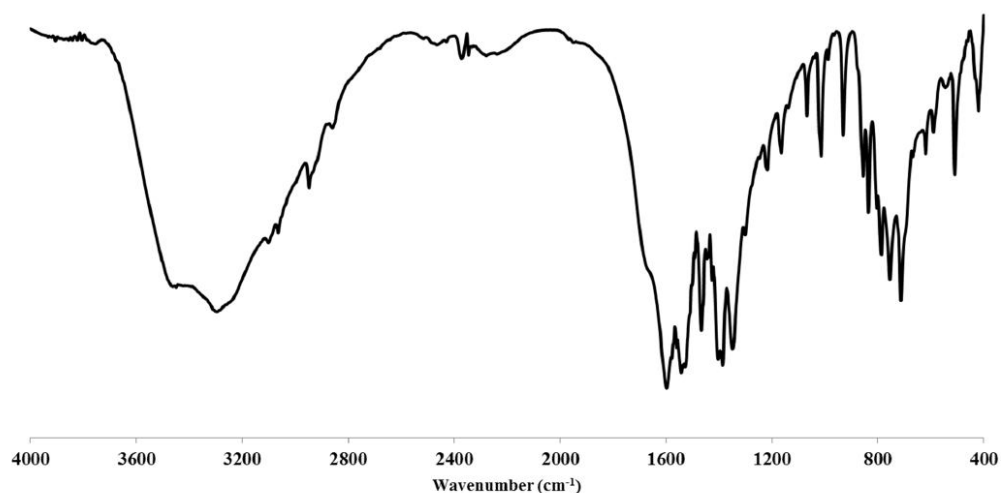


**Fig.4** The infrared spectra of  $[\text{Mn}_2(\mu\text{-}4,4'\text{-trimethylenedipyridine})(\mu\text{-}3\text{-nitrophthalate})_2(\text{H}_2\text{O})_4]_n$

### X-Ray powder diffraction and thermogravimetric analysis

Thermal stability of complex was examined by TG analysis under  $N_2$  atmosphere in the temperature range 50-1000 °C (Fig 5). The first decomposition (9.31 %) in the range 108 - 166 °C was assigned to the removal of four water molecules per formula unit (calculated 9.01 %) indicating dehydration of the complex. The second weight loss of 26.44 % occurred in the range 166-352 °C corresponded to loss of the 3-nitrophthalate ligand (cal. 26.92 %). The third weight loss was 21.01 % in the range 329-680 °C corresponding to loss of 4, 4'-trimethylenedipyridine ligand (cal. 24.81 %). On further heating the sample lost its weight continuously and the remained black residue was taken as a Mn oxide [14, 22-23].

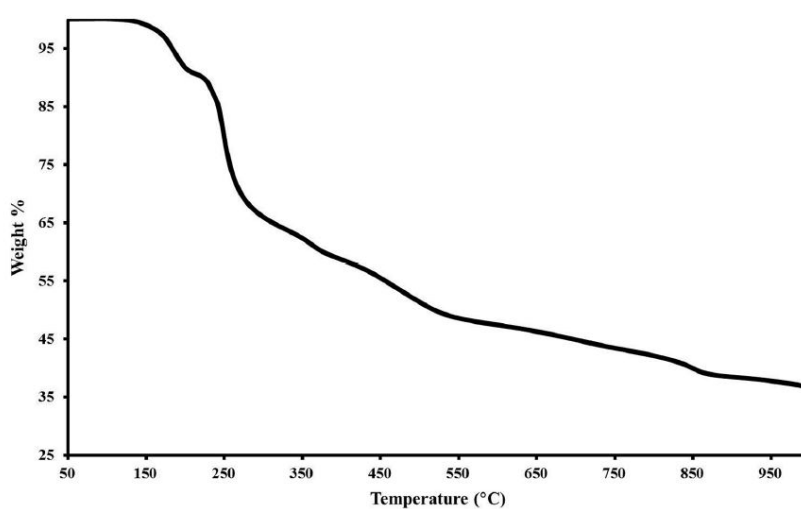


**Fig. 5** The TGA curve of  $[Mn_2(\mu-4,4'\text{-trimethylenedipyridine})(\mu-3\text{-nitrophthalate})_2(H_2O)_4]_n$

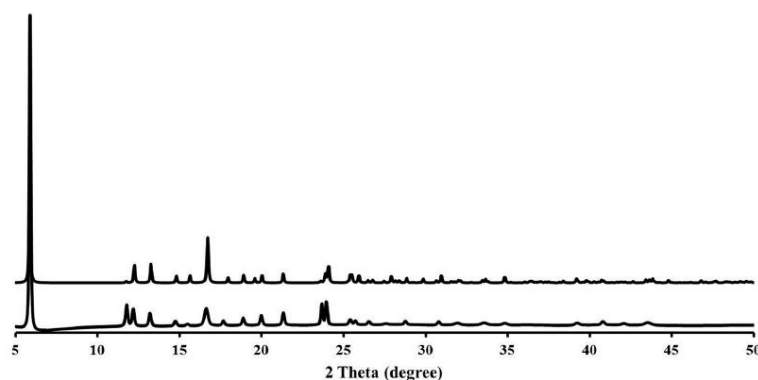


**Fig. 6** The simulated and measured PXRD patterns for  $[Mn_2(\mu-4,4'\text{-trimethylenedipyridine})(\mu-3\text{-nitrophthalate})_2(H_2O)_4]_n$



PXRD pattern of the complex agreed with the simulated pattern (Fig. 6) obtained from the single-crystal data using Mercury 3.5, indicating good phase purity of the synthesized product. The differences in the intensity may be due to the preferred orientation of the crystalline powder sample.

#### UV/vis absorption spectroscopy

The solid-state UV/vis spectra of 3-nitrophthalic acid and the complex at room temperature with BaSO<sub>4</sub> as the background are displayed in Fig. 7. The acid featured a strong absorption band in the ultraviolet region of 250-450 nm which can be assigned to the intraligand  $\pi$ - $\pi^*$  and  $n$ - $\pi^*$  transitions of the aromatic rings. No additional peaks were observed for Mn(II) complex due to the d-d spin-forbidden transition within the high spin  $d^5$  configuration causing the  ${}^6A_{1g}$  ground state to be doubly forbidden [28]. (Due to its unsuitableness for sample preparation, the spectrum of free 4,4'-trimethylenedipyridine ligand was not recorded.)

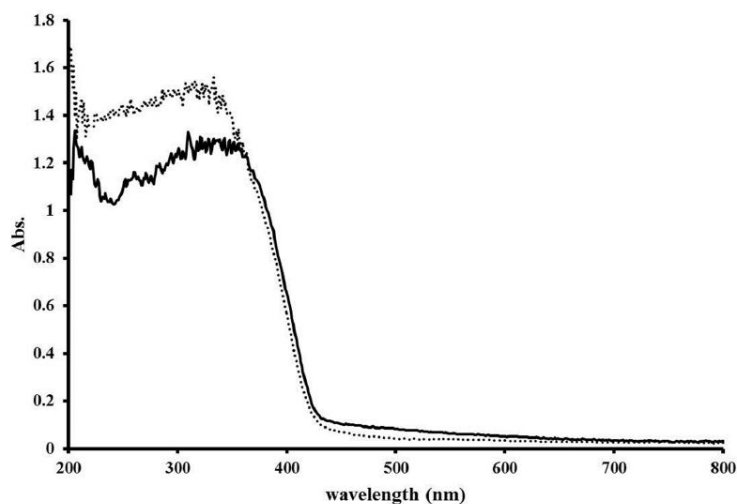


**Fig. 7** UV-vis absorption spectra for  $[Mn_2(\mu\text{-}4,4'\text{-trimethylenedipyridine})(\mu\text{-}3\text{-nitrophthalate})_2(H_2O)_4]_n$  (.....) and 3-nitrophthalic acid (—)

#### Photoluminescent spectroscopy

The emission spectra of the complex and the ligands were also investigated as shown in Fig. 8 with emission and excitation bands listed in Table 3. The complex exhibited a 25 nm blue-shift compared with free 4,4'-trimethylenedipyridine which might be assigned to a ligand to metal charge transfer (LMCT) after coordination. The fluorescent emission of 3-nitrophthalate ligand was not observable. The complex fluorescent emission is rather weak which could be the result of quenching by the strong electron withdrawing group of the carboxyl and nitro groups [29].

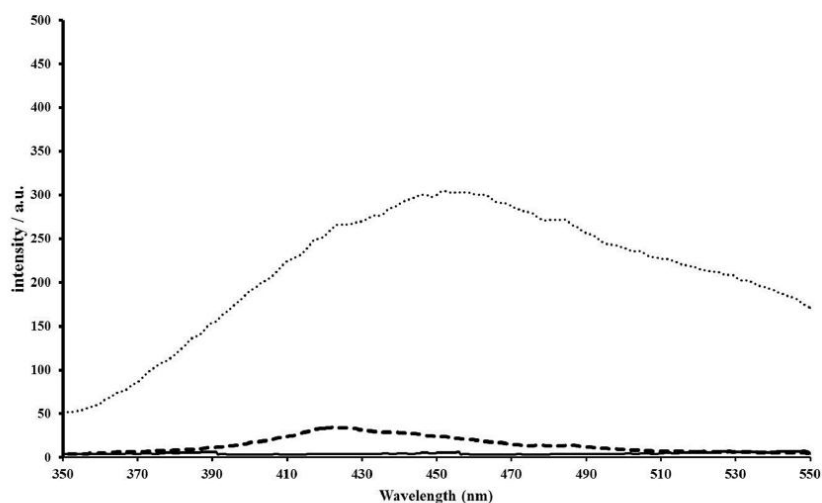


**Fig. 8** Solid-state emission spectra of  $[\text{Mn}_2(\mu\text{-}4,4'\text{-trimethylenedipyridine})(\mu\text{-}3\text{-nitrophthalate})_2(\text{H}_2\text{O})_4]_n$  (—), 4, 4'-trimethylenedipyridine (.....) and 3-nitrophthalic acid (---)(excitation at 327 nm)

**Table 3** Emission and excitation bands for 4, 4'-trimethylenedipyridine and complex

Ligand/complex	4, 4'-trimethylenedipyridine	complex
$\lambda_{\text{em}}$	445	420
$\lambda_{\text{ex}}$	327	327

## Conclusions

The complex  $[\text{Mn}_2(\mu\text{-}4,4'\text{-trimethylenedipyridine})(\mu\text{-}3\text{-nitrophthalate})_2(\text{H}_2\text{O})_4]_n$  was prepared from Mn(II) salt, 4, 4'-trimethylenedipyridine, and 3-nitrophthalic acid. The structure was obtained using single crystal X-ray diffraction which showed each Mn(II) coordinated to oxygen atoms from 3-nitrophthalic acid, water, and 4,4'-trimethylenedipyridine molecule to form an octahedral geometry. A 2D network is formed via the bridging by 3-nitrophthalate ligand linking adjacent manganese centers by syn-anti carboxylate groups. FT-IR spectroscopy, elemental and thermogravimetric analyses agree with the structure obtained from the single crystal X-ray diffraction.

### Supplementary materials

CCDC data 1404562 contain the supplementary crystallographic data for this paper. These data can be obtained free of charge via <http://www.ccdc.cam.ac.uk>, or from the Cambridge Crystallographic Data Centre (CCDC), 12 Union Road, Cambridge, CB2,1EZ, UK; fax: +44(0)1223-336033; e-mail: [deposit@ccdc.cam.ac.uk](mailto:deposit@ccdc.cam.ac.uk).

### Acknowledgments

This work was supported by the Songklanagarind Scholarship for Graduate Studies from Prince of Songkla University. We also would like to extend our thanks to the Department of Chemistry both at Youngstown State University and Prince of Songkla University, for providing X-ray and other supporting facilities.

### References

- [1] S. J. Hong, J. S. Seo, J. Y. Ryu, J. H. Lee, C. Kim, S.-J. Kim, Y. Kim, and A. J. Lough, *J. Mol. Struct.*, **22**, 751 (2005).
- [2] C.-D. Wu, A. Hu, L. Zhang, and W. Lin, *J. Am. Chem. Soc.*, **127**, 8940 (2005).
- [3] A. J. Fletcher, E. J. Cussen, D. Bradshaw, M. J. Rosseinsky, and K. M. Thomas, *J. Am. Chem. Soc.*, **126**, 9750 (2004).
- [4] E.-Y. Choi, K. Park, C.-M. Yang, H. Kim, J.-H. Son, S. W. Lee, Y. H. Lee, D. Min, and Y.-U. Kwon, *Chem. Eur. J.*, **10**, 5535 (2004).
- [5] K. S. Min, and M. P. Suh, *J. Am. Chem. Soc.*, **122**, 6834 (2000).
- [6] J. Fan, L. Gan, H. Kawaguchi, W.-Y. Sun, K.-B. Yu, and W.-X. Tang, *Chem. Eur. J.*, **9**, 3965 (2003).
- [7] L. M. Toma, R. Lescouëzec, J. Pasán, C. Ruiz-Pérez, J. Vaissermann, J. Cano, R. Carrasco, W. Wernsdorfer, F. Lloret, and M. Julve, *J. Am. Chem. Soc.*, **128**, 4842 (2006).
- [8] C. Jiao, F. Li, J. Zhang, Z. Li, S. Wang, Z. Wang, H. Yu, Z. Li, S. Liu, Z. Wang, X. Jiang, L. Sun, and F. Xu, *Dalton Trans.*, **42**, 1346 (2013).
- [9] S. P. Jang, J. I. Poong, S. H. Kim, T. G. Lee, J. Y. Noh, C. Ki, Y. Kim, and S.-J. Kim, *Polyhedron*, **33**, 194 (2012).
- [10] M. Bremer, J. Sandstrom, P. Jeppson, B. Anderson, M. Kaderbhai, K. Orhan, S. Zinoveva, L. Shengming, D.L. Schulz, and A.N. Caruso, *Polyhedron*, **26**, 2110 (2007)
- [11] R. Wang, D. Yuan, F. Jiang, L. Han, S. Gao, and M. Hong, *Eur. J. Inorg. Chem.*, **8**, 1649 (2006).
- [12] Bruker (2012). *APEX2, SAINT and SADABS* Bruker AXS Inc., Madison, Wisconsin,

USA.

- [13] G. M. Sheldrick, *Acta Cryst.*, **A64**, 112 (2008).
- [14] X. Yu, S. Ni, D. Zhang, Y. Zheng, and H. Zhu, *J. Mol. Struct.*, **1076**, 426 (2014).
- [15] C.-J. He, W.-Y. Wang, and Y.-F. Wang, *Synth React Inorg M.*, **44**, 492 (2014).
- [16] G.-L. Li, W.-D. Yin, G.-Z. Liu, L.-F. Ma, and L.-Y. Wang, *J. Solid State Chem.*, **220**, 1 (2014).
- [17] S. Konar, S. C. Manna, E. Zangrando, T. Mallah, J. Ribas, and N. R. Chaudhuri, *Eur. J. Inorg. Chem.*, **21**, 4202 (2004).
- [18] B. Li, G. Li, D. Liu, Y. Peng, X. Zhou, J. Hua, Z. Shi, and S. Feng, *CrystEng Comm.*, **13**, 1291 (2011).
- [19] M. Kalinowska, R. S'wislocka, and W. Lewandowski, *J Mol Struct.*, **993**, 404 (2011).
- [20] R. P. Sharma, A. Saini, P. Venugopalan, J. Jezierska, and V. Ferretti, *Inorg Chem Commun.*, **20**, 209 (2012).
- [21] G. B. Deacon, M. Forsyth, P. C. Junk, S. G. Leary, and W. W. Lee, *Z. Anorg. Allg. Chem.*, **635**, 833 (2009).
- [22] F. Lian, R. Wang, L. Han, F. Jiang, and M. Hong, *Z. Anorg. Allg. Chem.*, **631**, 2485 (2005).
- [23] X. Bu, Z. Wei, and S. Ren, *J Coord Chem.*, **68**, 471 (2014).
- [24] Y.-E. Cha, X. Li, X. Ma, C.-Q. Wan, X.-B. Deng, and L.-P. Jin, *CrystEng Comm.*, **14**, 5322 (2012).
- [25] W. Li, P. T. Barton, R. P. Burwood, and A. K. Cheetham, *Dalton Tran.*, **40**, 7147 (2011).
- [26] X. Ma, Y.-E. Cha, K. Zhao, X. Li, T.-T. Yan, X.-N. Liu, and L.-L. Feng, *J Coord Chem.*, **65**, 2500 (2012).
- [27] C. N. R. Rao, S. Natarajan, and R. Vaidyanathan, *Angew. Chem. Int. Ed.*, **43**, 1466 (2004).
- [28] J. Zhao, X.-L. Wang, X. Shi, Q.-H. Yang, and C. Li, *Inorg Chem.*, **50**, 3198 (2011).
- [29] Y.-H. Xu, Y.-Q. Lan, X.-L. Wang, H.-Y. Zang, K.-Z. Shao, Y. Liao, Z.-M. Su, *Solid State Sci.*, **11**, 635 (2009).



## VITAE

**Name** Miss Sirinart Chooset

**Student ID** 5510230028

### Educational Attainment

Degree	Name of Institution	Year of Graduation
B. Sc. (Chemistry)	Thaksin University	2010
M. Sc. (Applied Chemistry)	Thaksin University	2012

### Scholarship Awards during Enrolment

1. Songklanagarind Scholarship for Graduate Studies, Prince of Songkla University
2. The Thesis Research Fund through the Graduate School, Prince of Songkla University

### List of Publications and Proceedings

#### Publications

1. S. Chooset, B. Cunningham, A. Kantacha, M. Zeller and S. Wongnawa (2014). "Diaquabis (cinnamato- $\kappa^2$ O,O')cadmium" *Acta Cryst E.* 70, m106-m107.
2. S. Chooset, A. Kantacha, A. Nimthong, M. Zeller, and S Wongnawa. "Synthesis and X-ray crystal structure of novel 2D-Mn(II) coordination polymer with 4,4'-trimethylenedipyridine and 3-nitrophthalate as ligands" *Journal of Structural Chemistry.* xx, xxxx – xxxx (accepted, 2016).

**Proceedings**

1. S. Chooset, A. Kantacha, A. Nimthong, and S. Wongnawa (2015). "SYNTHESIS AND CHARACTERIZATION OF CADMIUM(II) COMPLEX WITH 4,4'-BIPYRIDINE AND CINNAMIC ACID" Pure and Applied Chemistry International Conference 2015 (PACCON2015) , Amari Watergate Hotel, Bangkok, Thailand, January 21-23, 2015.
2. S. Chooset, A. Kantacha, K. Chainok, and S. Wongnawa (2015). "Structural and spectroscopic characterization of zinc coordination polymer with 4,4'-bipyridine and 4-aminobenzenesulfonate" Pure and Applied Chemistry International Conference 2016 (PACCON2016) , Bangkok International Trade & Exhibition Centre (BITEC), Bangkok, Thailand, February 9-11, 2016.